

Flexibilisation of Biogas-Based Power-to-Gas Processes: A Techno-Economic and Experimental Assessment

Présentée le 5 septembre 2022

Faculté des sciences de base
Groupe Kröcher
Programme doctoral en chimie et génie chimique

pour l'obtention du grade de Docteur ès Sciences

par

Andreas GANTENBEIN

Acceptée sur proposition du jury

Prof. K. Sivula, président du jury
Prof. O. Kröcher, Dr T. J. Schildhauer, directeurs de thèse
Dr J. Krautwald, rapporteuse
Prof. M. Seemann, rapporteur
Prof. J. van Herle, rapporteur

Acknowledgements

I would like to thank my thesis advisor Prof. Oliver Kröcher for his scientific guidance during my thesis. I furthermore would like to thank Prof. Jan van Herle, Dr. Judith Krautwald and Prof. Martin Seemann for taking the time to be co-referees in this thesis, and Prof. Kevin Sivula for being the jury president.

I thank our group leader of the TCP group, Dr. Serge Biollaz, for giving me the opportunity to perform my work in his group.

My direct supervisor Dr. Tilman J. Schildhauer I would like to thank for giving guidance during my work, providing input when needed and answering questions when asked. I highly appreciate his valuable feedback, his friendly support, and that he always manages to find a way out of dead ends.

This thesis would not have been possible with the great joint effort of the team of technicians and engineers, who contributed to this work with creative technical solutions and critical input from a practical point of view. I would like to thank the whole team for building, maintaining, and operating our plants, and performing field experiments, which ultimately led to the data shown in this thesis: Alwin Frei, Marcel Hottiger, Peter Hottinger, Julian Indlekofer, Robert Janz, Martin Künstle, Daniel Meyer, Sergio Rodriguez Duran, Jörg Schneebeli, Hansjörg Wagenbach, Tanja Wieseler, and Daniel Wuillemin.

My office-colleagues of OVGA/104, Philipp Riechmann, Dr. Julia Witte, Dr. Frank Schillinger, and Dr. Emanuele Moioli, as well as Dr. Adelaide Calbry-Muzyka and Dr. Hossein Madi, I appreciated for being great co-workers. With you, I could not only exchange about positive and negative moments of my PhD, but I also learned a lot from you and could profit from valuable discussions.

I warmly thank Marlene Lasser for joining us for her master's thesis. She did a great job in performing process simulations and supporting the field experiments, which completed this work.

During my time at PSI, I had the opportunity to meet many other great people whose company I highly appreciated during coffee breaks, swimming and various other activities – thank you all for the great time!

I would like to take the opportunity to thank my parents, Karin and Paul, for being supportive over the past years and providing anything, which was necessary to reach this point.

I specially thank my partner Claudia for being there for me during the past years, enriching my life apart from work, and for her incredible support during the whole PhD time.

Zurich, July 2022

Andreas Gantenbein

Abstract

Biogas-based power-to-X technology allows storing renewable electricity, while producing CO₂-neutral products.

This work investigates the conversion and upgrading of digestion-derived gas mixtures with focus on increasing the operational flexibility of the overall process. Compensation of fluctuations in the feed gases enable a better economic predictability of the processes and increase the product gas output.

A techno-economic evaluation was performed on bubbling fluidised bed (BFB) methanation and biological methanation for CO₂ conversion in all-year operation. Each considered process was modelled and optimised to obtain grid-ready biomethane. Rate-based models were used for the main units (BFB reactor, H₂-separation membrane). For the biological methanation, simulated performance data from literature were included. The analysis revealed a 17 – 19 % lower production cost for BFB methanation, mainly due to lower investment cost for the main reactor vessel. Instead of using PEM electrolysis, high temperature electrolysis (SOE) would allow for heat integration with the BFB reactor, which increases the plant efficiency from 54 % to 73 % (LHV). A further production cost reduction can be achieved by direct methanation of biogas, omitting prior separation of CO₂.

Based on gas separation experiments with a commercial biogas upgrading module (Evonik Sepuran) performed in a TRL 5 plant, a flexible upgrading concept using a permeation model was developed. It allows to swiftly switch between conventional membrane-based CO₂ separation by a 2-stage membrane unit and direct methanation of biogas and subsequent H₂ recycling.

A techno-economic analysis was performed on the flexible upgrading concept. The operation hours of the electrolyser were determined by applying a threshold to the electricity price distribution of the past years. The sensitivity on electricity cost (*i.e.* PtG operation hours) is clearly reduced with the flexible processes, resulting in a better economic predictability of the overall process, compared to a pure PtG installation. System analysis shows the need to allow part load operation of the methanation.

Symmetric part load operation (reduced availability of CO₂ and H₂) was tested in a field experiment by direct methanation of biogas with subsequent H₂ recycling in the TRL 5 methanation pilot plant. Stable operation of the methanation plant could be achieved at part load levels from 45 % to 100 % with closed recycle loop. The BFB reactor alone was tested in a load range of 20 to 100 %. A dynamic experiment demonstrated fast, successive load changes while still producing grid-ready biomethane.

Asymmetric part load (only H₂ limiting) operation was investigated by process simulations and field experiments. Since CO₂ is present in the system in an over-stoichiometric amount, H₂ recycle and CO₂ separation have to be performed simultaneously. Process simulations showed that selecting a most ideal PtG configuration based on technical feasibility is difficult, as further constraints, such as overall economics and operation scheduling have to be considered in process design and evaluation. In all cases, the CO₂ separation from the integrated processes leads to a loss of H₂ and CH₄ from the process. The introduction of an additional membrane stage with a sweep stream is proposed to reduce the loss of reactive gases via the off gas stream.

Keywords:

Direct methanation, flexible biogas upgrading, grid-injection, techno-economic analysis, membrane, process intensification, part load operation, process integration

Zusammenfassung

Die Power-to-X-Technologie auf Basis von Biogas ermöglicht die Speicherung von erneuerbarem Strom bei gleichzeitiger Erzeugung CO₂-neutraler Produkte.

In dieser Arbeit wird die Umwandlung und Aufbereitung von aus der Vergärung stammenden Gasgemischen untersucht, wobei der Schwerpunkt auf der Erhöhung der betrieblichen Flexibilität des Gesamtprozesses liegt. Die Kompensation von Schwankungen der Rohgase ermöglicht eine bessere wirtschaftliche Vorhersagbarkeit der Prozesse und erhöht den Produktgasausstoß.

Es wurde eine techno-ökonomische Analyse der Prozesse durchgeführt, basierend auf der katalytischen Methanisierung in der blasenbildenden Wirbelschicht (BFB) und der biologischen Methanisierung zur CO₂-Konvertierung im Ganzjahresbetrieb. Jeder betrachtete Prozess wurde modelliert und so optimiert, dass Biomethan zur Netzeinspeisung erzeugt werden kann. Für die Hauptkomponenten (BFB-Reaktor, H₂-Abtrennmembran) wurden ratenbasierte Modelle verwendet. Für die biologische Methanisierung wurden simulierte Leistungsdaten aus der Literatur herangezogen. Die Analyse ergab, dass die Produktionskosten für die katalytische Methanisierung um 17 bis 19 % niedriger sind, was hauptsächlich auf die geringeren Investitionskosten für den Methanisierungsreaktor zurückzuführen ist. Anstelle der PEM-Elektrolyse würde die Hochtemperatur-Elektrolyse (SOE) eine Wärmeintegration mit dem BFB-Reaktor ermöglichen, was den Wirkungsgrad der Anlage von 54 % auf 73 % (bezogen auf den Heizwert) erhöht. Eine weitere Senkung der Produktionskosten kann durch die direkte Methanisierung von Roh-Biogas erreicht werden, wobei die vorherige Abtrennung von CO₂ entfällt.

Auf der Grundlage von Gasseparationsexperimenten in einer TRL 5-Anlage mit einem kommerziellen Membranmodul zur Biogasaufbereitung (Evonik Sepuran) wurde ein flexibles Aufbereitungskonzept entwickelt. Es ermöglicht einen raschen Wechsel zwischen der konventionellen membranbasierten CO₂-Abtrennung durch eine zweistufige Membraneinheit und der Direktmethanisierung von Biogas mit anschließendem H₂-Recycling. Aus den experimentellen Daten wurde ein Modell zur Gaspermeation entwickelt und in das ratenbasierte Simulationsmodell des Membranmoduls integriert.

Für das flexible Aufbereitungskonzept wurde eine techno-ökonomische Analyse durchgeführt. Dabei wurden die Betriebsstunden des Elektrolyseurs durch Anwendung eines Schwellenwertes auf die Strompreisverteilung der letzten Jahre bestimmt. Die Sensitivität der Produktionskosten gegenüber der Stromkosten (d.h. der PtG-Betriebsstunden) ist im Vergleich zu einer reinen PtG-Anlage bei den flexiblen Verfahren deutlich verringert, was zu einer besseren wirtschaftlichen Vorhersagbarkeit des Gesamtprozesses führt. Die Systemanalyse zeigt

die Notwendigkeit, einen Teillastbetrieb der Methanisierung zu ermöglichen und somit ihre Betriebsphasen zu verlängern. Dies senkt verlustreiche An- und Abfahrvorgänge und damit verbundenes Abfackeln nicht einspeisefähigen Gases, sowie Aufheizvorgänge.

Der symmetrische Teillastbetrieb (reduzierte Verfügbarkeit von CO_2 und H_2) der Direktmethanisierung von Biogas mit anschließendem H_2 -Recycling wurde in einem Feldversuch in der TRL 5-Pilotanlage getestet. Ein stabiler Betrieb der Anlage konnte im Teillastbereich von 45 % bis 100% mit geschlossenem Rezyklatstrom erreicht werden. Der BFB-Reaktor allein wurde in einem Lastbereich von 20 % bis 100 % getestet. Ein dynamisches Experiment zeigte, dass schnelle, aufeinanderfolgende Lastwechsel bei gleichzeitiger Produktion von einspeisefähigem Biomethan möglich sind.

Der asymmetrische Teillastbetrieb (nur H_2 -Limitierung) wurde durch Prozesssimulationen und Feldversuche untersucht. Da CO_2 im System in einer überstöchiometrischen Menge vorhanden ist, müssen H_2 -Recycling und CO_2 -Abtrennung gleichzeitig durchgeführt werden. Die Prozesssimulationen haben gezeigt, dass die Auswahl einer idealen Konfiguration auf der Grundlage der technischen Machbarkeit schwierig ist, da bei der Prozessauslegung und -bewertung weitere Randbedingungen, wie die Gesamtwirtschaftlichkeit und die Betriebsplanung, berücksichtigt werden müssen. In allen Fällen führt die CO_2 -Abscheidung aus den integrierten Prozessen zu einem Verlust von H_2 und CH_4 aus dem Prozess. Das Einführen einer zusätzlichen Membranstufe mit einem Spülstrom könnte den Verlust von reaktiven Gasen über den Abgasstrom verringern.

Schlagwörter:

Direktmethanisierung, flexible Biogasaufbereitung, Netzeinspeisung, techno-ökonomische Analyse, Membran, Prozessintensivierung, Teillastbetrieb, Prozessintegration

Contents

Acknowledgements	i
Abstract (English/Deutsch)	iii
List of symbols and terms	xi
1 Introduction	1
1.1 Motivation	1
1.2 The role of the gas grid	4
1.3 Energy storage and coupling of energy sectors	5
1.4 Objective and general methodology	6
2 Theoretical background	9
2.1 Biomass resources and biomass use	9
2.2 Biogas upgrading	11
2.3 Direct methanation of biogas	14
2.3.1 Catalytic methanation	14
2.3.2 Biological methanation	15
2.3.3 Long duration tests and commercialisation	16
2.4 Efforts towards a higher flexibility of methanation processes	17
2.5 Short overview on electrolyser technology	21
2.5.1 Alkaline water electrolysis	23
2.5.2 Polymer electrolyte membrane electrolysis	23
2.5.3 Solid oxide electrolyser cell	24
3 Techno-economic comparison of biological and fluidised bed methanation	27
3.1 Introduction	27
3.2 Methods	28
3.2.1 Process design	28
3.2.2 Main models	33
3.2.3 Cost calculations	40
3.3 Results and discussion	43
3.3.1 Heat integration	46
3.3.2 Investment cost	48

3.3.3	Operational expenses (OPEX)	51
3.3.4	Revenues and production cost	55
3.3.5	Sensitivity on electricity price and SOE investment cost	56
3.4	Conclusion	59
4	Seasonally flexible biogas upgrading: Upgrading concept	61
4.1	Introduction	61
4.2	Flexible process concept	63
4.3	Methods	64
4.3.1	Gas mixing	65
4.3.2	Membrane test unit	65
4.4	Results and discussion	67
4.4.1	Performance of the gas separation membrane as upgrading unit after methanation	67
4.4.2	Performance of the membrane unit in biogas upgrading	70
4.4.3	Technical concept of dual use of membrane technology to upgrade bio-methane and biogas	72
4.5	Conclusion	74
5	Seasonally flexible biogas upgrading: Membrane permeation model and TEA	77
5.1	Introduction	77
5.2	Development of a rate-based model of a hollow fibre membrane module	80
5.2.1	Gas mixing and membrane test set-up	80
5.2.2	Experiments for membrane characterisation	82
5.2.3	Permeability model	83
5.3	Process design and application of the membrane model	91
5.3.1	Case <i>PtG1</i> : Direct methanation of biogas with subsequent gas upgrading	91
5.3.2	Case <i>PtG2-2c</i> : Removal of CO ₂ by membrane separation and subsequent methanation	92
5.3.3	Case <i>PtG2-1c</i> : Membrane separation and subsequent methanation without recompression	92
5.3.4	Case <i>BG</i> : Membrane-based biogas upgrading	93
5.3.5	Combination of the processes	94
5.3.6	Unit models	96
5.3.7	Economic data and assumptions for process modelling	96
5.4	Results and discussion	98
5.4.1	Process simulations	98
5.4.2	Cost analysis	100
5.5	Conclusion	110
6	Symmetrical part load operation of a PtG process	113
6.1	Introduction	113
6.2	Materials and methods	115

CONTENTS

6.2.1	Pilot plant experiments	115
6.2.2	System analysis	118
6.3	Results and discussion	120
6.3.1	Field experiments	120
6.3.2	System analysis	123
6.4	Conclusion	131
7	Asymmetrical part load operation of a PtG process	133
7.1	Introduction	133
7.2	Concepts for asymmetrical part load and process simulations	134
7.2.1	Part load operation of <i>PtG1</i>	135
7.2.2	Part load operation of <i>PtG2</i>	136
7.2.3	Part load operation of <i>PtG3</i>	137
7.2.4	Energy loss	138
7.3	Validity of the permeance model	138
7.3.1	Results	139
7.4	Results and discussion – Asymmetrical part load scenarios	140
7.4.1	Reactor in slip stream after the compressor	140
7.4.2	Case <i>PtG2</i> – Slip stream to reactor after first membrane stage	142
7.4.3	Part load operation of <i>PtG3</i> – Split in the off-gas	145
7.4.4	Comparison of the process options	147
7.5	Experimental determination of H ₂ loss under asymmetrical part load operation	148
7.6	Sweep membrane concept	150
7.6.1	Introduction to the concept	150
7.6.2	Experimental	151
7.6.3	Results and discussion	152
7.6.4	Conclusion and outlook	155
8	General conclusion and outlook	159
8.1	Achieved results and conclusions	159
8.2	Outlook and recommendation for further work	163
A	Membrane characterisation experiments	167
B	Process simulations	173
	Bibliography	193
	List of publications	195
	Curriculum Vitae	197

Symbols and terms

Acronyms and abbreviations

AEL	Alkaline electrolysis
BFB	Bubbling fluidised bed
CAES	Compressed air energy storage
CAPEX	Capital expenses
CC	Counter-current
CEPCI	Chemical Engineering cost index
CO	Co-current
COSYMA	Container-based system for methanation
CSTR	Continuously stirred tank reactor
ESI	Energy system integration
GWP	Global warming potential
HEX	Heat exchanger
MEM	Membrane
MFC	Mass flow controller
MFR	Methane formation rate
μ GC	Micro gas chromatograph
NDIR	Non-dispersive infrared
O&M	Operations and maintenance
OPEX	Operational expenses
PEM	Proton exchange membrane
PHS	Pumped hydro storage
PSI	Paul Scherrer Institute
PtG	Power-to-Gas
PtM	Power-to-Methane

PtX	Power-to-X (generic species)
SNG	Synthetic natural gas
SOE	Solid oxide electrolyser
TRL	Technology readiness level
TSA	Temperature swing adsorption
WGS	Water-gas-shift
WWTP	Waste water treatment plant

Symbols

A	area	m^2
C, c	cost	€
E	energy	J, kWh
d	diameter	m
HHV_i	higher heating value of component i	kJ mol^{-1}
LHV_i	higher heating value of component i	kJ mol^{-1}
m_{cat}	catalyst mass	kg
\dot{n}	molar flow rate	mols^{-1}
P	power	J s^{-1} , W
Π_i	permeability of component i	$\text{mol m Pa}^{-1} \text{s}^{-1} \text{m}^{-2}$
P_i	permeance of component i	$\text{mol Pa}^{-1} \text{s}^{-1} \text{m}^{-2}$
p	pressure	Pa, bar
p_i	partial pressure of component i	Pa, bar
$\Delta p_{ln,i}$	logarithmic partial pressure difference	Pa, bar
Q	heat flow	W
r	ratio	-
T	temperature	K, °C
V	volume	m^3
\dot{V}	volumetric flow rate	m s^{-3}
vv_d	CH ₄ formation per reactor volume and day	$\text{m}_{\text{CH}_4}^3 \text{m}_{\text{reactor}}^{-3} \text{d}^{-1}$
x_i, y_i	molar fraction of component i	-

Subscripts

el	electric, electrolyser
$f, feed$	feed of the membrane

List of symbols and terms

<i>i</i>	generic compound
<i>meth</i>	methanation
<i>off</i>	off gas
<i>p, perm</i>	permeate of the membrane
<i>prod</i>	product
<i>PL</i>	part load
<i>r, ret</i>	retentate of the membrane
<i>re, react</i>	reaction, reactor
<i>rec</i>	recycle
<i>sc</i>	steam conversion
<i>sw</i>	sweep
<i>t, trans</i>	trans membrane

1 Introduction

1.1 Motivation

The worldwide energy system is highly relying on fossil sources, such as oil, coal, and natural gas [1]. These resources preserved the solar energy converted by photosynthesis millions of years ago, representing a limited source of energy today. Traditionally, humanity also relied largely on biomass as energy source in its history, whereas the extensive use of oil and natural gas is only a relatively recent activity during the past century [2].

Due to the extensive use of fossil resources, a large amount of CO₂ is emitted to the atmosphere. In 2019, the energy-related emissions amounted to 33 Gt of CO₂ [1]. These emissions result in a steady increase of the CO₂ concentration in the atmosphere, amounting to 416.9 ppm in December 2021 [3]. In the past decade, this concentration increased around 2.4 ppm each year [3]. Nowadays, this high CO₂ concentration causes severe effects to the earth's atmosphere and is one of the main contributors to the increase of the average global temperature. This temperature rise will present humanity with severe challenges during the coming decade, such as decreasing ice and snow coverage, rising of sea levels and weather extremes [2]. In the Paris Agreement of 2015, 196 countries negotiated to implement measures to limit the global warming to 1.5 °C, compared to pre-industrial levels. [4]. The so-called carbon budget is a way to estimate the total amount of greenhouse gases, which can still be emitted in the future while limiting the global warming to a given target temperature [5]. The remaining budget in 2018 was estimated to 580 Gt of CO₂ to keep the 1.5 °C global warming target [5–7]. This contrasts with a total emission of around 40 Gt of CO₂ per year in 2019 [6, 7].

In order to support the goals of the Paris Agreement and transform its energy system towards a higher sustainability, Switzerland decided upon the implementation of a new energy strategy (Energiestrategie 2050) [8]. This political strategy includes four main pillars:

- Increasing the energy efficiency to decrease the use of primary energy carriers.

- Development of renewable energies: solar, wind and geothermal power production shall be fostered.
- No permissions for newly built nuclear power plants will be granted anymore. Existing plants are allowed to operate as long as a safe operation is ensured.
- The transmission grid will be improved to fulfil the requirements of the future electricity system.

These measures imply that at least a part of the current nuclear power generation has to be replaced by renewable power sources, for example solar and wind energy. This has a large impact on the Swiss electricity market, as demand and production profiles undergo substantial transformations. On the production side, the loss of nuclear power has to be compensated, whereas on the demand side the general trend towards the electrification of various areas of life is leaving its mark. Current and future electricity management systems have to be adapted accordingly towards a higher flexibility and improved load [9].

Worldwide, the electricity generation system is highly dependent on fossil sources. The share of fossil primary energy carriers to be converted to electricity amounted to 63.1 % in 2019 [1]. In Switzerland, the role of fossil combustibles is almost negligible, due to the large share of hydropower and nuclear energy, which together account for 91.8 % of the total electricity generation of 2019 [10]. In order to keep the CO₂ emissions low in the future energy system, the lacking nuclear energy (35.2 % [10]) has to be replaced by renewable sources.

The shift from nuclear or any other thermal power source towards renewable energy means a shift from band energy towards higher fluctuating generation methods. Since the electricity grid cannot store energy by itself, suitable electricity storage technologies are required to maximise the efficiency of the overall system.

Due to its topological structure, Switzerland already has large capacities for pumped hydropower storage installed. In 2019, the total capacity amounted to 8850 GWh, which represents an important energy reserve in months with low electricity production [10]. This reserve and the possibility to use it as storage for excess electricity will be even more important in the future energy system. An increase of storage capacity is needed, but only a few projects were realised during the past years. Such hydropower projects state a strong impact on the environment and the landscape, which results in tedious approval procedures. Alternative pathways of storing or utilising excess electricity have to be found. A production and demand profile of the year 2019 of the Swiss electricity system is shown in Figure 1.1. A strong seasonal variation in production and demand can be observed. Hydropower plants experience a production peak in summer months as snow melt and higher precipitation increase the water discharge in rivers. Nuclear power plants use this overproduction in summer for scheduled maintenance operations, which results in lower production during summer months. The demand curve shows an increase in the winter months due to colder weather and increased heating activity. In 2019, around 10 % of the Swiss electricity consumption is caused by heating purposes [10].

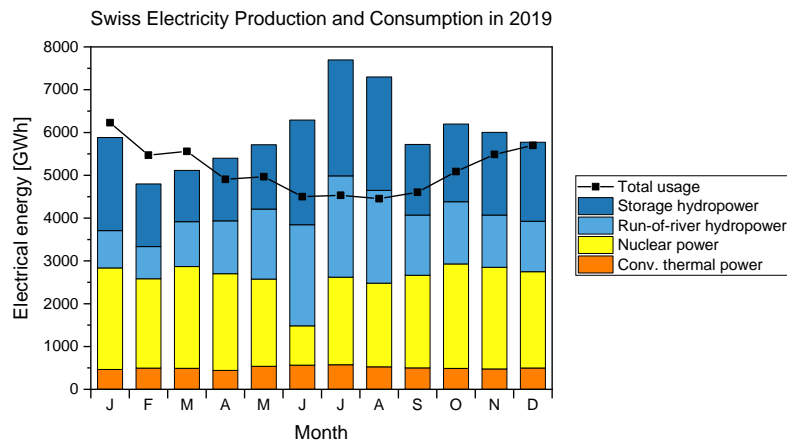


Figure 1.1: Monthly Swiss electricity total demand and generation of the four main generation sectors (stored hydropower, run-of-river hydropower, nuclear power, conventional thermal power) in 2019. Data source: [10].

Overall, Switzerland's electricity balance of the past years showed an overproduction in summer, allowing for electricity exports and some underproduction in winter, demanding for electricity imports [10]. Nevertheless, the discrepancy between demand and production is currently lowered by the pumped hydro storage facilities, allowing seasonal storage of electricity. In the future energy system, when the share of nuclear energy is lowered in favour of solar energy, the seasonal fluctuations in production are increased and the demand for the storage of unused electricity is higher.

A variety of electricity storage solutions is available. Best known from daily life are rechargeable batteries, which represent electrochemical storage solutions. Further technologies exist, which make use of the conversion of electricity to kinetic and potential energy. These include flywheel storage solutions, which store energy by the use of a rotating flywheel, which is connected to an electric motor and generator. Pumped hydro storage (PHS) uses the potential energy difference of two water basins at different elevations. Furthermore, compressed air energy storage (CAES) can be used when the topological structure of a region does not allow for PHS. CAES uses excess electricity to compress air in underground cavities formed by depleted salt deposits or rock caverns. This pressurised air is released later through a turbine, which generates electricity on demand. An additional advantage of CAES over PHS is its lower impact on landscape structure [11].

The chemical storage of electricity is possible by producing hydrogen in an electrolyser. The hydrogen can be further converted to hydrocarbons (*e.g.* CH_4 /biomethane). In any case, a suitable gas storage has to be available.

The applicability of the storage solution vary with the time scales the grid balancing is required. Providing balancing operations for short-term power fluctuations, (*i.e.* control reserve) requires relatively low storage capacities at high charge and discharge rates. It is therefore a

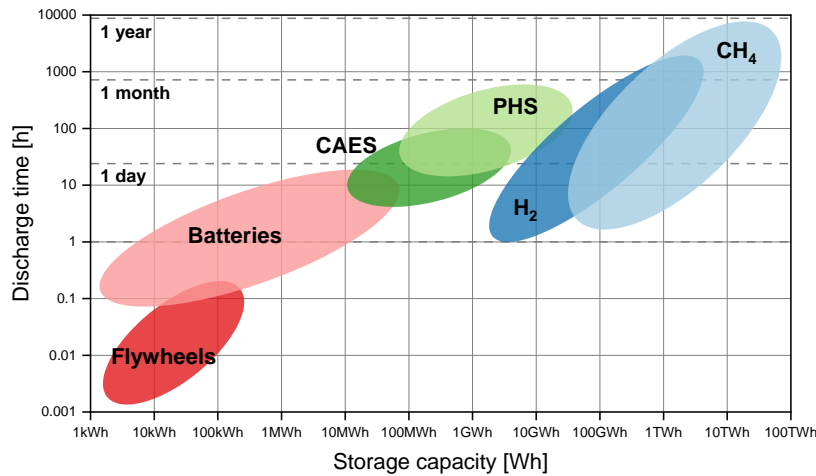


Figure 1.2: Electricity storage systems grouped according to their charge/discharge characteristics and their storage capacity. Adapted from Schaaf *et al.* [12].

suitable application for battery and flywheel storage solutions. Seasonal energy storage on the other hand is not dependent on fast discharge rates. Large energy quantities have to be stored for several weeks or months and are discharged over a similar time scale at later time [12–17]. Figure 1.2 [12] shows the different storage solutions by capacity and charge/discharge time, illustrating their respective operational flexibility.

1.2 The role of the gas grid

In 2019, the share of gas consumption among Swiss primary energy carriers amounted to 13.8 %, which corresponds to a total of 32 TWh [18]. This represents a substantial share of Switzerland’s primary energy consumption. Industrial processes consume around one third of the gas, mostly domestic heating and mobility use the remainder.

Currently, the share of renewable gas in the grid is very small. In 2019, only 361 GWh of biogas were injected to the gas grid [18], which comes up to only 1.1 % of the total consumption. Nevertheless, in order to foster the sustainability of the Swiss gas grid and support the goals of the energy transition, the Swiss gas industry decided to increase the share of renewable gas for domestic heating to 30 % by 2030 [19]. This goal shall be reached by connecting more biogas plants to the grid and importing of renewable gas.

The current gas storage capacity available for Switzerland amounts to around 1600 GWh, which corresponds to less than one month of the average annual gas consumption [20]. Apart from gas storage facilities, also the existing gas grid itself can serve as an energy storage by adapting its pressure level accordingly. Up to 5 % of the current storage capacity are associated with such pressure changes [20].

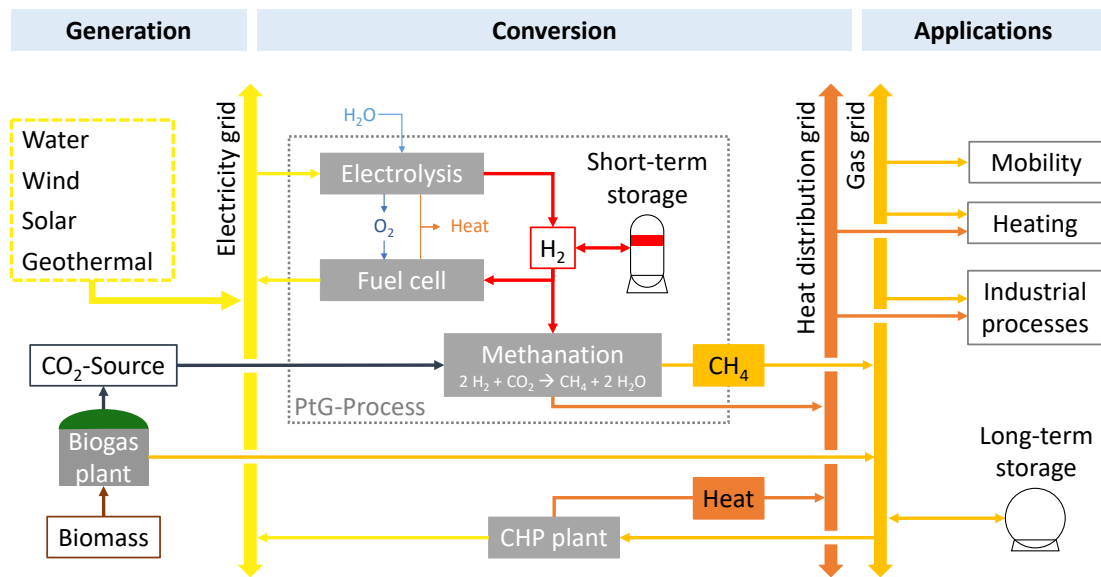


Figure 1.3: Methanation-based PtG as possible way to couple electricity, gas and heat distribution grids. By implementing appropriate conversion and storage technologies fluctuations in the connected grids can be compensated. As an example, digester-derived biogas is shown as CO₂-source for the methanation.

By increasing the share of renewable gas in the grid, the CO₂ emissions from the heating sector can be drastically reduced without high investments in new consumer infrastructure.

1.3 Energy storage and coupling of energy sectors

In order to cope with the fluctuations in the future electricity system a closer coupling of energy sectors is desirable. This includes the electricity grid, the natural gas grid, as well as heat distribution grids. Interconnecting these energy distribution grids allows to compensate production and demand discrepancies by respective energy conversion processes. An example of conversion pathways between the three distribution grids is shown in Figure 1.3.

Power-to-gas, using a biological process as CO₂ source, bears the potential to enhance the CO₂ neutrality of the gas grid on a short time-scale. Additionally, it allows storing unused electricity produced by renewable power sources (*e.g.* photovoltaic or wind) and avoids their curtailment [16, 21, 22]. The produced gas (biomethane) can be used in gas turbines to generate electricity at a relatively low round trip efficiency of around 20 to 38 % [12, 15]. Alternatively, methane is available for any other application in place today and represents a CO₂-neutral alternative to natural gas.

The mobility sector accounts to around 32 % of Swiss CO₂ emissions in 2019 [23], of which large share originates from private cars. Although an increasing share of new cars are electric,

battery electric vehicles are not feasible in all applications [20, 24]. Especially long-haul trucks require large fuel capacities, which battery systems currently cannot provide [24]. It is therefore required to operate these trucks with fuels of higher energy density, such as synthetic liquid fuels or biomethane. PtX and biomethane are therefore possibilities to indirectly electrify the long-haul mobility sector and lower the greenhouse gas emissions associated with it [20].

By using biomethane, already installed heating systems can be operated until end of their lifetime, while still reducing the CO₂ emissions. Furthermore, methane is still an important fuel in industry, especially for high temperature processes. Power-to-methane from renewable electricity and biogenic CO₂ sources can serve as a measure to lower the greenhouse gas emissions in various sectors. Nevertheless, it is required to drastically increase renewable power sources, as well as grid-injecting biomass conversion plants in near future.

1.4 Objective and general methodology

The aim of this thesis is to investigate the potential to increase the operational flexibility of biomass-based PtX processes. Due to the intermittency of renewable energies feeding the electrolysis and the relative operational inertia of the biomass conversion processes, different process states occur, depending on the availability of feed gases for the process. The goal of this thesis is to better understand how such processes should be designed and operated, especially when facing fluctuating feed streams. The use of expensive electricity (*e.g.* in winter) should be avoided, but the output of the product component may be maximised. By doing so, the specific cost for the upgrading unit can be decreased leading to a higher economic feasibility of such a process.

In order to better understand the effects of fluctuating feed streams of PtX processes, a mid-scale power-to-methane (PtM) plant operated with biogas from a digester unit is used as an example process. The plant consists of an anaerobic digestion unit, membrane upgrading and a PtG part.

Several process variations of different integration level of the membrane upgrading and the PtG plant are identified and evaluated based on technical and economic aspects. As a general restriction, each considered process has to fulfil the local grid injection limitations ([25], >96 % CH₄, <4 % CO₂, <2 % H₂). As an economic key performance indicator, the specific production cost per kWh of produced methane were determined.

The processes are numerically simulated by application of a rate-based model of a bubbling fluidised bed methanation reactor. The simulations are extended by the implementation of a rate-based counter-current model of a hollow fibre membrane for product gas upgrading.

In **Chapter 2**, a theoretical introduction is given, which gives an overview on biomass resources in Switzerland and subsequent biogas upgrading pathways. Furthermore, concepts for direct methanation of biogas are presented and applications at high Technology Readi-

ness Level (TRL) thereof. Due to its importance in PtX applications, a short introduction and overview in electrolyser technology is given.

Chapter 3 presents a detailed techno-economic analysis of three different PtM process chains including biological and catalytic bubbling fluidised bed methanation. Furthermore, the benefits of low and high temperature electrolysis are investigated. The process simulations and economic analyses in this chapter allow a direct comparison of CO₂ methanation and direct methanation of biogas.

In order to investigate its capability for removing excess hydrogen from the product gas stream, an experimental characterisation of a commercial biogas upgrading membrane is presented in **Chapter 4**. Based on the results of these tests, a flexible upgrading concept is explained, representing a first step towards seasonally flexible biogas upgrading.

In **Chapter 5**, a model for membrane permeance is developed, based on the previous experimental results. The model is applied in further process simulations and subsequent techno-economic assessment of the flexible upgrading concept presented in Chapter 4.

Chapter 6 reports on a field test performed with our TRL 5 methanation unit at a commercial biogas plant. During these tests, hydrogen recycling could be demonstrated for the first time using the pilot plant. Additionally, tests were performed, which demonstrated the part-load capabilities of the full process chain.

Chapter 7 presents a validation of the permeance model developed in Chapter 5. Based on previous process simulations, alternative part load scenarios are presented and explained. These part load scenarios allow a higher operational flexibility of the PtG process chain, independently from raw biogas storage. Furthermore, a modification of the membrane upgrading system is proposed, which should allow reducing the H₂ and CH₄ emissions during part load operation.

General conclusions are drawn in **Chapter 8**, along with an outlook to further work.

2 Theoretical background

2.1 Biomass resources and biomass use

Biomass as a renewable energy carrier can play a big role in the future energy system as a CO₂-neutral replacement for fossil raw materials. Especially the use of waste streams is favoured, as no competition with food production occurs.

Two main groups of biomass resources can be distinguished: woody biomass and non-woody biomass. The first includes wood from forests and landscape maintenance, wood residues, and waste wood. The second category consists of animal manure, sewage sludge, agricultural crop by-products, green waste from households and landscape, as well as organic waste from households and industry [26].

Thees *et al.* [27] and Burg *et al.* [26] assessed the potential for the energetic use of biomass in Switzerland. The total theoretical potential was estimated to 209 PJ of primary energy per year. Around one half originates from forestry wood (108 PJ a^{-1}) and one quarter derives from manure (49 PJ a^{-1}). From these theoretical potentials, the sustainably usable potentials were derived by estimating and deducing an individual set of environmental, technical, and economical restrictions for each biomass type. Furthermore, the biomass already used for energy purposes was taken into account. By this methodology, an additionally sustainably usable potential for each biomass was derived. The results of this analysis is shown in Figure 2.1 [26] for ten biomasses.

The analysis shows that the largest sustainable potentials are found in forestry wood (26 PJ a^{-1}) and animal manure (27 PJ a^{-1}). In addition, other non-woody waste biomasses shown in Figure 2.1 [26] (*i.e.* green waste, agricultural crop by-products, sewage sludge, and industrial bio-waste) bear a large combined sustainable potential of around 20 PJ a^{-1} , of which 8 PJ a^{-1} additional potential arise.

The energy content of the additionally available animal manure alone could cover around 2.2 % of the Swiss gross energy consumption (1103 PJ in 2019) [18, 28].

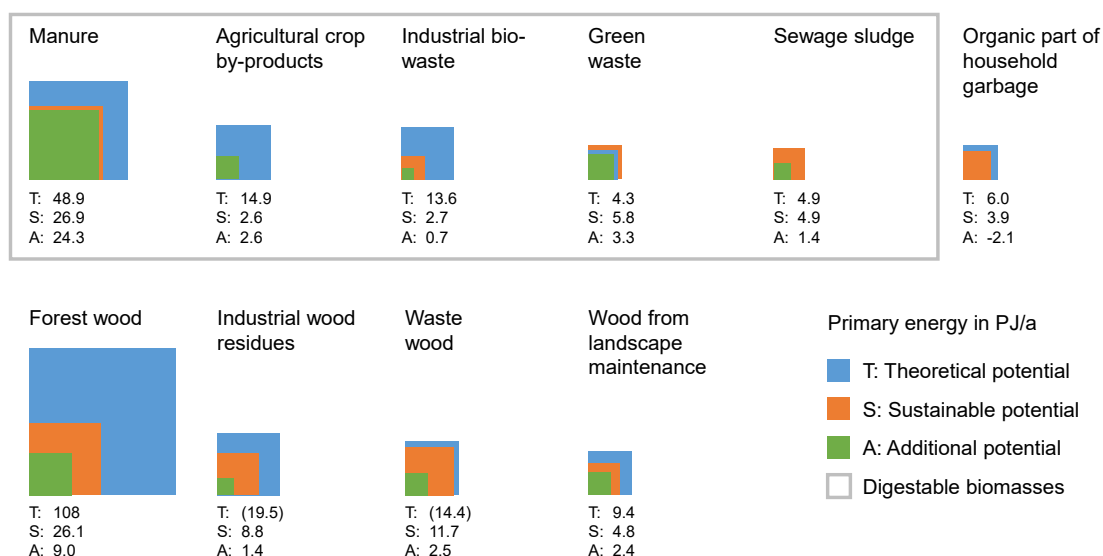


Figure 2.1: Theoretical and sustainable potentials for energetic use of 10 different biomass resources in Switzerland in PJ per year. The additional potential represents the share of currently unused, sustainable potential. Figure adapted from Burg *et al.* [26].

Another aspect of fostering the use of animal manure for energetic use arises from the greenhouse gas emissions associated with agriculture. In Switzerland, this sector accounts for 14 % of the total greenhouse gas emissions in 2019 [23]. Around 3 % of these emissions could be avoided by digesting animal manure instead of directly using it as fertiliser on the fields. This percentage could be even higher, as the energy obtained from this biomass could potentially replace fossil energy carriers [28, 29].

A variety of conversion pathways are available to make biomass available for energetic use [30, 31]. Besides waste incineration, anaerobic digestion (AD) is used for the conversion of non-woody biomass to methane [26]. Since the focus of this work lies in the upgrading of biogas for grid injection, other utilisation pathways are not discussed here.

Around 141 agricultural and industrial biogas plants are currently operated in Switzerland. Additional 291 plants use waste water or sewage sludge as substrate [32]. Most of these use the produced gas to operate combined heat and power (CHP) plants, as feed-in tariffs favoured electricity generation during the past decade.

Anaerobic digestion of biogas produces a raw gas, which consists of CH_4 and CO_2 as main components. The methane content varies depending on the substrate used in the digester ranging from 44 % to 69 %. Green waste has a tendency to yield lower methane content gases than manure or sewage sludge [33, 34].

Furthermore, low percentages of N_2 and O_2 may be present in the raw biogas [33]. Besides these bulk components, trace contaminants are present in the ppm-range, which are of high

importance for the downstream processes. These include H_2S , COS and sulphur-organic compounds, such as mercaptans, sulphides and thiophens [35, 36].

Also NH_3 is commonly found in raw biogas, as well as silicon containing trace compounds, such as siloxanes and silanes. Especially during the digestion of green waste, volatile organic compounds are formed (VOCs, *e.g.* terpenes, alkanes, furans, esters, alcohols etc.) [33, 37–39]. The quantity and occurrence of the trace compounds is highly dependent on the substrate fed to the digester. Siloxanes are more prominent in sewage sludge than in agricultural waste digestion, as they originate from consumer products (*i.e.* hygiene products, cosmetics, detergents etc.) [40].

Although the trace compounds are present at very low concentrations, they can directly affect the downstream processes. Especially sulphur contaminants can lead to catalyst poisoning or the formation of corrosive sulphur oxides. Siloxanes can also be oxidised and form SiO_2 microcrystallites, causing abrasion in moving parts and obstruction of porous structures [41]. Moisture and large VOCs can cause a problem in the gas cleaning section itself, as competitive sorption effects can occur, which then lead to an earlier breakthrough of the target molecule [42].

Gas cleaning gained a higher importance over the last years, as more complex and sensitive downstream applications are discussed. Gas motors operated with biogas are less sensitive to sulphur compounds than fuel cell applications, or the use for direct methanation discussed in this work [37, 43]. Figure 2.2 shows common conversion methods for energetic use of biogas and their respective tolerance against siloxane and H_2S contaminants. This data is compared to the contaminant concentration expected in different biogas types [37].

The Thermo-Chemical Processes (TCP) group at PSI focusses on sorbent-based gas cleaning. Various commercial low-temperature sorbents were tested for their capability of physisorption and chemisorption of contaminant species. It was shown that a two-stage gas cleaning allows to operate a methanation reactor with high stability [37]. The first stage of the gas cleaning is concerned with removal of bulk H_2S , whereas in the second stage organic sulphur compounds are removed. Nevertheless, due to competitive sorption and roll-up effects, field testing under application-specific conditions is important to obtain the right input parameters for bed sizing and sorbent choice [42].

2.2 Biogas upgrading

For conventional biogas upgrading, several well-established physical and chemical methods exist for the separation of CO_2 . Most commonly, these include water and amine scrubbers, as well as physical sorption methods like pressure swing adsorption (PSA) [44]. Scrubbers make use of the different solubility of methane and CO_2 in the respective medium. The raw gas is brought into the bottom of a first column, where water or an aqueous amine solution is injected into the top. Packings ensure a high gas-liquid contact area. The liquid phase

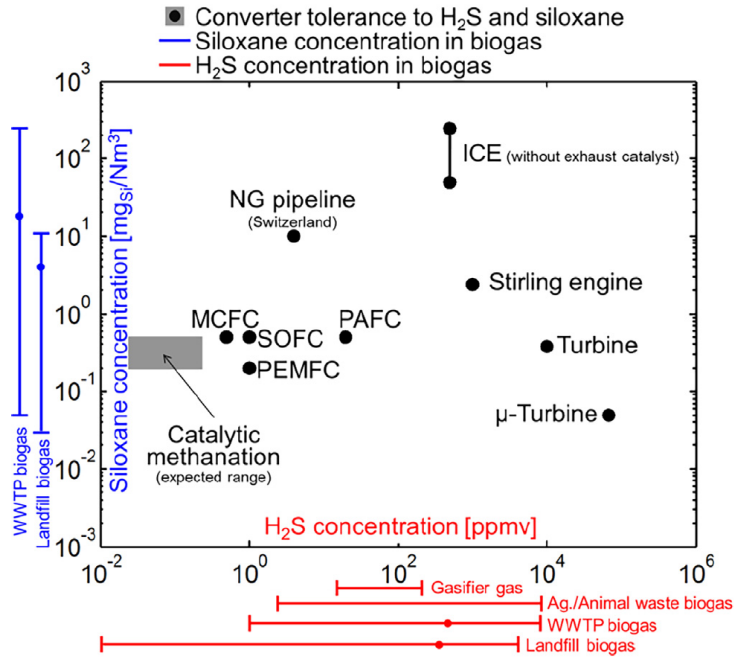


Figure 2.2: Concentration ranges of H₂S and siloxane contaminations in different types of biogas in combination with tolerances for the most common biogas utilisation pathways [37]. Reproduced with kind permission of Elsevier Publishing

absorbs the CO₂ and is regenerated in a second column. In a water scrubber, the regeneration occurs by lowering the pressure and stripping with air. The amine solution is regenerated by heating and partially evaporating it in a stripper column. This releases the chemically bound CO₂ from the solution. A condenser at the top of the column prevents the release of amine solution through the off gas stream [44]. The PSA operates in cycles with several pressure vessels in parallel to ensure continuous operation. During the adsorption cycle, CO₂ is selectively adsorbed on a solid sorbent (*e.g.* zeolite) and desorbed in the second cycle at lower pressure.

The scrubbing methods allow for the lowest methane slip, followed by PSA [38]. It is important that the processes are optimised to the respective applications in order to minimise the release of methane to the atmosphere. Methane slip has not only an impact on the economics of the process, but also on the environment, as CH₄ has a higher global warming potential (GWP) than CO₂. The methane loss should therefore not exceed 4 % of the feed gas [45]. Regulations in Switzerland [25] limit the maximum allowed methane slip to 2.5 % of the methane in the raw gas. In practice it is aimed to reach below 1 % of methane in the CO₂ released to the atmosphere, which corresponds to less than 0.5 % total methane slip.

Both separation methods require an external energy input: Scrubbers in the form of thermal energy and PSA as electrical energy for gas compression.

Another non-thermal upgrading method is performed by membrane separation. In recent years, membrane technology for biogas upgrading gained increasing market shares among newly installed plants. In 2019, almost one third of the installed plants rely on membrane upgrading [46].

The success of the membrane technology can be traced back to its simple scalability, operational flexibility and simplicity in operation. Apart from compressor equipment, no moving parts are required in the installation and the maintenance tasks are reduced to a regular replacement of membrane modules. Furthermore, the investment cost are in a similar range as other upgrading methods [47], which in the sum gives a clear incentive for membrane technology.

Two main types of industrial polymer membrane modules can be distinguished: spiral wound and hollow fibre modules, as shown in Figure 2.3. The first type consists of a sheet of membrane material and an impermeable spacer sheet. The spacer and the membrane material form a gas tight pocket, which is connected to a central tube. The two sheets are wound around the central tube and form the module. The feed gas passes through the module in axial direction along the membrane material. Permeating species collect in the pocket and are directed to the central tube representing the permeate outlet [48].

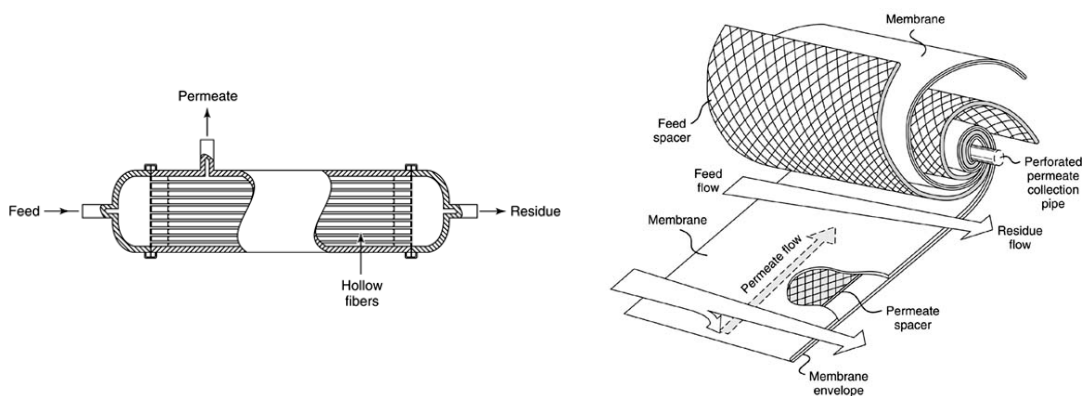


Figure 2.3: Two common types of commercially used membrane modules: hollow fibre module (left) and spiral wound module (right). Adapted from [49] and reproduced with kind permission of John Wiley & Sons, Inc.

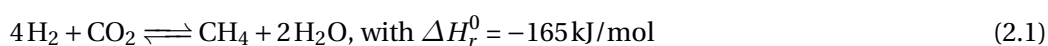
The second membrane type consists of hollow fibres made of carrier material, which is coated with a thin layer of active membrane polymer. A bundle of a few ten thousand fibres forms a cartridge, which is put into a pressure-resistant vessel. The feed gas is directed through the inside of the hollow fibres, penetrating species permeate through the fibre walls to the shell side and form the permeate stream. Some suppliers also reverse the flow, such that the feed gas is applied on the shell side [48, 50, 51].

In this work the focus is set on a commercial hollow fibre membrane for biogas upgrading, which is produced by Evonik Industries AG (Germany) and built into a module by

Apex AG (Switzerland). A selection of common membrane polymer types is given in the thesis of J. Witte [52].

2.3 Direct methanation of biogas

The upgrading technologies can be replaced by direct methanation of biogas. Instead of separating it from the gas stream, the CO₂ is directly converted to additional methane gas. The methanation reaction was discovered by Sabatier and Senderens in 1902 [53]. It is highly exothermic and limited by thermodynamic equilibrium:



Many metals from the group 8 – 10 are able to catalyse the reaction [54]. The most suitable for methanation are ruthenium, nickel, cobalt, iron and molybdenum [54, 55].

Most often, nickel-based catalysts are used, as the metal shows good selectivity towards CH₄, relatively high activity and a low raw material price [54, 56]. Ruthenium shows the highest activity for the methanation of CO and CO₂, or mixtures thereof, but its cost is significantly higher than that of nickel [54]. Although exhibiting a similar activity as nickel, cobalt is also more expensive and is therefore not as widely used as nickel [54]. Iron and molybdenum show a lower selectivity towards methane and are more suitable for the synthesis of higher hydrocarbons [54].

Commercial systems typically operate in the temperature range of 200 – 550 °C [54, 56]. In industrial scale, the methanation reaction is performed at elevated pressures up to around 30 bar, as reported for Haldor Topsøe's methanation technology [57, 58].

Alternatively, the methanation reaction can also be performed by specialised microorganisms in a mesophilic (35 to 40 °C) or thermophilic (55 to 65 °C) temperature range [59].

2.3.1 Catalytic methanation

Due to its strong exothermicity and equilibrium limitation, the methanation reaction requires reactor concepts, which maximise methane conversion by good heat removal to prevent hot-spot formation. In the case of direct methanation of biogas, the feed gas to the reactor already contains a large share of methane gas. The heat formation per volume flow is therefore dampened and hot-spot formation in catalytic reactors reduced [60].

In adiabatic fixed-bed reactors, temperatures up to 700 °C can be reached, which requires the catalyst to withstand cracking and sintering effects under such conditions [56, 61]. Often in

such systems, cascades of adiabatic fixed-bed reactors with intermediate cooling and product gas recycling are applied [12], or fixed-bed reactors with internal cooling systems [57].

Alternatively, fluidised bed technology allows for near-isothermal operation of the methanation reactor [62]. Especially when internal cooling systems are in place, the high turbulence and particle movement in the reactor allows an efficient distribution of the reaction heat. The particle movement also facilitates a uniform distribution of the heat production, as the reaction front is more distributed as in fixed-bed reactors.

Fluidised bed technology has been investigated and further developed since decades. Methanation is used as state-of-the-art technology for the removal of carbon oxide traces from feed- H_2 to the ammonia synthesis. Furthermore, methanation is used for coal gasification in the GW scale, mainly in China [63].

2.3.2 Biological methanation

In biological methanation, a water phase is required, which serves as living medium for the microorganisms catalysing the methanation reaction. In this water phase, also nutrients needed for the growth are dissolved and provided to the organisms. A variety of different growth media exist, depending on the organism used in the reactor [59]. They consist of a variety of salts, mainly containing phosphates, sulphates, carbonates and chlorides of potassium, ammonium, sodium, calcium and magnesium. Further trace minerals containing Zn, Ni, Mo, B, Mn and Fe in various concentrations are also added [59, 64–67]. Schill *et al.* [68] report the addition of Na_2S -solution as sulphur source. It was added pulse-wise in order to reduce stripping of H_2S from the liquid phase.

After all, Rusmanis *et al.* [59] state that the elemental composition of growth media used in biological methanation are not very different from those used in anaerobic digestion [69, 70]. Therefore, concepts exist, where effluent from an anaerobic digestion unit is directly used as medium [64, 69, 71].

In pilot tests, the biological methanation showed good performance in untreated raw biogas [72]. It was shown that sulphur contaminants present in the raw gas stream did not affect the performance of the methanation reactor, which shows that biological methanation is much more tolerant against sulphur contaminants.

In anaerobic methanation, the reaction is catalysed by microorganisms, which metabolise H_2 and CO_2 and produce CH_4 and water as side products. The two reactant gases are only available to the organisms when they are dissolved in the liquid phase. A big challenge for biological methanation is therefore to increase the gas-to-liquid mass transfer rate of H_2 , which is the main limiting factor for the methane conversion rate [73]. Especially at elevated pressures, CO_2 readily dissolves in water and is therefore less of a problem than hydrogen. Various reactor concepts are under investigation to overcome this problem. The

most dominant for biogas upgrading are continuously stirred tank reactor (CSTR)-based bubble columns and counter-current trickle bed reactors [59, 65, 71, 74].

In the bubble column reactor, vigorous stirring increases the gas-liquid interface area. The energy required for stirring amounts to around 0.7 to 2.5 % of the electricity used in the electrolyser, stating an efficiency loss of the same magnitude to the overall system [75, 76]. Often, these systems are operated at elevated pressures in order to facilitate the gas-to-liquid mass transfer.

For trickle bed reactors, an additional energy input is required, as the liquid phase has to be circulated in order to provide a liquid film and nutrients to the biofilm present in the bed. The recirculation of the liquid can either be done continuously or pulsated [65, 69]. Ullrich *et al.* [77] showed for trickle bed reactors, that increased system pressures indicate higher gas-to-liquid mass transfer and therefore result in a higher methane formation rates. This finding also holds for gassed CSTR systems [73].

2.3.3 Long duration tests and commercialisation

In both main technologies – catalytic and biological methanation – long duration tests using biogas were performed at TRLs of around 5. Such tests are important to prove the stability of the process and show the feasibility of the direct methanation technology [42].

In Denmark, long-duration tests were performed by the company Electrochaea using the CSTR-based biologic methanation [42, 74]. Furthermore, the company MicrobEnergy (now a subsidiary of Hitachi Zosen INOVA) has a combined experience of more than a several 1000 h for its stirred bubble column technology. Both companies work with thermophilic (60 – 70 °C) microorganisms. Electrochaea uses a single strain of archaea, whereas the technology of MicrobEnergy relies on a mixed set of organisms, which adapts itself to the conditions given by the digester effluent used as growth medium [71, 78]. Based on the technology of MicrobEnergy, the utility provider Limeco has built and commissioned a TRL 8 methanation plant in Switzerland [79]. The demonstration plant produces biomethane for grid injection, based on raw biogas from anaerobic digestion of sewage sludge. The electricity for electrolysis is generated on-site in the steam-cycle of a waste incineration plant [78].

Catalytic direct methanation of biogas was tested for 1000 h by Dannesboe *et al.* [58] in collaboration with Haldor Topsøe A/S. A two-stage fixed-bed methanation was used with intermediate cooling and condensation of reaction water, which allowed the production of grid-ready biomethane without further upgrading. The system was designed as boiling water reactor, producing steam at 280 °C (65 bar). The methanation was operated at 20 bar and a commercial Ni/Al₂O₃ catalyst was used. As no axial movement of the hot spot could be observed during the whole test, no catalyst deactivation was expected [58].

Specht *et al.* [80] reported successful operation of 25 kW_{el} and 250 kW_{el} methanation plants. The systems were mainly based on tubular fixed-bed reactors with molten salt (250 kW_{el}

system) and oil (25 kW_{el} system) cooling. The larger system had a plate reactor with water cooling installed. The systems were operated as two-stage reactors with intermediate gas cooling and condensation of product water. A part of the product gas was recycled to the feed in order to limit hot spot formation. The duration of the test runs is not known, nevertheless, the results lead to the implementation of the technology in a 6 MW_{el}-scale plant in Werlte, Germany in collaboration with Audi AG.

Our group performed a long duration test for direct methanation of biogas at the waste water treatment plant (WWTP) of Zurich, Switzerland. The experiments were performed using the TRL 5 methanation set-up COSYMA, which allowed to use a split-stream of the raw biogas produced in an anaerobic digester for sewage sludge. A part of the biogas also originated in an anaerobic digester fed with municipal green waste. The tests showed stable operation of the methanation plant for more than 1100 h [81]. To protect the methanation catalyst, two serial sorbent beds were included in the plant, which consisted of combinations of commercially available materials. During the long duration test, a slow activity loss of the catalyst could be observed due to sulphur poisoning. Several commonly occurring sulphur contaminants were regularly monitored during the field tests and the gas cleaning measures adapted accordingly [37]. The improvements in the gas cleaning reduced the deactivation rate to a level, which would allow the operation of the plant for a full year without catalyst exchange. Nevertheless, minor deactivation by coking effects could not be fully excluded [81].

The results from this long duration test was compared to the kinetics used in a simulation model for fluidised bed methanation developed in our group. The reaction temperature was varied during the experiments, leading to changing methane concentration in the product gas. The model was able to correctly predict the concentration maximum as a function of reaction temperature, which indicates that the kinetics applied describe CO₂ methanation appropriately [81].

2.4 Efforts towards a higher flexibility of methanation processes

In the following, a non-exhaustive overview is given for efforts increasing the flexibility of methanation and PtG systems. Namely fixed-bed, three-phase and biological methanation are discussed. The findings are summarised in Table 2.1.

Matthischke *et al.* [82] developed a one-dimensional fixed-bed reactor model for CO₂ methanation. They tested the start-up behaviour and load range of reactors operated under adiabatic conditions or with external cooling. They showed that product gas recirculation is highly beneficial for the operation of cooled fixed-bed reactors.

Cooled fixed-bed reactors were found to start up considerably faster than adiabatic reactors, as in the latter, more heat is required to increase the reactor temperature to a steady-state level, which corresponds to the hot-spot temperature. In the cooled system, the temperature is considerably lower and approaches the temperature of the cooling medium asymptotically.

In this study [82], the load range was set by adjustment of the feed flow rate. In the adiabatic reactor, increased product gas recirculation leads to a decreased hot-spot formation due to the cooling effect of the recirculated gas. At lower recycle rates, the conversion to methane is limited by equilibrium. With increasing recycle rates, the conversion rises due to a decreased hot-spot temperature. At high recycle rates, the reaction becomes kinetically limited, as a temperature profile forms along the reactor forming a hot-spot at the outlet of the reactor. Therefore, in adiabatic fixed-beds, an optimal recycle rate exists for a maximum conversion. In cooled reactors, recirculation of product gas also has a cooling effect, leading to a lower reaction rate and therefore less conversion. Nevertheless, this dampening effect has a positive impact on the stability of the reactor, when load changes are applied, as hot-spot formation and subsequent thermal deactivation is decreased. It furthermore increases the load range of the system.

In a prior study of Matthischke *et al.* [83], effects of the recycle stream and load ramps on an adiabatic fixed-bed reactor were experimentally investigated. In addition, the benefits of product gas recirculation on system stability could be shown. Experiments with load ramps (by feed flow rate) showed that the temperature response of the reactor is slower than the concentration response, due to the heat capacity of the catalyst bed and the reactor vessel. A recycle loop in the system allows to manipulate the reactor temperature and therefore the conversion of CO₂.

The dynamics of a three-phase methanation reactor were experimentally investigated by Lefebvre *et al.* [84]. The system consists of an unstirred slurry bubble column (DN25 and DN50) filled with a heat transfer liquid. Therein, a commercial Ni/Al₂O₃ catalyst is suspended. Similar to biological methanation systems, this system tends to be limited by the gas-to-liquid mass transfer rate. In steady-state experiments, they investigated the preferred conditions for maximum CO₂ conversion. They show that high partial pressures of H₂ favour the gas-to-liquid transfer and are beneficial for the methane formation rate. The partial pressure of CO₂ shows a lower influence, due to the higher solubility of CO₂ in the heat transfer liquid. In general, higher system pressure increases the CO₂ conversion. They emphasise that an optimum reaction temperature has to be found, which ensures high reaction rates and therefore high CO₂ conversions, but also ensures stability of the suspension, which is prone to decomposition at elevated temperatures. Increasing feed gas velocities resulted in an increase of the methane formation rate (MFR), but a decrease in CO₂ conversion, as larger bubbles are formed, which foster a larger bypassing of feed gas.

To assess the dynamic operation of the three-phase reactor, experiments with gas velocity steps were performed. They showed that the dead time of the concentration response of the reactor is shorter the higher when the feed gas velocity is increased. The reactor time constant was found to be solely dependent on the final gas velocity. It was found that the reactor time constant is only a function of the gas residence time. Therefore, the reaction kinetics are not limiting factors which influence the reactor time constant.

Giglio *et al.* [85] present a one-dimensional dynamic model for a multi-tubular, fixed-bed reactor. It was used for the dynamic simulation of a cascade of three boiling water-cooled CO₂ methanation reactors. The system allowed inter-stage feeding of CO₂ and condensation of water after the second and third reactor. The system was sized to a H₂ feed stream of 40 mol s⁻¹, which corresponds to an electrolyser size of 10 – 15 MW_{el}. Giglio *et al.* [85] tested the hot start-up and part-load operation of the system. They found, that after a hot stand-by, their system can reach grid-quality product gas within 130 s and requires a sequential start-up of the reactors in order to avoid hot-spot formation. In full-load operation, 39 % of the CO₂ is fed to the first reactor, the remainder is mixed to the feed gas of the second reactor. In part-load operation, the share of gas fed to the first stage decreases. At lower part loads, an increasing amount of CO₂ is fed to the feed of the third reactor. The inter-stage feeding was required, as the lower gas velocity in the reactors caused hot-spot formation.

In order to optimise the start-up control of a tubular, fixed-bed reactor, Bremer *et al.* [86] used a dynamic two-dimensional reactor model. The considered reactor tube is controlled via the cooling of the reactor jacket. The goal of this study is to avoid hot spot formation and to reduce the start-up time to reach a steady-state. They report an optimised temperature trajectory for the cooling medium, which initially serves as heating to reach reaction temperature in short time, but then is reduced in order to prevent hot spot formations in steady state.

Zimmermann *et al.* [87] present a simulation study, which investigates the dilution of the active material in a fixed-bed reactor and the introduction of catalyst particles with an active core and an inert shell. Sequential load changes were applied to the model and the step response analysed for several reactor designs. The reactors with core-shell catalysts revealed a significantly higher space-time yield, compared to diluted fixed-beds, leading to a reduction of tube length. This effect originates in the reduction of the effective reaction rate at high temperatures, as the mass transport through the inert shell becomes rate-determining and the effective reaction rate becomes almost independent on temperature. In a diluted fixed-bed reactor the effective reaction rate is equally reduced over the whole temperature range. The study reveals that fixed-bed reactors filled with core-shell catalysts are beneficial for load-flexible methanation, as no moving fronts were observed and steady-state was reached quickly.

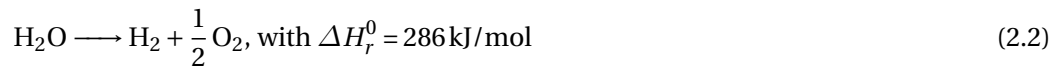
For the biological methanation, Inkeri *et al.* [75] developed a dynamic model of a tall, CSTR-based bubble column. The response of a 1 MW_{el} reactor to load changes was simulated, including an intermediate shut-down. The load profile applied two part load levels at 40 % and 80 %, which were set by reducing the feed gas flow. A single operation point was kept for 10 min. After each positive load change, spikes in the output gas flow were observed, which may be explained by the inability of the reaction to adapt fast enough to the new conditions, limiting the H₂ consumption. It could be seen, that after the load changes, the CH₄ concentration dropped below the desired 95 %-level, which demands for additional stabilisation mechanisms (*e.g.* storage, control logics). Nevertheless, the model showed that the reactor is able to regain steady-state in less than 10 min.

	Reactor type	Type of work	Investigated dynamics	Investigated load range	Results	Ref.
Fixed bed methanation	Adiabatic reactor with partial product recycle, cooled fixed-bed reactor without product recycle	Simulation: Unsteady-state, one-dimensional, pseudo homogeneous fixed-bed reactor model	Load flexibility with emphasis on load range and start-up time	Variation of volumetric flow rate, corresponding to the superficial velocity. Adiabatic reactor: 0.19 – 1.94 m/s Cooled reactor: 0.6 – 1.5 m/s	197 s for the cooled reactor to reach steady state after a warm start, 392 s for the adiabatic reactor; adiabatic reactor: maximum of methane content and temperature maximum are only slightly affected by the superficial velocity (broad load range); cooled reactor: narrower load range, very sensitive behaviour	[82]
	Three-stage, multi-tubular, cooled fixed-bed reactor cascade	Simulation: Transient, one-dimensional, pseudo homogeneous mathematical model	Start-up from hot standby and step reduction of the overall inlet flow	Without CO ₂ -staging: 80 % With CO ₂ -staging: 70, 65, 60, 55, 50 and 45 %	130 s to reach the targeted CH ₄ content after hot standby, 50 s to reach steady state at step reduction to 80 %, with CO ₂ staging the minimum partial load is 45 %, CH ₄ at reactor outlet is always above 95 %	[85]
Three-phase methanation reactor	Slurry bubble column reactor	Experimental: Columns with DN25 and DN50	Load variations using inlet gas velocity step changes	0.4 to 1.6 cm/s, 0.4 to 0.8 cm/s, 0.8 to 1.6 cm/s, incl. opposite step changes	The reactor time constant τ is halved when the gas velocity is doubled and reversely, τ is only a function of the gas residence time, reactor hydrodynamics or reaction kinetics are not the limiting factors influencing τ	[84]
Biological methanation	Continuously stirred biomethanation reactor	Simulation: Dynamic one-dimensional model for tall CSTRs	Load changes, start-up and shut-down of the methanation	Sequential load changes, each setting kept for 10 min: full load – 40 % – full load – shut-down – 80 % – full load	Steady-state could be reached in less than 10 min for all load changes, the CH ₄ content of the outflow gas does not remain above the desired 95 % level during load changes	[75]

Table 2.1: Studies on activities towards higher flexibility of methanation processes. Table adapted from [88].

2.5 Short overview on electrolyser technology

One of the key steps in any PtX process is the electrolyser, which provides hydrogen to the synthetic downstream process. Three major technologies can be distinguished: alkaline electrolysis (AEL), proton exchange membrane (PEM) electrolysis and solid oxide electrolysis (SOE). They are mainly classified by their operation temperature and the electrolyte, which separates the half-cell reactions. AEL and PEM technologies operate at temperatures below 100 °C, whereas the SOE is a high temperature technology and operates in the range of 650 to 1000 °C [89]. All of them split water into molecular hydrogen and oxygen by application of electrical and thermal energy:



The heat of reaction ΔH_r corresponds to the overall energy demand of the endothermal reaction 2.2 above. It can be partly supplied by heat (Q), while the Gibbs free energy part (ΔG_r) has to be supplied electrically:

$$\Delta H_r = \Delta G_r + Q \quad (2.3)$$

All enthalpies are temperature-dependent. The overall energy demand ΔH of the water splitting reaction varies only little with temperature. The enthalpy term, which enables heat integration increases with temperature. This positive temperature dependency allows to reduce the minimum electrical energy demand ΔG_r required for the water splitting reaction. The operation of the electrolysis at high temperature improve reaction kinetics and allow for a high heat utilisation of the cell's internal losses [90]. Furthermore, it allows for heat provision by steam, contrary to low temperature cells, where the latent heat of vaporisation is provided by electricity [90].

The reversible cell voltage U_{rev} represents the theoretical minimum cell voltage to perform the water splitting reaction. It is calculated according to the equation 2.4 and assumes that the whole heat demand Q is provided by an external heat supply.

$$U_{rev} = \frac{\Delta G_r}{zF}, \quad (2.4)$$

where F refers to the Faraday constant (96485 C/mol) and z the number of electrons transferred in the reaction ($z = 2$). As shown in Figure 2.4, U_{rev} decreases with raising temperature.

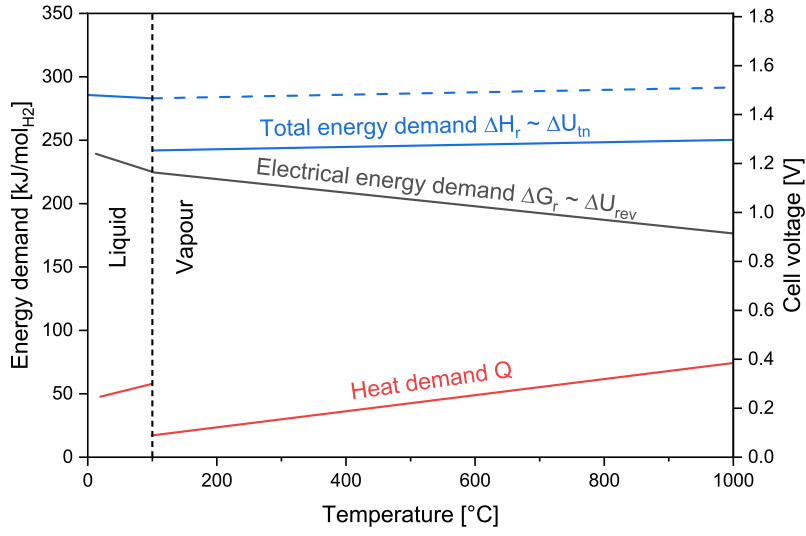


Figure 2.4: Total energy demand ΔH_r of an ideal electrolysis process as a function of temperature, along with the thermal and electrical energy demand (Q and ΔG_r). Adapted from [90].

If an electrolysis cell without any heat integration is considered, the minimum cell voltage is given by the thermoneutral cell voltage U_{tn} :

$$U_{tn} = \frac{\Delta H_r}{zF} \quad (2.5)$$

Under such conditions, the overall energy demand of the cell, including the heat, is supplied by electricity.

This has clear implications on the overall energy demand of an electrolyser cell: The thermoneutral voltage is around 1.47 – 1.48 V (284 – 286 kJ/mol_{H2}) when liquid water below 100 °C is fed to the system. This value reduces to 1.26 – 1.29 V (243 – 249 kJ/mol_{H2}) when steam is supplied in the temperature range of 100 – 1000 °C [90]. This allows to reduce the minimum electrical energy demand of steam electrolysis compared to liquid water electrolysis by the heat of vaporisation (41 kJ/mol at ambient pressure). As shown in Figure 2.4, the overall energy consumption of the cell is almost constant in the whole temperature range. By the application of high temperature electrolysis it is therefore possible to replace a part of the electrical energy provided to the cell by less valuable high-temperature heat [90, 91].

High temperature electrolyzers are operated at the thermoneutral voltage and isothermal conditions. Under such conditions, heat produced by internal irreversibilities is compensated by the endothermic electrolysis reaction. This operation mode is not possible for low temperature electrolyzers. These are operated above the thermoneutral voltage, as high internal

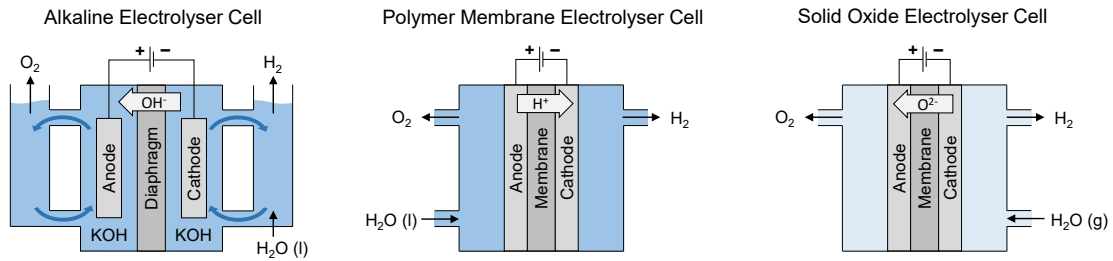


Figure 2.5: Schematic representation of the cells of the three electrolysis technologies. AEL and PEM are operated with liquid water, the SOE operates with steam. Figure adapted from [92].

losses and overvoltages cannot be compensated. It is therefore required to provide external cooling to such units to prevent overheating [90].

Figure 2.5 depicts a schematic design of the three electrolyser cells with an indication of the ions passing through the separator. Key characteristics of the technologies are summarised in Table 2.2.

2.5.1 Alkaline water electrolysis

Alkaline electrolysis is well established and has been industrially applied for several decades [89]. AEL are reliable, safe and reach lifetimes up to 15 years [89]. Therefore, they are the most widespread electrolyser technology in industry and stack sizes exist in MW-range [89, 93]. The alkaline electrolyte is a caustic potash solution (20 – 30 % KOH) in which the two electrodes are submerged [93]. These are separated with a diaphragm, which separates the product gases and is permeable for hydroxide ions and water molecules [93].

The major draw-backs of AEL technology are a low part load range, limited current density, and therefore limited specific hydrogen production due to the high ohmic losses across the liquid electrolyte and the diaphragm [93]. Furthermore, the operation pressure is limited to low levels, which negatively impacts system size and hydrogen production cost [92, 93]. Also, cross-diffusion of product gases and diffusion of oxygen into the cathode chamber decrease the system's efficiency [93].

2.5.2 Polymer electrolyte membrane electrolysis

This type of electrolyzers make use of a solid polymer electrolyte membrane, which was first introduced by General Electric in the 1960s to overcome the draw-backs of the AEL technology [92, 93]. Although less mature than AEL, industrial suppliers for PEM systems are available [94]. The polymer membrane has high proton conductivity, but prevents gas crossover, which enables high operation pressures [93]. Membrane thicknesses are in a range

of approximately 20 – 300 μm , which enable high current densities resulting in compact system designs [93]. A further important economic aspect is the capability of the PEM electrolyser to work under a wide load range. This is due to the proton transfer through the membrane quickly reacting to changes in the input power. In comparison to PEM technology, in alkaline electrolyzers the response time is limited, due to the high inertia of the liquid electrolyte [93]. In these systems, the minimal part load is limited due to the higher hydrogen permeability of the diaphragm. When AELs are operated at reduced load, the formation of H_2 and O_2 is reduced accordingly, while the permeation of H_2 through the diaphragm remains constant. This causes potentially high concentrations of H_2 in the anode cell and prevents AELs from being operated at very low loads [93].

Due to the compact design of the PEM cell and the structural properties of the solid electrolyte membrane high differential pressures are possible between the anode and cathode side. This allows producing compressed hydrogen directly from stack, without needing further mechanical compression in the downstream part of the plant. Prototypes with stack pressures up to 350 bar were reported [95, 96]. However, commercially available units operate in the range of 20 – 50 bar [90].

2.5.3 Solid oxide electrolyser cell

The SOE represents the least mature among the three discussed technologies. It makes use of a solid oxide as an electrolyte, which allows the passage of O^{2-} ions at high temperatures. Often, yttria-stabilized zirconia is applied as ion-conducting ceramic [97]. This material enables the operation at high temperatures with the advantage of increased electrical efficiency. This high operation temperature on the other hand causes a high thermal stress on the components, especially during start-up and shut down procedures. This is also one of the key challenges to solve in further development, as significant material degradation is occurring, which limits the lifetime of the stack [93, 97]. Another interesting application of the SOE cells is their ability to reverse their operation to fuel cell operation [17, 90]. Furthermore, systems are investigated, which allow co-electrolysis of CO_2 producing syngas for the production of synthetic hydrocarbons [90]. However, the industrial application of SOE stacks is still very limited, as only a single commercial supplier for SOE system is reported by Buttler *et al.* [90].

Due to the high temperatures and therefore reduced mechanical stability pressurising a SOE system is challenging. In the HELMETH project [91, 98], this problem was solved by enclosing the whole electrolyser stack in a pressure-resistant vessel, where it was operated up to 15 bar.

		AEL	PEM	SOE
Operation parameters				
Cell temperature	°C	60 – 90	50 – 80	700 – 900
Typical pressure	bar	10 – 30	20 – 50	1 – 15
Current density	A/cm ²	0.25 – 0.45	1.0 – 2.0	0.3 – 1.0
Flexibility				
Load flexibility ^a	%	20 – 100	0 – 100	±100 ^b
Cold start-up time		1 – 2 h	5 – 10 min	hours
Warm start-up time		1 – 5 min	10 s	15 min
Efficiency				
Nominal stack efficiency (LHV)		63 – 71 %	60 – 68 %	100 % ^c
... specific energy consumption	kWh/m ³	4.2 – 4.8	4.4 – 5.0	3
Nominal system efficiency (LHV)		51 – 60 %	46 – 60 %	76 – 81 %
... specific energy consumption	kWh/m ³	5.0 – 5.9	5.0 – 6.5	3.7 – 3.9
Available capacity				
Max. nominal power per stack	MW	6	2	<0.01 ^d
H ₂ production per stack	m ³ /h	1400	400	<10 ^d
Cell area	m ²	<3.6	<0.13	<0.06 ^d
Durability				
Life time	kh	55 – 120	60 – 100	(8 – 20) ^d
Efficiency degradation	%/a	0.25 – 1.5	0.5 – 2.5	3 – 50
Economic parameter				
Investment cost	€/kW _{el}	800 – 1500	1400 – 2100	(>2000) ^d

^a Of nominal load

^b Fuel cell operation possible

^c At thermoneutral voltage U_{tn}

^d Uncertainty due to pre-commercial technology

Table 2.2: Key parameters of water electrolysis technologies according to Buttler *et al.* [90].
Table adapted from [90].

3 Techno-economic comparison of biological and fluidised bed methanation

3.1 Introduction

The integration of biomass in the future energy system bears a large potential for the decarbonisation of society. Switzerland's gas providers agreed on increasing the share of renewable gas in the distribution grid to 30 % of the residential heating consumption by 2030 [99]. The largest potential in unused domestic bio-resources is associated with biogas from digestion processes [27]. In order to make use of this potential, biogas upgrading and utilisation processes on a relatively small scale are necessary. Methanation of such biogenic gases also enables a flexible way of integration and seasonal storage of renewable electricity in the future energy system. The Power-to-Gas technology can provide a large, yet unused potential for such chemical energy storage [56, 100]. The technology allows the coupling between different energy sectors (*i.e.* electricity, gas, heat) and has also a large potential in reducing the carbon footprint of the existing gas grid [20]. The underlying methanation reaction is currently being tested in a variety of lab-scale and demonstration-scale projects [101]. The technologies investigated involve mostly fixed-bed and biological methanation concepts [101].

In previous work, Witte *et al.* [102] compared the cost structure of catalytic fixed bed and catalytic bubbling fluidised bed (BFB) methanation. It could be shown, that also fluidised bed methanation and subsequent membrane upgrading can provide a cost-efficient way to produce biomethane [102]. The maturity of the technology could be demonstrated by stable operation for more than 1000 h with subsequent grid injection [81], but no demonstration project is in operation yet.

While biogas proved to be a cost-efficient carbon source for direct methanation of biogas, any other CO₂ source can be used [42, 103]. Direct air capture and similar technologies to

Chapter 3 is based on the post-print version of the publication: A. Gantenbein, O. Kröcher, S. M. A. Biollaz, T. J. Schildhauer, "Techno-Economic Evaluation of Biological and Fluidised-Bed Based Methanation Process Chains for Grid-Ready Biomethane Production", *Frontiers in Energy Research*, vol. 9, Mar. 2022. DOI: 10.3389/fenrg.2021.775259

A. G. performed all process simulations and economic analyses, created all diagrams and wrote the text.

obtain CO₂ are associated with high cost. However, also waste streams of almost pure CO₂ are available and can be used for methanation. These include for example the off-gas streams of conventional biogas upgrading units. The Store&Go demonstration plants make use of different technologies, such as direct air capture, waste-CO₂ from a waste water treatment plants, as well as a CO₂ stream from a bioethanol plant [104]. The carbon source, as well as the source of electricity for the electrolysis highly influence the profitability of the overall process, as a higher selling price for biomethane can be achieved by renewable sources [105].

Due to the high share in operation cost, the efficiency of the electrolyser technology has a large influence on the overall production cost of the biomethane [102]. Alkaline electrolysis (AEL) is the most commonly used technology [106]. Nevertheless, proton exchange membrane (PEM) technology allows for higher current densities and higher operation pressures than conventional alkaline electrolysis. This technology is increasing its industrial maturity and commercial applications are now available on the market. The solid oxide electrolysis cell (SOE) technology is still under development, mainly because stack lifetime issues due to material degradation need to be solved [106]. SOE technology allows an increase of electrolyser efficiency by integration of an external heat source, for example catalytic methanation [91].

This work provides a bottom-up techno-economical evaluation of three different Power-to-Gas (PtG) process chains in two different scales. For each of these processes the size and performance of the main equipment is determined, and its capital and operation costs are evaluated. The study compares the cost structure of the bubble column-based biological methanation and catalytic bubbling fluidised bed methanation. Furthermore, the influence of electrolyser technology and cost is investigated.

3.2 Methods

3.2.1 Process design

The processes evaluated in this work are divided into two scales corresponding to the electrolyser power of two demonstration projects. The first scale corresponds to the 1 MW_{el} BioCat plant in Avedøre (Denmark), based on biological methanation [74]. The second scale refers to the 6 MW_{el} Audi e-gas project in Werlte (Germany), which operates alkaline electrolyzers with cooled, fixed-bed methanation reactors [56]. Furthermore, two methanation technologies are compared, namely bubbling fluidised bed methanation and biological methanation in a stirred bubble column.

As electrolyser technologies, proton exchange membrane, as well as high-temperature electrolysis by solid oxide electrolysis cells are considered. Based on the available electrolysis power and subsequent H₂-feed, a CO₂ feed stream is calculated according to the respective needs of the methanation technology. For the cases including the SOE technology, the hydrogen output

Case	Electrolysis power	Electrolyser technology	Methanation technology
B1	1 MW	PEM	Biological
B6	6 MW	PEM	Biological
C1 /C1bg	1 MW	PEM	Catalytic BFB
C6 /C6bg	6 MW	PEM	Catalytic BFB
C1S /C1Sbg	1 MW _{eq}	SOE	Catalytic BFB
C6S /C6Sbg	6 MW _{eq}	SOE	Catalytic BFB

Table 3.1: Process options considered for the techno-economic analysis.

of the electrolyser is kept the same as in the PEM-cases. Therefore, plant costs are comparable to the PEM-BFB case.

An overview on the considered cases is given in Table 3.1.

The combination of biological methanation with solid oxide electrolysis is not considered in this work since the temperature level of excess heat from biological methanation is too low for integration with high temperature electrolysis. Such a process would either require the addition of an external high temperature heat source or result in a decreased electrical efficiency of the SOE.

The two catalytic processes were furthermore evaluated for the case of direct methanation of biogas. In this case, the electrolyser power is fixed to the respective CO₂-case and a biogas-feed containing the necessary CO₂ is provided to the process. The raw biogas is assumed to have a methane content of 60 vol.-%. The cases with biogas as feed are marked with “bg.”

Cases B1 and B6: Biological methanation with PEM electrolysis (PEM-Bio)

The process in cases B1 and B6 consist of a biological methanation unit fed by a PEM electrolyser in the 1 MW and 6 MW-scale, as shown in Figure 3.1. A purified CO₂ feed stream is compressed to the operation pressure of the reactor and mixed with hydrogen from the electrolyser. The CO₂ feed stream to the plant and the water feed stream to the electrolyser are chosen according to the electrolyser power and the H₂/CO₂-ratio required in the feed of the reactor. The water feed stream is compressed to the operation pressure of the PEM-electrolyser, which is 30 bar. The valorisation of oxygen produced by the electrolyser is optional, but not part of this work.

The feed gas mixture is then pre-heated to the reactor inlet temperature, which is 60 °C in the case of biological methanation. As this temperature level is low and temperature differences of the feed gases relatively small compared to the required temperature, no heat exchanger equipment is considered in the upstream part of the plant. Furthermore, the feed gas is injected into a large volume of liquid, which allows for fast adjustment of the temperature.

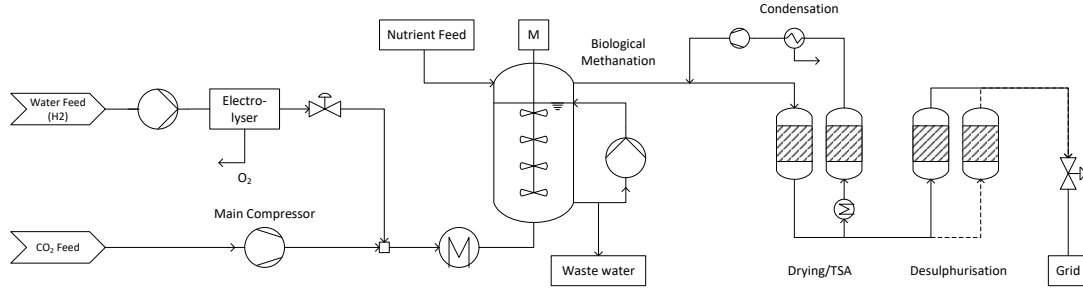


Figure 3.1: Process chain for the biological methanation of CO₂.

Parameter		B1	B6
Electrolyser power	P_{el} [MW _{el}]	1.0	6.0
Reactor volume	V_{re} [m ³]	8	115
Reactor diameter	d_{re} [m]	1.0	2.4
Reactor height	h [m]	10	24.5
Impeller diameter	d_{im} [m]	0.5	1.2
Stirring power	$P_{stirrer}$ [kW]	11	56
Product gas flow (methane)	$\dot{V}_{CH_4,Prod.}$ [m ³ /h]	54	324
Heat production	Q [MW]	0.16	0.97

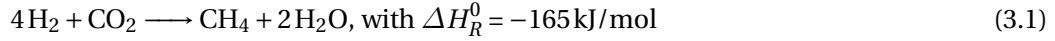
Table 3.2: Data used to estimate the performance of the biological methanation system according to Inkeri *et al.* [75]. The methane production rate was corrected according to equations 3.2 and 3.3 .

The biological methanation reactor is a tall continuously stirred tank reactor (CSTR) unit with multiple stirrer stages. The design of the sizing of the unit is given by the data in the work of Inkeri *et al.* [75], summarised in Table 3.2. The rate-based model developed in this study was validated by comparison of model predictions with literature data. The biological methanation kinetics itself are based on the growth of the archaeon *Methanobacter thermoautotrophicum* obtained from the work of Schill *et al.* [68]. The upscaled reactor system operates at a temperature of 60 to 65 °C.

The reactor geometry is fixed for both scales to 1:2:20 for the stirrer diameter (d_{im}), reactor diameter (d_{re}) and reactor height (h). The stirrer furthermore consists of 10 impeller stages along the height. The study of Inkeri *et al.* [75] furthermore provides data for the reactor volume (V_{re}), the power required for stirring ($P_{stirrer}$), the methane product gas flow rate ($\dot{V}_{CH_4,Prod.}$) and the heat production of the reactor system (Q).

In biological methanation, the reaction is catalysed by one or multiple strains of microorganisms. In addition to the suitable temperature and pressure conditions, those organisms also have to be provided with nutrients in order to foster their growth. Therefore, these nutrients are provided as solution to the reactor. To avoid the accumulation of potentially toxic metabolites in the liquid phase, a part of the slurry has to be discarded as wastewater. This

wastewater stream furthermore contains the water produced by the methanation reaction according to equation 3.1. To ensure a proper distribution of nutrients and microorganisms along the reactor height, a part of the slurry is pumped from the bottom of the reactor to the top. Inkeri *et al.* [75] provides a liquid feed rate D_L of 0.05 h^{-1} and a recycle ratio of 0.75, which allows the calculation of the required nutrient feed.



The wastewater flow also contains a small amount of dissolved gases. In order to avoid insufficient CO_2 supply at the top of the reactor, 1 % excess CO_2 is fed to the system [75]. For the calculations, a H_2/CO_2 ratio of 3.96 is chosen. The methane production rates published by Inkeri *et al.* [75] are slightly above the stoichiometric possible values. They were corrected for this work by equations 3.2 and 3.3, and listed in Table 3.2. We assumed that the CO_2 is fully dissolved in the liquid phase and the raw biomethane leaving the reactor only contains CH_4 and unreacted H_2 . This assumption can be confirmed by measurements at the Solothurn pilot plant [107].

$$\dot{n}_{\text{H}_2} = \frac{P_{el} \cdot \eta_{PEM,LHV}}{LHV_{\text{H}_2} \cdot MW_{\text{H}_2}} \quad (3.2)$$

$$\dot{n}_{\text{CH}_4, \text{biomethane}} = \dot{n}_{\text{H}_2} \left(\frac{1 - x_{\text{CH}_4, \text{biomethane}}}{x_{\text{CH}_4, \text{biomethane}}} + 4 \right)^{-1} \quad (3.3)$$

The hydrogen production rate \dot{n}_{H_2} is calculated from the nominal power of the electrolyser P_{el} and its efficiency $\eta_{PEM,LHV}$. The efficiency is given by 65 %, based on the lower heating value (LHV), a value applying for alkaline as well as PEM technology [75, 94, 103].

The product gas stream contains around 98 % CH_4 and fulfils grid injection limitations. Nevertheless, it is saturated with water and contaminated with volatile metabolites from the biological process. Therefore, a temperature swing adsorption (TSA) process for drying and a sorption step for desulphurization is considered. The TSA consists of two vessels operated alternately, one in the main product gas stream in adsorption mode and the other in regeneration mode. The adsorption process occurs at ambient temperature, whereas for desorption the vessel is electrically heated to 200°C and flushed with a part of the dried product gas stream. This water-saturated stream is then fed to a condenser and recompressed to be fed to the main stream again. This procedure allows to regenerate the sorbent without losing product gas or contaminating the product gas with other components, such as air or nitrogen. In the TSA, silica gel is used as a sorbent.

The desulphurisation step consists also of two vessels, which are filled with a specialised activated carbon-based sorbent for biogas polishing described in a later section. The first

vessel is in operation mode and fed with the main gas stream whereas the second one serves as back up in case of maintenance or sorbent replacement.

The now cleaned and dried biomethane can be expanded to the required grid pressure and injected to the gas distribution network.

Cases C1 and C6: Bubbling fluidised bed methanation with PEM electrolysis (PEM-BFB)

The process consisting of the bubbling fluidised bed methanation is designed as shown in the process flow diagram in Figure 3.2. It consists of the same upstream equipment as the process in PEM-bio case and is based on a previous study by Witte *et al.* [103] on direct methanation of biogas. Again, cleaned CO_2 and water for electrolysis are fed to the plant and compressed to the operation pressures of the electrolyser and reactor. Hydrogen is mixed to the main CO_2 stream. This feed gas has to be preheated to the minimal feed temperature of the reactor, which is set to a 280°C . This temperature is the minimum useful operation temperature of the nickel-based catalyst. The catalyst has to be protected from contamination with sulphur compounds and subsequent deactivation [81]. Since biogenic CO_2 still contains a small amount of such contaminants a gas polishing step is introduced in the CO_2 feed stream [37].

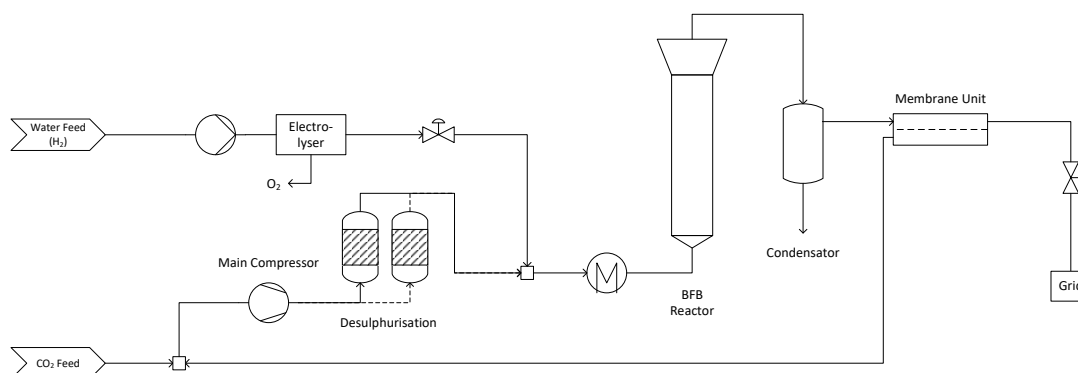


Figure 3.2: Process chain for bubbling fluidised bed methanation of CO_2 using a PEM electrolyser as hydrogen source.

In order to avoid coking and subsequent deactivation of the catalyst, an over-stoichiometric ratio of H_2/CO_2 of 4.01 is fed to the reactor. The product gas of the reactor is led to a heat exchanger and a condenser, which allow the valorisation of the off gas heat and removal of product water. The heat removed in these units is used to pre-heat the feed streams of CO_2 and H_2 .

The heterogeneous methanation reaction is limited by the thermodynamic equilibrium, which results in hydrogen concentrations of more than 2 vol.-% in the dry product gas. In order to fulfil grid injection limitations, excess H_2 has to be removed to allow the use of the biomethane in CNG cars whose tanks are certified for 2 % H_2 fraction at maximum. As previous work

showed, membrane separation can be a cost efficient way to do so [102]. We implemented a counter-current hollow fibre membrane upgrading system to obtain full grid compliance. The resulting H_2 -rich recycle stream, which also contains CH_4 and CO_2 , is fed to the CO_2 feed stream before the main compressor. This recycle stream directly influences the gas composition in the reactor feed, which demands an adjustment of the CO_2 feed stream in such way that the required H_2/CO_2 is fulfilled.

Cases C1S and C6S: Bubbling fluidised bed methanation with high temperature electrolysis (SOE-BFB)

This case represents a modification of the previous system: the PEM electrolyser is replaced by a high-temperature solid oxide electrolyser system. This allows the comparison of the cost structure, when BFB methanation is combined with an SOE system. Instead of liquid water, steam is used for electrolysis, which allows the provision of heat by an external heat source. The stack itself can be operated at a thermoneutral voltage, where the heat flux from the stack is zero [108]. This allows a very high electrical efficiency of the stack, as a part of the energy for the electrolysis is provided by the thermal energy of the steam [90]. In this study, a stack efficiency η_{stack} of 89 % (LHV) and a steam conversion efficiency η_{sc} of 90 % were assumed [91].

Such SOE systems are under experimental investigation in pilot scale, such as in the Helmeth project [98]. In this project, a hot-box is used to keep the temperature of the stack constant and to allow heat integration between the feed streams and hot product gas streams. Furthermore, this box allows the pressurisation of the sensitive high temperature components and enables an operation pressure up to 15 bar [98]. For this work, a similar design is assumed, where heat exchangers allow the pre-heating of the feed water and superheating of the steam by the product gas streams ($H_2 + H_2O$ and O_2). The heat required for evaporation of the feed water is provided by the off-heat from the methanation reactor.

Instead of scaling this process by the electrical input, the electrolyser was scaled by the same hydrogen output as in the previous cases. This allows a direct comparison of the plant cost structure and indicates the benefits of including a SOE system in the methanation process.

All other process units are designed the same way as in case PEM-BFB.

3.2.2 Main models

Bubbling fluidised bed reactor

This work considers an internally cooled, bubbling fluidised bed reactor with a nickel-based methanation catalyst. The model of this unit is based on a pseudo-homogeneous two-phase approach according to Kopyscinski *et al.* [109], which applies hydrodynamic correlations of

freely bubbling fluidised beds. This model was already modified and used in previous studies by Witte *et al.* [103]. The two-phase approach of the model is shown in Figure 3.3.

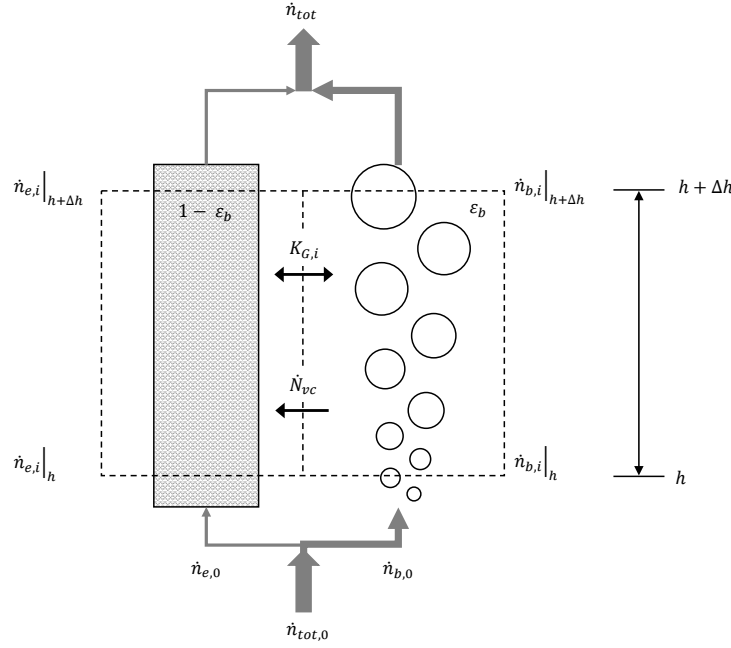


Figure 3.3: Schematic representation of the BFB model used.

The inlet gas stream $\dot{n}_{tot,0}$ is split into a stream going to the bubble phase $\dot{n}_{b,0}$ and a flow in the dense phase $\dot{n}_{e,0}$. The flows are divided according to the volumetric fraction of the bubble phase ϵ_b and the emulsion phase $\epsilon_e = (1 - \epsilon_b)$. The initial fraction of the bubble phase is determined by superficial gas velocities u and bubble diameter d_b . The bubble diameter is determined by a correlation from Hilligardt *et al.* [110]:

$$u_b = \psi (u - u_{mf}) + 7.11 v \sqrt{g d_b} \quad (3.4)$$

$$\epsilon_b = \psi (u - u_{mf}) / u_b \quad (3.5)$$

The two parameters for the bubble rise velocity v and visible bubble flow ψ are dependent on the different Geldart types of particles [111], as well as the reactor height and diameter. The Geldart classification allows a characterisation of the fluidisation regime in a reactor, based on the ratio of the particle size and particle density [111].

The molar balances of the two phases for each component i are as follows:

$$0 = -\frac{d\dot{n}_{b,i}}{dh} - K_{G,i} \cdot a \cdot A_{cross} \cdot (c_{b,i} - c_{e,i}) - \dot{N}_{vc} \cdot x_{b,i} \quad (3.6)$$

$$0 = -\frac{d\dot{n}_{e,i}}{dh} + K_{G,i} \cdot a \cdot A_{cross} \cdot (c_{b,i} - c_{e,i}) + \dot{N}_{vc} \cdot x_{b,i} + (1 - \epsilon_b) (1 - \epsilon_{mf}) \cdot \rho_P \cdot A_{cross} \cdot R_i \quad (3.7)$$

The volume fraction of the dense phase is represented by the factor $(1 - \epsilon_b)$, while $(1 - \epsilon_{mf})$ expresses the volumetric fraction of particles in the emulsion phase at minimal fluidisation conditions. The overall reaction term is defined as:

$$R_i = \sum v_{i,j} \cdot r_j, \quad (3.8)$$

where j represents the methanation and water-gas-shift reactions taking part.

The total bulk flow from the bubble to the dense phase is represented in factor \dot{N}_{vc} , which is the sum of the molar losses due to the reactions and the mass transfer to the dense phase:

$$\dot{N}_{vc} = \frac{\dot{n}_{vc}}{dh} = \sum K_{G,i} \cdot a \cdot A_{cross} \cdot (c_{b,i} - c_{e,i}) + (1 - \epsilon_b) (1 - \epsilon_{mf}) \cdot \rho_P \cdot A_{cross} \cdot \sum_i R_i \quad (3.9)$$

The reaction kinetics implemented in the reactor model are expressed as Langmuir-Hinshelwood-type rate equations. The kinetics of CO₂ methanation are expressed as a water-gas-shift (WGS) reaction coupled with CO methanation as shown in equations 3.10 and 3.11 [103, 109, 112]:

$$r_{WGS} = \frac{k_{WGS} \left(K_\alpha p_{CO} p_{H_2O} - \left(\frac{p_{CO_2} p_{H_2}}{K_{eq,WGS}} \right) \right)}{p_{H_2}^{0.5} \left(1 + K_C p_{CO}^d p_{H_2}^e + K_{OH} p_{H_2O} p_{H_2}^{-0.5} \right)^2} \quad (3.10)$$

$$r_{Meth} = \frac{k_{Meth} K_C p_{CO}^a p_{H_2}^b \left(1 - \left(\frac{p_{CH_4} p_{H_2O}}{K_{eq,Meth} p_{CO} p_{H_2}^3} \right) \right)^c}{\left(1 + K_C p_{CO}^d p_{H_2}^e + K_{OH} p_{H_2O} p_{H_2}^{-0.5} \right)^2} \quad (3.11)$$

The temperature dependence of the rate and adsorption coefficients are based on the Arrhenius and Van't Hoff approach according to equations 3.12 and 3.13:

$$k_i = k_{i,T_{ref}} \exp \left(\frac{E_{A,i}}{RT_{ref}} \left(1 - \frac{T_{ref}}{T} \right) \right), i = WGS, Meth \quad (3.12)$$

Parameter	Value	Unit
$k_{WGS,T_{ref}}$	8.4	-
$k_{meth,T_{ref}}$	1.08	-
$E_{A,WGS}$	155.7	kJ/mol
$E_{A,meth}$	63.1	kJ/mol
$K_{\alpha,ref}$	0.36	bar ⁻²
$K_{C,ref}$	2.53	bar ^{-1.5}
$K_{OH,ref}$	0.67	bar ^{-0.5}
ΔH_{α}	-1.7	kJ/mol
ΔH_C	-50.7	kJ/mol
ΔH_{OH}	-87.5	kJ/mol
a	0.5	-
b	1	-
c	1	-
d	0.5	-
e	0.5	-
T_{ref}	598.15	K

Table 3.3: Kinetic parameters used in the BFB model according to [103, 112].

$$K_j = K_{j,T_{ref}} \exp\left(\frac{\Delta H_j}{RT_{ref}} \left(1 - \frac{T_{ref}}{T}\right)\right), j = \alpha, C, OH... \quad (3.13)$$

The adsorption coefficient of the intermediate carbon species of the rate determining step is given by K_C . K_{OH} refers to the adsorption coefficient of OH and K_{α} is a combined adsorption coefficient of the species CO, H₂, CO₂, and OH [113]. Detailed information can be found in [113]. The values of the kinetic parameters are listed in Table 3.3.

Hydrodynamics in the reactor is the second main influence on the performance. This influence is expressed through bubble size correlations, from which bubble rise velocities and the bubble hold-up ϵ_b can be determined. These values allow the estimation of the total bubble surface area available for inter-phase mass transfer.

A variety of bubble size correlations exist in literature, but they are only valid for conditions with no heat exchanger internals present in the reactor. Therefore, the bubble growth correlation with the smallest overall bubble size d_B by Werther *et al.* [114] was used in the model and it was further modified by a factor of 0.5 in order to account for the internals present in the reactor that significantly inhibit the bubble growth in the reactor [115, 116].

$$d_b = 0.5 \cdot 0.835 \left(1 + 0.272 (u - u_{mf})\right)^{1/3} (1 + 0.0684 \cdot h)^{1.21} \quad (3.14)$$

As shown in equation 3.14, the bubble diameter d_b is dependent on the gas velocity u in the reactor and the gas velocity required for minimal fluidisation of the bed u_{mf} .

The reactor model is based on the following assumptions:

- Steady-state conditions and ideal gas behaviour
- No reaction in the bubble phase
- Laminar boundary layers around the catalyst particles and influence of pore diffusion are neglected. Therefore, the gas concentration in and on the particles equals the dense phase concentrations.
- Radial gas concentration gradients are neglected

Catalyst deactivation is not considered in the model. The economic analysis includes an annual replacement of the full catalyst load in order to compensate for minor deactivation effects. Field experiments showed that a stable operation of fluidised bed methanation in biogas is possible for more than 1000 h [37, 81]. In order to account for deactivation effects and the additional reactor height needed for particle settling, the reactor height and catalyst mass was multiplied by a design factor of 1.5 prior to cost calculations.

Biological methanation reactor

Data published by Inkeri *et al.* [75] was used to estimate the process performance in the work presented here. The study chose the scale of well-known demonstration projects for methanation, namely the Danish BioCat project [74], the Audi e-gas project [80] in Germany, as well as a large electrolysis plant in Finland, which is not considered in this work. The BioCat project consists of a biological methanation reactor, which is fed by a 1 MW_{el} electrolysis unit. The Audi e-gas project is a pilot plant consisting of a fixed bed methanation reactor in the 3 MW_{CH₄}-scale [80].

The work of Inkeri *et al.* [75] estimates the gas-liquid mass transfer by a lumped mass transfer coefficient, taking into account the reactor height, stirring energy and stirrer geometry. Furthermore, the influence of physical properties of gas and liquid phase components on the bubble size and subsequently the gas-liquid mass transfer are approximated. This approach, based on simplified fundamental equations describing physical phenomena allows a scale-up of the reactor model.

Inkeri *et al.* [75] verified the scale-up of their model using estimated dimensions of the plant in Avedøre (Denmark). In the meantime another pilot plant by the same technology was operated in Solothurn (Switzerland) as part of the Store&Go-project [117]. This plant was designed for a hydrogen input corresponding to a 700 kW_{el} electrolysis unit, which required a vessel volume of around 7 m³. Furthermore, a second biological methanation plant of 2.5 MW_{el} is currently

under construction in Switzerland. This plant uses the technology of microbEnergy [71], which is also based on a stirred bubble column, but makes use of strains of microorganisms already present in the waste water treatment plant. Limited technical information is accessible, but based on the available illustrations, we estimate the reactor size to around 45 m³ [79]. These values indicate that the dimensions given by Inkeri *et al.* [75] are in a valid range for such systems.

Biological systems, where substantial gas formation occurs in the liquid phase, tend to form large amounts of foam. This foam formation has to be minimised, as it can cause severe problems in the downstream part of the plant. Usually, anti-foaming agents are added to the slurry and technical equipment for de-foaming is used [104]. These measures are beyond the scope of this work, nevertheless, we assumed an additional 2 m of reactor height for foam protection.

The data used is summarised in Table 3.2.

Hollow fibre gas separation membrane

For the gas separation unit required for the removal of excess hydrogen after BFB methanation, a rate-based model from literature was implemented. Makaruk *et al.* [118] published an algorithm simulating a counter-current hollow fibre membrane. This algorithm is based on an iterative finite difference Gauß-Seidel method. The discretisation into c discrete points is done along the length of the membrane as shown in Figure 3.4.

The trans-membrane flow is expressed along the membrane length l by:

$$\frac{d\dot{n}_p}{dl} = \dot{n}_{trans} = P_i (x_i p_F - y_i p_P) A_L \quad (3.15)$$

Where P_i refers to the permeance of the respective membrane material, the driving force of the separation is expressed as the partial pressure difference ($x_i p_F - y_i p_P$) and A_L refers to the available separation area per length.

The flow gradients are approximated by a first order upwind finite difference scheme. This allows the calculation of the molar flow of each component i on the retentate and permeate side of the membrane at a specific point j along the one-dimensional grid. The boundary conditions are defined at the points with index $j = 1$.

$$\dot{n}_{f,i,j}^{k+(1/2)} = \dot{n}_{f,i,j-1}^k - P_{i,j} (x_{i,j}^k p_F^k - y_{i,c-j+2}^k p_P^k) A_L \Delta L \quad (3.16)$$

$$\dot{n}_{p,i,j}^{k+(1/2)} = \dot{n}_{p,i,j-1}^k + P_{i,j} (x_{i,c-j+2}^k p_F^k - y_{i,j}^k p_P^k) A_L \Delta L \quad (3.17)$$

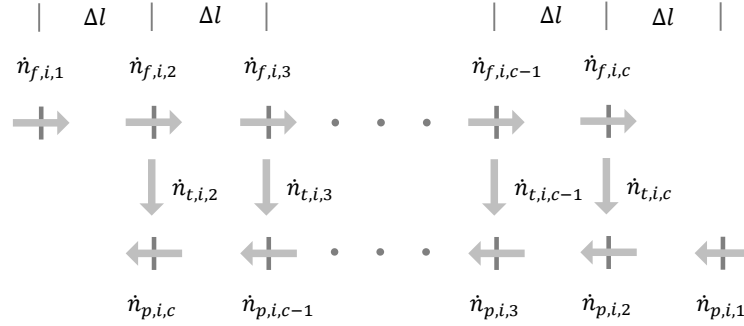


Figure 3.4: Discretisation scheme for the counter-current membrane model along the length of the module. Adapted from [118].

The iteration variable k denotes the state of the variables before the iteration and $k + (1/2)$ the half-step variables. The full iteration step at $k + 1$ is extrapolated by:

$$\dot{n}_{f,i,j}^{k+1} = \dot{n}_{f,i,j}^k - \omega \left(\dot{n}_{f,i,j}^{k+(1/2)} + \dot{n}_{f,i,j}^k \right) \quad (3.18)$$

$$\dot{n}_{p,i,j}^{k+1} = \dot{n}_{p,i,j}^k - \omega \left(\dot{n}_{p,i,j}^{k+(1/2)} + \dot{n}_{p,i,j}^k \right) \quad (3.19)$$

The initiation of the iteration requires an initial guess for the concentration profiles on the retentate and permeate side.

The counter-current membrane model is based on the following assumptions:

- Ideal gas behaviour
- Axial dispersion is neglected
- Pressure drop on bore and shell side is neglected
- The influence of the gas composition on the permeability is neglected. Therefore, the permeability parameter is set constant.

In this work, a constant value for membrane permeance is introduced, based on the commercial polymer type *Matrimid*. Permeability data for the relevant species were taken from work of Zhang *et al.* [119]. Since there was no permeability determined for water, we assumed it to be equal to the permeability of hydrogen. This is justified by other commercial biogas upgrading membranes, which indicate a higher permeability for water than for hydrogen [51]. In order to obtain the permeance parameter, the permeability has to be divided by the effective thickness of the separation layer. The actual separation layer is only a fraction of the wall thickness of

the membrane fibre and has to be estimated for this case. These thicknesses range from 500 to even less than 100 nm [48]. In this work, we assumed the effective thickness to be 100 nm.

Auxiliary units

For all auxiliary process units short-cut models are used, which are based on correlations [103].

For the PEM electrolyzers, a specific electricity consumption of 4.6 kWh/m³ (H₂, NTP) is considered, which is an average value for PEM and alkaline technology [90]. This value corresponds to an efficiency of 65 % (LHV). The data used to calculate the stack performance of SOE is given in Table 3.4.

The TSA unit is based on a zeolite sorbent with a maximum capacity of 0.15 kg_{H₂O}/kg_{sorbent}. A cycle time of 8 h and a regeneration temperature of 200 °C is assumed.

For the desulphurisation after the biological methanation and in the feed of the BFB methanation, we assume an inlet concentration of 50 ppm H₂S. Vessel size calculations are based on a conservative maximum load of 7 wt.-% H₂S on the sorbent. Further data is based on the commercially available sorbent Sulfatrap R7 [37].

Pumps and compressors are based on thermodynamic correlations, with an electrical efficiency of 0.8.

The heat exchanger equipment was sized based on heat transfer coefficients available as correlations for different systems [120]. The exchangers are assumed to be shell and tube systems in counter-current operation.

All units, including the membrane model are implemented in a process simulation environment based on Matlab (Matlab 2021a). The BFB reactor model is built in the software product Athena Visual Studio (V14.2).

All volumetric flow rates reported in this work refer to standard conditions at 1 atm and 0 °C according to DIN 1343 [121].

3.2.3 Cost calculations

The comparison of the cost structure of the three processes is performed by determining the operational cost (OPEX) and capital cost. Based on the technical performance and size of the units, cost functions for the units are applied, which were obtained from Ulrich and Vasudevan [120] and already part of previous work [102]. These functions have the following structure:

$$C_{BM} = C_P \cdot F_{BM}, \text{ with } F_{BM} = f(F_M, F_p) \quad (3.20)$$

		C1	C1S	C6	C6S	C1bg	C1Sbg	C6bg	C6Sbg
Reaction conditions									
T_{react}	°C	360	360	360	360	360	360	360	360
$T_{r,feed}$	°C	280	280	280	280	280	280	280	280
p_{react}	bara	10	10	10	10	10	10	10	10
$d_{HEX-tubes}$	m	0.02	0.02	0.02	0.02	0.02	0.02	0.02	0.02
r_{H_2/CO_2}^a	mol/mol	4.01	4.01	4.01	4.01	4.01	4.01	4.01	4.01
T_{cond}	°C	30	30	30	30	30	30	30	30
Number of membrane modules (counter-current, 4 inch)									
N_{mod}	-	2	2	11	11	4	4	22	22
Electrolysis									
T_{soec}	°C		800		800		800		800
$\eta_{el,stack}$ (LHV)	-	0.65	0.89	0.65	0.89	0.65	0.89	0.65	0.89
η_{sc}^b	-		0.9		0.9		0.9		0.9
$p_{electrolysis}$	bara	30	15	30	15	30	15	30	15

^a at reactor feed

^b steam conversion efficiency, fraction of steam converted by the electrolyser

Table 3.4: Input parameters for the bubbling fluidised bed-based processes for CO₂ methanation.

The bare module cost C_{BM} consists of the purchased equipment cost C_P , which is multiplied by a bare module factor F_{BM} . This factor is a function of the material factor F_M and the pressure factor F_p , which are given in literature and consider the cost increase by the use of special materials and elevated pressures. The accuracy of such cost evaluations is within the range of $\pm 20\%$ [120].

In order to obtain the investment cost $C_{inv,k}$ for a unit k , the cost for piping, instrumentation and further surrounding equipment have to be considered. Such costs are approximated by a factor of the bare module cost, as shown in equation 3.21. The plant cost factors F_{PC} considered in this work are summarised in Table 3.5 [102, 122].

Plant cost factor F_{PC}	Value
Piping	0.4
Instrumentation	0.1
Electricals	0.2
Buildings and foundations	0.13
Engineering and approval	0.3

Table 3.5: Plant cost factors F_{PC} applied to calculate the installation cost of the equipment [102, 122].

$$C_{inv,k} = C_{BM,k} \left(1 + \sum F_{PC}\right) \cdot F_{CEPCI} \quad (3.21)$$

The investment cost also include a factor F_{CEPCI} , which quantifies the cost increase of equipment [120] according to equation 3.21. It consists of the Chemical Engineering plant cost index (CEPCI, I_{2019}), listed in Table 3.6. The reference value $I_{ref(2004)}$ was 400 in 2004 [120].

$$F_{CEPCI} = \frac{I_{2019}}{I_{ref(2004)}} \quad (3.22)$$

The annualised capital expenses (CAPEX, C_{CAPEX}) are calculated, based on the annual interest rate i and the plant lifetime a , both shown in Table 3.6:

$$C_{CAPEX} = C_{inv,tot} \frac{(1+i)^a \cdot i}{(1+i)^a - 1} \quad (3.23)$$

The cost for the nutrient solution for biological methanation was estimated based on a total nutrient concentration of 2 g L^{-1} of slurry [59, 65]. In case of an artificial nutrient solution fed to the reactor, this growth medium has to be mixed from a variety of chemicals at an estimated cost of around 20 €/kg. We therefore estimate the cost for growth media provision to around 40 €/m³. Alternatively, the reactor can also be supplied with digester efflux, which provides all necessary nutrients [69]. Nevertheless, also the integration of such a waste stream and its conditioning is associated with certain costs, which may be in a similar range as shown above.

For the membrane unit, a module geometry of 1 m length and 4 inch diameter is considered. A commercial 2 inch version of such a module was tested in the next chapter for its capability for hydrogen recycle in Power-to-Gas applications. The separation area of the module was estimated to be around 65.12 m², which corresponds to a fourfold area of the 2-inch membrane module [52]. The module consists of a cartridge fixed into a tubular, pressure-resistant case, which itself provides all the connections to the plant. The cartridge contains the hollow fibres and is sealed with a resin. Due to ageing effects, the cartridges have to be replaced after a certain time interval. The replacement cost were obtained from Ulrich and Vasudevan [120], which indicate 50 \$/m² in 2004. As the cartridges also maintain pressure and require specialised sealing, we assumed a twice as high cost for the membrane material. Considering the CEPCI, this cost is 126 €/m², which is in a similar range as a quote obtained by a supplier. This cost refers to the replacement cost of the membrane cartridge, which does not include further installations. We consider this replacement cost as operational expenses, analogously to sorbent and catalyst replacement cost. For the initial installation cost of the membrane modules, we consider the same amount, but include also the plant cost factors.

Cost factor	Value	Unit	Source
Electricity	0.05	€/kWh _{el}	[123]
Heat revenues @ 280 °C	0.04	€/kWh	[102]
Heat revenues @ 165 °C	0.04	€/kWh	[102]
Heat revenues @ 60 °C	0.0	€/kWh	
Biomethane revenue	0.11	€/kWh	[102, 105]
Raw biogas cost	0.06	€/kWh	[102]
Fresh water	0.1	€/m ³	Own estimate
Desalinated process water	0.25	€/m ³	Own estimate
Waste water treatment	1	€/m ³	Own estimate
Nutrient solution	40	€/m ³	Own estimate
Membrane cost	63.3	€/m ²	[120]
Membrane replacement interval	2	years	Own estimate
Electrolysis cost (PEM)	930	€/kW _{el}	[94]
Electrolysis cost (SOEC)	2800	€/kW _{el}	[92]
BFB Catalyst cost	90	€/kg	[102]
Sorbent cost (desulphurisation)	8.96	€/kg	Supplier's quote
Sorbent cost (TSA)	5	€/kg	Own estimate
Operation hours	8322	h/y	(95 % availability)
Interest rate	5 %		[120]
Plant lifetime	15	years	[120]
CEPCI (2019)	607.5	-	[124]

Table 3.6: Cost assumptions for the base case scenario.

For the two methanation reactor types, a detailed cost analysis was performed, based on the reactor vessel itself, as well as the auxiliary units required for operation and heat utilisation. For the fluidised bed system, this includes the cooling cycle, the internal heat transfer tubes and a vessel for catalyst activation as already used by Witte *et al.* [102]. The biological system also includes an external cooling system, internal cooling coils, which also serve as baffles, as well as the multi-stage stirring system.

3.3 Results and discussion

All process options evaluated produce biomethane, which is ready for grid injection at a level of 10 bar (absolute). The input parameters were taken from the publication of Inkeri *et al.* [75] in the case of biological methanation, or based on previous work of Witte *et al.* [102, 103] for BFB methanation. Compared to the earlier studies, the input parameters for the BFB cases were slightly modified to result in a process, which is comparable to the biological one. These were namely the BFB reactor temperature (360 °C) and the system pressure (10 bar). Nevertheless they are in a comparable range to the optimal conditions reported by Witte *et al.* A summary of the input parameters for the process simulations can be found in Table 3.4. The

values obtained from the process simulation are given in Tables 3.8 and 3.7. Based on these parameters, further cost analysis was performed.

Parameter		B1	B6
TSA			
Vessel diameter	m	0.42	0.77
Vessel height	m	1.27	2.31
Sorbent mass (total)	kg	144	861
Bioreactor			
Nutrient feed	m ³ /h	0.10	1.44
Waste water	m ³ /h	0.30	4.31

Table 3.7: Additional technical data for the biological methanation processes

For each process, investment cost, operation cost and revenues from gas and heat sales are determined. The costs are grouped according to system compartments. The H₂-path contains the electrolyser and required water feed. In the main reactor section, the main vessel is considered as well as all units and heat exchanger equipment, which are required to remove the reaction heat. In the case of biological methanation, this also includes the stirrer. Membrane upgrading is required to ensure grid injection compliance and is only needed in the case of BFB methanation. The membrane upgrading also removes water, which replaces TSA drying in the BFB cases. As supporting modules, the units required for grid injection are considered, *i.e.* process analytics and gas odorisation. These units are assumed to be independent of methanation technology and scale. The cost for external heat exchanger equipment considers the equipment required for heat integration between feed gas and product gas (condenser). In the case of high temperature electrolysis, this also includes the heat exchangers required to recover the off-heat of the SOE stack and pre-heat feed steam. For the biogas cases, a water evaporator is considered to add steam to the feed gas. This steam is required to reduce catalyst stress due to the high methane content.

The efficiency of the processes was calculated based the molar product gas flows, considering the newly formed methane ($\dot{n}_{Prod.,CH_4}$) and the unreacted hydrogen ($\dot{n}_{Prod.,H_2}$, $x_{H_2} < 2\%$), using the higher heating value (HHV). The electrical input energy is given by the nominal power of the electrolyser P_{el} according to equation 3.24:

$$\eta_{HHV} = \frac{\dot{n}_{Prod.,CH_4} \cdot HHV_{CH_4} + \dot{n}_{Prod.,H_2} \cdot HHV_{H_2}}{P_{el}} \quad (3.24)$$

Technical parameters		B1	B6	C1	C6	C1S	C6S	C1bg	C6bg	C1Sbg	C6Sbg
Raw gas feed flow	m ³ /h	54.77	328.59	54.47	326.88	54.47	326.91	136.67	820.31	136.67	820.31
Feed compressor	kW	3.96	23.76	5.11	30.30	5.12	30.38	11.88	70.80	11.88	70.80
Evaporator area	m ²	n/a	n/a	n/a	n/a	n/a	n/a	2.3	13.81	2.3	13.81
H ₂ /CO ₂ (plant feed)	mol/mol	3.96	3.96	3.98	3.98	3.98	3.98	3.97	3.97	3.97	3.97
Electrolysis (power)	kW	1000	6000	1000	6000	737	4423	1000	6000	737	4423
Reactor											
Diameter	m	1	2.4	0.38	0.83	0.42	0.83	0.48	0.96	0.48	0.96
Height	m	12	26.5	1.77	2.28	1.50	2.26	1.16	1.74	1.16	1.74
Cat. mass	kg	n/a	n/a	71	427	71	427	72	434	72	434
Internal HEX area	m ²	22.9	138.6	11.5	68.9	11.5	69.0	11.7	70.1	11.7	70.1
Heat exchanger equipment											
Total condenser area	m ²	n/a	n/a	6.6	39.4	6.8	41.0	9.7	58.1	9.8	58.4
Total HEX area SOE	m ²	n/a	n/a	n/a	n/a	17.3	103.9	n/a	n/a	17.3	103.9
Electr. heater SOE	kW	n/a	n/a	n/a	n/a	6.9	41.1	n/a	n/a	6.9	41.1
Desulphurisation vessels (2x)											
Diameter	m	0.48	0.86	0.47	0.86	0.47	0.86	0.64	1.17	0.64	1.17
Height	m	1.43	2.59	1.42	2.59	1.42	2.59	1.93	3.52	1.93	3.52
Sorbent mass (total)	kg	513	2792	510	3059	510	3059	1279	7677	1279	7677
Excess heat											
Reactor	kW	-160	-970	-111	-667	-5	-32	-105	-627	0	0
Condenser @ 165 °C	kW	n/a	n/a	-54	-325	-56	-336	-80	-482	-80	-482
Grid compliance											
x_{H_2}		1.4 %	1.1 %	1.1 %	1.3 %	1.1 %	1.3 %	1.4 %	1.6 %	1.4 %	1.6 %
x_{CO_2}		0.0 %	0.0 %	0.7 %	0.8 %	0.7 %	0.8 %	0.6 %	0.7 %	0.6 %	0.7 %
x_{CH_4}		98.6 %	98.9 %	98.2 %	97.9 %	98.2 %	97.8 %	97.9 %	97.5 %	97.9 %	97.5 %
$\dot{n}_{tot,out}$	mol/s	0.679	4.066	0.683	4.106	0.683	4.107	1.719	10.343	1.719	10.343

Table 3.8: Technical data for the considered processes. The processes marked with “bg” are operated using biogas as feed.

Analogously, the process efficiency was also determined based on the lower heating value (LHV). The efficiency is independent of the scale of the plant, the results shown in Table 3.9 are therefore summarised for the 1 MW and 6 MW plants. The only difference in the electricity-to-methane conversion is the electrolyser technology applied. The methanation step towards grid-ready biomethane is identical in all considered cases. Efficiency discrepancies caused by slightly different gas composition are negligible.

	C1/C6	B1/B6	C1bg/C6bg	C1S/C6S	C1bg/C6bg	C1Sbg/C6Sbg
η_{HHV}	60 %	60 %	60 %	81 %	60 %	81 %
η_{LHV}	54 %	54 %	54 %	73 %	54 %	73 %

Table 3.9: Electricity-to-biomethane efficiencies of the processes.

The use of high-temperature electrolyser technology has a clear impact on the overall process efficiency, especially when the provision of process heat to external processes is restricted. When PEM electrolysis is applied, the PtG process efficiency is 54 % based on LHV and 60 % based in HHV. These values can be increased by over 19 %-points by the use of an SOE to 73 % and 81 %, respectively.

3.3.1 Heat integration

The high-temperature BFB methanation processes presented here allow two ways of heat utilisation: The pre-heating of the feed gases using the off-heat of the water condenser and in the case of high-temperature electrolysis the steam generation via the use of off-heat from the reactor. The second option was justified via pinch point analysis, as shown in Figure 3.5. The cold streams (blue) correspond to the heat requirement of the feed water to the electrolyser. Water enters the plant at 20 °C and is heated to 193 °C, which corresponds to the vaporisation temperature at the operation pressure of 15 bara. The heat requirement in the evaporator is indicated by the horizontal part. The steam is then superheated to the operation temperature of the electrolyser. The last 50 K of temperature increase have to be provided by an electrical heater, whose energy demand is indicated by a horizontal shift of the curves. This point also corresponds to the minimal temperature approach of the hot and cold streams, which was set to 50 K. The hot streams correspond to the combined heat provision by the product gas streams from the electrolyser (hydrogen and oxygen). Specialised heat exchanger equipment is necessary to valorise the heat of both gases efficiently. Concepts for such equipment are under development [125, 126].

The hot streams (red) correspond to the product gas streams cooled to 60 °C. In the first step, the hot product gases are cooled to 287 °C, where the freed enthalpy is used to superheat the incoming steam to 750 °C. The reactor provides heat at a temperature level of 287 °C, which is sufficient in quality and quantity to provide heat to the evaporator. Subsequently, the product gases are further cooled by the incoming water feed. Part of the steam remains in the hydrogen product gas, as it is not fully converted in the electrolyser. This steam is condensed at a

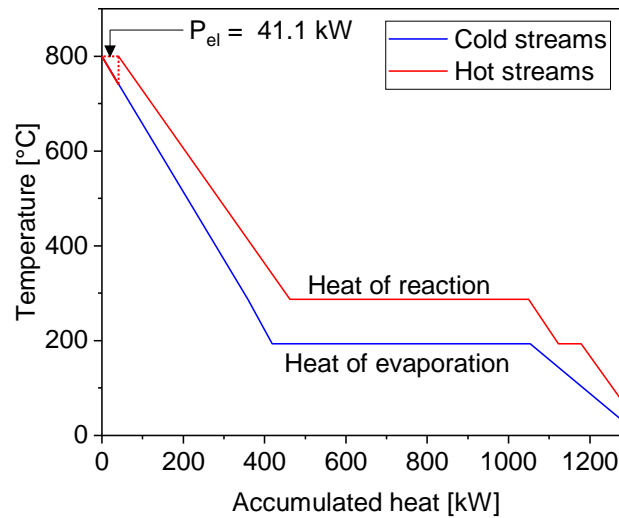


Figure 3.5: Pinch point analysis for the heat integration between the reactor and the high-temperature electrolyser in the 6 MW-scale. The cold composite curve (blue) corresponds to the water fed to the electrolyser, where the horizontal part represents the energy required to evaporate the feed water at 15 bar. The hot composite curve (red) represents the hydrogen and oxygen product gas streams. The heat capacities are combined as both are used to superheat the incoming steam. The horizontal part represent the available heat from the reactor. Both curves have a minimal approach temperature of 50 K.

temperature level of 193 °C, visible as small horizontal part in the hot composite curve (red). The remaining cooling duty can be provided by air cooling, which is not further discussed in this work.

The reactor analysed in this work is cooled by a thermo-oil system and internal heat exchangers. This cooling system is directly connected to the evaporator providing an efficient heat transfer. The remaining heat after the water evaporation can be further utilised at a temperature level of around 280 °C. Other concepts combining fixed bed methanation with high temperature electrolysis make use of direct, internal steam generation in the reactor [58, 127]. In order to provide an efficient heat transfer, the water has to be kept in a boiling state. Depending on the reactor temperature, this requires high operation pressures, which increases equipment cost substantially and decreases cost efficiency.

As shown in this pinch point analysis, the heat provided by the off-gas streams and the reactor is sufficient to produce and superheat the steam required for the high-temperature electrolysis. Additional electrical heating is necessary to reach isothermal conditions in the stack. Nevertheless, the corresponding electrical energy demand represents only a small share of the total electrolyser power.

3.3.2 Investment cost

As shown in previous work [102], the investment cost of Power-to-Gas systems are highly dominated by the electrolyser expenses. The cases considered in this work are shown in Figures 3.6 and 3.7 and summarised in Table 3.11. The hydrogen path contributes to at least 50 % of the total cost in case of 1 MW biological methanation, and to up to 92 % in the case of BFB methanation with 6 MW_{eq} SOE. This extreme originates mainly in the high assumed cost for the SOE stack in the base case. Nevertheless, even in the case of a commercial PEM electrolyser, the cost share amounts to 69 % in the 1 MW and 86 % in the 6 MW scale.

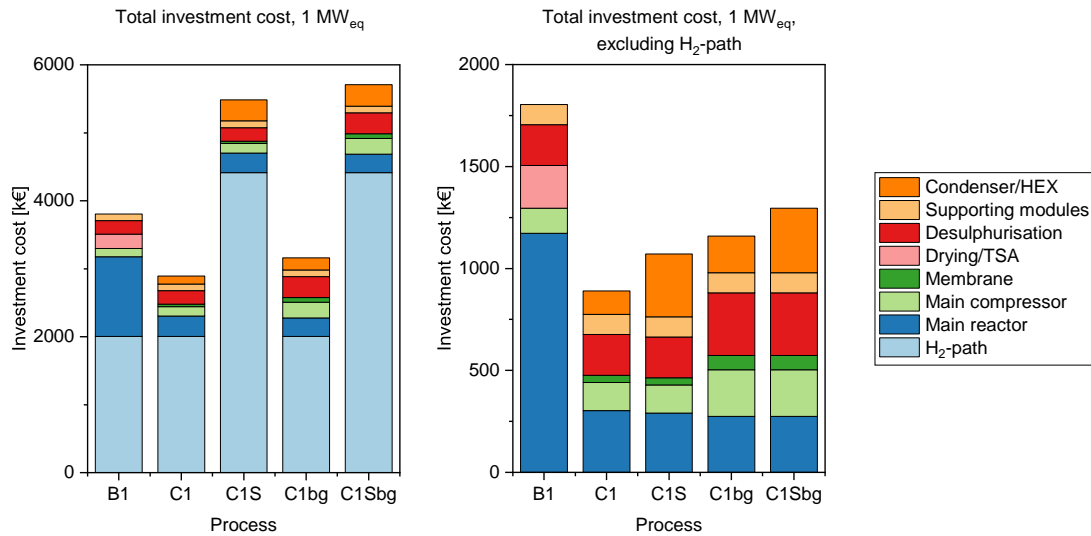


Figure 3.6: Investment cost of the 1 MW_{eq} processes in k€. The cost including the H₂-path are shown on the left, the right side shows the cost structure without the H₂-path.

When a Power-to-Gas plant is in planning, two main considerations can be identified: An overall cost analysis for a newly installed plant, or a retrofit project, where the decision between methanation technologies has to be taken. In the first case, the hydrogen path has to be included in the considerations. For the second case, as the hydrogen path is identical for all methanation technologies, it can be excluded from the consideration. In some of these cases, existing electrolyser units are retrofitted with PtG equipment. It is therefore important to compare technologies based on total investment cost, as well as only based on methanation equipment cost.

The second-largest share of investment cost is the reactor vessel itself. As shown in previous work by Inkeri *et al.* [75] and pilot plant projects, biological methanation requires a large reactor volume to produce utility-scale biomethane. This is also represented in the data discussed in this work, as for the operation with pressurised hydrogen and potentially corrosive slurries, *i.e.* CO₂ dissolved in water, a pressure resistant stainless steel tank is required. Although BFB methanation needs a smaller reactor volume, it also requires pressure and

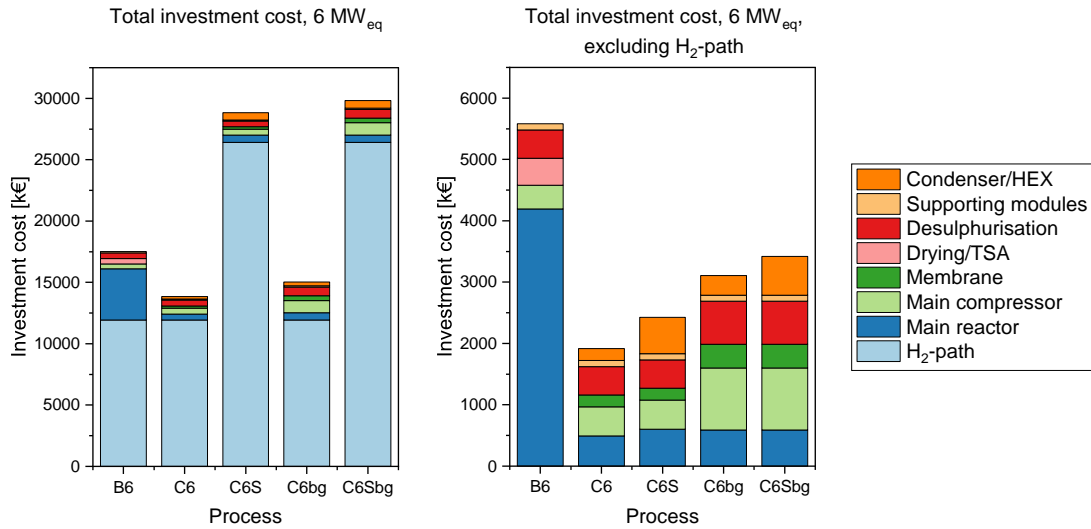


Figure 3.7: Investment cost of the 6 MW_{el} processes in k€. The cost including the H₂-path are shown on the left, the right side shows the cost structure without the H₂-path.

corrosion resistance at high temperatures. Nevertheless, mainly due to the size difference, the investment cost for the BFB vessel is less than a third of the cost of the bioreactor.

The data provided by the simulations of Inkeri *et al.* [75] indicate a methane evolution rate of 168 vvd^I in the 1 MW case and 70 vvd in the 6 MW case, based on the reactor sizes given in Table 3.2. Other biological reactor concepts are available and under investigation [59]. For fixed film reactors, which include trickle bed reactors, the projects reported by Rusmanis *et al.* show an average methane evolution rate of around 18 vvd [59]. Compared to the total methane formation in CSTR systems, such rates would result in large vessel sizes. Even though these reactors are operated at atmospheric pressure, such volumes will result in high investment cost for the main reactor, exceeding the system considered in this study. The demonstration project ORBIT is a trickle bed reactor operated at pressures up to 12 bar, but also here, a methane formation rate of only 8.4 vvd is reported [67]. This indicates that further development towards higher methane formation rates is necessary.

The catalytic BFB methanation requires a larger main compressor than the biological system, since the membrane upgrading unit creates a recycle stream, which increases compression duty.

A further cost factor in the BFB-based processes is the heat exchanger equipment required for utilisation of the product gas stream and subsequent integration with the feed gas stream. This cost is not considered in the bioreactor, since the latter is operated at a low temperature level, which results in a low water content in the product gas. In the case with SOE electrolysis, more exchangers are required for heat management in the electrolyser. In the 1 MW-case,

^Ivvd: methane production per reactor volume and day, in m³_{CH₄}/m³_{reactor}/d

this doubles the cost for heat exchanger equipment compared to the PEM-BFB case, for the 6 MW-case this results even in a three-fold increase.

In addition to the CO₂ base cases, the process was furthermore simulated using biogas as carbon source. The feed stream was adjusted to match the CO₂ content with the electrolyser power. This results in a 2.5 times higher total feed flow rate than in the pure CO₂-cases due to the additional methane. This higher total flow rate causes a cost increase of the supporting units, namely the compressor and desulphurisation. The reactor cost on the other hand is almost not affected. As the absolute amount of CO₂ remains identical, the same amount of catalyst is required for the methanation unit. Furthermore, the internal heat exchanger area remains equal, as the same reaction heat has to be dissipated. The gas composition itself has therefore less influence on the reactor dimension and subsequently on the corresponding investment cost than on the supporting units.

Rough estimates for plant scaling are obtained by relating the capacity increase of equipment to the cost increase by an exponential law according to equation 3.25 [128]:

$$\frac{C_2}{C_1} = \left(\frac{6 \text{ MW}}{1 \text{ MW}} \right)^\alpha \quad (3.25)$$

Such scaling exponents are obtained for all three processes and listed in Table 3.10. For the electrolyser we assumed a linear relationship of cost to the rated power, implying that there is no economy of scale applicable. Again, due to the dominance of the expenses for the H₂-path, this somewhat conservative assumption has a high influence on the scaling exponent. For the total plant, the exponent is close to unity. When only the methanation plant is considered, the exponent for the biological system is close to 0.6, which is a common rule of thumb value for the scaling of vessels and therefore reflects the dominance of the cost for the reactor vessel. The scaling exponents for the catalytic system are in the range of 0.4 to 0.5, which implies that there is a strong decrease in specific expenses with increase of the scale.

	PEM-bio	PEM-Cat	SOE-Cat
Full system w/o H ₂ path	0.63	0.43	0.46
Full system incl. H ₂ path	0.85	0.87	0.93

Table 3.10: Scaling exponents for the considered methanation processes.

The annualised capital cost is calculated according to equation 3.23.

The specific investment cost for the biological methanation without the hydrogen path amount to 2975 €/kW in the 1 MW_{el} case (B1) and 1538 €/kW in the 6 MW_{el} case (B6), related to the energy output of the produced biomethane. Mörs *et al.* [129] and Schlautmann *et al.* [130] estimate the specific investment cost for the pilot plant in Solothurn, which corresponds to a biomethane output of 0.325 MW, to 4320 €/kW. They furthermore provide estimates for specific investment cost for plants scaled to 1 MW_{biomethane} and 5 MW_{biomethane}, which amount to 2172 €/kW and 940 €/kW, to the produced biomethane. In Figure 3.8, the estimates

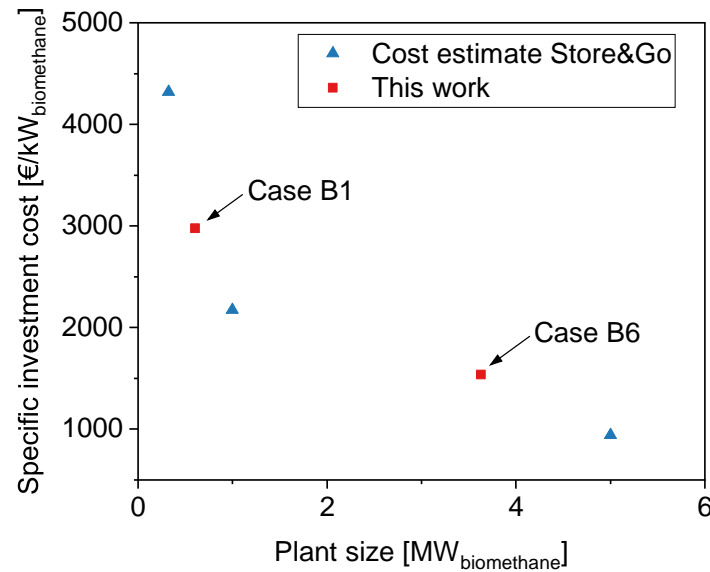


Figure 3.8: Specific investment cost estimates of cases B1 and B6 in comparison with estimates from the Store&Go project reported by Mörs *et al.* [129] and Schlautmann *et al.* [130]. The plant scale refers to the energy output of the produced biomethane.

of the Store&Go project are compared to the results provided in this study. Although the estimates provided in the current study fit well within the estimates reported by Schlautmann *et al.* [130], they are slightly more conservative. Especially the value for the larger plant size indicates that the cost-related scaling factor provided in this study is lower than the one by Schlautmann *et al.* [130]. It is difficult to assess such differences in detail, as the full cost assessment and detailed methodology of the Store&Go project is not known to the authors.

3.3.3 Operational expenses (OPEX)

The annual operational expenses for the processes are shown in Figures 3.9 and 3.10 and summarised in Table 3.12.

The obvious main driver for operational cost of the Power-to-Gas process is the electricity cost. In both scales, the cases PEM-Bio (B1 and B6) and PEM-BFB (C1 and C6) are comparable in terms of electricity consumption. The SOE introduced in cases C1S and C6S has a higher electrical efficiency, which can be considered as a reduction of electricity use per hydrogen produced.

The annual operation cost also includes labour and maintenance cost (O&M), which are estimated by 1.5 % of the investment cost for the electrolyser and 5 % of the total investment cost for the rest of the plant. This differentiation takes into account that electrolyzers do

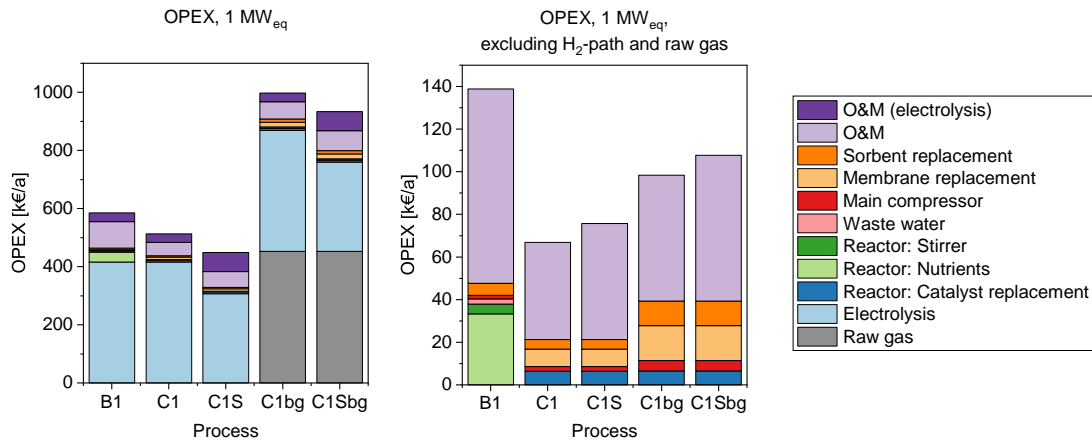


Figure 3.9: Operation cost (OPEX) of the 1 MW_{el} processes in k€ per year. The OPEX including the H₂-path are shown on the left, the right side shows the cost structure without the H₂-path and the corresponding O&M cost.

not have any moving parts and require therefore less servicing. Due to the dominance of electrolyser costs, the O&M costs are also separated in two parts.

When excluding the H₂-path in this analysis, the main contribution to the OPEX is the O&M cost for the rest of the plant. The actual consumables and utilities used in the process amount only to around one half of the remaining OPEX. For the biological methanation, the largest share of its OPEX are related to the nutrient cost. In the BFB processes, the largest contribution comes from the bi-annual membrane replacement, followed by the catalyst replacement, which occurs on an annual basis. According to our assumptions, the nutrient provision cost are around four times higher than the annual catalyst replacement cost in the 1 MW catalytic case. For the 6 MW case the amount increases tenfold. The amount of nutrients required scales with the volume of the biological system, subsequently there is a disproportionate increase compared to the energy scale.

Investment cost [k€]	B1	C1	C1S	C1bg	C1Sbg	B6	C6	C6S	C6bg	C6Sbg
H ₂ -Path	2002	2002	4413	2002	4413	11925	11925	26409	11925	26409
Main reactor	1173	303	291	275	275	4193	493	602	590	590
Main compressor	123	138	138	229	229	387	475	476	1010	1010
Membrane	0	35	35	70	70	0	192	192	384	384
Drying/TSA	209	0	0	0	0	437	0	0	0	0
Desulphurisation	200	200	200	307	307	464	463	463	705	705
Supporting modules	99	99	99	99	99	99	99	99	99	99
Condenser/HEX	0	116	309	179	316	0	193	592	318	630
Sum	3806	2893	5484	3161	5709	17504	13839	28834	15030	29827

Table 3.11: Investment cost of the processes in k€.

Operation cost [k€/a]	B1	C1	C1S	C1bg	C1Sbg	B6	C6	C6S	C6bg	C6Sbg
Raw gas	0	0	0	453	453	0	0	0	2718	2718
Electrolysis	417	417	307	417	307	2499	2499	1843	2499	1843
Reactor: Cat. replacement	0	6	6	7	7	0	38	38	39	39
Reactor: Nutrients	33	0	0	0	0	479	0	0	0	0
Reactor: Stirrer	5	0	0	0	0	23	0	0	0	0
Waste water	2	0	0	0	0	36	0	0	0	0
Main compressor	2	2	2	5	5	10	13	13	29	29
Membrane replacement	0	8	8	16	16	0	45	45	90	90
Sorbent replacement	6	5	5	11	11	31	27	27	69	69
O&M	91	46	54	59	68	281	98	123	157	177
O&M (electrolysis)	30	30	66	30	66	178	178	396	178	396

Table 3.12: Operation cost of the processes in k€/a, based on base case assumptions indicated in Table 3.6.

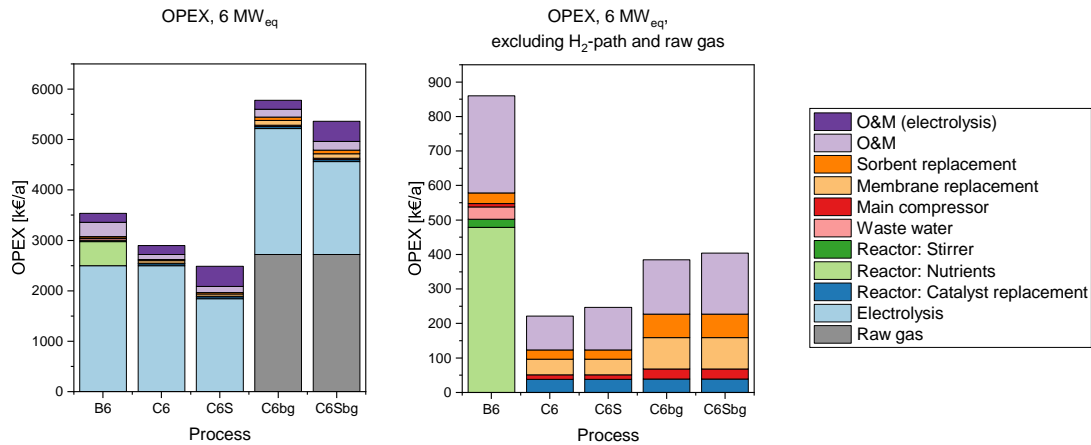


Figure 3.10: Operation cost (OPEX) of the 6 MW_{el} processes in k€ per year. The OPEX including the H₂-path are shown in on the left, the right side shows the cost structure without the H₂-path and the corresponding O&M cost.

The stirring power required for the bioreactor amounts to 0.9 – 1.1 % of the electrolyser power, as shown in Table 3.2. This corresponds to less than 1 % of the total OPEX, but remains in a similar range as the cost caused by other supporting units, such as the main compressor and sorbent replacement costs.

Nevertheless, when including the H₂-path in the calculation of the pure CO₂ cases, the costs for utilities and consumables are marginal. The cost for the H₂-path, including the corresponding O&M expenses make up 76 – 92 % of the total.

The charges for membrane replacement have a direct influence on the OPEX, however it represents only a minor part of the total OPEX. Therefore, the sensitivity towards the replacement interval is only low. An annual replacement would double the share of membrane replacement cost compared to the base case represented in Figures 3.9 and 3.10.

The total OPEX for catalytic methanation operated with biogas are almost twice as high as in the corresponding base cases. The additional cost originates from the price paid for the raw biogas, which can be considered as an opportunity cost for biogas upgrading through an alternative method. Apart from the increase of the total OPEX, the influence on the OPEX related to the methanation equipment is also visible: Due to higher gas throughput, the electricity consumption of the compressor increases, as well as the amount of sorbent required each year. Additionally, the membrane replacement cost approximately doubles. Although roughly the same amount of CO₂ and H₂ has to be separated from the product gas stream a larger amount of membrane modules is required. The increased number of modules compensates for the higher total gas flow rate, as the permeation rate of CO₂ and H₂ remains constant.

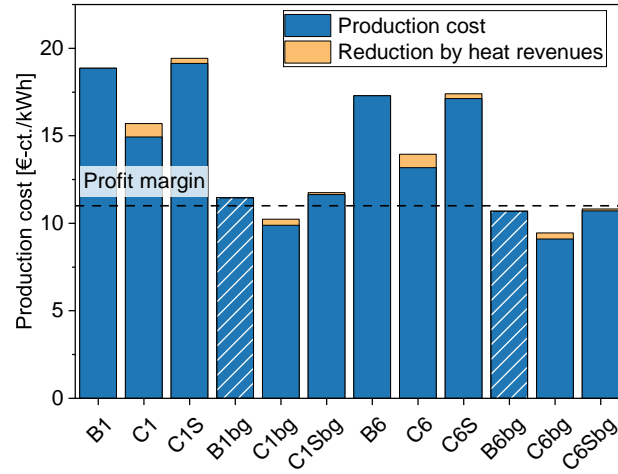


Figure 3.11: Production cost of biomethane for each considered process under the base case assumptions indicated in Table 3.6. The projected cost for biological methanation operated with biogas is indicated with shaded bars.

3.3.4 Revenues and production cost

The energy content of the biogas injected to the grid is determined according to equation 3.26 from the higher heating values of the species CH_4 and H_2 .

$$E_{\text{biomethane}} = \dot{V}_{\text{biomethane}} (x_{\text{CH}_4} \text{HHV}_{\text{CH}_4} + x_{\text{H}_2} \text{HHV}_{\text{H}_2}) \quad (3.26)$$

The total revenues from biogas sales are then obtained by multiplication with the biogas selling price. The heat revenues are calculated by considering the high and mid temperature level off-heat. In order to account for heat losses in the heat extraction equipment, we assumed that only 70 % of the heat produced can be sold. The specific production cost per kWh of gas injected to the grid are calculated by dividing the total annual cost of the plant (OPEX + CAPEX) by the biogas sales. The values obtained for the different processes are summarised in Table 3.13.

The absolute production cost per kWh of biomethane injected to the grid are indicated in Figure 3.11. The values correspond to the base case scenario represented by the input parameters in Table 3.6. For this case, neither of the pure CO_2 processes can be operated economically. Using biogas as feed reduces production cost by around 26 – 39 %. This causes the two PEM-based catalytic processes to reach a profitable range (cases C1bg and C6bg) at a production cost of 10.2 and 9.5 €-ct./kWh. The process including high-temperature electrolysis is right at the profit margin at a scale of 6 MW.

As we have no full model for biological methanation available, the production cost for biological methanation (cases B1 and B2) using biogas were projected as shown in Figure 3.11.

The analysis of the investment and operation expenses showed that for the catalytic cases, the change of the feed gas to biogas does hardly affect the cost related to the reactor but increases the expenditures for auxiliary units. We therefore assume that approximately the same cost decrease occurs for the biological system as for the catalytic technology. Even though there is a significant step towards profitability possible, the margin is not yet reached under base case assumptions.

The 1 MW-scale SOE-BFB process has the highest production cost, mostly caused by high investment cost for the SOE stack. The cost decreases with scale, but remains the highest among the technologies. When switching to biogas methanation, the production cost decreases by 39 %, which is the highest relative decrease among the technologies. This is a result of the higher electrical efficiency of the SOE stack, which reduces the relative OPEX due to lower expenses for electricity while still producing the same amount of biomethane.

For both feed gases, the 6 MW PEM-BFB case indicates the lowest production cost, which is a result of scaling effects, lower- cost electrolyser technology, as well as a small reactor size. Therefore, switching the technology from biological methanation to BFB-based technology can lead to a cost reduction of 17 % (1 MW) and 19 % (6 MW) in the case of pure CO₂ methanation. When using biogas, this benefit even increases to 24 % (1 MW) and 26 % (6 MW).

A further decrease of production cost is achieved by valorising the process heat. For the PEM-BFB cases a cost reduction of around 5 %, and for the SOE-BFB cases a reduction of around 2 % is possible. The latter cases do have a limited heat output due to the heat requirement of the SOE. Furthermore, when biogas is used only very limited heat sales are possible, as part of it is redirected to feed water evaporation. The valorisation of the oxygen produced in the electrolysis would be another opportunity to decrease cost. However, this is challenging to realise at most sites and is therefore not considered in this work.

3.3.5 Sensitivity on electricity price and SOE investment cost

The electricity cost states the largest influence on the operation cost of the processes. The base case used above is based on an electricity price of 5 €-ct./kWh. This value is comparable to the production cost of wind and large-scale photovoltaic electricity [123]. Figure 3.12 indicates the production cost for each process as a function of the electricity price. The profit margin corresponds to the selling price of renewable gas indicated at 0.11 €/kWh_{biomethane}. As shown in Figure 3.11 for the pure CO₂ cases, the 6 MW PEM-BFB case shows the lowest production cost and therefore reaches profitability at the highest electricity cost of approximately 3.2 €-ct./kWh_{el}. The corresponding 1 MW-case with the second-lowest production cost reaches profitability at 2.2 €-ct./kWh_{el}, whereas the larger-scale biological methanation process requires an electricity price as low as 1.2 €-ct./kWh_{el} to reach the profit margin. The 1 MW-scale biological process only reaches a profitable range when electricity is provided at 0.3 €-ct./kWh_{el}. The performance of the SOE-based processes is inferior, as no profitability is reached, even if no electricity cost is considered. Nevertheless, it is notable, that the SOE-based

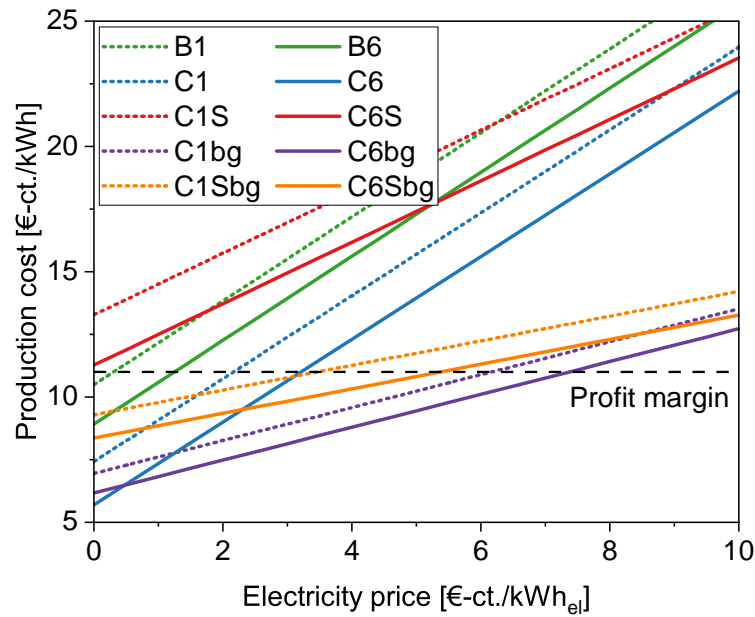


Figure 3.12: Production cost in cents per kWh of biomethane as a function of the electricity price for each considered process. The profit margin is indicated as a dashed line at 11 €-ct./kWh, which indicates the selling price for renewable gas.

processes are less sensitive towards electricity cost, *i.e.* the production cost do not rise as fast with the electricity price as in the PEM-based cases. This is a direct consequence of the higher efficiency of the SOE stack and the heat integration with the BFB reactor.

Biogas as feedstock increases the total amount of methane produced per kWh of electricity. Generally, the processes are therefore less sensitive towards the electricity price than in the case of pure CO₂ methanation. This can be seen in Figure 3.12 by a decreased slope of the corresponding lines. The 6 MW-scale PEM-BFB process reaches profitability at 7.4 €-ct./kWh_{el} and at 6.2 €-ct./kWh_{el} in the 1 MW case. Lower, but still above the pure CO₂ processes, the methanation with high temperature electrolysis reaches the margin: At 5.4 €-ct./kWh_{el} for the 6 MW case and 3.5 €-ct./kWh_{el} for the 1 MW scale, respectively.

In order to make the SOE-based processes profitable, the investment cost and subsequent CAPEX for the SOE stack have to decrease considerably. Schmidt *et al.* [92] estimate the cost for the SOE technology to be in a range of 3000 to 1900 €/kW_{el} in the year 2030, depending on R&D funding and production scale. This is still around three times as high as their estimate for PEM electrolyzers. Figure 3.13 shows the influence of the investment cost of the SOE stack on the production cost of biomethane. Electricity prices of 5 €-ct./kWh_{el} or 2.5 €-ct./kWh_{el} are taken into account.

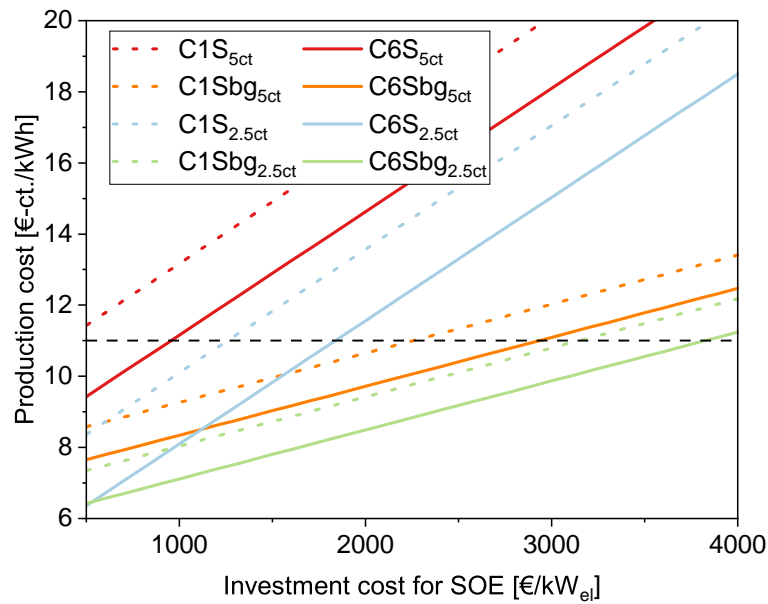


Figure 3.13: Production cost in €-ct./kWh of biomethane of the SOE-based processes as a function of investment cost for the SOE stack. Two different electricity prices are considered: 5 €-ct./kWh_{el} and 2.5 €-ct./kWh_{el}.

Depending on the feed gas, two further cost ranges can be identified: The case for pure CO₂ methanation and the case for direct methanation of biogas. As in the latter a larger amount of methane is fed to the grid based on the same nominal power of the electrolyser, biogas methanation has a higher profitability range and allows for higher investment cost for the electrolyser. For the same reason, the production cost for direct methanation is less sensitive towards the electrolyser investment cost and the corresponding lines appear with a reduced slope in Figure 3.13.

As shown in Figure 3.11, the two SOE-based processes for CO₂ methanation exhibit production costs of 19.4 €-ct./kWh_{el} for the 1 MW-scale and 17.4 €-ct./kWh_{el} for the 6 MW-scale respectively. To reach a profitable range, the production cost has to be reduced to below 11 €-ct./kWh_{el}. As shown in Figure 3.13, for the higher electricity price this will be at investment costs lower than 500 €/kW_{el} for the 1 MW case and lower than 960 €/kW_{el} for the 6 MW-scale. This is a very ambitious cost decrease, nevertheless, under favourable circumstances, a capital cost lower than 1000 €/kW_{el} in future is considered possible [92, 131]. Literature indicates that capital cost for SOEs may adjust to a similar range as PEM or AEC technology [90, 92]. A halving of the electricity cost to 2.5 €-ct./kWh_{el} results in an increase of the allowed investment cost in the 1 and 6 MW case of approximately 2.6-fold to 1260 €/kW and 1.9-fold to 1840 €/kW, respectively.

	B1	C1	C1S	C1bg	C1Sbg	B6	C6	C6S	C6bg	C6Sbg
Biomethane production										
1000 m ³ /a	456	458	458	1154	1154	2731	2757	2758	6946	6946
MWh/a	5045	5031	5032	12671	12671	30200	30241	30243	76183	76183
Revenue [k€/a]										
Biogas sales	561	559	559	1408	1408	3356	3360	3360	8465	8468
Heat revenue	0	39	14	43	14	0	231	86	258	86
Production cost										
€-ct./kWh	18.86	15.69	19.42	10.24	11.75	17.30	13.95	17.40	9.45	10.82
Production cost reduction by heat sales										
€-ct./kWh	0.00	-0.77	-0.28	-0.34	-0.11	0.00	-0.76	-0.28	-0.34	-0.11
Production cost without nutrient cost										
€-ct./kWh	18.20					15.71				

Table 3.13: Biomethane production, subsequent revenues and specific production cost of the considered processes.

Due to the reduced production expenses for direct methanation, the maximum allowed electrolyser investment increases to 2260 €/kW_{el} (1 MW_{el}) and 2930 €/kW_{el} (6 MW_{el}) for the two scales based on an electricity price of 5 €-ct./kWh_{el}. Using the lower electricity cost, this numbers increase to 3150 €/kW_{el} and 3820 €/kW_{el}. This indicates, that even with moderate improvements in the investment cost of the SOE, profitability of the process can be achieved.

Again, the profitability range can be further extended by also including heat utilisation and oxygen sales. For the heat utilisation, a production cost decrease of around 2 % is possible in the pure CO₂ case.

3.4 Conclusion

A techno-economic analysis of three CO₂ methanation process chains in two different scales (1 MW_{el} and 6 MW_{el}) was performed. The focus was set on the comparison of biological CO₂ methanation in a stirred bubble column with catalytic bubbling fluidised bed methanation. Furthermore, the benefits of including high-temperature electrolysis compared to industrially mature PEM electrolysis was investigated. For all investigated cases, fulfilling the grid injection limitations (mainly a H₂-content of <2 %) was required. For the investigated catalytic processes, we also included the case of direct methanation of biogas, which showed a clear cost benefit over CO₂ methanation.

In general, the investment and operation cost of the process chains are highly dominated by the hydrogen path. On one hand, there is the high specific investment cost for the electrolyser unit, which is more than twice as high in the case of high-temperature electrolysis. On the

other hand, electricity cost directly influences the operation cost of the process. Nevertheless, these costs are specific to the electrolyser technology applied and are independent from the methanation technology. Therefore, for cost comparison in between the technologies, a focussed view on the respective cost without the H₂-path may be advisable.

The investment cost for biological methanation is highly dominated by the large reactor vessel required. The investment cost benefit for the BFB technology mainly originates from the significantly smaller reactor vessel required for catalytic methanation. The investment cost of biological methanation can only be reduced when smaller reactor volumes are applicable. The required reactor volume on the other hand is directly linked to the gas-to-liquid mass transfer. As long as this coefficient cannot be increased, the methane formation per volume is limited. A possibility of decreasing the vessel cost would be the reduction of the operation pressure. Nevertheless, this results in a reduced mass transfer rate and therefore again to a larger required reactor volume.

The nutrient provision for biological methanation states the largest influence on the OPEX of that process option. This cost causes the OPEX to exceed the annual cost of the PEM-BFB process. Concepts exist where nutrients are provided by feeding digester efflux to the reactor, which may cause a cost decrease. Still, even when no cost is associated with nutrient provision the production cost for the biological system remains higher than the cost of the catalytic system.

The integration of high-temperature electrolysis leads to a higher electrical efficiency of the Power-to-Gas process chain. Nevertheless, the reduction in electricity cost does not compensate for added capital expensed due to the high stack investment cost and additional heat transfer equipment needed. Currently, SOE cells are still under investigation, which results in high investment cost in near future. Based on an electricity price of 5 €/ct./kWh_{el} and a biomethane selling price of 0.11 €/kWh, the investment cost for SOE technology have to decrease to 950 €/kW_{el} for 6 MW plant size to reach profitability. However, such a cost decrease is not unfeasible if the technology is further developed.

Direct methanation of biogas reduced the production cost in all investigated cases by 26 to 39 %, which resulted in biomethane production cost of less than 11 ct/kWh for the 1 MW_{el} and 6 MW_{el} PEM-BFB cases, as well as the 6 MW_{el} SOE-BFB case. Even though direct methanation showed also great cost reduction potential in biological methanation, profitability could not be reached in the 1 MW_{el} case. In the 6 MW_{el}-scale, our calculations indicate a production cost slightly below the profitability limit, in the same range as the 6 MW_{el} SOE-BFB case.

Methanation of CO₂ and biogas are technologies on a high TRL (catalytic 6 – 7, biological 7 – 8) and allow for fast integration of biogenic gases into the future energy landscape. This study shows that the underlying technologies can play a cost-efficient role in the seasonal storage of renewable electricity.

4 Seasonally flexible biogas upgrading: Upgrading concept

4.1 Introduction

In the previous chapter, a clear cost benefit of direct methanation of biogas compared to CO₂ methanation was shown. When working with biogenic gases, a separation step is required in order to obtain a pure CO₂ stream. As shown, this initial separation step can be avoided by direct methanation of the raw biogas and lead to a significant cost benefit. The removal of contaminants is still necessary, as the methanation catalyst has to be protected from sulphur poisoning and subsequent deactivation [35, 37].

The synergetic combination of energy grids is becoming a major issue in future energy systems, especially when facing an increased share of renewable energy in the electricity grid [8, 132]. This higher influence of renewable energy carriers causes high fluctuations on the production side of the market, which must be balanced in order to follow the demand curve and to use renewable electricity efficiently [9, 21, 22]. Power-to-Gas is a technology to connect the power grid with the natural gas distribution network, which enables the storage of electricity that cannot be used at the time and place of production, in the form of methane gas in an existing infrastructure. One of the goals of Switzerland's Energy Strategy 2050 is to further exploit biomass as primary energy source [133]. Also, as a measure for rapid reduction of fossil CO₂, the share of renewable gas used for heating should be increased significantly to a final goal of 30 % by 2030 [99].

To allow for unlimited injection into the natural gas grid, biogas has to be upgraded by separation or conversion of the carbon dioxide to yield biomethane, according to local grid injection specifications (>96 % CH₄, <4 % CO₂, <2 % H₂ [25, 134, 135]). The simplest case of biogas upgrading for injection into the grid requires the separation of CO₂ by well-known and

Chapter 4 is based on the post-print version of the publication: A. Gantenbein, J. Witte, S. M. A. Biollaz, O. Kröcher, T. J. Schildhauer, "Flexible application of biogas upgrading membranes for hydrogen recycle in power-to-methane processes", *Chemical Engineering Science*, vol. 229, Jan. 2021. DOI: 10.1016/j.ces.2020.116012
J. W. initially conceptualised, planned, and performed experiments.
A. G. planned and performed experiments, created the diagrams and wrote the text

widely applied technologies such as amine-, water- or organic solvent-based scrubbers, as well as pressure swing adsorption [44, 46]. The alternative, non-thermal purification technology is the membrane-based gas separation. It can especially be used, when no economic waste heat source for solvent regeneration is available and electricity is relatively inexpensive [44]. This technology is very well-suited for small-scale biogas upgrading plants, as it can be scaled down without large efficiency losses and does not depend on hazardous chemicals [44, 136, 137]. These technical and economic advantages are reflected in the increasing share of membrane-based upgrading units, which were put into operation over the last few years [46]. The technologies for conventional biogas upgrading discussed above separate CO₂ from the raw gas and release it to the atmosphere. Increased benefit can arise by the direct methanation of biogas where the renewable carbon dioxide is used as feedstock in the Power-to-Gas process. Hydrogen from electrolysis with renewable electricity is converted with the CO₂ in the biogas to additional methane and steam. This approach combines the Power-to-Gas technology with biogas grid injection, resulting in a higher yield of renewable methane per amount of biomass introduced [56].

Currently, the direct methanation of biogas is being tested in various demonstration units and different technologies are put into operation under industry-like conditions [58, 60, 65, 71, 74, 81, 104, 138–140]. Two of these technologies, *i.e.* biological and catalytic fluidised bed methanation, were economically compared in the previous chapter.

As shown in the previous chapter and in literature [56, 102, 141], an inherent problem of all PtX-systems arises from their high sensitivity to the underlying electricity price. Subsequently, when the cost of renewable hydrogen, generated by electrolysis is high, their operation might become economically unattractive. In the case of Switzerland, this is especially the case during winter months, when the domestic production by renewable photovoltaics is low and electricity has to be imported [9] (*c.f.* Figure 1.1). Such fluctuations in the electricity cost require an increased flexibility of the downstream processes in order to maintain an economic operation. Further challenges arise when the CO₂ used in the PtG chain originates from a continuous process, such as fermentation or digestion. Especially these biological processes are difficult to interrupt in a short-term timescale [142–144]. The raw biogas cannot be used in the PtX system, it has to be either stored or flared in another process. Storage of raw gas is difficult, as low pressure tanks with large volumes are required [144]. Therefore, the fluctuation of the availability of hydrogen might be a major drawback in the economic feasibility of the overall process. In order to cut down total expenses, it would be advantageous to flexibly switch between biogas upgrading and Power-to-Gas operation and bridge times where renewable hydrogen is not available at reasonable cost.

This chapter focuses on experiments with a polymeric gas separation membrane and presents a Power-to-Gas concept, where it is possible to switch swiftly between biogas upgrading and PtG operation. The technical performance of a commercially available fibre-based membrane produced by Evonik AG (Germany) is investigated under co- and counter-current operation.

In addition, the effect of pressure changes and different concentrations in the feed of the gas components (methane, hydrogen and carbon dioxide) is tested.

4.2 Flexible process concept

Processes for the direct methanation of biogas often need an upgrading unit to reach the injection specifications for the natural gas grid. While high methane concentrations are relatively easy to reach in the exothermic methanation step, the necessary low hydrogen contents (<2 %) are a challenge. This is due to thermodynamic equilibrium in catalytic methanation reactors at temperatures above 250 °C [12] and mass transfer limitations in biological methanation [76]. For the final conversion or removal of hydrogen, two concepts are available. Water removal to shift the thermodynamic equilibrium by reaction product removal and a subsequent further methanation step, or hydrogen separation by polymeric membranes and recycle to the main reactor [102, 103].

Thus, a flexible process concept, where it is possible to switch swiftly between biogas upgrading and Power-to-Gas operation, requires the same type of membranes for two different upgrading tasks: in biogas upgrading, a high amount of CO₂ needs to be separated from the methane, whereas in direct methanation post-upgrading, a low amount of hydrogen has to be separated.

Figure 4.1 illustrates how the dual use of the membrane upgrading unit affects the yield of methane. For this example, a hypothetical biogas plant was assumed delivering biogas containing 40 % carbon dioxide in 60 % methane. The biogas has to be cleaned prior to the upgrading process in order to protect the methanation catalyst from poisoning. Sorbent-based removal of H₂S and other sulphur-containing species proved to be successful in removing harmful species down to concentration levels of 1 ppm required for fluidised bed methanation [37, 81]. The gas cleaning also provides protection to the membrane unit and minimises premature degradation of the materials.

By separating the CO₂ from the raw gas stream, 60 % of the biogas volume can be injected into the gas grid.

In the direct methanation mode, the feed stream to the membrane unit contains mainly methane, around 10 % hydrogen, and traces of CO₂ and humidity. 40 % of that methane flow were produced from the CO₂ by methanation. By means of the membrane separation, most of the hydrogen can be recycled (accompanied by some methane) back to the reactor, while the volumetric flow (at STP) injected to the gas grid is as large as that of the incoming biogas. As obvious from this example, the feed flow rates to the membrane units are in a similar range. Therefore, in both cases, the sizing of the membrane units can be based on a similar feed flow rate, which is tested experimentally in this work.

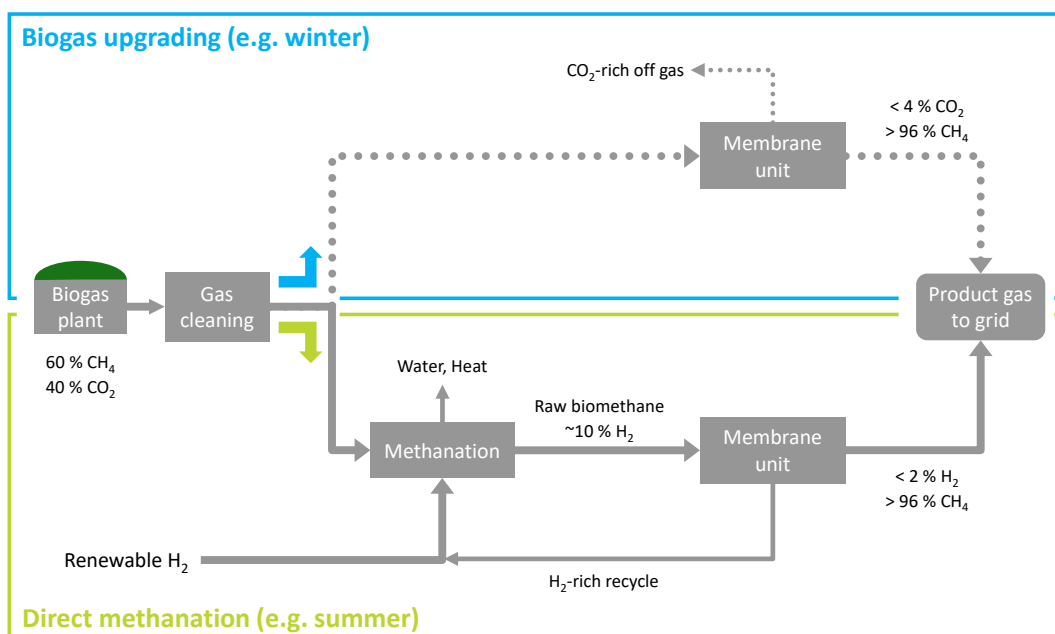


Figure 4.1: Example illustrating the change in production of renewable product gas when using either of the two operation modes. This idealised example is based on a biogas plant delivering raw biogas (60 % CH₄ and 40 % CO₂). In the biogas upgrading mode, 60 % of the volumetric flow can be delivered as methane to the grid. When direct methanation is used, the CO₂ in the raw gas is nearly completely converted to methane using a slightly over-stoichiometric amount of hydrogen. The excess hydrogen can be fed back to the methanation unit.

4.3 Methods

The membrane unit (Evonik SEPURAN[®] Green, diameter: 2 inches) was installed in a TRL 5 methanation set-up (10 – 20 kW), which can be used either for CO₂ methanation or for direct methanation of biogas [81].

The post-upgrading of product gas from the methanation (raw-biomethane) poses different requirements to the membrane separation than the upgrading of biogas. Raw biogas consists to a large extent of carbon dioxide (30 to 50 %) in methane (50 to 80 %) [81, 137]. In this work, we set the carbon dioxide content to 40 %. Previous work [81] showed an average composition of raw-biomethane of 88 % CH₄, 10.6 % H₂ and 1.4 % CO₂. This corresponds to the product gas of a bubbling fluidised bed methanation reactor reaching thermodynamic equilibrium at regular operation pressure using a biogas feed. Therefore, the concentrations for the methanation base-case was set to 88 % CH₄ and 12 % H₂; carbon dioxide was not

considered, as the concentration is already lower than the grid injection limitations (generally around 1 %).

The experiments were carried out using the product gas from the reactor, as well as gas mixtures simulating raw-biomethane or biogas. The operation conditions are summarised in Table 4.1.

Case	Gas composition	Range of volumetric flow rate	Pressure difference across membrane
Real product gas from methanation	2.7 % CO ₂ , 18 % H ₂ in CH ₄	7.45 L min ⁻¹	2 bar
Simulated product gas from methanation	12 % H ₂ in CH ₄	42 L min ⁻¹	3 – 9 bar
Simulated biogas, Stage 1	40 % CO ₂ in CH ₄	28 – 65 L min ⁻¹	3 – 8 bar
Simulated biogas, Stage 2	75 % CO ₂ in CH ₄	28 – 52 L min ⁻¹	1.5 – 6 bar

Table 4.1: Summarised operating conditions applied during experiments.

4.3.1 Gas mixing

The membrane unit was installed in the Power-to-Gas pilot plant COSYMA (COntainer-based SYstem for MethAnation), according to the schematic shown in Figure 4.2. A more detailed description of the set-up is available in [81]. The gas mixtures used for the experiments were produced using a set of mass flow controllers (MFCs) connected to gas tanks. For the experiments with methanation gas, the reactant gases were fed to the bubbling fluidised bed methanation reactor where carbon dioxide and hydrogen were converted to methane and water over a nickel-based catalyst. For the remaining experiments, the gas was led through the empty reactor or a reactor bypass. Experiments where the methane flow exceeded 40 L min⁻¹ were performed using a second MFC, originally calibrated for carbon monoxide. The flow rate indicated by this device was corrected by a conversion factor of 0.7637 to account for the use with methane gas [145].

4.3.2 Membrane test unit

For this study, an adapted membrane module was purchased from Apex AG, Däniken/Switzerland. The whole module was submerged in a heated water bath, which ensured the temperature control of the set-up. The feed line to the membrane module was equipped with a coiled section of tube, which was also placed in the water bath and served as a heat exchanger to pre-heat the gas mixture before entering the module. On the shell side, which represents the permeate side, the unit was equipped with two outlets at both ends, which allowed switching between co- and counter-current mode. The gas composition of the inlet flow of the membrane was monitored by micro gas chromatography (μ GC, Varian CP-4900) and non-

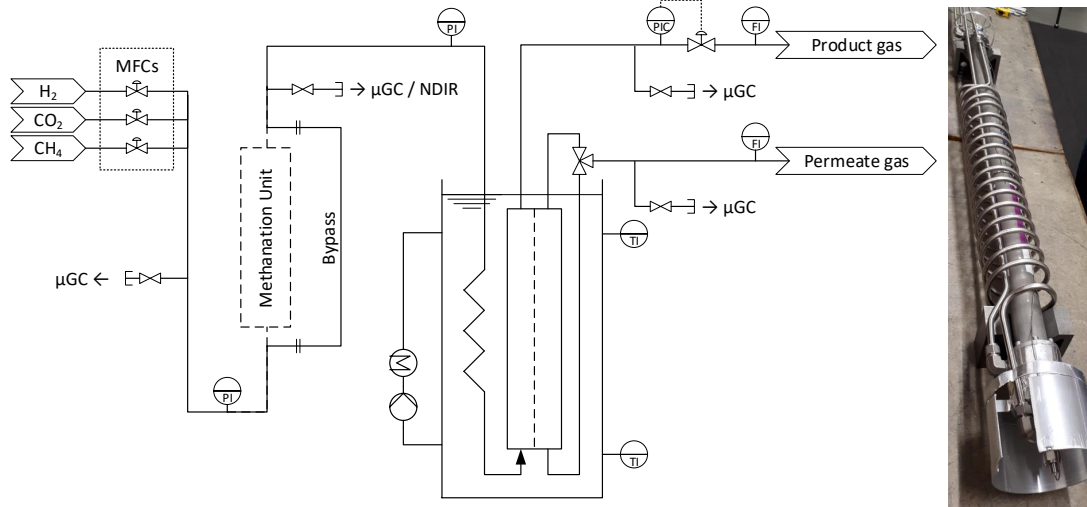


Figure 4.2: Schematic of the membrane test set-up included in the methanation pilot plant. The gas mixtures generated with MFCs are fed through the methanation reactor or a bypass. Before entering the membrane module, the gas is pre-heated in a coiled length of tube. The permeate gas can be released from both ends of the membrane module. It is therefore possible to switch between co-current and counter-current operation. The whole membrane module including the heat exchanger are submerged in a temperature-controlled water bath. In the right picture, one can see the membrane module with the coil serving as feed pre-heater.

dispersive IR spectroscopy (NDIR, Siemens Ultramat 23). The composition of the permeate and retentate flows were monitored using the μGC . The μGC was calibrated according to the methodology given in [146], which ensures a low influence of viscosity effects of the sampled gas on measurement accuracy. Since only two gas streams could be analysed by the μGC at the same time, one inlet was manually switched between the feed stream of the membrane and the permeate. The retentate composition was monitored constantly. Each operating condition was maintained for at least 30 min in order to obtain stable concentration measurements and equilibrate the membrane module. The volumetric flow rate of the retentate was measured by a gas meter (Wohlgroth G4), whereas the permeate flow was determined using a flow meter (MesaLabs Defender 530+). The pressure of the whole system was controlled at the retentate side of the membrane by a pressure retention valve. The permeate was released at ambient pressure. In order to assess the pressure drop in the membrane unit, also the feed pressure was measured. Since temperature, pressure, volumetric flow rate and gas composition were monitored in every stream entering and leaving the membrane module, it is possible to derive molar balances for all components.

During the data evaluation process a systematic deviation of the total molar balance could be observed. This deviation originated mainly from the gas meter in the retentate branch and could be corrected by a linear function with an offset:

$$\dot{V}_{ret,corr.} = m \cdot \dot{V}_{ret,measured} + q \quad (4.1)$$

The use of this function can be justified by a lower limit of the measurable gas flow rate of the gas meter and a systematic deviation depending on the gas flow rate run through the device. Applying the correction allowed to close the total molar mass balance for most of the data points within a margin of $\pm 5\%$ of the feed flow rate, a few cases exceeded this range, but were always within $\pm 10\%$ of the feed flow rate. All indicated volumetric flow rates refer to standard conditions at 1 atm and 0 °C, commonly used in gas industry according to DIN 1343 [121].

4.4 Results and discussion

4.4.1 Performance of the gas separation membrane as upgrading unit after methanation

In this section, we refer to the product gas (raw-biomethane) from the methanation reaction as inlet gas to the membrane.

The feed pressure of the membrane was set to 2.15 bar and the permeate released at ambient pressure. Operating the methanation reactor resulted in a membrane inlet concentration of 79.3 % CH₄, 2.7 % CO₂, and 18 % H₂ at total volumetric flow rate of 7.45 Lmin⁻¹ (*c.f.* Table 4.1). The membrane was operated in counter-current mode and at four different temperatures. The influence of the temperature is clearly visible as the total permeation flow almost doubles between 15 °C and 45 °C. With increasing temperatures, the transport by diffusion increases, as does the permeability [147, 148]. The composition of the permeate and retentate is also influenced by the temperature. The methane concentration in the retentate increases with the temperature due to enhanced permeation of all components. However, in the permeate, the methane concentration is also increased. At 15 °C, the permeating volume flows of methane and hydrogen are about equal. At 45 °C the shares of methane and hydrogen in the permeate shift towards two thirds and one third. Due to the larger permeation rates, it is likely that the membrane behaves less selective at higher temperatures, similarly to the case of the selectivity of hydrogen to nitrogen, which can be found in literature [149]. Nitrogen and methane have similar properties regarding their permeabilities and can replace each other in this case. The changing behaviour of the membrane for different temperatures is expressed within the permeability factor. However, this effect is not considered in various membrane unit models in literature [150–154]. A comparison of the ratios of the permeate flow rates of CO₂ and CH₄ show a similar trend as the ratio of H₂ to CH₄. This indicates that the selectivity towards H₂ is lower at higher temperatures.

Considering the whole process of the CO₂ methanation including the membrane, the retentate flow is the product flow and the permeate flow is a recycle flow directed back to the meth-

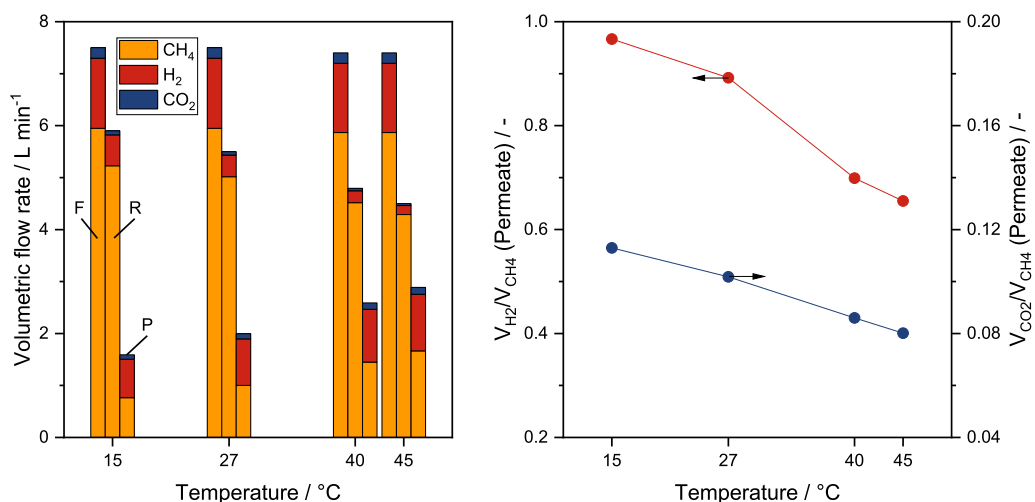


Figure 4.3: Left: Temperature dependency of the separation of hydrogen and carbon dioxide from methane. F: Feed, R: Retentate, P: Permeate. The membrane shows a clear increase of overall permeability with temperature, as the total permeate flow increases. Right: Ratio of permeate flow rates as indicator for the selectivity. With rising temperature, the selectivity of the separation towards H₂ and CO₂ decreases, as their relative shares in the permeate decrease.

anation reactor so that the reactants and the product methane are not lost (see Figure 4.1). Increasing the temperature of the membrane helps to purify the retentate flow, on the other hand it produces a large recycle flow with a significant share of methane. This recycle must be compressed again before it enters the reactor, therefore a larger recycle flow enlarges the whole process and results in particular in increased compression and reactor costs.

The temperature dependency of the selectivity as seen in these experiments indicate the importance of a stringent temperature control in the process. An uncontrolled drift of operating temperature results in an undesired process state, which may have a negative effect on the overall performance.

The low feed pressure of 2.15 bar of the experiment, shown in Figure 4.3, prevents further separation of hydrogen so that at 45 °C still a hydrogen concentration of about 4 % is present in the retentate.

In the following experiments, the focus was set on the influence of the retentate-side pressure on the membrane separation performance. Therefore, no prior methanation was done, such that the feed volumetric flow could be chosen appropriately to the membrane size and pressure. A volumetric flow rate around 42 L min⁻¹ was taken for our experiments as a base-case. This flow rate allows reaching all relevant gas mixtures with the installed mass flow controllers. The temperature of the membrane module was fixed to 40 °C, which was assumed as realistic operation temperature in practical applications. This temperature allows a high gas through-

put at a slightly reduced selectivity. Furthermore, no cost-intensive active cooling equipment is required in industrial installations.

The experiments were performed using gas from bottles, simulating the separation of remaining hydrogen and carbon dioxide from the raw-biomethane stream (see Figure 4.5). The retentate stream is the product gas, which is to be injected into the gas grid. The methane-depleted permeate stream of the membrane is mixed with the raw gas from the digester before being compressed again and recycled to the methanation reactor. In our experiments, the gas quality representing raw-biomethane was approximated by a 12 %-mixture of hydrogen in methane.

The gas separation experiments were performed in co-current as well as counter-current mode by selecting the respective permeate outlet (see Figure 4.4).

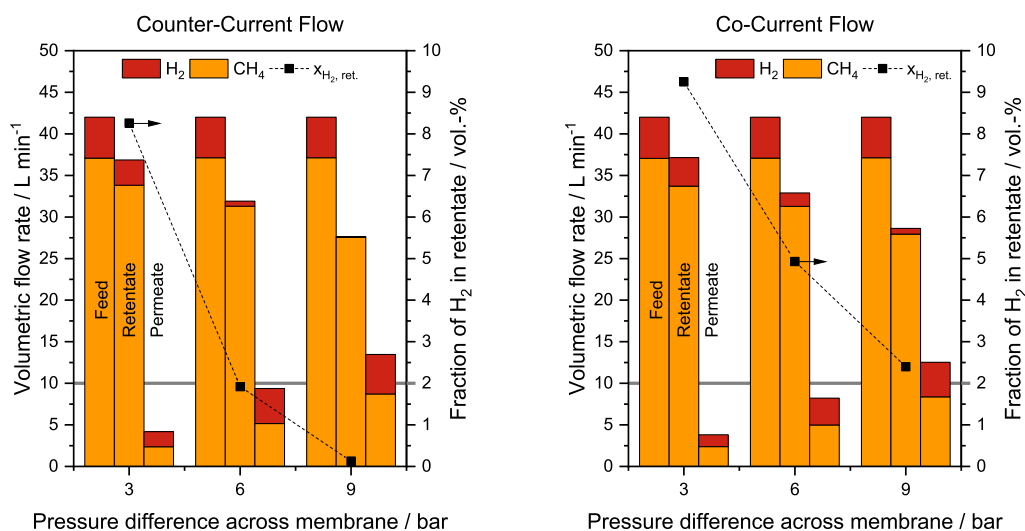


Figure 4.4: Upgrading of simulated raw-biomethane in counter-current mode (left) and co-current mode (right). The tests were performed with a mixture of 12 % H₂ in methane at a total feed flow rate of 43 L min⁻¹. Grid injection limitations are fulfilled above a pressure level of 6 bar, when using the counter-current mode.

As expected, the counter-current operation proved to be more efficient than the co-current mode. This is due to the higher average concentration difference across the membrane in counter-current operation, which states the driving force for this separation process. It was possible to reach grid injection specifications at pressure differences above 6 bar. In co-current case, the amount of hydrogen in the retentate remained at 2.4 %, but the observed trend indicates that the limitation can be reached at pressures slightly above 9 bar.

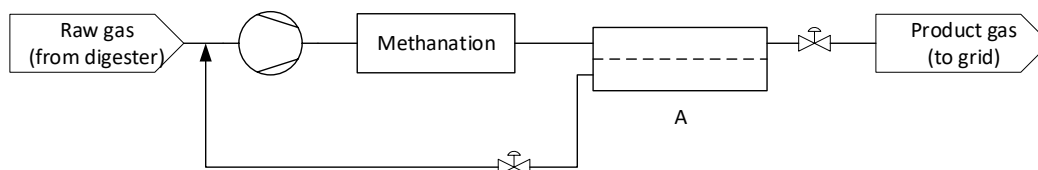


Figure 4.5: Flow diagram of a biomethane upgrading process. Leaving the methanation, the raw-biomethane is fed into a membrane module A, which separates remaining hydrogen and carbon dioxide from the product gas stream. The recycle stream is fed back to the raw gas stream and compressed again before entering the methanation reactor.

4.4.2 Performance of the membrane unit in biogas upgrading

The separation task for upgrading anaerobic digestion-derived biogas corresponds to the separation of carbon dioxide from methane. The amount of H_2 present in the biogas is supposed to be negligible [137]. The experiments were therefore performed with a mixture of 40 % CO_2 in methane at pressure differences across the membrane unit between 3 bar and 8 bar. The total volumetric feed flow rates were varied between 28 L min^{-1} and 65 L min^{-1} . The module was operated in counter-current mode only, as this configuration promises more efficient separations.

In our experiments, we could reach grid injection quality ($\leq 4 \text{ \% } CO_2$) in a single upgrading step at pressure differences above 6 bar at flow rates of 28 L min^{-1} and 42 L min^{-1} . At 65 L min^{-1} , the CO_2 -concentration was still slightly above 4 %. At higher pressure differences, lower concentrations of CO_2 were present in the retentate stream. Also, the permeate flows of CO_2 and CH_4 increase due to the higher pressure difference. The increased permeate flows can be explained by higher differences of the partial pressures, which correspond to the driving force responsible for the permeation. At higher feed flow rates, the injection specification is harder to reach. The permeate streams at these flow rates are higher at the same pressure difference than at lower feed flow rates. This increase in flow rate is mostly the result of higher CO_2 permeation as the absolute methane flow in the permeate stays almost the same. This behaviour can be explained by the interplay of two effects: on one hand, the higher permeability of the CO_2 compared to methane, on the other hand, the change of the partial pressure differences of the two components along the membrane. At higher flow rates, a larger total amount of CO_2 and CH_4 is present at the retentate side. Keeping the same pressure level and concentration of the gases in the feed, their initial partial pressure stays the same. As the permeation through the membrane is the rate limiting step of the overall transport, the presence of a higher amount of a species at higher flow rates results in a slower decrease of partial pressure on the retentate side, compared to lower flow rates. This flatter partial pressure profile leads to a higher average partial pressure difference across the membrane and therefore a larger driving force, which furthermore increases the permeating flow.

Due to the higher permeability of CO_2 and H_2 compared to methane, their average partial pressure difference is more affected by the change of feed flow rate than the one of methane. Finally, this leads to a larger change in permeate flow rate of the species with the higher permeability upon change of the feed flow rate, compared to less permeating species.

Methane-depleted recycle stream (permeate)

The permeate leaving the first membrane is enriched with CO_2 , but still contains a high amount of methane. In order to be released to the atmosphere, or be sent to a storage facility, the CO_2 off-stream is supposed to contain $<1\%$ methane, an arbitrary benchmark set due to the impact caused by the global warming potential of methane. This limit is also in the concentration range of commercial biogas upgrading systems, which lie around 0.7% for membrane-based systems, 0.07% for amine-based plants and 0.4% for water scrubbers [155]. Assuming that the permeate of the first membrane contains a mixture of 75% CO_2 in methane, further tests were performed at this concentration level. This time, the main goal is to keep the methane flow across the membrane as low as possible. This can be achieved by sustaining a low pressure difference across the membrane and a high volumetric flow rate at the retentate side.

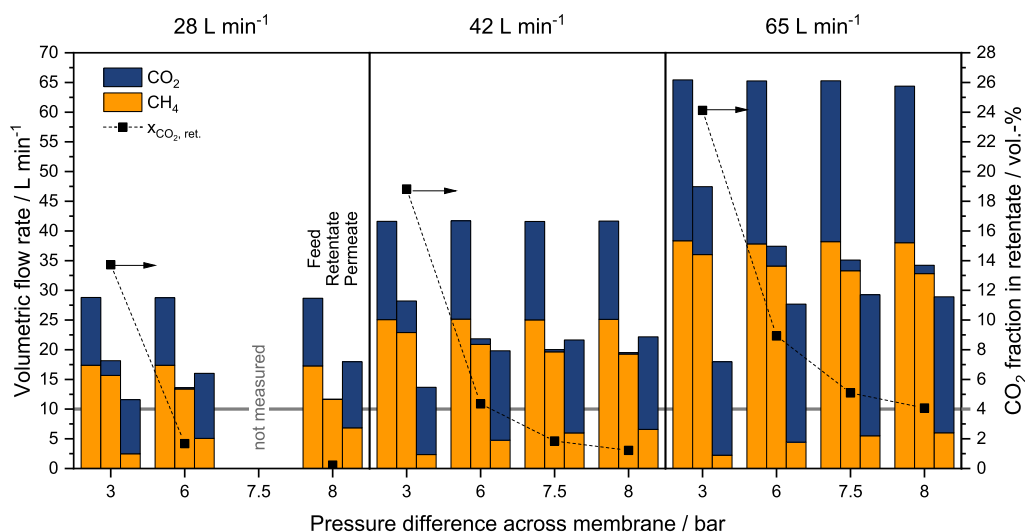


Figure 4.6: The biogas upgrading was tested using a mixture of 40% CO_2 in methane. This situation corresponds to membrane A in Figure 4.7. At flow rates of 28 L min^{-1} and 42 L min^{-1} , grid injection limitations are reached above 6 bar pressure difference. At 65 L min^{-1} , the limitation would be reached above 8 bar . The permeate stream still contains a high amount of methane and requires further upgrading before being released to the atmosphere.

In our experiments, we were not able to fully meet the injection limits: the lowest achieved methane concentration was 2.8% . However, due to the pressure drop caused by the instruments and equipment downstream the retentate outlet, and the fixed atmospheric pressure

at the permeate side, we were not able to achieve pressure differences below 1.5 bar. Further decreasing this pressure would result in an improved performance of the system. Another, more theoretical option to increase the separation of methane from the CO₂ off-gas is the cooling of the membrane module from 45 °C to 15 °C (*c.f.* Figure 4.3), which increases the selectivity and therefore the purity of the off-gas stream. This would generally decrease the permeate flow (off-gas), which must be compensated in order to retain the capacity of the upgrading unit. This can be achieved by either increasing the pressure difference, lowering the feed flow rate, or increasing the membrane area by adding more modules in parallel. All these measures tend to have a negative effect on investment or operation cost. Nevertheless, a reduced methane-slip is a key success factor for biogas upgrading units and requires therefore closer attention during process evaluation.

The retentate of this separation step can be fed back to the biogas stream entering the plant.

4.4.3 Technical concept of dual use of membrane technology to upgrade biomethane and biogas

Using the two-step configuration for biogas upgrading as shown in Figure 4.7 requires a matching flow rate of the permeate of module A and the feed of module B. The data shown in Figure 4.6 indicates that operation at 42 L min⁻¹ and 7.5 bar pressure difference results in a permeate stream of around 22 L min⁻¹. In order to match the feed flow rate shown in Figure 4.8 at 1.5 bar pressure difference, it is required to operate at least three identical modules. Two of them are connected in parallel whereas one serves as the second stage of the biogas upgrading plant, assuming the same type and size of the modules used. Alternatively, a module with higher surface area can be used. Membrane separation is a rate-based process, therefore the residence time of the gas inside a fibre should not be changed during the scaling of the process in order to retain the desired separation properties. Therefore, the length of the module has to be kept constant, an increase of surface area requires an increase in number of parallel fibres or modules, respectively.

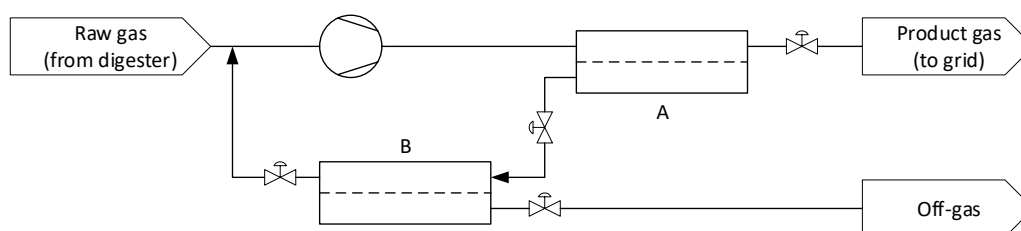


Figure 4.7: Flow diagram of the biogas upgrading process. The biogas bypasses the methanation unit and enters membrane A where a gas quality is reached, which is suitable for grid injection. The permeate of the membrane module A is fed to a second module B, where CO₂ is separated from the recycle stream and released to the atmosphere.

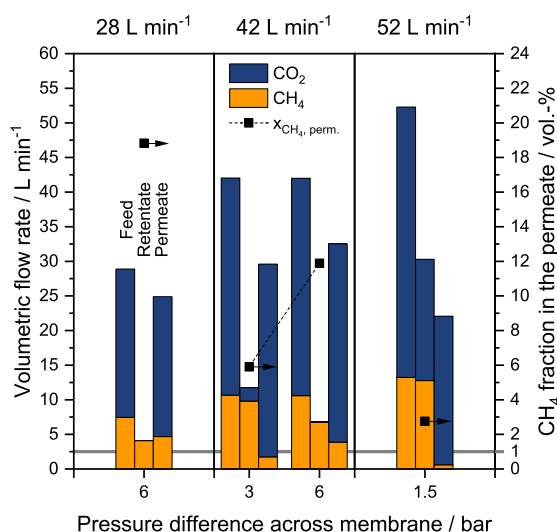


Figure 4.8: Experiments simulating the gas composition of the recycling stream (75 % CO₂ in methane). Three feed flow rates were tested at different pressure levels. The goal was to minimise the methane content in the permeate (off-gas) in order to reduce emissions.

Considering the upgrading of methanation product gas according to Figure 4.5, only the membranes of stage A are in operation. Assuming the same amount of biogas available, its CO₂-content of 40 % would be converted to the same amount of additional methane by a slightly over-stoichiometric amount of H₂. This would result in a membrane feed gas stream, which is only few 10 % higher than in the case of biogas upgrading. Therefore, biogas upgrading and methanation product gas upgrading operate in similar flow ranges, which enables the use of the same set of membrane modules.

Figure 4.9 shows a possible concept: when in biomethane upgrading mode, the interconnecting 3-way-valve is set to position 1 and the two membranes A1 and A2 remove hydrogen and CO₂ from the raw biomethane. When in biogas upgrading mode, the 3-way-valve is set to position 2. The membranes A1 and A2 are needed to remove CO₂ from the product gas, whereas membrane B is necessary to keep the methane in the recycle stream and reduce emissions. As previously described, membranes A1 and A2 could also be replaced by a module of larger surface area, but same length. With the described combinations of membrane modules, it will be possible to operate a flexible process concept as was presented in Figure 4.1.

The system presented here also provides an intrinsic back-up to the biogas upgrading by direct methanation of biogas. During failure or maintenance of the methanation unit the plant can still be operated in the biogas upgrading mode and is still able to inject methane to the grid.

In both cases, biomethane and biogas upgrading, the system should be operated in such way that the required concentration of hydrogen and CO₂ is just reached. A further increase of pressure difference leads to higher permeate flows and an increased amount of methane in

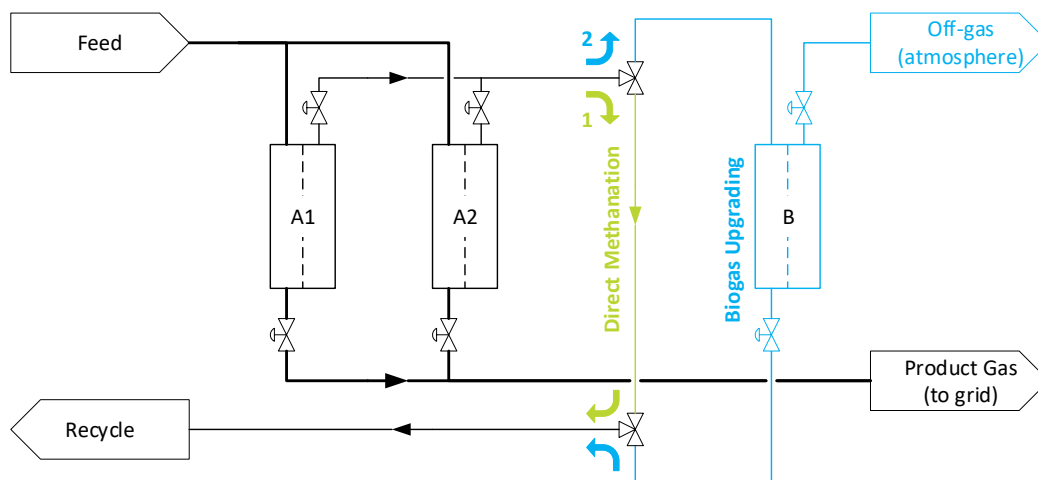


Figure 4.9: Concept for dual use of membrane modules as biogas upgrading and Power-to-Gas post upgrading units. The unit consists of at least two membrane modules in counter-current operation whose trans-membrane pressures can be regulated by valves at the permeate and retentate outlets of the modules. The interconnecting 3-way-valve serves as a switch between biomethane and biogas operation: when in position 1, modules A1 and A2 remove hydrogen from biomethane, when in position 2, the third module B retains methane in the recycle stream.

the recycling streams, which has a negative effect on the economics of the overall processes due to the larger gas stream to be recompressed.

Adjusting the pressure difference across the modules allows the compensation of ageing effects occurring to the modules due to contaminants in the gas stream or material degeneration. In case of decreasing permeability or selectivity, the desired retentate concentration can be maintained by increasing the pressure difference across the modules. Therefore, within a limited range, it is possible to restore the functionality of the upgrading system.

Using a membrane module with higher selectivity towards separation of CO_2 and H_2 from CH_4 would lead to a reduction of the residual methane concentration in the permeate and therefore also to lower recycling streams. An overall economic assessment has to be performed, which also includes material costs of the membrane module, as well as the membrane area required to maintain the current separation performance.

4.5 Conclusion

The primary goal in this chapter was to test a commercial membrane module for its feasibility as an upgrading device for raw-biomethane in a 10 – 20 kW methanation pilot plant. As a

benchmark, we used the Swiss gas injection limitations ($>96\%$ CH_4 , $<4\%$ CO_2 , $<2\%$ H_2 [25]), which define the gas quality at point of injection. This first task involved the separation of 12% hydrogen from the product gas stream in order to fulfil gas grid injection limitations and recycle unreacted hydrogen. In counter-current mode, we were able to reach the desired gas quality ($<2\%$ H_2) above 6 bar pressure difference across the membrane. In co-current mode, the limitations were not reached, but the observed trend leads to the conclusion that it will be reached at pressure differences above 9 bar. In both flow patterns, the grid injection limitations can be reached using a single membrane module, which reduces the complexity of the separation step, and therefore capital expenses.

In the second separation task presented here, the suitability of the membrane module as an upgrading device for digestion-derived biogas (40% CO_2 in CH_4) was investigated. These tests showed that the quality requirements could also be reached with a single membrane unit in counter-current operation. The retentate pressure required for this task was dependent on the total gas flow rate at the feed and increased with rising flow rate. The methane-depleted permeate stream still contained around 25% CH_4 and required further upgrading. This condition was simulated by a mixture of 25% CH_4 in CO_2 . The methane slip through the CO_2 off-gas stream must be reduced to a level acceptable for release to the atmosphere. The methane levels reached in the tests stayed around 2.8% . This value was obtained by increasing the total volumetric feed flow rate and decreasing the pressure difference across the membrane. In order to reach lower residual methane contents, a further reduction of the pressure difference or another increase of the feed flow rate is required.

We propose a concept of combining two operation modes of a biogas plant with grid injection: the separation of CO_2 from biogas, and the direct methanation of biogas using renewable hydrogen. Both processes require gas upgrading steps, which can be realised with membrane modules. The two upgrading tasks are not performed at the same time due to availability of renewable hydrogen. Therefore, the same type of membrane unit can be used for both tasks, which allows a swift change of operation mode to flexibly react to fluctuations in the energy market. By utilising synergies between the two process variants, the proposed combined process may cut down overall cost and lead to a higher yield of biogas. It furthermore increases the availability of the plant since in case of a malfunction in the methanation unit, membrane-based biogas upgrading is still available as an intrinsic back-up option. This process should make direct injection of biogas a more competitive player in the future energy system.

5 Seasonally flexible biogas upgrading: Membrane permeation model and techno-economic analysis

5.1 Introduction

On the way towards CO₂-neutrality, the future energy sector will experience a higher penetration of renewable energy carriers [156]. Especially in PtG, the intermittent nature of the electricity production causes a high number of changes in the feed gas availability to the system. Such perturbations can affect the downstream process on short time scales (hours) due to short power fluctuations caused by wind and solar energy [21, 22]. On the other hand, long-term fluctuations occur due to seasonal availability changes of the input streams [42, 157].

In the previous chapter a concept for flexible biogas upgrading was presented and demonstrated by gas separation experiments. It allows for a swift change between conventional, membrane-based biogas upgrading and biomethane production via direct methanation. This concept allows avoiding the use of electricity for PtG when it is expensive and enables a simple way to integrate flexible electricity storage into a biogas upgrading plant. It was shown that membrane upgrading technology can be a simple way to increase the operational flexibility of the overall system without the need of altering the dynamic capabilities of the reactor itself. The technical and economic feasibility of the proposed concept will be explained in this chapter.

Furthermore, the experiments in the previous chapter showed that commercial biogas upgrading membranes can serve as a hydrogen recycle unit in methanation systems in order to produce grid-compliant biomethane.

Chapter 5 is based a publication in preparation: A. Gantenbein, M. Lasser, T. J. Schildhauer, "A rate-based membrane model to simulate seasonally flexible electricity storage by Power-to-Gas and conventional biogas upgrading".

A. G. planned and performed experiments, evaluated the data, performed the process simulations and economic analyses, created all diagrams, and wrote the text. A. G. supervised the master's thesis of M. L., who contributed to the model benchmarking, supported process simulations, and data evaluation.

Process simulations to obtain cost estimates of plant designs require reliable unit models of the underlying process steps. In a PtG process, apart from the main reactor, a critical step is the membrane-based upgrading of the product gas [103]. Nevertheless, models of such commercial membrane modules are often proprietary and not available for common use.

In this chapter, a permeation model for the previously presented membrane module is developed. The model is based on the data presented in the previous chapter, as well as on new measurements.

In membrane separation processes, a trade-off between high selectivity and high permeability exists [158]. To operate an upgrading process economically, a membrane material with suitable properties has to be used. Previous investigations by Witte *et al.* [52, 103] indicated that for methanation product gas upgrading, a combination of high permeability and medium selectivities are most beneficial. It was shown that a higher selectivity allows to reach the required product gas quality faster, whereas a high permeability reduces the required membrane area and therefore the investment cost [52, 103].

A variety of approaches to model whole gas separation membranes in co- and counter-current operation are available in literature [150–154]. They are based on diffusion by Fick's Law [152–154] or on resistance by Ohm's Law [150]. Often, constant permeability factors to describe the mass flow through the membrane material for each gas component are assumed.

However, the permeability Π_i of a component i through a membrane material is strongly dependent on the pressure difference Δp applied, the temperature T in the system, and the gas composition x_i :

$$\Pi_i = f(\Delta p, T, x_i) \quad (5.1)$$

Therefore, ideal permeabilities often reported in literature do not represent well the permeability of a component in a gas mixture [52, 159, 160]. Using such ideal values in process simulation can lead to misleading size and performance estimates of the upgrading steps.

In literature, several approaches exist to estimate the permeabilities based on pressure and concentrations, of which the most prevalent is the 'dual-mode sorption, partial-immobilisation model' [147]. It assumes the permeability to be the product of solubility S_i and diffusivity D_i of a gas in the membrane polymer:

$$\Pi_i = S_i \cdot D_i \quad (5.2)$$

A similar process as in dissolution of gases in liquids is assumed: the permeating gases first dissolve on the polymer surface and secondly diffuse across the polymer material. The partial pressure difference between the high and low-pressure side of the membrane serves as the driving force. The temperature dependency of the diffusion process can be described by an Arrhenius-type approach [148]:

$$D_i = D_{i,0} \exp\left(\frac{-E_{A,D_i}}{RT}\right), \quad (5.3)$$

where E_{A,D_i} represents the activation energy and $D_{i,0}$ the pre-exponential factor, respectively.

The 'dual-mode sorption, partial-immobilisation model' describes the transport in glassy polymers below the glass transition temperature T_g . It assumes two different sorption sites to be present in the polymer: Henry-type sorption sites in the relaxed volume (concentration C_H), and Langmuir-type sorption sites in the unrelaxed part of the volume (C_L) [148, 161]. The sorption isotherm of a gas in a polymer membrane can therefore be described in the following form [161–163]:

$$C_m = C_H + C_L = S \cdot p = H \cdot p + \frac{C_{L,max} \cdot B \cdot p}{1 + B \cdot p} \quad (5.4)$$

Equation 5.4 consists of two terms: The first describes the Henry-type sorption in the polymer and contains the Henry's law constant H . The second term corresponds to a Langmuir sorption isotherm, containing the maximum sorption capacity $C_{L,max}$ and the Langmuir affinity constant B .

Extended to n components, equation 5.4 becomes [161, 163]:

$$S_i = H_i + \frac{C_{L,max,i} \cdot B_i}{1 + \sum_{j=1}^n B_j \cdot p_j} \quad (5.5)$$

This 'dual-mode sorption' model was first proposed by Barrer *et al.* [148] and has been modified by many others inter alia [162, 164, 165].

Due to the presence of two types of environments in the membrane material, also two different diffusion coefficients can be defined: D_H for the mobility in the relaxed and D_L for the diffusion in the unrelaxed volume fraction of the polymer. The flux J through the membrane can be expressed by Fick's law:

$$J = -D_H \cdot \frac{dC_H}{dx} - D_L \cdot \frac{dC_L}{dx} \quad (5.6)$$

By substituting equation 5.4 into equation 5.6, and integration across the membrane, the following expression for the permeability Π of a single component can be obtained [161]:

$$\Pi = H \cdot D_H + \frac{D_L \cdot C_{L,max} \cdot B}{1 + B \cdot p} \quad (5.7)$$

Due to the lack of performance data under real operation conditions, which can serve as a foundation for rigorous process simulations, a commercial, hollow fibre membrane module (Evonik SEPURAN[®] Green, diameter: 2 inches) was tested and characterised. Based on the obtained data, a permeability model was developed, which was included in a numerical, rate-based membrane model. This work provides new data for a commercially available membrane, determined using gas mixtures in a full membrane module. The membrane model allows a reliable simulation of biogas and Power-to-Gas-related separation problems, which enables subsequent cost analysis for a case study of seasonally flexible electricity storage by Power-to-Gas and conventional biogas upgrading.

5.2 Development of a rate-based model of a hollow fibre membrane module

In this study, a commercial, hollow-fibre membrane module was experimentally characterised for its separation performance of $H_2/CO_2/CH_4$ -based gas mixtures. Subsequently, a permeation model was proposed and its parameters fitted against the experimentally determined permeances. The model was then included in the numerical model by Makaruk *et al.* [118].

A single membrane module was installed in a TRL 5 methanation set-up (10 – 20 kW). As shown in a long-term (1000 h) field experiment, this plant can either be used for direct methanation of biogas or CO_x methanation [81]. For the current set of experiments, the pilot plant was installed on the Energy System Integration (ESI) platform at PSI, which ensured gas provision. A process flow diagram of the set-up is depicted in Figure 5.1.

5.2.1 Gas mixing and membrane test set-up

The gas mixtures required for the membrane tests were prepared by a set of mass flow controllers (MFCs) connected to gas tanks. As no reactive experiments were performed, the bubbling fluidised bed methanation reactor was bypassed. For gas mixtures exceeding a methane flow rate of 40 Lmin^{-1} , a second MFC was required. This device was originally calibrated for carbon

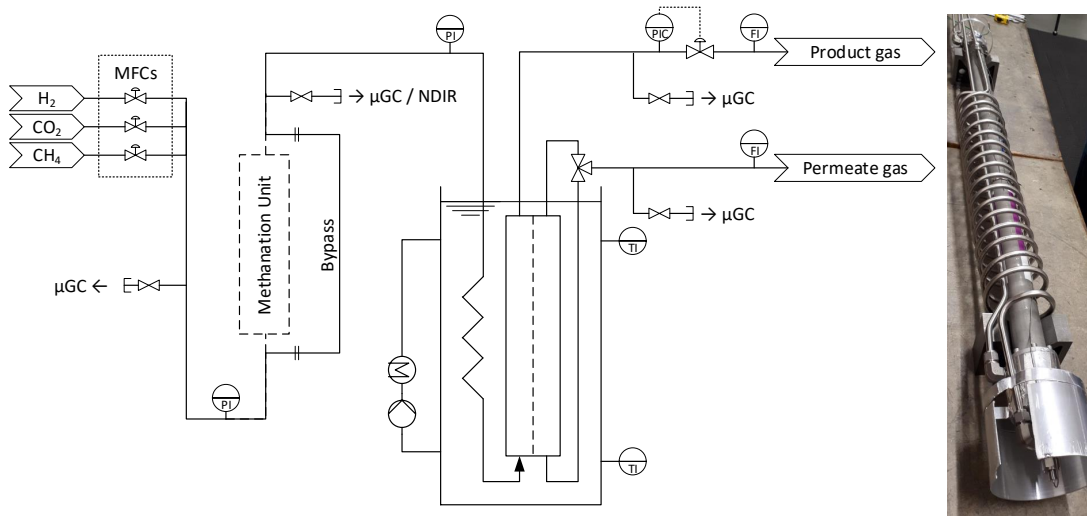


Figure 5.1: Experimental set-up for membrane characterisation experiments. Gas mixtures are prepared by a set of MFCs and fed to the membrane module (right), which was submerged in a water bath to ensure temperature control.

monoxide. We therefore corrected the flow rate by a conversion factor of 0.7637 in order to account for usage with methane gas [145, 166].

In order to provide stringent temperature control during experiments, the whole module was submerged in a heated water bath. Furthermore, a coiled length of tube was added to the module to ensure temperature equilibration in the feed stream. On the shell side, which corresponds to the permeate side of the membrane, the unit was equipped with two outlets at both ends, which allowed switching between co- and counter-current operation.

The gas composition of the inlet flow of the membrane was monitored by micro gas chromatography (μ GC, Varian CP-4900) and non-dispersive IR spectroscopy (NDIR, Siemens Ultramat 23). The composition of the permeate and retentate flows were monitored using the μ GC. We only analysed two gas streams by the μ GC at the same time, one inlet was manually switched between the feed and the permeate stream of the membrane. The retentate composition was monitored constantly. Each operating condition was maintained for at least 30 min in order to obtain stable concentration measurements and equilibrate the membrane module. At each gas sampling position, at least five subsequent concentration measurements were obtained and averaged during data evaluation. The deviation in these five measurements was always within the observed mass balance deviation of the experiment. The volumetric flow rate of the retentate was measured by a gas meter (Wohlgroth G4), whereas the permeate flow was determined using a flow meter (MesaLabs Defender 530+). The pressure of the whole system was controlled at the retentate side of the membrane by a pressure retention valve. In order to assess the pressure drop in the membrane unit, also the feed pressure was monitored. The permeate side of the membrane was kept at ambient pressure. Temperature, pressure,

volumetric flow rate and gas composition were monitored in every stream entering and leaving the membrane module, allowing us to derive molar balances for all components [166].

During evaluation of raw data, systematic deviations in the total molar mass balance were observed. A linear regression of the absolute deviation along the measured retentate flows provided us with the parameters (slope m and intercept q) for a correction function (see equation 5.8).

$$\dot{V}_{ret,corr.} = m \cdot \dot{V}_{ret,measured} + q \quad (5.8)$$

As already described in previous work [166], we associated the deviations mainly to the gas meter installed in the retentate stream of the membrane. The use of the correction function can be justified by a lower measurement limit of the gas meter and a systematic deviation depending on the gas flow rate run through the device. Applying this correction allowed to close the total molar balance for most of the data points within a margin of $\pm 5\%$ of the feed flow rate, up to $\pm 10\%$ for a few cases.

All indicated volumetric flow rates refer to standard conditions at 1 atm and 0 °C (normal temperature and pressure, NTP), commonly used in gas industry according to DIN 1343 [121].

5.2.2 Experiments for membrane characterisation

For the characterisation of the membrane model, a set of gas separation experiments was performed in addition to previous work [166]. In the current experiments, the gas composition, pressure difference through the membrane, feed gas flow rate, as well as co- and counter-current operation was varied. Furthermore, experiments using ternary gas mixtures were performed using hydrogen and carbon dioxide in methane. In each experiment, a different flow rate, pressure, and concentration regime was tested.

The range of conditions tested during this work was defined by concentration ranges expected during membrane-based biogas upgrading and methanation product gas upgrading. The concentrations were furthermore extended to the limits given by the technical installations of the plant. The analysis included binary and ternary gas mixtures, as well as a set of pure gas measurements by Witte *et al.* [52]. The conditions set for the characterisation experiments are summarised in the tables of the following section. All experiments were performed at 40 °C. This temperature ensured a high permeability of the membrane module with a somewhat reduced selectivity [52, 166], which ensures a high gas throughput in practical applications.

All nine single gas experiments, which were within a molar balance deviation of $\pm 5\%$ were used for the parameter estimation. From the binary experiments performed, 83 data points fulfilled the balance requirement. From this data set, 56 data points were used in the parameter

estimation, as no partial pressure equilibrium was reached. The number of ternary gas mixtures tested amounted to 27, whereof 15 were used for the parameter estimation. In total, 119 data points were evaluated, of which 80 were used for the permeance parameter estimation.

All experimental ranges summarised in Table 5.1 refer to the performed set of experiments, including the data sets, which were excluded before the parameter estimation shown in the appendix.

Series 1: Initial characterisation experiments using single gases and binary mixtures of CO₂ and H₂ in methane. The experiments were performed in co- and counter-current configuration, if not otherwise indicated.

Series 2: The experiments from series 1 were partially repeated with extended flow rate. All experiments were performed in co-current configuration.

Series 3: For this set of experiments, we further extended the maximum flow rate by using a secondary MFC for methane provision, as described in section 5.2.1. The flow rate increase was necessary to obtain a larger number of data points in the non-equilibrium range.

Series 4: Simulation of the behaviour of the second membrane stage in membrane upgrading mode. For this set of experiments, the conditions in the second membrane stage were simulated according to the bi-seasonal upgrading concept.

Part of this data was already published in Chapter 4 and previous work [166]. Detailed ranges of conditions can be found in the Appendix A.

5.2.3 Permeability model

Previous reports by Witte *et al.* [52] showed a high discrepancy between membrane permeances from literature, which were determined under ideal laboratory conditions using pure gases, and permeances using gas mixtures in a real membrane module and own experiments. It is therefore not advisable to use ideal gas permeances and selectivities for process simulations and subsequent techno-economic analyses, as it may under-estimate the membrane area required for separation. We therefore decided to implement a sub-model for gas permeance in the membrane model, in order to represent the pressure and composition dependency of the permeance of the gas components.

A standard model to describe gas permeance through dense polymer membranes is the 'dual-mode sorption, partial immobilisation' model (see Chapter 5.1). David *et al.* [149] used it to describe the permeation of H₂/CO/N₂/CO₂ gas mixtures through a polymer membrane (equation 5.9):

$$P_i = A_{1i} + \frac{A_{2i}}{1 + \sum_{j=1}^N b_j f_j} \quad (5.9)$$

	Concentration range	Feed flow rate L/min	Retentate pressure bar
Series 1: Single gas experiments			
H ₂ (co only)	100 %	90	1.5
CO ₂ (co only)	100 %	40	2
CH ₄ (co & cc)	100 %	20 – 30	4 – 10
Series 1: Binary gas experiments (co- & counter-current)			
H ₂ in CH ₄	3 – 30 %	41 – 43	4 – 10
CO ₂ in CH ₄	3 – 30 %	36 – 43	4 – 10
Series 2: Binary gas experiments (co-current)			
H ₂ in CH ₄	3 – 30 %	40 – 56	4 – 9
CO ₂ in CH ₄	3 – 30 %	40 – 56	4 – 9
Series 2: Ternary gas experiments (co-current)			
H ₂ and CO ₂ in CH ₄	3 – 6 % CO ₂ 12 – 30 % H ₂	46 – 61	4 – 9
Series 3: Binary gas experiments (co- & counter-current)			
H ₂ in CH ₄	3 – 30 %	39 – 105	4 – 6
CO ₂ in CH ₄	3 – 30 %	76 – 106	4 – 7
Series 3: Ternary gas experiments			
H ₂ and CO ₂ in CH ₄ (co-current)	3 – 6 % CO ₂ 12 – 30 % H ₂	40 – 115	4 – 5.5
H ₂ and CO ₂ in CH ₄ (counter-current)	3 – 6 % CO ₂ 12 – 30 % H ₂	45 – 61	4 – 8
Series 4: Binary gas experiments (counter-current)			
H ₂ in CH ₄	40 %	39 – 105	4 – 6
CO ₂ in CH ₄	12 – 80 %	76 – 106	2.2 – 9

Table 5.1: Experimental conditions used for the membrane characterisation

A permeance P_i is obtained for each component i of a mixture of N components as a function of the fugacity f . For each species i , three parameters are required: A_{1i} , A_{2i} and the affinity b_i . In the work of David *et al.* these parameters were obtained by fitting experimental data [149].

The current work focuses on a similar approach. A mixture of three main components (H₂, CO₂ and CH₄) requires the fitting of 9 parameters to obtain the permeances for each component. Due to the scarcity of the underlying data set, we decided to introduce a new permeation model based on a Langmuir-Hinshelwood-type equation, which is commonly used in chemical kinetics. This new model represents a simplification of the 'dual-mode sorption, partial immobilisation' model by neglecting the parameter A_{1i} , which contains the gas mobility through the equilibrium free volume of the polymer [149].

The new permeability model is shown in equation 5.10:

$$P_i = \frac{K_{1,i}}{1 + K_{H_2} \Delta p_{ln,H_2} + K_{CO_2} \Delta p_{ln,CO_2} + K_{CH_4} \Delta p_{ln,CH_4}} \quad (5.10)$$

This way, the number of parameters was reduced to two per component. The parameter $K_{1,i}$ can be regarded as a lumped parameter, accounting for sorption on the polymer and subsequent diffusion through it, similar to the work presented by David *et al.* [149]. Instead of partial fugacities, partial pressures p_i are used, as in this application only moderate pressures are present (up to 10 bar). Therefore, the non-ideal behaviour of gases is not considered and the activity coefficients are assumed to be unity.

From the characterisation experiments, only integral measurements were available, *i.e.* the concentration profiles along the membrane fibres are unknown. The driving force for the gas separation is the partial pressure difference on either side of the membrane. As the local conditions are unknown, an average partial pressure difference had to be calculated. Due to the similarity between heat and mass transfer, a methodology known from heat exchangers was adapted as proposed by Pettersen *et al.* [151], see equation 5.11:

$$\Delta p_{ln,i} = \frac{\Delta p_{i,max} - \Delta p_{i,min}}{\ln \frac{\Delta p_{i,max}}{\Delta p_{i,min}}} \quad (5.11)$$

In counter-current operation, $\Delta p_{i,max}$ refers to the partial pressure difference between the feed of the membrane and the permeate. $\Delta p_{i,min}$ is the partial pressure difference between the retentate outlet and the closed end of the permeate. At this position, the partial pressures are assumed to be zero, therefore, $\Delta p_{i,min}$ equals the partial pressures of the retentate streams. In case of co-current operation, the retentate flow is reversed and $\Delta p_{i,max}$ refers to the partial pressure difference between the feed and the closed end of the membrane. $\Delta p_{i,min}$ then becomes the partial pressure difference between the retentate and the permeate stream.

After correction of the raw data using formula 5.8, the data was filtered prior to parameter estimation. This way, all measurements were removed from the dataset where the equilibrium partial pressure was reached for any component. These data points were identified by $\Delta p_{i,min}$ below zero. Furthermore, all data points were removed where the total molar balance deviation of $\pm 5\%$ of the feed flow rate was exceeded. The data sets of co- and counter-current experiments were combined, as the flow configuration is assumed to have no influence on the local permeance of the membrane material. The configuration of the membrane flows is already accounted for by using equation 5.11 in the respective form.

The parameter estimation was performed by a least-squares minimisation using the *lsqnonlin* function in Matlab. For the optimisation, the following equation 5.12 was minimised:

$$0 = \frac{\dot{n}_{p,exp,i}}{A_{MEM}} - \frac{\sum_{i=H_2,CO_2,CH_4} K_{1,i} \cdot \Delta p_{ln,i} \cdot sel_i}{1 + K_{H_2} \Delta p_{ln,H_2} + K_{CO_2} \Delta p_{ln,CO_2} + K_{CH_4} \Delta p_{ln,CH_4}} \quad (5.12)$$

For every data point consisting of a pressure and concentration setting, three permeate flow rates – one for each component – are fitted. Therefore, in order to be used in the mentioned subroutine, the values obtained from equation 5.12 had to be converted in a single-value vector using a selection variable sel_i during parameter estimation. This selection variable was set to 1 according to for which species the permeate stream was calculated.

Therefore, for each component i the parameters $K_{1,i}$ and K_i were simultaneously fitted to experimentally determined permeate flow rates. The results are shown in Table 5.2.

Parameter	Value	Unit
K_{1,H_2}	$92.7 \cdot 10^{-5}$	$\text{mol bar}^{-1} \text{m}^{-2} \text{s}^{-1}$
K_{1,CO_2}	$125.3 \cdot 10^{-5}$	$\text{mol bar}^{-1} \text{m}^{-2} \text{s}^{-1}$
K_{1,CH_4}	$5.5 \cdot 10^{-5}$	$\text{mol bar}^{-1} \text{m}^{-2} \text{s}^{-1}$
K_{H_2}	-0.67	bar^{-1}
K_{CO_2}	0.13	bar^{-1}
K_{CH_4}	0.07	bar^{-1}

Table 5.2: Parameters obtained from the fit of the permeance model to the experimental data.

The parity graphs are shown in Figure 5.2. The permeate flows predicted by the model are shown in comparison to the experimentally determined values. For methane and CO_2 , a satisfactory agreement was achieved. Due to the limited data available for hydrogen, especially in an intermediate concentration range, the regression is less precise. Nevertheless, it is sufficient to predict the behaviour of the membrane module.

The methanation reaction produces a large amount of water, which has to be removed from the product gas stream prior to grid injection. In the process chains considered in this work, a simple condensation is used. In commercial scale plants, cooling water or air cooling is often the most economical way to provide cooling duty to such units, which allow only a cooling to relatively high temperatures. We therefore assumed a condenser temperature of 40 °C in our processes. Since the dew point in the product gas is not sufficiently low for grid injection, a part of the remaining moisture also enters the membrane upgrading unit. SEPURAN®-type membranes are also permeable for water [51] and can therefore be used to remove such remaining moisture.

According to the manufacturer [51], the permeance for water is at least in the same range as hydrogen. We therefore included the water permeance in the membrane model by adding a term to equation 5.10 representing water. The coefficients K_{1,H_2O} and K_{H_2O} were set identical to the ones of hydrogen.

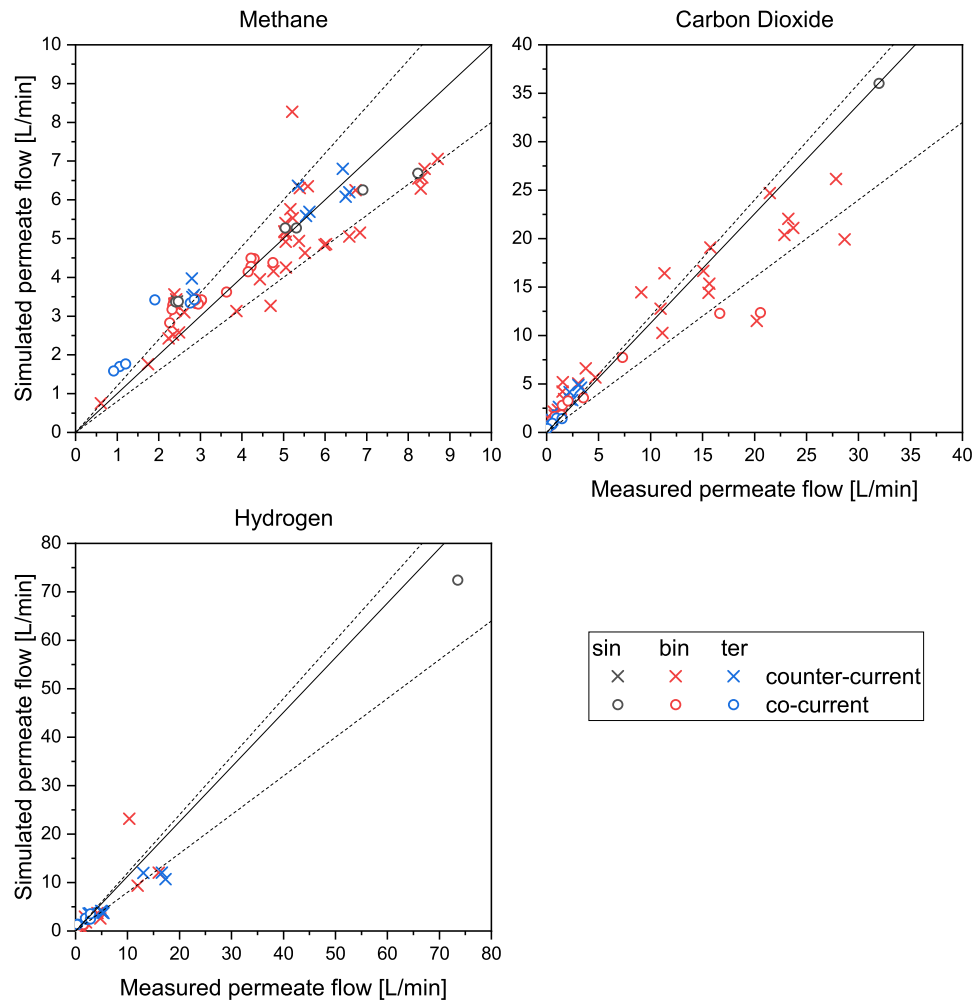


Figure 5.2: Parity plot for each component, showing the model prediction vs. the component's flow rate measured in the experiment. The dashed lines indicate the $\pm 20\%$ deviation from the parity line (solid). The colour coding refers to the different types of experiments, which were performed using pure gases (sin), binary (bin) and ternary (ter) gas mixtures.

Membrane model

The membrane model used is based on a rate-based counter-current algorithm developed by Makaruk and Harasek [118]. The model was implemented in the Matlab-based process simulation environment, which was used in previous work [167] and Chapter 3.

The correct working of the membrane model was verified by comparison with permeance and simulation data published by Makaruk and Harasek [118] (not shown here).

Benchmarking of the membrane model with data of an existing membrane upgrading plant

To investigate the validity of the membrane model presented in this work for the case of biogas upgrading, a comparison was made with an existing membrane upgrading plant in Reinach AG (Switzerland), for which a detailed report exists [168]. The modules used in this plant originate from the same manufacturer and are of the same type as the one used in this work, we therefore assume that they are made of similar material and that the assumptions made in the model are applicable. Hence, it is assumed, that a direct comparison of the two cases is possible.

The demonstration plant makes use of the patented, three-stage upgrading process from Evonik Fibres GmbH (Germany) [169], as shown in Figure 5.3. Two detailed process flow diagrams are given, where flow rates, pressures and methane concentrations are indicated. According to the report, this data does not represent directly measured data, it corresponds to simulated values obtained from a proprietary software by the manufacturer of the membrane modules. One process state was simulated using the membrane model developed in our work (see Table 5.3).

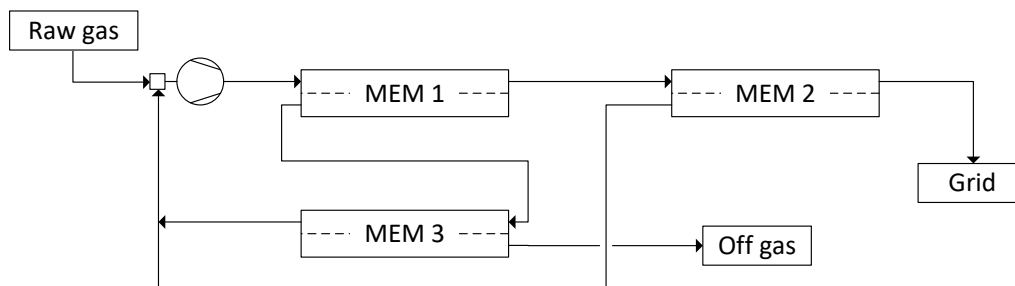


Figure 5.3: Membrane configuration used by the upgrading process at the biogas plant in Reinach AG, Switzerland [168].

According to the report, the first stage consists of a single module, stages 2 and 3 of two modules each. The modules used in this plant have twice the diameter of the module tested in this work. Therefore, the membrane surface area available is assumed to be four times larger.

Furthermore, it is stated that the membrane modules are of a newer type with higher capacity. We therefore assumed a factor 1.5 in membrane area to account for this performance increase. Therefore, the separation area used for the simulation of this upgrading plant amounts to 97.68 m^2 per module.

The volumetric flow rates and the CH_4 content of the off gas and product gas streams are simulated using the newly developed membrane model, as well as based on literature data for the polymer *Matrimid* [119]. The results for this simulation are then compared to the data presented for the plant in Reinach AG.

	Value	Unit
System pressure	17.5	bar
Biogas feed	48.73	m^3/h
CH_4 in feed	62.8	vol.-%
Permeate pressure membrane 1	2.2	bar
Permeate pressure membrane 2	1.05	bar
Permeate pressure membrane 3	1	bar

Table 5.3: Input parameters for the simulation of the Reinach AG biogas upgrading plant. This process is based on a three-stage upgrading process.

The results of the simulation of an operating point of the biogas upgrading plant in Reinach AG are shown in Figure 5.4. This data is compared to simulations based on the membrane model introduced in the current work. The output streams (*i.e.* the CH_4 -rich product gas stream and the CO_2 -rich off gas stream) simulated with the newly developed membrane model show good agreement with the values reported by Müller *et al.* [168]. The grid and off gas volumetric flow showed a deviation of 0.1 % and 1.3 %, respectively. The deviation of the CH_4 concentration in the grid stream is 0.3 %. The simulated off gas stream shows a relatively high deviation for the reported CH_4 concentration, but it is still close to the self-set limit of 1 %. This concentration limit is set, as the off gas is released to the atmosphere, and therefore a low CH_4 concentration is desired, but it does not refer to an official regulation.

When the upgrading plant is simulated using the literature data for the *Matrimid* material (see Zhang *et al.* [119]), the deviations for the volumetric flow to the grid (6.0 %) and the volumetric flow of the off gas stream (11 %), as well as the CH_4 concentration in the grid stream are all higher than in the Evonik-case. The CH_4 concentration in the off gas is even 13.2x higher than the reported value. Compared to the newly developed permeation model, the values are clearly higher. Especially in the off gas stream the CH_4 concentration is increased and in contrast to the new permeation model, the concentration exceeds the 1 % margin clearly. The comparison leads to the conclusion, that biogas upgrading plant in Reinach AG is better described by the permeance model developed in this work than by literature data from the material *Matrimid*. We therefore conclude, that the membrane model in combination with the newly developed permeability sub-model gives a realistic representation of the behaviour of the Evonik SEPURAN[®] membrane module.

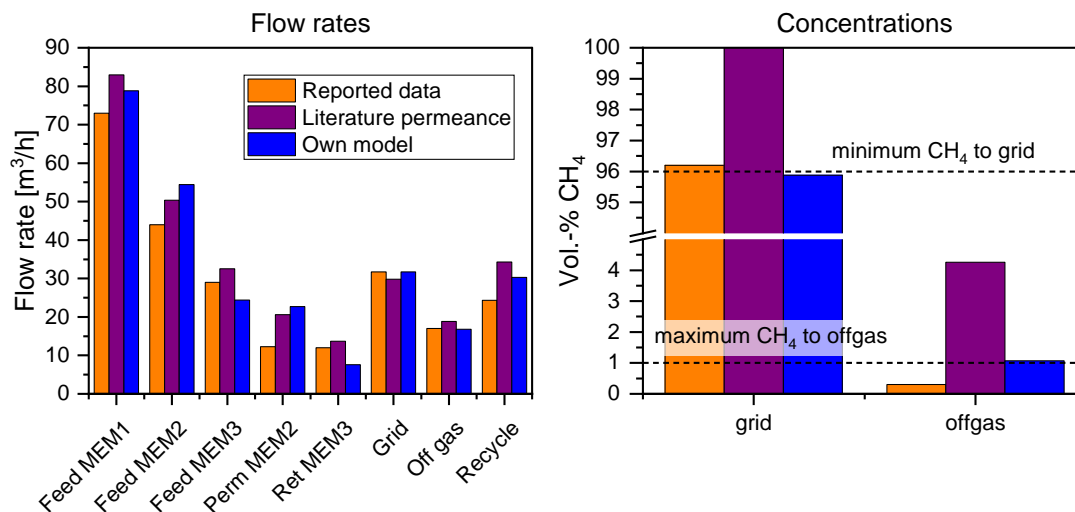


Figure 5.4: Comparison between reported flow rates (left) and molar fractions (right) at the Reinach AG biogas upgrading plant (Reported data) and two simulations, based on the newly developed permeability model of the Evonik membrane module (Own model), and literature data from the *Matrimid* polymer (Literature permeance).

Regarding the internal volumetric flows in the plant, the highest deviation can be seen in the permeate of the second membrane (ca. 84 %), since the first membrane stage insufficiently separates CH₄ and CO₂. The reported data and the simulated retentate of membrane one deviate by almost 24 %. Because of the retentate of membrane two (product gas stream) being almost identical in the report and in our simulation, the volumetric flow in the permeate of membrane two has to be higher in the simulation. This leads to an overestimation of the recycle flow and a larger feed of membrane one in our calculations. This can possibly be explained by the different development stage of the membrane modules used, which could not be covered by assuming a capacity factor 1.5. Furthermore, the model developed in this study is based on experiments performed with a module produced in 2012, whereas the modules in Reinach AG and the simulation from the same supplier correspond to a newer type of polymer (2015) and therefore experienced less ageing effects than the module tested in our work.

The simulation with our model suggests that in the first separation step, the permeation of CO₂ and CH₄ is lower, leading to a lower CO₂ concentration in the second membrane step, resulting in a good agreement with the reported grid stream.

The verification of the rate-based membrane model is considered successful. The deviation of the volumetric flow rates of the simulations and the reported data never exceeded 37 %. A better agreement of the results could be achieved using the newly developed permeance model than with literature data of the polymer type *Matrimid*.

5.3 Process design and application of the membrane model

Three process chains for direct methanation of biogas were simulated in this work. All of them allow a fast switching between membrane-based biogas upgrading (*i.e.* CO₂ separation) and power-to-gas functionality, according to the concept proposed in previous work [166]. The goal of this concept is to provide grid-quality biomethane [25] over the whole year while avoiding negative impact on the process economics by high electricity cost. This can be achieved by bypassing the methanation system and the addition of a second membrane stage, which removes excess CO₂ from the system. An overview on the concept can be found in Figure 5.5. All cases are based on a pre-cleaned biogas stream of 200 m³/h with a CO₂ content of 40 % in methane.

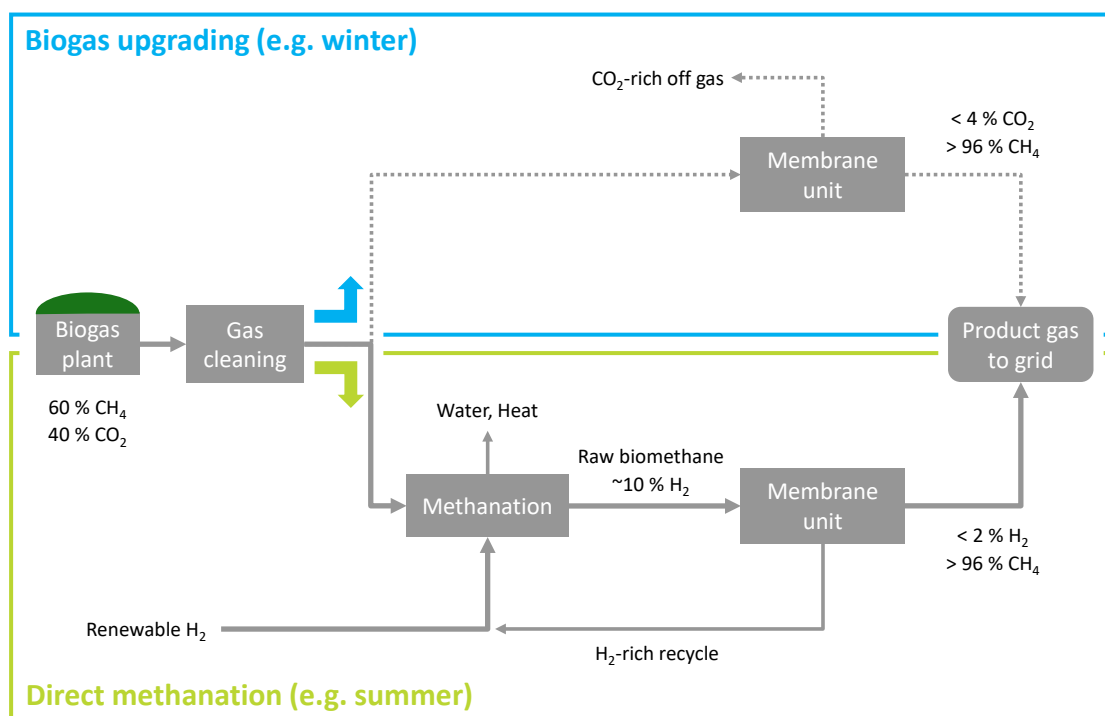


Figure 5.5: Concept for seasonally flexible upgrading of biogas, using either methanation (PtG-mode, bottom) or conventional membrane-based upgrading (top) [166].

5.3.1 Case PtG1: Direct methanation of biogas with subsequent gas upgrading

This case refers to the classical biogas-based power-to-gas process chain, originating in an all-year-round operation of the methanation reactor, as shown in the process flow diagram in Figure 5.6. The raw gas coming from the digester unit is pressurised to the desired system pressure and mixed with hydrogen prior to being fed to the reactor system. The product gas passes through a condenser unit and is subsequently directed to the membrane upgrading unit. This way, the focus of the process design lies in the removal of excess hydrogen from the raw biomethane for subsequent grid injection. The resulting recycle stream is merged with the

feed gas and recompressed. The process conditions used in the simulation are summarised in Table 5.4.

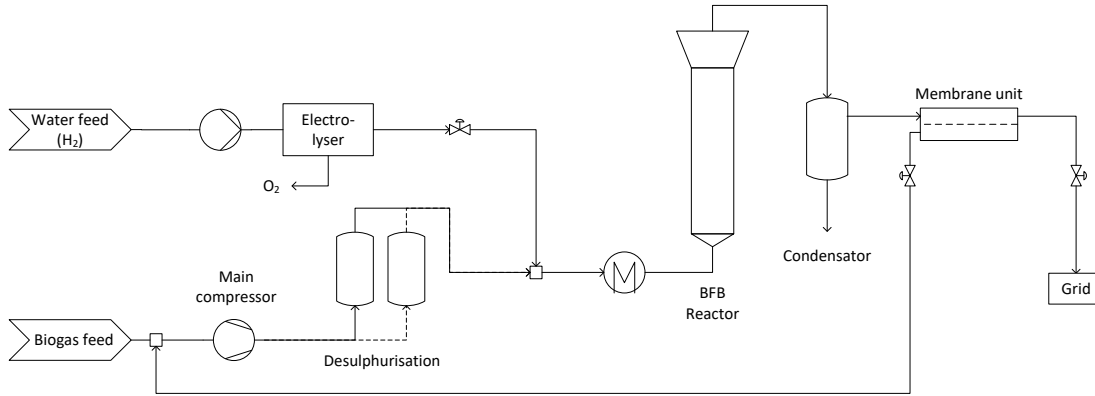


Figure 5.6: Process flow diagram of process *PtG1*. The raw biogas is mixed with the appropriate amount of H_2 (c.f. Table 5.4) and methanised in the reactor. The membrane unit separates excess H_2 from the product gas stream and produces a recycle stream back to the main compressor.

5.3.2 Case *PtG2-2c*: Removal of CO_2 by membrane separation and subsequent methanation

In this process chain (*PtG2-2c*), the main gas stream is fed directly to the first stage of the two-stage membrane upgrading system, where grid-compliant biomethane is produced and injected to the distribution network. This way, a large part of the methane is removed from the system and is directly injected to the grid. The CO_2 -rich permeate is mixed with the appropriate amount of hydrogen and fed to the methanation system. As the permeate side of the membrane is kept at a pressure of 1 bar, a second compressor is required to operate the methanation at an optimal pressure of approximately 6 bar. Due to the initial separation of most of the methane, the burden to the reactor is lowered, which allows a reduction of equipment size.

This process version corresponds to a retrofitting case where an existing membrane-based biogas plant is equipped with flexible PtG functionality. Furthermore, the product gas stream leaves the system at the pressure level defined by the main compressor.

5.3.3 Case *PtG2-1c*: Membrane separation and subsequent methanation without recompression

This process represents a modification of case *PtG2-2c* as shown in Figure 5.7, with only a single compressor considered (*PtG2-1c*). The main biogas stream is directed to the membrane upgrading unit and a large quantity of the methane injected directly to the grid. Other than in

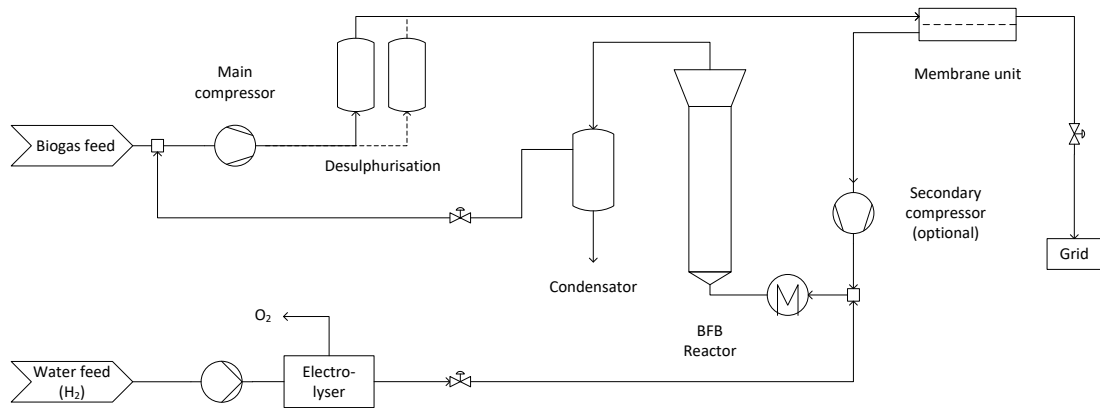


Figure 5.7: Process flow diagram of the options *PtG2-1c* and *PtG2-2c*. The secondary compressor is optional and only considered in option *PtG2-2c*.

case *PtG2-2c*, the permeate stream is not recompressed and directly mixed with hydrogen and fed to the methanation unit. This requires a higher system pressure at the retentate side of the membrane.

The goal of considering this process is to see whether it is beneficial to remove the secondary compressor to rather increase the duty of the main compressor. An operational margin is required to reliably operate the methanation reactor. It is therefore required to maintain a minimum operation pressure to adapt to fluctuating gas flow rates and compositions. The reactor pressure was therefore set to 4 bar.

5.3.4 Case BG: Membrane-based biogas upgrading

According to the proposed flexible concept, when the plant is not in power-to-gas operation (e.g. “winter” mode), the process should be switched to conventional, membrane-based upgrading. This option was simulated by a simple process containing a main compressor and a two-stage membrane unit, as shown in process flow diagram Figure 5.8. The two-stage set-up was chosen as a simple, working example for a biogas upgrading unit. Nevertheless, it can also be replaced by an existing design containing a different membrane configuration (c.f. section 5.2.3).

During process simulations we observed, that this biogas upgrading case requires more membrane area than hydrogen recycle in PtG operation. Therefore, the membrane upgrading case defines dimensioning of the membrane upgrading unit. The system pressure was set to 15 bar and the permeate pressure of the first stage to 3 bar. As seen in the process diagram, this pressure level corresponds to the feed pressure of the membrane stage two as well as the pressure in the recycle stream. The permeate of the membrane stage two is rich in CO₂ and is released as off gas to the atmosphere or other processes requiring a clean CO₂ stream.

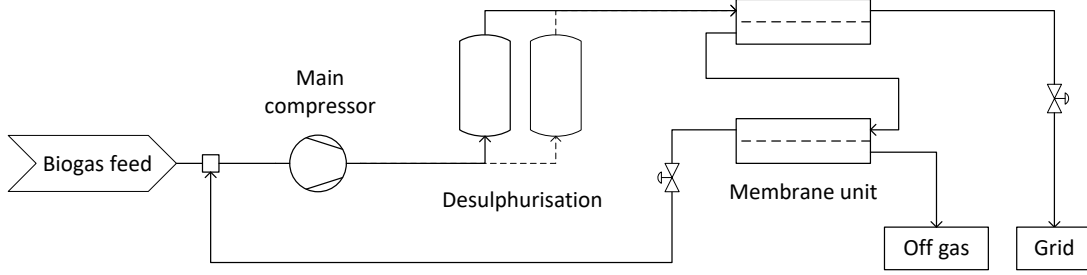


Figure 5.8: Process flow diagram of the 2-stage conventional biogas upgrading process, referred to as “BG”. The first membrane stage provides grid-ready biomethane to the grid. In the second membrane stage, CO₂ is separated from the recycle stream and removed from the process as off gas.

Parameter	Unit	BG	PtG1	PtG2-2c	PtG2-1c
System pressure	bar	15	12	10	20
Permeate pressure, stage 1	bar	3	2	1	4
Permeate pressure, stage 2	bar	1	n/a	n/a	n/a
Pressure in the methanation reactor	bar	n/a	12	6	4
Reactor temperature	°C	n/a	360	360	360

Table 5.4: Main process conditions applied in the simulation.

5.3.5 Combination of the processes

In this work, we want to point out synergies between direct methanation-based and membrane-based biogas upgrading. We therefore combined the process options and excluded duplicate units from further evaluations, by considering only the more expensive unit. Thus, the membrane-based and the *PtG*-based upgrading processes are simulated as two separate processes. From the total annual operation time, a share is assigned to be operation hours in *PtG* operation. The remaining time is assumed to be membrane-based biogas upgrading. The procedural combination of the *BG* and *PtG* processes is performed by combination of investment and operation cost (OPEX) according to operation hours during the year as shown in Table 5.5. The expenses for labour and maintenance (O&M) are calculated as a percentage of the total investment cost. For the electrolyser, they are assumed to be 1.5 % of the C_{inv} , as no moving parts are present. For the rest of the equipment, an addition of 5 % is assumed.

The combined processes generally result in a higher investment cost than the underlying non-flexible upgrading processes. The maximum biomethane production is limited by the underlying all-year operating *PtG* process. Therefore, no additional biomethane can be obtained with the flexible process, which results in higher specific production cost of the combined processes if a constant average electricity price is assumed. This additional cost

	Investment cost C_{inv}	OPEX
Raw biogas	n/a	$\text{sum}(c_{BG}, c_{PtG})$
H ₂ -path (incl. electrolysis)	$\max(c_{BG}, c_{PtG})$	c_{PtG}
Reactor	c_{PtG}	c_{PtG}
Main compressor	$\max(c_{BG}, c_{PtG})$	$\text{sum}(c_{BG}, c_{PtG})$
Secondary compressor	$\max(c_{BG}, c_{PtG})$	$\text{sum}(c_{BG}, c_{PtG})$
Membrane stage 1	$\max(c_{BG}, c_{PtG})$	$\max(c_{BG}, c_{PtG})$
Membrane stage 2	c_{PtG}	c_{PtG}
Desulphurisation	$\max(c_{BG}, c_{PtG})$	$\text{sum}(c_{BG}, c_{PtG})$
Supporting units	$\max(c_{BG}, c_{PtG})$	$\text{sum}(c_{BG}, c_{PtG})$
Heat exchanger equipment	$\max(c_{BG}, c_{PtG})$	c_{PtG}
O&M (electrolyser)	n/a	calculated from C_{inv}
O&M	n/a	calculated from C_{inv}

Table 5.5: Cost calculation of flexible PtG processes, based on estimated expenses of all-year conventional and all-year PtG-based biogas upgrading. The total operation time and operation cost is split into phases where the PtG-part of the plant is active (*PtG*) and where the membrane-based upgrading is active (*BG*). The combination of both phases result in the flexible process. The values c_{BG} and c_{PtG} refer to the respective investment or operation cost of the underlying process.

can be regarded as penalty for increased flexibility, as it originates – compared to the *PtG* case – from additional investments due to a larger membrane upgrading unit and thus additional investment cost for the biogas case.

In order to have a comparison between the combined processes (PtG/upgrading) with seasonal flexibility and a pure PtG process, which operates only part of the year due to seasonal variation of electricity prices, we included such a process in the analysis. This simplified process is based on the assumption of a *PtG1* process, which is only operated a part of the year. During the remaining time, the raw biogas still has to be processed, as it cannot be stored for longer time. Instead of membrane-based upgrading, it is flared. Therefore, the raw biogas still generates a cost throughout the year, but no additional methane is produced. Except for the raw gas cost, the cost structure of this process only consists of the cost of the underlying *PtG1* process without investments for additional flexibility.

In addition, the heat from flaring may be valorised. Therefore, also the revenues from the respective heat sales were considered in the calculation of the production cost, based on a heat value of 4 €-ct./kWh. Such a heat usage can be a direct use by an industrial combustion process, where the raw biogas can be added to the feed gas. Alternatively, the gas can be burned on site in order to heat a high temperature heat storage, which facilitates the start-up of the methanation reactor.

As a further option, the valorisation of CO₂ is considered. Since the flexible process options allow for an intrinsic CO₂ separation, this product gas stream can be sold for further use

or sequestration of clean CO₂. It therefore generates another income for the flexible biogas upgrading.

5.3.6 Unit models

The process unit of the methanation reactor was simulated using a rate-based reactor model of bubbling fluidised bed methanation. This model was already used in previous studies, described in detail there [103, 167, 170].

For membrane separation steps, the model developed in this work was applied.

Auxiliary process units were simulated using short-cut models, based on correlations, as used in previous work [103, 167].

For the electrolyser unit a specific electricity consumption of 4.6 kWh/m³ H₂ (273.15 K, 1 atm) was used, an average value representing alkaline and PEM-technology [90]. This value corresponds to a LHV-based efficiency of 65 %.

The raw gas is assumed to contain an inlet concentration of 50 ppm H₂S. The sizing of the sorption vessels is based on a conservative maximum load of 7 wt.-% H₂S on the sorbent. Further calculations are based on supplier's information of the commercial sorbent SulfaTrap R7 [37].

Pumps and compressors are based on isentropic correlations, with an assumed electrical efficiency of 0.8.

The sizing of heat exchanger equipment was based on correlations for heat transfer coefficients for different systems [120]. The exchangers are assumed to be shell and tube systems in counter-current operation.

5.3.7 Economic data and assumptions for process modelling

The data used for electricity cost are obtained from the European Electricity Exchange (EEX) [171], which are available in 1 h resolution for the past years. The data sets from the years 2007 to 2019 were used in order to obtain a representative depiction of the Swiss electricity market during the past years. Although data for 2020 is available, we excluded this year from the evaluation due to the pandemic situation and its subsequent non-representative character.

For each year, the data sets were sorted by ascending electricity prices to obtain a distribution of electricity cost along the operation hours of the year. Along this distribution curve, a cumulative average was determined, which corresponds to the average electricity price at a certain cheapest number of operation hours per year. Additional hours of leap years were removed in the centre of this distribution curve, in order to obtain a uniform number of 8760 hours per year. The distribution curves of all considered years were averaged in order to obtain a mean average electricity price per operation time per year. As an example, the

cost distribution over the year 2018 is shown in Figure 5.9, along with the cumulative average electricity cost, obtained as average from the whole time period.

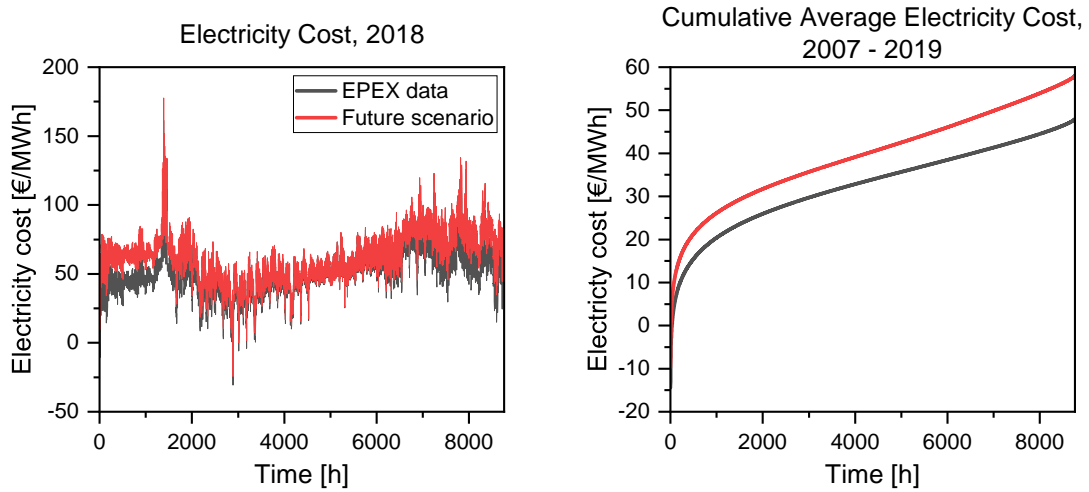


Figure 5.9: Left: Electricity cost along the year 2018, as historical data and with the hypothetical future scenario, including a solar radiation profile. Even in the historical data, a higher electricity price during winter months can be seen. This effect is more pronounced when a solar profile is added. The right side shows the cumulative average electricity cost, as an average over the years 2007 to 2019.

This data is then used as a basis to analyse the sensitivity of the considered processes towards operation hours in power-to-gas mode.

In the current electricity generation portfolio of Switzerland, the influence of new, fluctuating renewable energies such as photovoltaics and wind energy is well below 5 % of total electricity generation [172]. Therefore, we assume their influence on current electrical energy cost is negligible.

The future energy system of Switzerland is expected to have a larger share of renewable energy carriers included [8], especially wind and solar power. If these renewable electricity sources reach a high market penetration, they can impose high load fluctuations on the electricity grid. If storage technologies are not capable of absorbing excess load or other power plants cannot compensate shortages adequately, these fluctuations also affect the electricity cost distribution.

We therefore implemented a simplified prediction of the possible future electricity cost. We assumed that solar power is available according to the solar irradiation profile. We therefore used the climatological data of the Zurich Airport, which is located in the Swiss Plateau region, provided by the national weather service [173]. We assumed that the electricity prices are inversely proportional to the solar irradiance per month I_{solar} . The solar profile was therefore normalised, inverted and added to the electricity cost distribution according to equation 5.13.

$$C_{future,Solar} = C_{current} + \frac{\max(I_{solar})}{I_{solar}} \cdot \bar{C}_{current} \cdot 0.5 \quad (5.13)$$

This estimate is based on the assumption that 50 % of the long-term average electricity cost $\bar{C}_{current}$ is added to the current electricity price $C_{current}$, at maximum. It is furthermore assumed that very low or negative electricity prices do not occur in higher frequency, as low energy costs foster the demand from storage utilities or other end users. This increased demand will form a support to energy price and prevent the formation of negative electricity prices.

The cost calculations were performed as described in previous work [102, 167] and based on cost assumptions explained in Chapter 3.

In each process chain, a hydrogen buffer tank with a capacity of 12 h is considered. The investment cost for this unit is assumed to be 50 €/m³_{H₂} (at normal conditions).

5.4 Results and discussion

5.4.1 Process simulations

Membrane-based biogas upgrading

All considered processes were optimised to produce a grid-ready biomethane. In a first step, the membrane-based biogas upgrading was analysed and the number of membrane modules adapted such that grid injection limitations were fulfilled. Furthermore, the CO₂-rich permeate stream from the second membrane stage was supposed to contain less than 1 % of methane. This common limit was set to account for the higher global warming potential of methane compared to CO₂ and the subsequent negative impacts of methane emissions on the overall eco-balance of the plant.

Process simulations for 200 m³/h raw biogas showed that grid injection and off-gas limits are fulfilled using 48 4-inch modules in the first membrane stage and eight modules in the second stage. The membrane in the second stage has to be operated at high flow rate and low pressure difference to avoid an increased CH₄-slip, as the relatively low selectivity of CO₂ to CH₄ limits the CO₂ removal capacity. Furthermore, a large recycle stream is produced, which is more than two times larger than the raw biogas feed stream. Using a configuration with a third membrane results in a reduction of the recycle stream, as one can see in the previous section. Under the current pressure conditions, as shown in Table 5.4, the power duty of the main compressor is 60.3 kW, as shown in Table 5.7.

Power-to-gas process chains

Based on the membrane configuration obtained in the conventional upgrading case, the power-to-gas process options were evaluated.

The system pressure of process *PtG1* could be set to 12 bara, such that the injection limitations were fulfilled using the membrane area available in the first stage. In the PtG-mode, the first membrane stage serves for hydrogen recycling, therefore, the second membrane stage is not considered for the technical analysis. In the case *PtG1*, the dried raw biomethane contains around 6.8 % hydrogen and less than 2 % CO₂ in methane. This gas is fed to the membrane stage one and upgraded to grid-ready biomethane. From the simulated gas compositions, it can be seen that apart from 18.4 % hydrogen and 4.5 % of CO₂, a large amount of CH₄ is recycled to the feed of the plant as permeate. Nevertheless, the total recycle flow only amounts to around 50 % of the feed flow rate. This is due to the methane, which was removed from the main gas stream and injected to the grid.

In the system *PtG2*, the share of CO₂ being fed to the membrane amounts to more than 20 % of the total gas flow. This is the CO₂ from the raw biogas diluted by the methane produced in the methanation unit.

Grid compliance	BG	PtG1	PtG2-1c	PtG2-2c
x_{H_2}	0.0 %	1.0 %	0.6 %	0.4 %
x_{CO_2}	3.9 %	0.2 %	1.1 %	0.7 %
x_{CH_4}	96.1 %	98.8 %	98.3 %	98.8 %
Dew point	n/a	−9.5 °C	−9.4 °C	−18.4 °C

Table 5.6: Product gas composition of the process options. All conditions are fulfilled, referring to the Swiss grid injection regulations [25].

The compressor duty for both cases PtG2 is almost twice as high as in case *PtG1* due to the product gas of the reaction, which has to be recompressed again to the higher system pressure. On one hand, the recycle stream to be recompressed is around twice as large as in case *PtG1*, on the other hand, in case of the single compressor system, the system pressure is also 8 bar higher. In case *PtG2-2c*, the overall compressor duty is around 3 kW lower than in *PtG2-1c*. Since the pressure difference in the first membrane stage is lower in case *PtG2-2c* than in the case with a single compressor, the permeate stream of the membrane module is lower. Also, the relative share of CO₂ to CH₄ is larger in the two compressor case. Therefore, less methane passes through the methanation unit and has to be recompressed again. For this reason, the recycle stream is smaller in the case *PtG2-2c*. In both cases, the hydrogen separation in the membrane works well and the recycled hydrogen accumulates to around 11 % in the recycle stream. Interestingly, the relative hydrogen concentration in case *PtG1* is almost twice as high in the permeate. The reason for this lies again in the dilution of the methanation product gas by the raw biogas in the cases of process chain *PtG2*. The absolute flow of excess H₂ in the raw biomethane is similar for both cases *PtG1* and *PtG2*, as the same amount of CO₂

is converted to methane. This results also in a similar absolute H_2 flow in the membrane permeate. Nevertheless, it is diluted by CO_2 and methane.

The feed compositions to the reactor are very different in cases *PtG1* and *PtG2*; variances between cases *PtG2-1c* and *PtG2-2c* are only minor. In case *PtG1*, the feed biogas with a composition of 40 % CO_2 and 60 % CH_4 is mixed with the recycle steam. A large amount of methane is recycled, resulting in a methane concentration of around 64 % and 28 % of CO_2 prior to addition of new hydrogen.

	Unit	BG	PtG1	PtG2-1c	PtG2-2c
Main Compr.	kW	60.3	25.4	46.2	27.4
Second Compr.	kW	n/a	n/a	n/a	15.6
Electrolyser power	kW	n/a	1478	1454	1460
\dot{V}_{biogas}	m^3/h	200	200	200	200
$\dot{V}_{prod.}$	m^3/h	124	202	200	200
$\dot{V}_{recycle}$	m^3/h	441	108	215	178
Composition of recycle stream					
$x_{rec.,H_2}$		0.0 %	18.4 %	12.1 %	11.5 %
$x_{rec.,CO_2}$		86.5 %	4.5 %	2.9 %	2.7 %
$x_{rec.,CH_4}$		13.5 %	76.1 %	83.9 %	85.0 %
Membrane stage one, feed and permeate concentrations ^a					
x_{f,H_2}		0.0 %	6.8 %	6.3 %	5.4 %
x_{f,CO_2}		72.4 %	1.6 %	20.6 %	22.5 %
x_{f,CH_4}		27.6 %	91.2 %	72.5 %	71.8 %
x_{p,H_2}		0.0 %	18.4 %	11.5 %	11.0 %
x_{p,CO_2}		88.3 %	4.5 %	39.1 %	47.1 %
x_{p,CH_4}		11.7 %	76.1 %	48.4 %	41.2 %

^a Retentate corresponds to product gas (*c.f.* Table 5.6)

Table 5.7: Result of the process simulations: Power consumption of compressors and electrolyzers, gas compositions in relevant gas streams.

5.4.2 Cost analysis

Cost comparison between the three *PtG*-cases and conventional biogas upgrading (*BG*) – all-year operation

The investment and annual cost for the underlying four processes, assuming all-year operation, was obtained (*i.e.* 8322 h/a, 95 % availability). For the electricity cost, the average value for the considered time period was used (*i.e.* 4.899 €-ct./kWh_{el}).

Investment cost The investment cost for conventional biogas upgrading corresponds to around 50 % of the investment expenses of the *PtG* processes (see Figure 5.10 and Table 5.8).

The electrolyser and hydrogen storage dominate the investment cost of PtG processes, resulting in more than 58 % of the total investment cost. When excluding the hydrogen path and the buffer tank from the comparison, it can be seen that for the conventional biogas upgrading case (*BG*), similar investments are required as for the PtG cases. In the *BG* case, the dominating expenses are the investment cost for the compressor and for the membrane upgrading, *i.e.* mainly the first stage. As mentioned before, the *BG* case requires a relatively high system pressure and has a large internal recycle stream, which results in an expensive compressor unit.

The difference in system pressure is also the reason for the slightly varying cost for the desulphurisation step among the cases: Although an identical amount of contaminant is transported to the plant and therefore the same amount of sorbent is used, the investment cost for the vessel are different in each case. The desulphurisation units are located in the high-pressure part of the plant, therefore a different pressure factor has to be considered in the cost evaluation (see equation 3.20).

A comparison between the three considered PtG cases shows that the investment cost for all cases is in a similar range between 5.6 and 5.9 M€. The two extremes correspond to the processes *PtG2-2c* and *PtG2-1c* and can be associated with the influence of the system pressure. The main difference between the three processes originates from the investment cost for the compressor unit. Since a large recycle stream is present and high system pressures are required, the *PtG2* process with a single compressor unit shows the largest required expenditures. Interestingly, the second compressor in case *PtG2-2c* has only minor influence on the total investment cost. Nevertheless, it decreases the cost indirectly by shifting load from the main compressor and allowing for a lower system pressure. The largest cost share, which corresponds to the membrane upgrading unit, is identical for all process options. This is due to the process design procedure, where a fixed membrane area was defined by the *BG* process and the system pressure was used as measure to ensure compliance to grid injection limitations.

Investment Cost [k€]	BG	PtG1	PtG2-1c	PtG2-2c
H ₂ -Path	0	3362	3307	3320
Reactor	0	352	276	290
Main compr.	871	409	685	436
Second compr.	0	0	0	70
Membrane, stage 1	830	830	830	830
Membrane, stage 2	144	0	0	0
Desulphurisation	420	389	472	326
Supporting modules	99	99	99	99
Condenser/HEX equipment	0	196	191	191

Table 5.8: Investment cost required for the all-year operating upgrading processes.

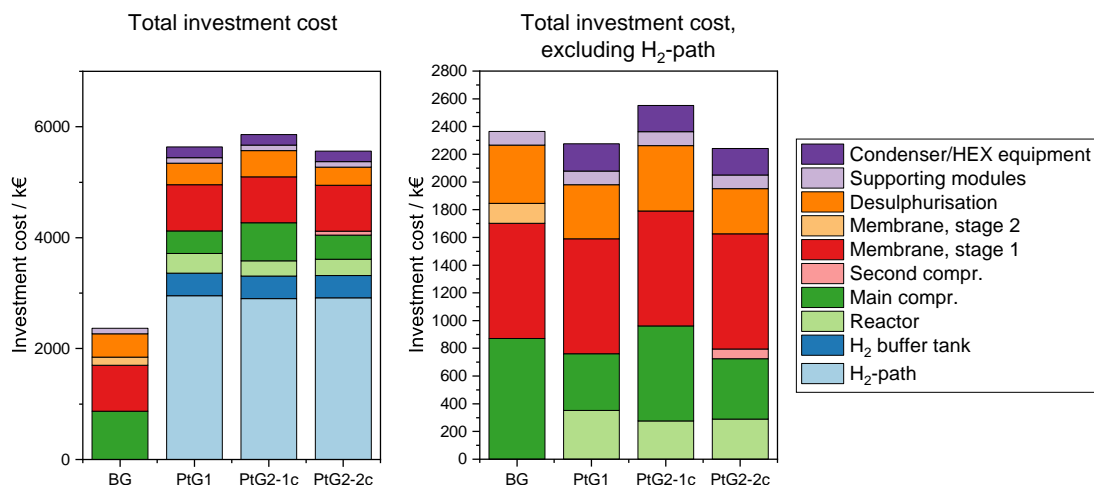


Figure 5.10: Total investment cost of the all-year operating membrane-based (*BG*) and methanation-based (*PtG*) upgrading processes.

The processes *PtG2* were introduced with the goal of reducing the burden to the reactor unit by separating methane gas from the reactor feed. This is reflected in the investment cost for the reactor unit, as it decreases compared to process option *PtG1*. Nevertheless, the cost difference is balanced by higher cost for other process units, mainly the compressors.

Annual cost The annual costs for all-year operation were calculated based on the assumption of full-load operation of the different processes throughout the whole year (see Figure 5.11 and Table 5.9). A comparison between the investment cost and the annual cost of the processes reveals a similar picture on total cost basis: the annual cost for the conventional upgrading process (*BG*) represents around 60 % of the *PtG* processes.

The expenses for raw gas are identical for all processes, as the same amount of biogas is processed. Obviously, around 25 to 30 % of the total cost of the *PtG* processes originate in the electricity needed for the electrolysis, which represents the main difference between the *BG* process and the *PtG* processes.

Again, an exclusion of the H₂-path and the raw biogas cost provides a more detailed view on the operation cost on the process level. The capital expenses are a further dominating share of the annual cost, present in the same distribution as the investment cost in the previous section. Another contribution derived from the investment cost are the operation and maintenance expenses. Apart from these cost contributions, the main remaining cost share originates from the replacement cost of the membrane unit. In this evaluation, a replacement interval of two years is assumed. This means that every second year, the membranes have to be fully replaced and the purchasing cost of the modules has to be spent. Decreasing the interval to an annual replacement would double these expenses. This is of course highly depending on the stability of the membrane material and its subsequent ageing behaviour. Practical experience in the

operation of such a plant have to show how ageing-resistant a membrane module under the particular conditions is.

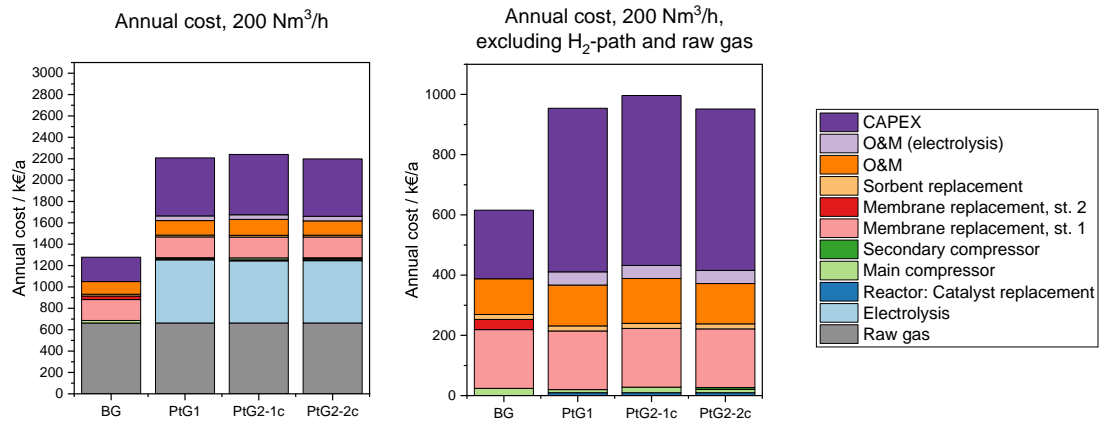


Figure 5.11: Annual cost in k€/a for all-year operating upgrading process chains. The processes are operated during the whole year (8322 h), injecting biomethane to the grid.

Annual Cost [k€/a]	BG	PtG1	PtG2-1c	PtG2-2c
Raw gas	663	663	663	663
Electrolysis	0	591	581	583
Reactor: catalyst replacement	0	10	10	10
Main compressor	24	10	18	11
Secondary compressor	0	0	0	6
Membrane replacement, st. 1	195	195	195	195
Membrane replacement, st. 2	34	0	0	0
Sorbent replacement	17	17	17	17
O&M	118	135	149	134
O&M (electrolysis)	0	44	43	43
CAPEX	228	543	565	536

Table 5.9: Annual cost in k€/a for all-year operating upgrading process chains. The processes are operated during the whole year (8322 h), injecting biomethane to the grid.

Cost analysis of the combined processes

The conventional biogas upgrading process and the three *PtG* processes were combined on the cost level. In order to obtain a cost estimate for the flexible process, the investment and operation expenditures were combined as shown in Table 5.5.

In order to obtain a comparison of the cost structure of the resulting three flexible processes, the costs were calculated for 4000 operation hours in *PtG* mode and a corresponding electricity price of 3.285 €/ct./kWh.

The combined *PtG* processes were compared with another flexible process, which operates methanation equipment, but assumes simple raw biogas flaring when *PtG* is unfeasible instead of membrane upgrading. As mentioned before, this process based on the option *PtG1* serves as benchmark, simulating a *PtG* process only operated during a part of the year. This way, investment and annual cost related to them are considered for the full year, but the remaining annual expenditures only for the operation time in *PtG* mode.

In Figure 5.12, the investment cost comparison between the processes can be seen. All three flexible *PtG* processes show very similar investment expenses around 6.2 M€. As less compression cost and no second membrane stage is necessary, the process option *PtG-flare* indicates lower required costs around 5.6 M€. The three processes *flexPtG1* and *flexPtG2* are highly influenced by the underlying conventional biogas upgrading process (*BG*). This process determines the investment cost for the membrane upgrading, as well as the cost for the compressor unit. The investment cost of all flexible *PtG* processes are again highly dominated (>50 %) by the cost for the buffer tank and the electrolyser. The remaining cost variation between the processes *flexPtG1* and *flexPtG2* originate mainly from the cost difference in the reactor unit and the second compressor unit in the case *flexPtG2-2c*.

The annual cost (Figure 5.13 and Table 5.11) are again dominated by contributions from the raw gas and electricity purchasing price, as well as costs directly derived from the investment costs (O&M, CAPEX). The replacement cost for the membrane upgrading unit are also directly based on the *BG*-case. They are also identical for all processes. The only remaining cost difference originates from the annual cost of the reactor, the gas cleaning and the electricity cost for the compressors. Nevertheless, these differences among the *flexPtG* processes are marginal. The process *PtG-flare* shows a slightly lower annual cost, which is the result of lower investment cost and the missing second membrane upgrading unit. Although this process has a lower annual cost, one has to consider that less biomethane is injected to the grid and the specific production cost is higher in the current consideration.

Overall, the investment and operation cost difference between the different *flexPtG* processes is marginal. Only the process which considers flaring of the raw gas shows a lower annual cost. Decisions leading to investments in such a flexible *PtG* process should therefore not only be based on the cost calculations such as shown in this work. Furthermore, aspects on the plant operation or potential future developments should also be considered.

Sensitivity of the combined processes towards electricity cost and annual operation hours

The *PtG* processes will only be operated when inexpensive electricity is available. As explained in previous sections, the electricity price has a high influence on the annual operation cost. Nevertheless, the higher biomethane output to the grid has a positive impact on the specific production expenses.

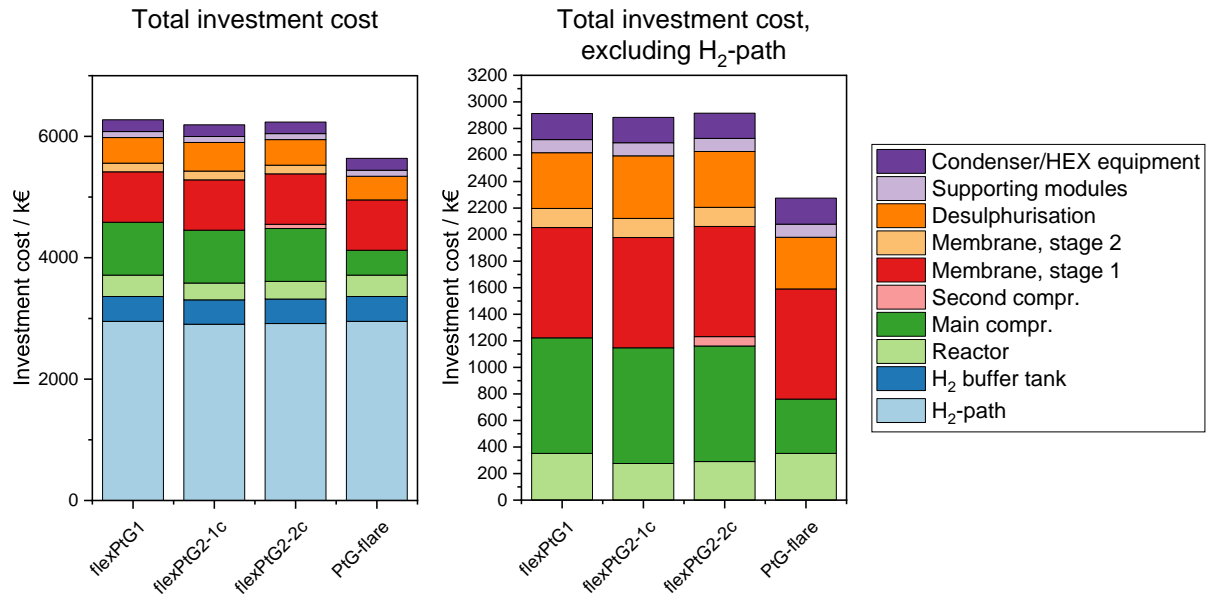


Figure 5.12: Investment cost in k€ required for the four considered upgrading options. The process *PtG-flare* is a modification of the process chain *PtG1*.

Investment Cost [k€]	flexPtG1	flexPtG2-1c	flexPtG2-2c	PtG-flare
H ₂ -Path	3362	3307	3320	3362
Reactor	352	276	290	352
Main compr.	871	871	871	409
Second compr.	0	0	70	0
Membrane, stage 1	830	830	830	830
Membrane, stage 2	144	144	144	0
Desulphurisation	420	472	420	389
Supporting modules	99	99	99	99
Condenser/HEX equipment	196	191	191	196

Table 5.10: Investment cost in k€ of the combined, flexible process options.

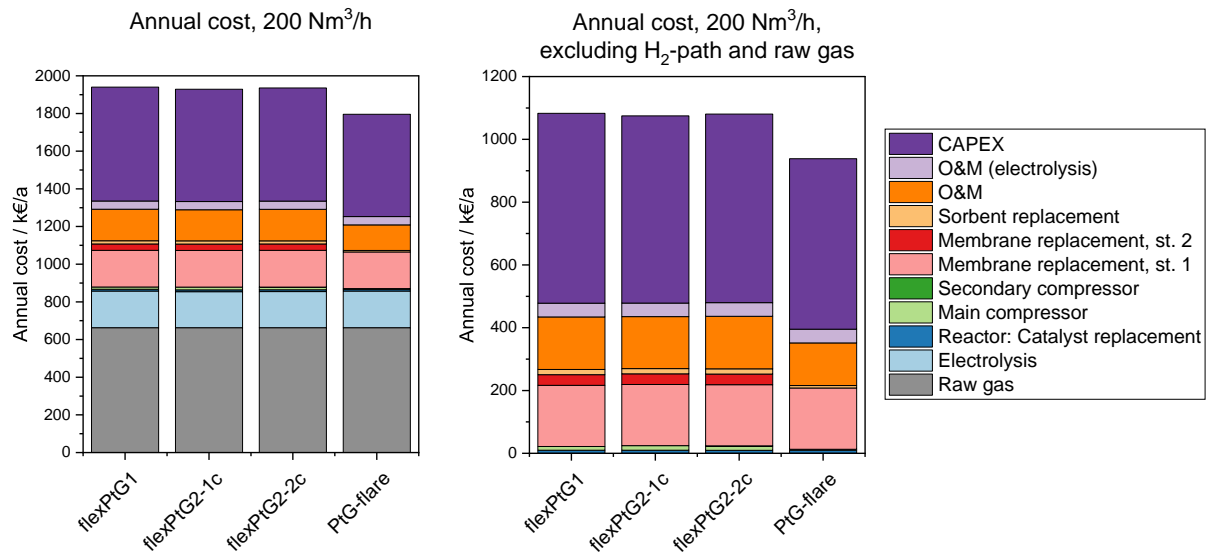


Figure 5.13: Annual cost of the flexible processes in k€/a, based on a PtG operation time of 4000 h per year.

Annual Cost [k€/a]	flexPtG1	flexPtG2-1c	flexPtG2-2c	PtG-flare
Raw gas	663	663	663	663
Electrolysis	194	191	192	194
Reactor: catalyst replacement	10	10	10	10
Main compressor	12	15	12	3
Secondary compressor	0	0	2	0
Membrane replacement, st. 1	195	195	195	195
Membrane replacement, st. 2	34	34	34	0
Sorbent replacement	17	17	17	8
O&M	167	166	167	135
O&M (electrolysis)	44	43	43	44
CAPEX	604	596	601	543
Sum	1940	1929	1935	1796

Table 5.11: Annual cost of the flexible processes in k€/a, based on a PtG operation time of 4000 h per year.

The electricity price directly relates to the average operation time of the PtG unit per year under the assumption that the PtG unit is only operated during the least expensive hours of the year. The electricity price distribution used in this analysis is shown in Figure 5.9.

In Figure 5.14, the specific biomethane production cost for the flexible PtG processes is shown in relation to the PtG operation hours. As a comparison, the production cost for the conventional biogas upgrading process and for the three PtG processes without added flexibility are shown. For these processes, the production cost are indicated as single data points at the maximum operation hours. Correspondingly, the all-year conventional biogas upgrading is indicated at zero PtG operation hours. It can be seen that the all-year PtG processes show a slightly higher production cost than the conventional biogas upgrading case. Although the total expenditures are higher over the year, the additionally produced biomethane allows for a reduction of the specific production cost.

The production cost of the flexible processes is highest at a low number of operation hours. Although a very low electricity price is favourable for the electrolyser operation cost, this is counter-acted by high investment cost for the additional flexibility. As the PtG process is only operated for small time intervals and only a small additional amount of biomethane is produced by methanation, the specific production cost are high. With increasing operation hours of the PtG process, the production cost decreases as more biomethane can be injected to the grid. Although the average electricity price increases, this additional expenditure is compensated by a higher biomethane injection. The two effects equalise at high operation hours, which results in a plateauing of the curve under the current electricity price distribution.

The process considering raw gas flaring shows the highest increase in production cost when decreasing the operation hours. The flaring results in a direct monetary loss since the raw biomethane cost still have to be paid. This lower income due to decreasing amounts of injected biomethane at constant operation expenses results in a disproportionate increase in specific production cost. Nevertheless, this process option shows the production cost development of a non-flexible PtG process, which is not operated full-time. This justifies the use of a system with added flexibility, as the sensitivity of the production cost is much lower than in the flaring option. Especially when a flexible process is operated less than the amount of hours indicated by the intersection point of the *flexPtG* and the flaring option, the flexible option has clear financial advantages. To decrease the expenditures by an additional income, the raw biogas can be energetically used for heating purposes, as shown in Figure 5.15. If such a process is available in proximity, the raw biogas can be directly burned in a high temperature processes. Alternatively, the heating of a high-temperature storage is possible, which facilitates the start-up of the methanation reactor.

It can be seen that the production cost for the PtG with flaring decreases below the cost for the *PtG1* process. This is the effect of lower average electricity price at lower operation hours. When the operation hours would exceed the indicated 8322 h/y, the plant would also be operated during the most expensive electricity prices and the production cost would adjust to

the value indicated for the case *PtG1*. Furthermore, the *BG* and *PtG* processes were evaluated at 8322 h/y using the average electricity price over the whole year. This also causes a certain discrepancy due to the lower gas injection to the grid.

Implementing a flexible process results in a production cost increase of around 0.6 €-ct./kWh during all-year operation of the *PtG* plant for the present electricity price curve. For example, this means, that instead of flaring biogas it can be energetically used down to a *PtG* operation time of 5500 h/a without exceeding production cost of 13 €-ct./kWh.

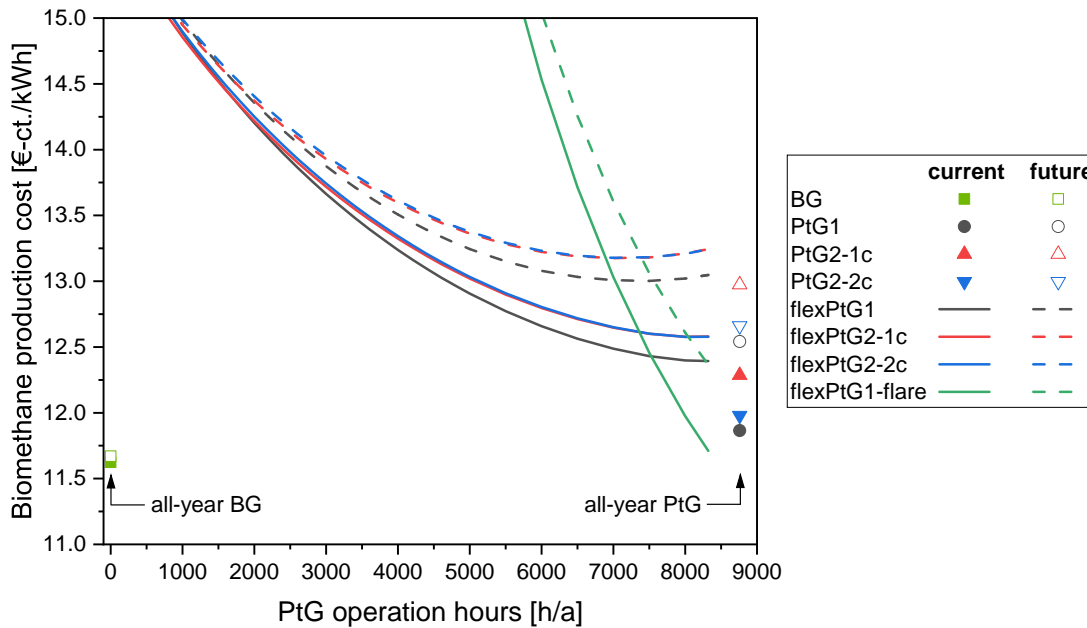


Figure 5.14: Production cost of the flexible *PtG* processes in relation to the *PtG* operation hours per year. The operation hours directly relate to the cumulative average electricity price, which defines one of the main contributions to the processes OPEX. For comparison, the underlying membrane-based upgrading processes are shown, as well as the *PtG* processes in full-year operation. Values based on the current electricity price are indicated in solid lines and full symbols, the future scenario in dashed lines and empty symbols, respectively.

Future development In this work, we also make an assumption for a future electricity price distribution, based on a solar irradiation profile from Switzerland. As shown in the previous section, it generally increases the electricity price and the number of more expensive hours. This results in a distribution, which has a higher slope and is shifted towards higher electricity price. This directly reflects in the cumulative average curve, which is used to relate operation hours and electricity price.

The processes were analysed again using the modified electricity cost distribution, which allows a projection on how such processes would be operated in a future energy system. Along with the electricity cost, the specific production cost also increases. As shown in Figure 5.14, the predicted production cost of the flexible processes are close to the current scenario at low operation hours, but deviate towards higher production cost when operated for longer time spans in PtG mode. The curve even forms a minimum, as towards higher PtG operation hours, high electricity prices as a cost factor dominate over the income from the additional biomethane and increase the specific production cost.

Having a higher variance in the underlying electricity price distribution results in a more pronounced minimum in the biomethane production cost curve and therefore an optimal number of PtG operation hours. In the future energy system, when photovoltaic and wind energy have a higher penetration, such operation hours with high energy cost can occur more often. Especially if this minimum is located at a lower number of PtG operation hours than the flaring option, this justifies the use of a flexible system. Although one has to face higher production costs at a higher number of PtG operation hours, due to the flat nature of the cost development towards lower operation hours, biomethane can be produced with higher cost efficiency even under economically harsh conditions.

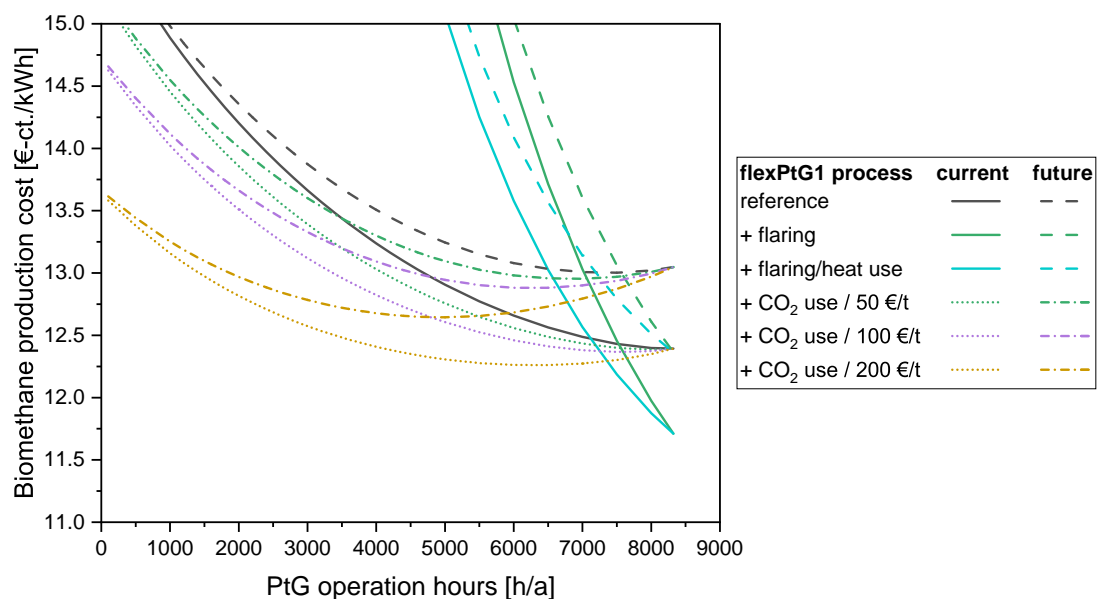


Figure 5.15: Based on process option *PtG1*, the influence of valorising the heat from flaring is shown for the current electricity market and the future scenario are shown. If a profit from CO₂ separation can be generated, a clear benefit towards lower production cost is possible. For comparison, the production cost of *PtG1* is indicated for the current and the future electricity market.

Negative carbon emission process In the flexible upgrading process, depending on PtG operation hours, CO₂ separation from a biogenic carbon source is performed. Such a separation is necessary, as the total oxygen content in the molecules of the feed gas stream is higher than the oxygen content of the desired product (methane). In order to increase the product gas value, the oxygen content has to be reduced, either by methanation and subsequent water formation, or CO₂ separation [30]. The flexible process presented in this work consists of an inherent CO₂ separation and enables biomass-based, negative emission operation. It is therefore possible to provide a clean CO₂ stream to a process for further utilisation or sequestration of CO₂.

To evaluate the cost benefits through CO₂ separation and utilisation, the *PtGI* process chain was evaluated with an income from the CO₂ stream. Three different revenues for the CO₂ stream were assumed (50, 100 and 200 €/t), which cover the price range for current CO₂ emission certificates (89.9 €/t, 15.02.2022 [174]).

As shown in Figure 5.15, the production cost clearly benefit from CO₂ valorisation. Under the current electricity cost and very high price for CO₂ (*i.e.* 200 €/t at the biogas plant), the production cost show a clear optimum at around 6000 h/a. There is no optimum at lower CO₂ prices, nevertheless the production cost is still lower than in the base-case scenario without CO₂ utilisation, and the flat character of these curve indicates that the costs are not too dependent on the exact number of PtG operation hours, alleviating the requirements on the control system. In the future electricity price scenario, the cost minimum occurring at high CO₂ prices is even more pronounced and shifted down to around 4500 h/a. In this case the production costs of *flexPtGI* are as low as the costs of a PtG-only plant (*c.f.* to the points in Figure 5.14 at 8760 h). For low PtG operation hours, the production cost trends converge at a price mainly dominated by the specific investment cost of the plant and the revenues by CO₂ sales. This value is largely independent on the electricity cost. On the other hand, at high PtG operation hours, there is less CO₂ separated and only small revenues are possible. The production cost is therefore dominated by the underlying PtG process and therefore highly sensitive on the electricity cost development.

The CO₂ separation can also be used independently from the PtG functionalities. In the base-case scenario only considering membrane based upgrading around 1171 t of CO₂ can be separated. Combining the revenues from the CO₂ sales with the upgrading cost result in lower production cost of 11.1 €/ct./kWh, 10.6 €/ct./kWh and 9.5 €/ct./kWh for a CO₂-price of 50 €/t, 100 €/t and 200 €/t, respectively. This corresponds to a specific biomethane production cost reduction of 4.6 to 18.3 %. Selling CO₂ for at least 100 €/t renders the membrane-based biogas upgrading profitable even without increasing the biogas price above 11 €/ct./kWh.

5.5 Conclusion

The goal of this work is to investigate the economic potential of a flexible upgrading concept proposed in earlier work [166]. This concept allows for a fast switching between conventional

biogas upgrading by membrane separation and upgrading by direct methanation of biogas, depending on the availability of hydrogen from electrolysis.

In order to have a reliable model for membrane separation in hand, characterisation experiments were performed on a commercial hollow-fibre membrane module produced by Evonik. The experimental range covered the conventional biogas upgrading case, as well as hydrogen recycling after PtG operation. This data allowed the fitting of parameters for a permeation model, which was included as a sub-model in a numerical, rate-based simulation model for counter-current membrane operation. The model was benchmarked with literature data and showed good agreement. For this benchmarking, data from a real biogas upgrading plant was considered.

In this work, we present three power-to-gas process chain options for the production of bio-methane based on biogas. Additionally, a two-stage conventional membrane-based upgrading system was considered. A techno-economic analysis was performed on each of those process chain options in order to investigate their cost structure. The processes were merged to model the flexible concept by suitable combination of investment and operation cost.

As a key performance indicator for process comparison, the specific production cost per kWh of injected product gas were taken into account. The three PtG processes showed only small variation in investment cost between 5.5 and 5.8 M€. The investment expenses are highly dominated by electrolyser and H₂ buffer tank cost, accounting for more than 50 % of total investment cost. Only for conventional biogas upgrading, a significantly lower total investment of 2.4 M€ is necessary. In all processes, membrane and compressor cost account for a large share of expenditures not related to the H₂-path.

Operation cost reveal a similar picture: the OPEX is fully dominated by raw gas and electricity purchase cost, as well as capital expenses and O&M cost directly proportional to the investment cost.

Overall, the all-year biogas upgrading results in the lowest production cost (11.7 €-ct./kWh). The classical PtG process (PtG1) shows the lowest production cost (11.8 €-ct./kWh) among the PtG process chains, whereas the inverted process with a single compressor results in the highest (12.2 €-ct./kWh).

The flexible processes revealed also a very similar production cost among the process options. As expensive equipment, such as the compressor and the membrane upgrading are defined by the biogas case, the cost variation is limited among the *flexPtG* cases. Only the inverse process chain with two compressors (*flexPtG2-2c*) shows a slightly higher investment and operation cost. It shows therefore also the highest production cost among the *flexPtG* processes. The least expensive flexible case is still based on the classical PtG process chain (*PtG1*).

Naturally, the production cost of the flexible processes are highly sensitive to operation hours and electricity cost. The production cost decrease with increasing number of PtG operation

hours. The decrease is lower at higher numbers of operation hours. This allows for an operation of the PtG process down to 5500 h per year without exceeding a production cost of 13 €-ct./kWh. On the other hand, by allowing for a production cost increase of around 0.5 €-ct./kWh, a PtG process can be equipped with additional flexibility to ensure all-year biomethane injection.

The proposed system allows for a more predictable economic situation, even if electricity cost allows only for a very low number of PtG operation hours.

Under the assumption of more hours of expensive electricity in future, the flexible system allows to avoid the use of the most expensive periods. In contrary to the PtG-flaring process, this results in an optimum number of PtG operation hours where production cost are lowest. In the future cost scenario considered in this study, the optimum PtG operation time can be located in the range of 6500 – 8000 hours per year.

Further decrease of production cost and better economic predictability of the process is possible when the CO₂ separation capabilities of the flexible process are used. This synergy allows to profit from additional revenues when the PtG process is inactive. Even at low CO₂ prices of 50 €/t, a clear biomethane production cost benefit of around 0.25 €-ct./kWh can be realised.

6 Symmetrical part load operation of a Power-to-Gas process

6.1 Introduction

In the energy system of the future, fluctuating power generation techniques, such as wind and solar power will gain importance [156]. Power-to-Gas (PtG) technologies can be a way to absorb and store electricity production from these sources [21, 22] that cannot be used at the time or place of its production. Simultaneously, PtG allows decreasing the carbon footprint of the natural gas grid by using renewable hydrogen and biogenic or not avoidable CO₂ as feedstock. A cost efficient way to access biogenic CO₂ is the direct methanation of biogas and subsequent grid injection [102, 141].

While catalytic processes, such as methanation, present some flexibility to operate on fluctuating feed streams, synergistic combinations with adequate buffer solutions are required to increase the resilience of such processes and to optimise the operation of the reactors.

The highest operational flexibility is required in the electrolysis, which represents the first process step. State-of-the-art technology enables a fast ramping of the nominal power in order to follow the supply curves of electricity [90]. Gorre *et al.* [157] state that proton exchange membrane electrolyzers (PEM) are capable of ramping up to full load from cold stand-by within 10 s. Furthermore, the load range can be varied from 0 to 100 % [90]. For alkaline electrolyzers (AEL), the minimum load is limited to around 20 % [90] and load changes of 20 %/min are possible [157].

For the methanation case, Gorre *et al.* [157] presented a Monte Carlo-based simulation study where hydrogen storage size and methanation capacity were economically optimised for a 10 MW alkaline electrolyser. The study considers three different power sources (wind, solar and grid balancing operation) and two different operation concepts to compensate for H₂ overproduction by the size difference of the methanation and the electrolyser. The study shows that a gas production cost decrease of up to 17 % is possible by optimising the methanation capacity. Nevertheless, it also indicates that no single optimum system design is possible, but rather a range of capacities where the production cost change is only limited. The fixed-bed

methanation considered in this study operates down to an assumed part load level of 40 % and varies linearly with the tank level (*i.e.* pressure in the tank). The methanation is only started at around 50 % tank level in order to prevent frequent on-off cycles.

Gorre *et al.* [157] found the largest required H₂ tank sizes when solar energy is used, as regular day/night periods have to be compensated. Less storage capacity is required when a PtG plant is connected to a wind farm, as the fluctuations are distributed over the full day. The grid balancing scenario required the least capacity, as only short-term peaks and under-coverages had to be compensated.

Inkeri *et al.* [175] present a similar study, which considers further parameters of thermal dynamics for the reactor, such as a load ramp, thermal ramp, a cooling rate and a maximum stand-by time. Their considerations are also based on a fixed-bed methanation reactor. The storage capacity for H₂ was varied between 2 and 12 h. Similar to the study of Gorre *et al.* [157], the methanation is operated in a load range between 20 % and 100 % depending on the H₂ storage level. Apart from a scenario where H₂ is produced by overproduction from wind and solar power, a further scenario is considered where grid electricity is used below a fixed price threshold.

Both studies show that specific optimisations of unit sizes (*i.e.* electrolysis, methanation and H₂ storage size) have to be performed based on the purpose of the plant and the temporal availability of electricity.

In the previous chapter (see Chapter 5), the necessity to increase the flexibility of power-to-gas process chains was discussed. Especially during times when electricity costs are high, operating a PtG facility might be uneconomic. Phases with high electricity cost are likely to increase in the future energy system, as renewable energies reach a high penetration in the market. This will lead to a high fluctuation on the production side of the electricity market, which subsequently requires additional flexibility at the demand side. A measure to monitor and react to such fluctuations is the European Power Exchange (EPEX) spot price, which reflects the settling price of short-term electricity auctions [171].

A flexible PtG and biogas upgrading system was presented in previous work (see Chapter 4 and [166]), which allows for a fast switching between PtG operation and membrane-based biogas upgrading. The system was analysed for its economic feasibility in the previous chapter, based on a bi-modal operation mode. In this mode, the plant is either operated in full-load membrane-based upgrading or in full-load PtG operation depending on the availability of hydrogen, which itself is generated using renewable electricity. It could be shown that additional flexibility in the PtG plant allows for a more economic production of biomethane even at lower possible PtG operation hours per year by actively avoiding times of scarce and thus expensive electricity.

In this work, we investigate to what extent such a flexible system can be improved by operating the methanation in part load. This is done by i) experimental investigation, performed at

TRL 5, which has a high relevance for industry-like applications, and ii) by analysing operation heuristics based on the electricity cost distribution.

Here, we consider a part load case where hydrogen is fed to the methanation process according to the stoichiometric requirement, based on the availability of biogas or CO₂. Such part load situations occur when the biogas production fluctuates or the carbon-containing gas can be stored for longer time periods. When the CO₂ source is limited, full-load PtG operation is not possible and the H₂ supply can be throttled. Therefore, part load in the reactor as well as in the hydrogen recycle membrane can be expected and is investigated in this work.

6.2 Materials and methods

In this work, experimental work during a field campaign was performed to prove part load of the methanation reactor alone and in combination with the membrane based upgrading system. Furthermore, an algorithm was developed, which allows the analysis of the operation of a power-to-methane plant.

6.2.1 Pilot plant experiments

The experiments in this work were performed in a container-based methanation set-up (COSYMA, 10 – 20 kW, TRL 5). As shown in a previous campaign, this plant can be used for direct methanation of biogas [81] and biogas upgrading [37]. In this experimental campaign, the COSYMA pilot plant was installed at a biogas plant (Swiss Farmer Power Inwil, SFPI) in Inwil (Switzerland). This biogas plant mainly uses manure and municipal biowastes as feedstock. The composition of the biogas feed-stream coming to the plant was not monitored continuously. Although it was prone to fluctuations, frequent measurements showed a composition of around 40 % CO₂ and 60 % CH₄. The relevant gas compositions were recorded by μ GC in a 3 – 4 min interval during the experiments.

The main components of the pilot plant were identical to the previous experimental campaigns, as shown in Figure 6.1. The gas mixtures used in the experiments were prepared using biogas from the digester plant, mixed with additional gas from cylinders (H₂), dosed with thermal mass flow controllers (MFCs). The biogas from the digester plant was compressed to system pressure and fed through two sorbent beds to remove contaminants to prevent poisoning of the methanation catalyst and damage to the biogas upgrading membrane. After the main compressor, a cooled condensate trap was installed (4 °C), which removed condensable contaminants. The gas flow rate to the sorbent beds was monitored with a Coriolis mass flow meter (Promass A, Endress+Hauser, Switzerland).

The raw gas mixture was pre-heated to reaction temperature and mixed with steam (approx. 0.5 mol_{H₂O}/mol_{CO₂}) to prevent coke formation and reduce catalyst stress.

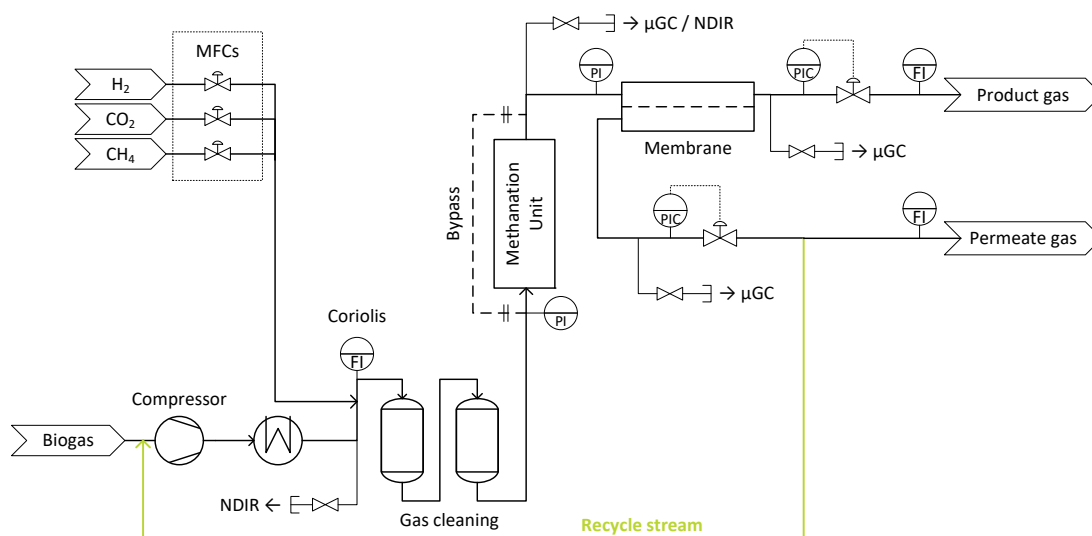


Figure 6.1: P&ID of the COSYMA plant in the configuration for symmetrical part load experiments. The optional connection for H₂ recycling is drawn in green. For reasons of readability, the water bath for temperature control in the membrane module is not shown and the reactor unit is drawn in a simplified way.

The methanation reactor was filled with a commercial Ni-based catalyst in suitable size. The reactor vessel had an inner diameter of 5.2 cm. In contrary to larger-scale BFB reactors [176], the only internals present in the reactor volume were lances for gas sampling and temperature probing. The vessel was cooled by a heated air stream, which was passed through a shell from the bottom to the top of the reactor. This way, a near-isothermal temperature profile could be achieved, as shown by Witte *et al.* [81].

The product gas from the reactor was fed to a condenser unit, cooled to 4 °C in order to remove reaction water. The dried product gas was then directed to the gas separation membrane.

The single biogas upgrading membrane module (Evonik SEPURAN[®] Green, 2 inch) was already used to perform the membrane characterisation experiments of the previous chapters. It remained installed in a temperature-controlled water bath to ensure a constant temperature. To ensure pre-heating of the feed gas, it was fed through a coiled section of tube, which was also submerged in the water bath. Throughout the complete experimental work, the membrane module was operated at 40 °C.

The permeate side of the module was equipped with two exits, which allowed to change the flow configuration from co-current to counter-current operation. For the experiments in this work, counter-current operation was chosen. For tests investigating the performance of the complete plant (and not only of the reactor itself), the permeate was recycled to the inlet of the compressor. At the retentate outlet, as well as on the permeate outlet, pressure regulators were installed to set a defined pressure regime in the membrane module. The volumetric flow

rates of the retentate and permeate streams were recorded by two mechanical gas meters (Wohlgroth G4).

Throughout the plant, various sampling positions were available for the analysis of the gas composition. All three streams entering and leaving the membrane module were monitored by micro gas chromatography (μ GC, Varian CP-4900), which allowed a full concentration measurement every 3 – 4 min. Furthermore, as part of the control system, the plant had two non-dispersive IR spectroscopy (NDIR, Siemens Ultramat 23) devices available, which continuously recorded the gas composition before the gas cleaning and the product gas of the reactor.

Part load operation with limited biogas and H₂ supply

In the experiments, the part load behaviour of the methanation pilot plant should be investigated for the case, where the carbon source and the hydrogen supply are limited to the same extent. In this case, the reactor operates with a slightly over-stoichiometric amount of hydrogen, but at a fraction of the full methanation capacity, *i.e.* the overall feed gas flow rate is reduced.

Operation window of the methanation reactor and of the complete PtG plant

In a first experiment, the part load option of only the methanation reactor was tested. The membrane module was used for single-stage hydrogen removal with an open hydrogen recycle loop, therefore the permeate of the membrane module was merged with the product gas stream again and not recycled. During these first tests, the lower limit of the reactor operation window was defined by the minimum flow rates that could be provided by the compressor and the MFCs. The maximum possible load was given by the maximum cooling rate of the reactor, which was identified as the point where the reactor temperature could be kept constant at the full cooling rate. This maximum point was determined for different fluidisation states.

The feed flow rate to the reactor was determined by the Coriolis flow meter. The conversion to a volumetric flow was performed using the NDIR concentration measurement, assuming that H₂ can be calculated from the sum of all other species (CO₂, CH₄ and traces of CO).

In a second series of experiments, the possible part load range of the complete PtG plant was tested, *i.e.* including the hydrogen separation and recycle. For this operation with a closed recycle loop, the permeate stream of the membrane was merged with the raw biogas stream at the main compressor's inlet.

Load profile

In order to simulate the dynamic operation of a PtG plant and to demonstrate the capability of a fluidised bed methanation with membrane-based upgrading in sequential part load operation, a load profile was followed during the experiments that is based on the availability

of renewable energy. The load profile was defined as part of the ReMaP^I project [177–179], where a local hydrogen demand for public transport is covered by PV, wind turbines and a seasonal storage system combining a battery, an electrolyser, a hydrogen tank, a methanation unit, and a steam reformer unit. The sequence of part load levels tested in the methanation plant was 45 %, 100 %, 89 % and 59 %. In real systems, load changes in the PtG plant more frequently than few times per day are not needed due to the dampening effect of the hydrogen tank. Such a tank has to be installed, as the methanation – due to its thermal inertia – cannot follow directly the production curve of the electrolyser. The goal of the experiments was therefore to maintain stable operation at each load level for 1 h and then change to the next level.

6.2.2 System analysis

To understand the potential of part load for the operation of a PtG plant under the condition of fluctuating electricity prices, a system analysis was performed to identify advantages such as longer operation and less start-up/shut-downs of the methanation plant.

Three different algorithms for the operation scheduling of the electrolyser and the methanation unit were developed. In all of them, no part load of the electrolyser unit is considered, *i.e.* the electrolyser is either switched off or runs at full load. In this base-case, we assume that the methanation unit and the electrolyser are equally sized. Meaning that the nominal hydrogen output of the electrolyser corresponds to the stoichiometric requirement of the methanation plant of full load. The H₂ tank size was defined as a capacity in hours, relative to the H₂-feed of the methanation unit under full-load operation. Four different main tank sizes were considered in the analysis: 3 h, 6 h, 12 h, 24 h. Two extreme values were added (48 h and 200 h) to investigate the influence of very large storage capacity.

In all algorithms, the electricity price curve is monitored at the market and based on a pre-defined threshold value the electrolyser is switched on or off. This threshold range was varied between 5 €/MWh and 200 €/MWh. As a time-horizon for the analysis, we obtained market data from the European Power Exchange and considered the years from 2007 to 2019 [171].

Such a consideration based on pure electricity cost does not directly reflect the use of renewable electricity and does not automatically lead to a renewable PtG process. Nevertheless, it is assumed that renewable electricity generation will have a higher influence in the future energy system and will affect the electricity cost based on their present availability. An increased, but stochastic availability of wind energy and the more predictable availability of solar energy might cause a high overproduction of electricity during certain times, and this will lead to higher fluctuations in the energy market, an increasing share of renewable energies and therefore to a more sustainable energy system.

^IRenewable Management and Real-Time Control Platform, Homepage: <https://remap.ch/>

The hydrogen storage tank cannot only serve as a decoupling unit of the electrolyser and the methanation unit; it may also extend the methanation activity under highly fluctuating conditions on the electricity supply. In order to enable this behaviour, the electrolyser requires a higher nominal capacity than the methanation unit does. In this work, an electrolyser capacity increase of 10 %, 20 %, 60 % and 100 % was considered, while the existing CO₂ source (biogas plant) defines the size of the upgrading unit – either methanation or membranes.

When the hydrogen production rate of the electrolyser is increased above the maximum capacity of the methanation unit, excess hydrogen is produced during long periods of low-cost electricity. As storage is limited, a strategy for handling the excess is required. Gorre *et al.* [157] fix the electrolyser power and either optimise the tank size and methanation unit size to allow for a full use of hydrogen or they even allow for a certain discarding of H₂ by flaring biomethane. Having a limited amount of biogas available for methanation, flaring is not an option. In this work, the electrolyser is switched off as soon as the tank level reaches the maximum. This is based on the assumption, that the plant is connected to the electricity grid and not required to perform balancing operations.

Basic algorithm (full load, FL) – no part load allowed

In the basic version of the algorithm, the electrolyser is switched on, as soon as the electricity cost of the upcoming 1 h-period is below the pre-defined threshold value. In the first priority, the H₂ storage tank is filled to the maximum level. As soon as the tank is full, the methanation unit is started and runs at full capacity until the storage tank is empty. Depending on the electricity cost, hydrogen production is ongoing or not, causing the tank level to remain constant or not. The methanation unit is shut down as soon as the tank is empty. It is only restarted again when the tank level is at maximum.

Algorithm PL1

This algorithm operates the same way as in the basic version, but it considers part load operation of the methanation unit. When the tank is emptied below a level of 50 % of the full capacity, the methanation unit changes operation to 50 % part load, extending its operation time. The part load operation is maintained until the tank is empty and the methanation is shut down, or the tank reaches full capacity, which causes the methanation to switch again to full capacity.

Algorithm PL2

This algorithm also allows part load operation of the methanation unit. In addition to the operation concept explained in the previous section, this algorithm also enables 50 % part load during the filling of the storage tank. As soon as the tank level reaches 50 % capacity, the methanation is switched on at 50 % part load. The load of the methanation unit is increased

to 100 % when the tank reaches the maximum capacity, turned down to 50 % part load at 50 % tank filling, or it is shut down when the tank is empty. Although we only consider discrete load changes, this operation mode corresponds in principle to the heuristics implemented in the simulations of Gorre *et al.* [157] and Inkeri *et al.* [175].

6.3 Results and discussion

6.3.1 Field experiments

Part load operation of the methanation reactor

The heat removal limit of the fluidised bed methanation reactor was determined without a closed recycle stream. It was identified as operation point, where the temperature in the reactor rises although the cooling was set to the maximum level.

The operation limit was tested at four different system pressures between 4 and 7 barg (see Table 6.1). As shown by the red points in Figure 6.2, higher pressures lead to lower maximum flow rates. The heat production is proportional to the molar flow of biogas, as full conversion is targeted for all pressures. Therefore the slightly lower operation limits at higher pressures indicate the impacts of the fluid-dynamics in the reactor where higher molar flows and lower pressures both lead to higher linear gas velocities and in consequence to more particle movements and better heat transfer to the cooling surface. Even larger capacity of the reactor would be possible by installing more heat transfer area within the given catalyst volume, *i.e.* by smaller hydraulic diameter of the reactor.

H ₂ flow rate L/min	Biogas flow rate L/min	$x_{ret.,H_2}$ %	$x_{ret.,CO_2}$ %	$x_{ret.,CH_4}$ %	System pressure barg
53.0	33.0	1.0	0.0	98.9	7.0
56.0	34.3	2.3	0.1	97.6	6.0
61.3	37.6	4.8	0.2	94.9	5.0
67.0	41.2	8.4	0.5	91.1	4.0

Table 6.1: Experimental settings used to determine the upper limit of the plant's operation window, given by the maximum heat removal rate in the reactor. The plant was operated with an open recycle loop, the gas quality after the membrane upgrading is given by the retentate concentration measurement.

Further constraints are given as minimum and maximum fluidisation states in the reactor. Those are values based on experience with BFB methanation. The lower limit ensures a minimal fluidisation in the catalyst bed, which allows sufficiently high mass and heat transport for isothermal operation. More importantly, this also prevents the catalyst bed from settling, which would lead to fixed-bed-like behaviour, subsequent hot spot formation and catalyst

deactivation. Operation of the reactor above the upper limit would lead to slightly increased attrition and carrying-out of the bed material.

As shown in Figure 6.2, the highest H_2 flow rates applied were 67.0 L min^{-1} . The lowest tested flow rate amounted to 13.3 L min^{-1} , which corresponds to a part load level of 19.8 %. Note that this lowest operation point in Figure 6.2 was reached by using mass flow controllers mimicking the biogas composition, as the operation line of the installed compressor would not allow such low flow rates at low pressures. In commercial scale systems, such operation points can be operated with a bypass flow around the compressor.

Part load operation of the complete PtG plant

While the previous tests showed that 20 % part load in the reactor is possible, the performance of the complete plant with closed recycle loop had to be tested in a subsequent experiment to determine the maximum possible flow rate, *i.e.* the upper operation limit. Due to the manual regulation of the compressor duty and hydrogen supply to the plant, maintaining a stable operation was challenging to achieve. During several pre-tests, it could be observed that a slight over- or under-stoichiometric amount of hydrogen in the reactor's feed could lead to positive/negative feedback effects in the system. The compressor operates with a fixed volumetric flow rate at a certain duty. When the hydrogen concentration in the reactor feed largely exceeds the stoichiometric ratio, a correspondingly large amount of unreacted hydrogen enters the membrane separation. Due to the high permeance of H_2 , the permeate stream increases, which displaces raw biogas from the compressor's feed. This causes the amount of CO_2 fed to the plant to decrease, which increases the amount of unreacted hydrogen in the product gas even more. It could be seen that the gas hold-up of the current set-up could be replaced by accumulated hydrogen within a few minutes. The same effect occurs when an over-stoichiometric amount of CO_2 is fed to the reactor leading to a CO_2 accumulation in the loops.

The NDIR provided fast measurements of the CO_2 concentration after the reactor. During dynamic testing, this value proved as a reliable indicator for the gas compositions in the feed. As soon as the hydrogen concentration approached an under-stoichiometric level, the CO_2 concentration in the product gas stream increased, which allowed a timely adjustment of the process parameters.

A hydrogen flow of 49.5 L min^{-1} was found as the maximum possible energy input for this configuration while still allowing to reach grid injection specifications. This means that not the heat removal, but the upgrading performance of the installed membrane limits the operation window.

Operation of the plant at this H_2 flow rate showed a certain instability of the overall process, leading to the risk of accumulation of H_2 in the system. In order to maintain a larger margin in adjusting process parameters and therefore a higher stability of the process, the maximum

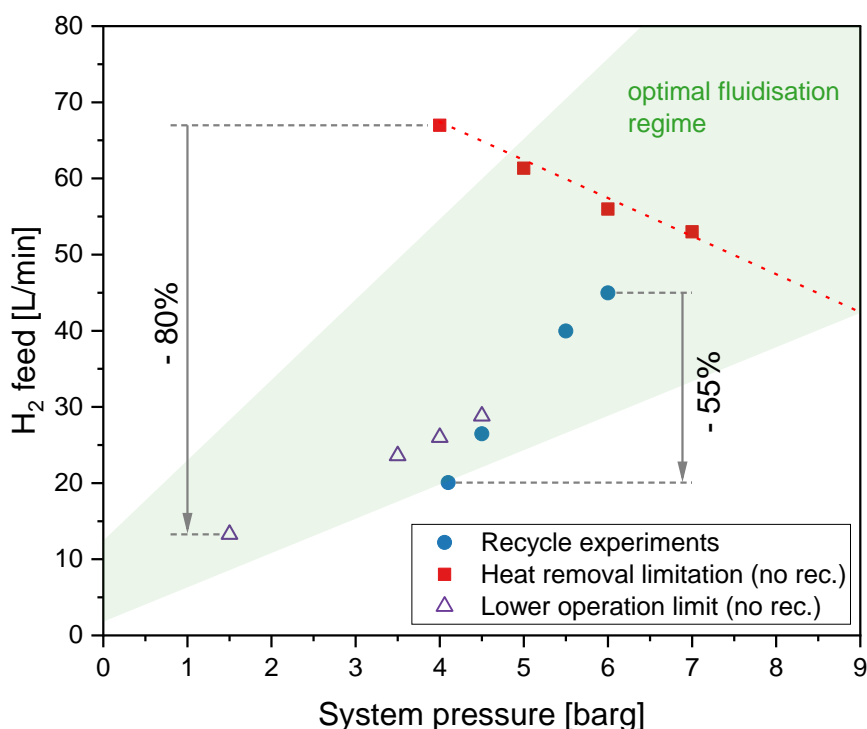


Figure 6.2: The operation window of the plant COSYMA is shown in terms of system pressure and H₂ feed flow (energy input). The optimal fluidisation regime of the reactor is indicated by green shading. Three sets of experiments are shown: Sequential load change experiments (45 % to 100 % load) with H₂ recycling, the determination of the upper operation limit (plant operation limited by heat removal capacity, no recycling loop operated), and tests of the plant at the lower operation limit.

hydrogen feed flow rate for the subsequent series of part load experiments was reduced to 45 Lmin⁻¹, which was defined as the 100 % load operation. To allow higher H₂ feed flow rates at the given pressure difference in the membrane without the H₂ concentration in the product gas exceeding the 2 % limit, a larger membrane module would be required to ensure grid quality. Therefore, in the current set-up, the compressor (which has a lower operation limit) and the membrane unit are limiting factors. As discussed above, with a bypass around the compressor (and more installed membrane area), also the complete PtG plant could reach a larger operation window, similar to that of the methanation reactor. Alternatively, in case of low fluidisation in the reactor, a short-cut connection between the membrane feed and the permeate could be operated, which directly recycles methane-rich product gas. At the same time, the total gas flow rate in the membrane module is reduced, which allows reaching grid injection limitations at lower pressure differences.

Sequential load changes

The final goal of the field test was to sequentially go through different part loads in a dynamic experiment, while still producing grid-compliant biomethane. In between the constant operation phases, the feed flows, pressure levels and compressor duties had to be adapted manually. The sequence is shown in Table 6.2 with the corresponding flow rate and pressure settings.

Load level	H ₂ flow rate L/min	Biogas flow rate L/min	$x_{ret.,H_2}$ %	$x_{ret.,CO_2}$ %	$x_{ret.,CH_4}$ %	System press. barg
45 %	20.1	11.6	1.4	0.7	97.9	4.1
59 %	26.5	15.6	1.7	0.6	97.7	4.5
89 %	40.0	22.7	1.5	0.6	97.9	5.5
100 %	45.0	24.6	1.7	0.3	98.0	6.0

Table 6.2: Part load levels tested during the sequential experiment with corresponding average process conditions and product gas concentrations.

The composition of the product gas stream is shown in Figure 6.3. In this dynamic experiment, each setting was kept constant for around 1 h. After each load change, several adjustments of process parameters were required to maintain a stable operation of the process. As shown by the concentration measurement in the product gas stream, the grid injection limitations for CO₂ and CH₄ were fulfilled throughout the whole experiment. The H₂ concentration showed a slight violation of the 2 % limit after each load change. This is caused by an accumulation of hydrogen in the permeate stream, which was recycled to the feed of the plant. Since there was no faster concentration measurement than the μ GC available in the recycle stream, it was challenging to adjust the H₂ flow to the reactor. It was therefore not possible to immediately compensate the overshooting H₂ concentration in the product gas stream by reducing the H₂ feed to the plant, which lead to limit violations for around 5 – 25 min after each load change. This indicates that with improved process analytics (*e.g.* NDIR to record all carbon-species) and more automated process control procedures, a load change would be possible in much shorter time on one hand and with less hydrogen accumulation in the recycle loop, on the other hand.

The operation points of the sequential load test are indicated in the operation window of the COSYMA plant in Figure 6.2.

6.3.2 System analysis

An analysis of the current EPEX electricity cost data was performed using the three algorithms presented before. Based on a threshold cost for electricity, these algorithms decide when the electrolyser unit is active, and subsequently they calculate the hydrogen storage tank level and the load of the methanation unit.

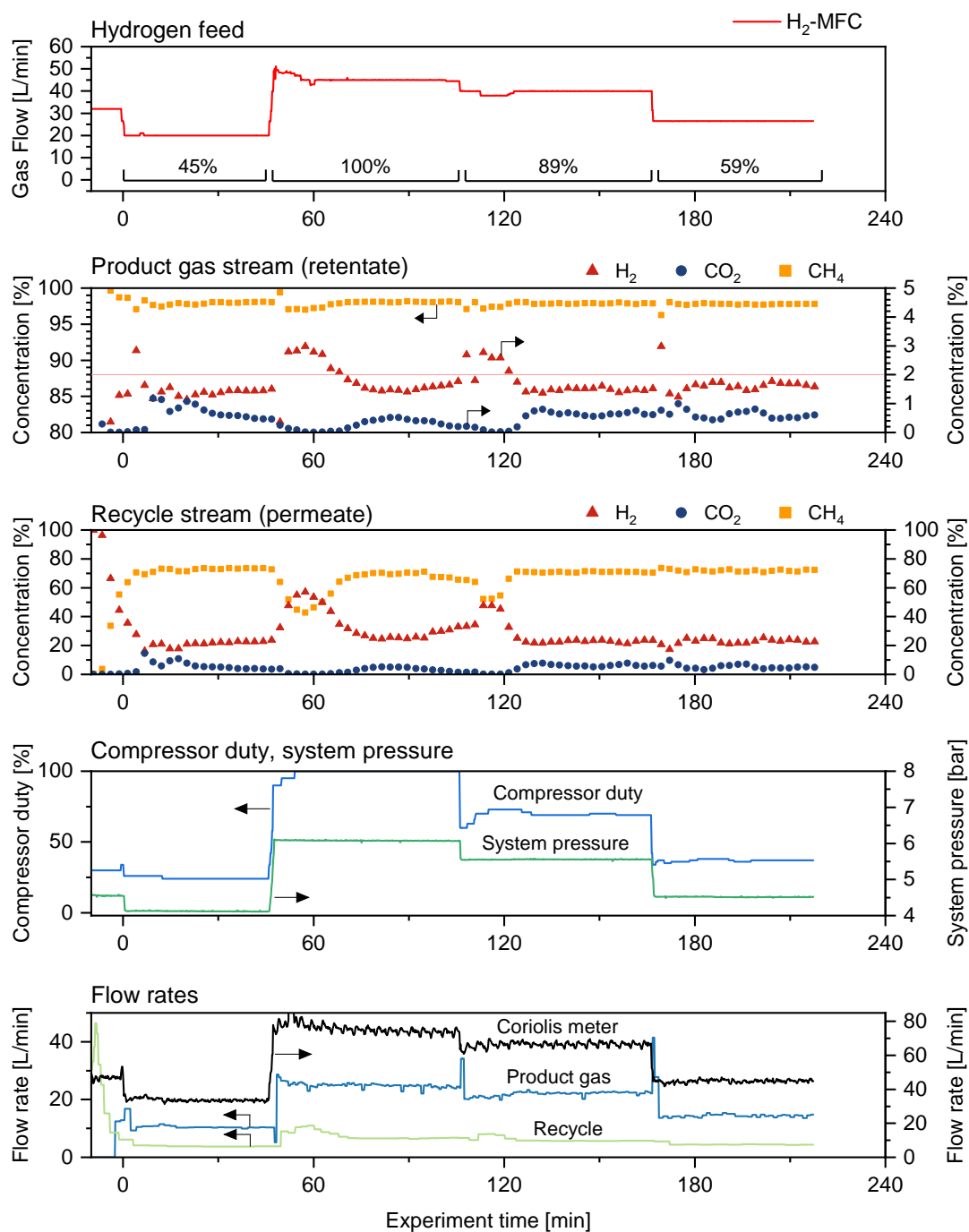


Figure 6.3: Dynamic methanation experiment – the most important process conditions and resulting concentration measurements are shown along the experimental time.

With increasing threshold value, more activity hours of the electrolyser are possible, and the higher is the amount of hydrogen produced. Obviously, that also leads to a longer operation span of the methanation unit. In this consideration, we decouple the operation of the electrolyser and the methanation unit by using the hydrogen storage tank. This means, that we can effectively use the hours with low electricity cost.

The buffer tank serves as accumulation unit to avoid short operation phases of the methanation unit that are connected to start-up and shut downs, thermal stresses in the plant, electricity consumption for re-heating and performance loss. For each algorithm, the number of start-ups of the methanation unit per year was determined. This gives an indication on the efficiency of the overall process, as each start-up operation is associated with a short operation state where grid injection limitations are not met and the product gas has to be flared. Figure 6.4 shows the average number of start-up operation per year for the three algorithms at four different tank sizes (3 h, 6 h, 12 h and 24 h). The underlying electricity cost distribution corresponds to the current market situation.

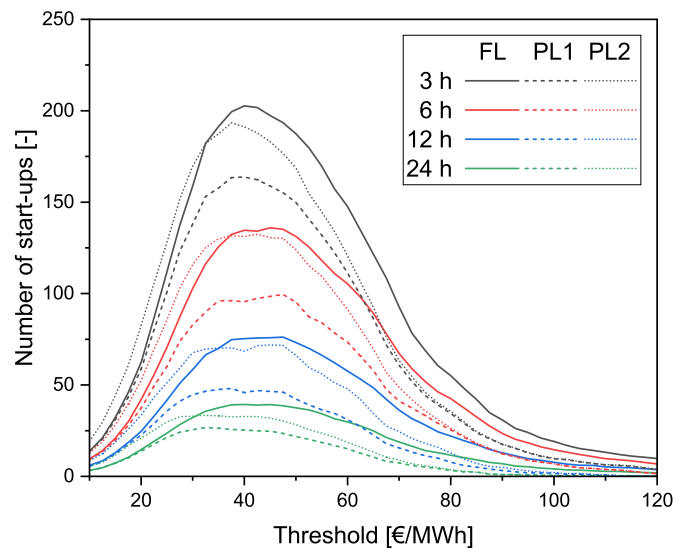


Figure 6.4: Average number of start up operations per year based on the price threshold for electricity is shown for all algorithms and tank sizes between 3 h and 24 h capacity.

As a general trend, it can be seen that larger tank sizes lead to a lower number of switching operations. Obviously, having a larger storage capacity available allows to bridge larger time spans with no hydrogen production on one hand, as well as operating the methanation unit longer with a single tank filling. Therefore, less start ups and shut downs are necessary.

Algorithm FL can be considered as a reference, as it only allows for full-load operation after the buffer tank is completely filled. In the case of a 6h tank size, this leads to a maximum number of around 135 switching operation per year at a threshold of 40 – 50 €/MWh. At lower

thresholds, the starts are less frequent, as the threshold is too low to produce large amounts of hydrogen. Above a threshold of 50 €/MWh, the number of switching operations decreases again for all algorithms. In this case, the threshold is above the main fluctuations and only peaks with high electricity cost cause the electrolyser to stop. Therefore, the methanation unit only shuts down for shorter periods of longer-term high electricity cost.

The maximum number of 135 starting operations mentioned before correspond to a start up every 2 to 3 days. This number decreases to around 55 in the case of 12 h tank size and 40 in the case of 24 h tank capacity. The maximum of this curve represents the threshold where the methanation is active for more than half of the year.

Similar to the full-load algorithm, the two part load versions show a steep increase of switching operations at low thresholds. The PL1 case even shows an identical behaviour as the full-load case, which is a consequence of the condition that the methanation is only allowed to start at full tank level. The algorithm PL2 allows a start of the methanation unit in part load operation at 50 % tank level. This reflects in higher starting operations at low thresholds. In this case, the methanation is started in part load at relatively low tank level and therefore only operates for short times. It is therefore advisable to store hydrogen until at least one full tank capacity can be methanated. The advantage of part load starting can only be seen at high thresholds leading to high availability of hydrogen.

The algorithm PL1 initially shows an identical behaviour as the full-load case, but in the mid-range of thresholds, it leads to a lower amount of switching operations. This is the effect of switching the methanation to part load as soon as 50 % tank level is reached. This leads to an extension of the operation time of the methanation, which ideally merges with the next operation period. Instead of several full-load operation cycles, an extended part load at 50 % level is possible. As mentioned before, this leads to a reduction of starting and shut down operations, which unavoidably produce product gas losses and decrease the overall process efficiency.

It is important to mention that the number of full-load-equivalent operation hours of the electrolyser and the methanation unit are identical in all cases as the two units are designed for the same hydrogen capacity. Only the distribution over the year is different. Furthermore, the specific production costs of the biomethane are not directly affected as the same amount of biomethane is produced. An indirect contribution originates from the difference in tank size, *i.e.* lower CAPEX.

The hydrogen buffer tank acts as an integration unit for electricity cost. It is only filled when the current cost for electricity is below a certain threshold. The methanation operation hours can therefore be associated with the corresponding averaged electricity cost.

In Figure 6.5 (left), the operation hours of the methanation unit are shown against the electricity threshold cost. With increasing threshold, more of the electricity price curve can be

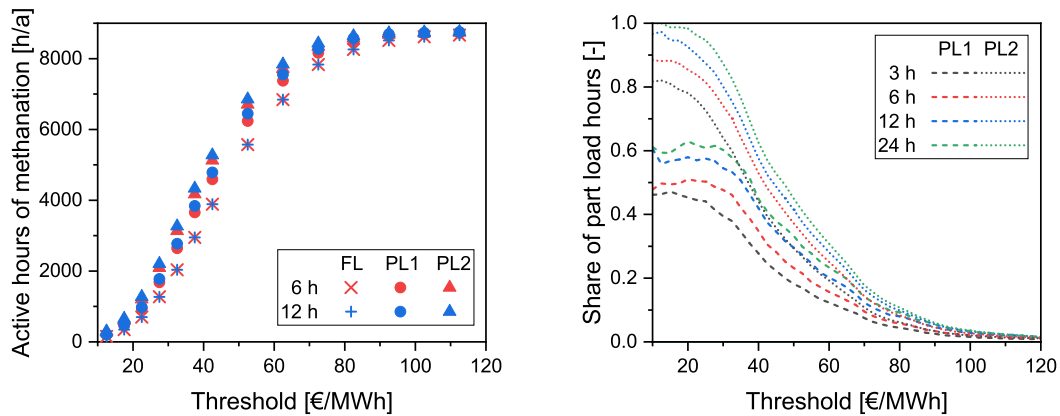


Figure 6.5: On the left side, the activity hours of the methanation unit, based on different threshold prices for electricity are shown. The right side shows the share of activity hours, where the methanation unit is operated in part load, in dependence of electricity threshold cost.

covered, and a higher operation time of the electrolyser and the methanation unit is reached. The operation hours are shown for all three algorithms and tank sizes of 6h and 12h capacity.

The distribution for the full-load algorithm is identical for all tank sizes. This algorithm does decouple the operation times of the electrolyser and the methanation, but does not extend the operation time of the methanation unit. This leads to a rescheduling of the activity of the methanation unit and a merging of short operation phases according to the tanks capacity.

The operation times of the methanation unit can only be extended when part load is allowed. In this operation, a certain influence of the tank capacity can be observed, nevertheless, as presumably large fluctuations cannot be covered by this relatively small tank sizes, the influence on operation cost is marginal.

The largest influence on the operation hours of the methanation unit has the chosen algorithm. This means that the heuristics of plant management are crucial in the effective use of the resources. Compared to the full-load algorithm at a threshold of 50 €/MWh, the part load algorithm increases the operation time by almost 1000 h per year, the second part load algorithm by around 1500 h per year. It is important to mention that this does not change the overall biomethane output of the plant, as a share of this operation hours refer to part load operation. As a fraction of these operation hours refer to operation in part load, this mode has also no influence on the cost of the electricity, which was used in the electrolyser, therefore no cost benefit arises from the current design. It simply allows the plant to be kept at operation temperature for 1000 h and 1500 h more per year, which decreases intermediate cooling cycles or unproductive hot-standby phases.

As shown in Figure 6.5 (right), the operation heuristics of the plant have a great influence on the load-level of the methanation plant. At low thresholds, the first part load algorithm favours

full-load operation, whereas the second operates almost only at part load. With increasing thresholds, the hydrogen production phases become more continuous and the share of part load hours of the methanation unit decreases. Even at thresholds around 50 €/MWh, the values obtained with algorithm PL1 are clearly lower than for the second but still at around 20 to 30 % part load operation.

The analysis shows that the two part load algorithms have different influence on the share of part load and full-load operation hours. The first algorithm clearly favours full-load operation, which is more desirable from plant operation perspective. It allows for an operation closer to the design specifications of the plant and therefore a more efficient use of resources. The first algorithm furthermore triggers less start-up cycles of the plant, which is another key advantage and efficiency gain of this heuristic.

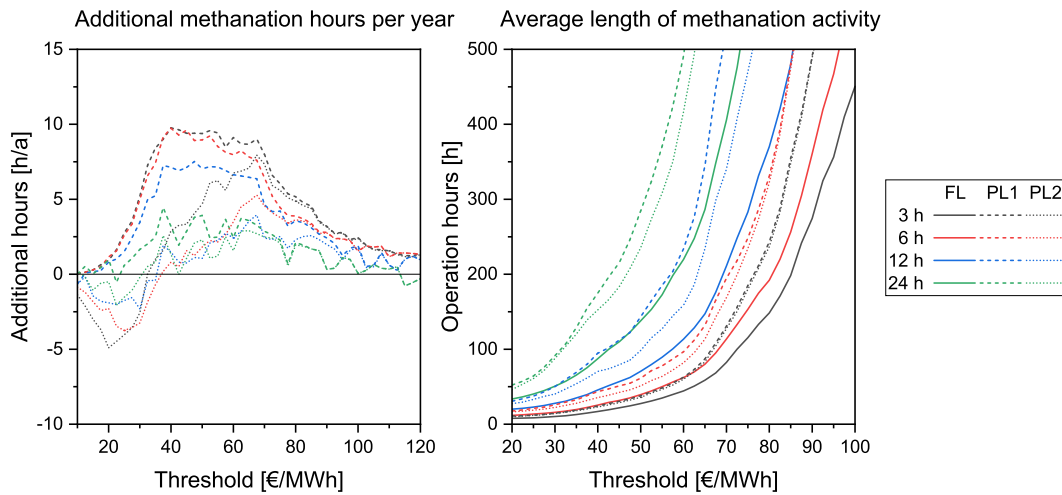


Figure 6.6: Left: Average number of additional biomethane production hours per year, compared to the full-load algorithm at different electricity cost thresholds. Each start-up operation is associated with a penalty of 15 min lost gas production time (*i.e.* flaring). Right: Duration of a methanation operation phase regardless of load level, as an average over the whole considered time period.

Figure 6.6 (left) shows the benefit of introducing part load capability in the plant in terms of additional biomethane production time, compared to the full-load algorithm. It considers 15 min of gas flaring during the start-up of the methanation reactor. The algorithm PL1 shows a clear positive influence at all considered tank sizes. Using 3 h and 6 h tanks, the algorithm allows an increase of 10 h per year. Larger tank sizes decrease the benefit even further, as generally less start-ups are performed. The second algorithm shows even a negative effect, which is caused by short part load intervals at low thresholds.

In Figure 6.6 (right), the operation time spans of the methanation unit are shown as an average over the whole considered time period. Both part load algorithms clearly increase the operation time compared to the full-load reference case. Already relatively low tank capacities

allow to bridge interruptions in H_2 supply and increase the methanation activity. At the larger tanks sizes investigated, it can be seen that the algorithm PL1 results in a larger increase of methanation activity. The methanation activity spans start to increase over-proportionally with larger tank sizes and higher price thresholds. This is a result of more short-termed fluctuations, which are bridged.

The benefit indicated here is almost negligible in terms of additional methane production and therefore also in terms of cost. Nevertheless, in terms of plant operation, it is important to see that there is no negative impact on the methane production due to starting procedures.

Increasing the electrolyser power

Increasing the capacity of the electrolyser compared to the methanation results in a more frequent start-up of the methanation unit. A larger amount of hydrogen is available and the tank level reaches the trigger point to start the methanation faster.

The second part load algorithm becomes more beneficial with increasing electrolyser power. The number of additional PtG operation hours and therefore the amount of produced bio-methane increases with higher electrolyser power. Algorithm PL2 provides better use of the produced hydrogen, as it allows for a start-up of the methanation plant before the storage is full. Therefore, a higher amount of hydrogen can be converted through the system than with the first part load algorithm or no part load at all.

A beneficial effect of the tank and the electrolyser size on the average cost of the electricity used could only be observed at extreme cases. Increasing the tank size to 200 h capacity and oversizing the electrolyser by 100 %, resulted in an increase of the operation time of the methanation unit of around 1000 h per year in the mid-range of the distribution curve. Such a tank and electrolyser size are economically unfeasible for a stand-alone biogas plant to realise. Nevertheless, if tank and electrolyser are available from another process, flexible methanation can be included as a synergy. Although this is only a simplified consideration, which opens room for further optimisation, these insights justify the use and the need for part load capability of the methanation unit. On one hand to decrease gas losses by flaring during start-up procedures, on the other hand by decreasing time-consuming heating of the methanation unit by enabling hot-standby phases. Overall, a process with higher stability in the downstream part is possible. This is especially also favourable in terms of lifetime of the methanation unit, as less thermal stress is caused and catalyst deactivation is reduced due to more stable process operations. An additional aspect refers to the adsorptive raw gas cleaning, which can also be operated more stably, which reduces desorption of contaminants and subsequent poisoning of the methanation catalyst [37].

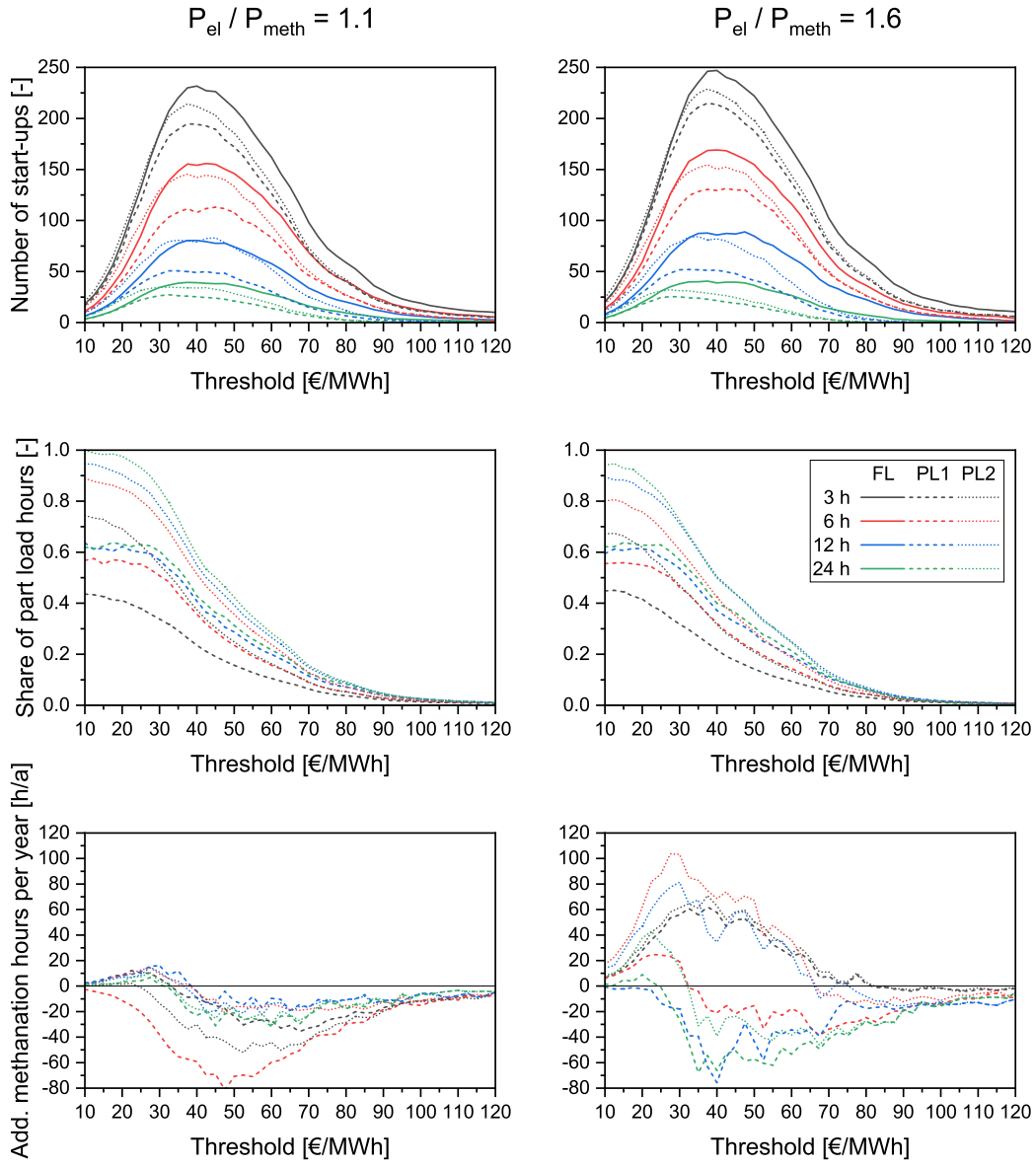


Figure 6.7: Effect of increasing the electrolyser power 10 % and 60 %, relative to the methanation capacity.

6.4 Conclusion

In this work, we investigated how part load operation increases the flexibility of a PtG process chain for biogas upgrading. The system considered is based on a concept of earlier work, which allows a flexible upgrading of biogas, either by direct methanation or by membrane separation of CO₂.

The part load behaviour of the process chain was tested in a TRL 5 methanation pilot plant during a field campaign using real biogas. In a first set of experiments, it was shown that the load maximum of the plant was given by the heat removal capacity in the reactor. In a second set of experiments, the minimum load of the bubbling fluidised bed reactor was determined to be 20 % of the full load (based on H₂ flow rate).

A stable operation of the full process chain including the upgrading membrane and subsequent H₂-recycling could be successfully shown. Grid-ready biomethane was produced in a load range of 45 to 100 %. Nevertheless, special attention had to be taken to prevent H₂ and CO₂ accumulation in the recycle loop, which led to a displacement of raw biogas in the plant's feed and subsequently to a decreased conversion in the reactor. In newly designed plants, specific sensors and automated control mechanisms could prevent such feedback loops. The lower part load limit was given in this specific set-up by the installed membrane area, which was insufficient to remove H₂ at lower pressure levels.

In a dynamic experiment, four sequential load changes in the range of 45 % to full load were run. It could be shown that a stable operation in the whole range is possible and grid-ready biomethane can be produced. During short periods after load changes the H₂ limit in the product gas was exceeded. Nevertheless, by implementing improved control mechanisms, such events can be significantly reduced.

Our field experiments showed that dynamic part load operation of the full methanation process chain is possible and stable operation can be achieved after each load change. The biogas upgrading membrane successfully removes excess H₂ from the product gas down to a limit of <2 % and enables grid injection at all operation levels.

Furthermore, a system analysis (regarding electrolyser, H₂ storage tank, and methanation) was performed, which shows the necessity to enable part load operation of the PtG plant. Operation times of the methanation unit could be increased, as part load operation phases bridge between times, where cheap, renewable electricity is available. Larger H₂ tank sizes further decrease the average number of start-up operations of the methanation unit per year. To find the optimum tank size, further optimisation is required, which includes economic factors in the analysis.

In the system analysis, three different heuristics for plant operation were tested. It revealed that the trigger point for methanation start up (*i.e.* H₂ storage tank level) has a high influence on the average number of start up and shut down operations. Allowing the methanation plant

to start up in part load before the H₂ storage level reaches its maximum results in a higher number of short operation phases of the methanation unit. Accumulating H₂ in the tank to be able to run the methanation for at least one tank capacity proved to be more favourable in terms of start up operations and consecutive methanation operation.

7 Asymmetrical part load operation of a Power-to-Gas process

7.1 Introduction

In the previous chapter, symmetrical part load scenarios were discussed. It was assumed that the CO₂ source either limits the capacity of the methanation plant or can be stored for a certain time when H₂ is the limiting component. This refers to an integrated plant concept as presented in Chapter 4, which is capable of biogas upgrading as well as methanation product gas treatment.

Alternatively, an existing biogas upgrading plant with a clean CO₂ off gas stream can be considered. The CO₂ stream can be methanated depending on the availability of H₂. Such a design causes a similar, symmetrical part load behaviour as shown in the previous chapter. The disadvantage of such a design is that two separate plants are built, each with its own membrane upgrading system. As full load PtG operation should be possible, the size of the methanation plant has to match the maximum CO₂ production of the biogas plant. By integrating the methanation unit into the biogas upgrading process, the investment and operation cost of a second membrane upgrading unit after the methanation might be saved.

The operational flexibility of anaerobic digester units is limited. It is tested to influence the biogas production by different feeding strategies with the goal for a demand-driven biogas production. Nevertheless, in such a system with high residence times, the changes take effect only after several hours or days [142–144]. Also, storage capacity for raw biogas is limited to several hours, as often only low pressure tanks are available [144]. The biogas plant therefore provides a CO₂ stream with fluctuations on a rather long time scale. If PtG is used for biogas upgrading and only limited H₂ is available for methanation, only part load operation of the plant is possible. In such a case, the system has to cope with an excess of CO₂. As hydrogen and the carbon source are not equally reduced, we refer to this scenario as asymmetrical part load operation.

In symmetrical part load operation as shown in the previous chapter, all units are operated under part load conditions. In this case, CO₂ and H₂ are equally limited and can be fed to the

reactor in a stoichiometric ratio. Such a case occurs when excess biogas can be temporarily stored (*e.g.* by inflatable rooftops [144]) and H_2 production is reduced, or if H_2 provision is synchronised with biogas production. Previous simulations and experiments showed the feasibility of such an operation mode.

In an asymmetrical part load scenario as described above, CO_2 has to be selectively removed from the system. In the flexible upgrading system presented in the current chapter, this can be achieved by bypassing the methanation reactor and only converting a part of the CO_2 fed to the plant to CH_4 .

When only part of the CO_2 can be converted to methane, the remainder of the raw biogas (ca. 60 % CH_4 and 40 % CO_2) has to be upgraded otherwise. Since the product gas stream from the methanation contains around 10 % of unreacted hydrogen, it requires a membrane upgrading step to fulfil grid injection limitations. If the same membrane unit is used for CO_2 separation from the remaining biogas stream, part of the H_2 is lost through the off gas stream along with the vented CO_2 .

The presence of H_2 and CH_4 in the CO_2 -rich exhaust gas stream might not only be problematic in terms of operational safety, it also caused a loss of reactant gas and represents a direct efficiency decrease for the plant.

Such process integration leads to further issues, which have to be addressed. Especially since the membrane upgrading produces a recycle stream to the feed of the plant, its flow rate is important for plant sizing as recompression of this gas stream is required. Furthermore, an altered gas flow rate and composition affects the performance of the membrane upgrading and therefore the composition of the product gas. It is therefore required to adjust the process conditions (pressures and flow rate per membrane module) accordingly.

To investigate these challenges, simulations were performed in order to investigate the feasibility and to identify peculiarities of the process variations.

7.2 Concepts for asymmetrical part load and process simulations

The process simulations presented in this work are a modification of the concept presented in the previous chapter. There, a way to increase the operational flexibility of a power-to-methane process at moderate cost increase was presented. It could be shown that by simulations using rate-based models for a hollow-fibre gas separation membrane and a bubbling fluidised bed methanation reactor, a process operating in the two extreme cases (membrane-based biogas upgrading and methanation) is feasible. This data provides the general sizing of the membrane upgrading and main compressors.

In this work, we present process simulations, which investigate the behaviour of these process chains under an asymmetrical part load scenario, *i.e.* a part of the gas is upgraded, and a part is converted by PtG. The basis for this bottom-up process simulations is the rate-based model

for bubbling fluidised bed methanation and the counter-current membrane model presented in Chapter 3.

Based on previously investigated process options for flexible biogas upgrading, further alternative process configurations are proposed, which allow for an operation under part load conditions. The goal is to identify a process, which maintains the cost structure of the previously investigated full-load processes, but enables combined part load of both, membrane upgrading and PtG. Extensive cost calculations are thus obsolete, since the investment costs are given by the full-load processes and operation costs are also not exceeded.

The integrated process options considered for further evaluation mainly differentiate in the position where the split stream to the reactor is positioned. The underlying process design is based on the 2-stage membrane process for biogas upgrading, where the first membrane stage is used to produce grid-ready biomethane and the second stage to remove CO₂ from the recycle stream (see Chapter 4). In all part load cases, it is important to ensure the possibility to adjust the pressure level in the reactor independently from the membrane upgrading unit. In case of part load operation, the methanation unit is impinged with a lower flow rate than in full load operation; therefore, the fluidisation in the reactor has to be maintained by lowering the pressure, while the separation performance of the membrane upgrading can be adjusted independently.

In asymmetrical part load operation, the split ratio r_{split} defining the share of the gas being directed to the methanation unit, is determined by the feed stream of CO₂ to the plant $\dot{n}_{CO_2,feed}$ and the part load ratio r_{PL} . The split ratio is multiplied with each partial stream entering the stream splitter $\dot{n}_{i,splitterfeed}$ in order to determine the feed to the methanation unit.

$$\dot{n}_{CO_2,split} = \dot{n}_{CO_2,feed} \cdot r_{PL} \quad (7.1)$$

$$r_{split} = \frac{\dot{n}_{CO_2,split}}{\dot{n}_{CO_2,splitterfeed}} \quad (7.2)$$

$$\dot{n}_{i, meth.} = r_{split} \cdot \dot{n}_{i, splitterfeed} \quad (7.3)$$

7.2.1 Part load operation of PtG1

This process option is a modification of the process *PtG1* (see section 5.3.1). In full-load operation, the product gas from the methanation unit would be directed to the feed of the first membrane stage. The second membrane would be bypassed and is not in operation (see Figure 7.1).

The methanation unit stays in this configuration as long as no adjustment of the fluidisation state is necessary. As soon as a lower operation pressure of the reactor is required due to

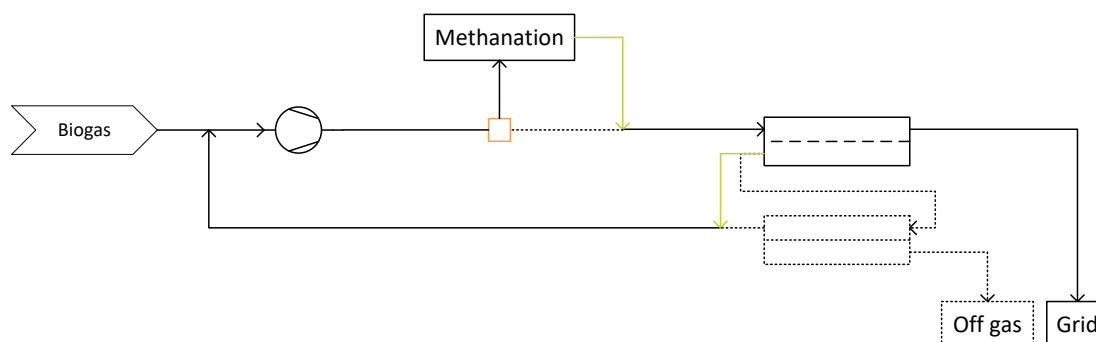


Figure 7.1: *PtG1* configuration in full load operation: The green connections are only active during full load operation of the plant.

lower part load, the pressure difference in the membrane upgrading unit becomes too small. Therefore, the configuration of the plant has to change as shown in Figure 7.2. The product gas is merged at the plant's feed with the recycle flow coming from the second membrane stage. This re-configuration of the plant can be achieved by appropriate piping and valve switching, no alteration of the main units is required.

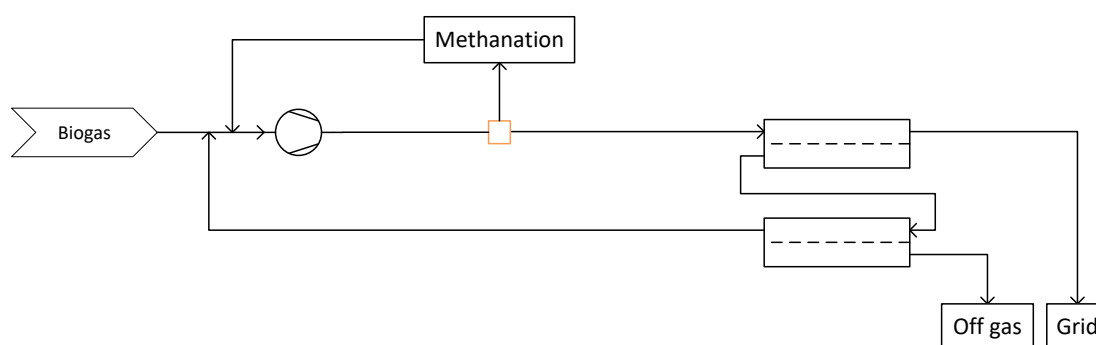


Figure 7.2: *PtG1* configuration in part load operation: To independently adjust the pressure in the BFB reactor and the membrane unit the product gas from the methanation has to be merged with the feed of the plant.

7.2.2 Part load operation of *PtG2*

Compared to the *PtG1* case, these process options refer to an inverted process chain, as shown in Figures 7.3 and 7.4. Under full-load operation, the raw gas enters the membrane unit first and the CO_2 -rich permeate is then methanated. Since only a single stage is required for the separation of unreacted H_2 from the product gas stream, the second membrane stage is bypassed. This configuration includes a secondary compressor, which recompresses the

feed stream to the reactor. The second membrane stage is only put in operation when the methanation is inactive, or if asymmetrical part load operation is desired. In such a case, the split stream through the reactor can either be drawn from the permeate of the first membrane stage (Figure 7.3), or from the retentate leaving the second stage (Figure 7.4).

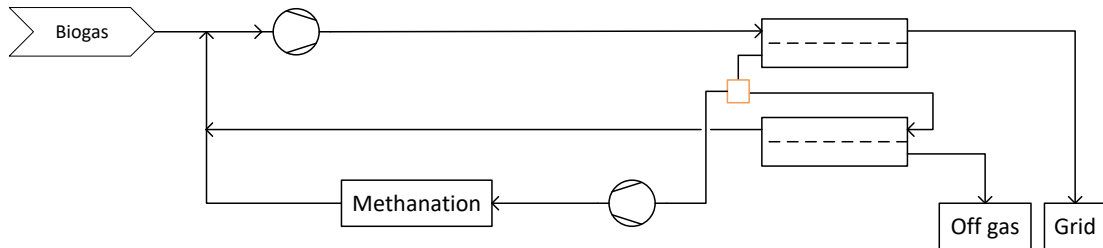


Figure 7.3: Process *PtG2*, split stream to the reactor in the permeate of the first membrane stage.

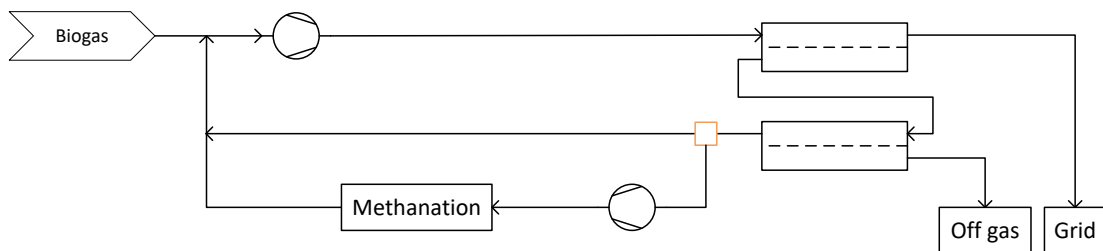


Figure 7.4: Process *PtG2*, split stream to the reactor in the retentate of the second membrane stage.

7.2.3 Part load operation of *PtG3*

This process option enables a refurbishing of an existing membrane upgrading plant. The CO₂ off-gas stream is partially fed to a methanation unit and the product gas merged with the plant's recycle stream (see Figure 7.5). In full-load operation, the feed gas for the reactor would directly be the permeate of the second membrane stage, analogously to the previous process variant. For all comparisons, a reactor pressure level of 6 bara was considered and the temperature set to 360 °C. Although there is a certain influence of the process conditions on the product gas composition, it hardly affects the performance of the overall process. Therefore, no further evaluation of reaction conditions was performed.

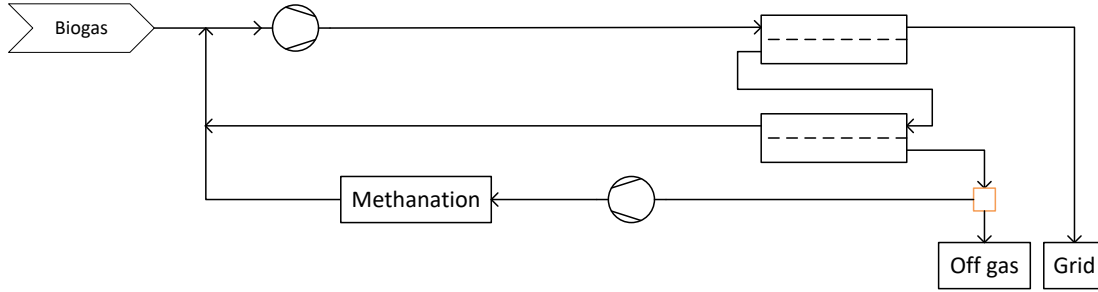


Figure 7.5: Process *PtG3*, the slip stream to the reactor is drawn from the off gas stream.

7.2.4 Energy loss

The share of energy lost through product gas in the exhaust stream during part load operation was calculated from the feed and off gas streams of H_2 and CH_4 according to:

$$r_{E,loss} = \frac{\dot{n}_{offgas} (x_{offgas,CH_4} \cdot HHV_{CH_4} + x_{offgas,H_2} \cdot HHV_{H_2})}{\dot{n}_{CH_4,plantfeed} \cdot HHV_{CH_4} + \dot{n}_{H_2,in} \cdot HHV_{H_2}} \quad (7.4)$$

The molar feed flow of CH_4 to the plant was identical in all cases, as all cases are based on a biogas feed of $200 \text{ m}^3/\text{h}$ with 60 % CH_4 . For the membrane-based upgrading process presented in the previous chapters, the methane loss amounted to 0.6 % of the incoming methane flow. This corresponds directly to the energy loss, as no other combustible compound is present.

7.3 Validity of the permeance model

The field experiments explained in Chapter 6 allowed to check the validity of the membrane model presented in Chapter 5. The experiments provided us with a new, independent data set, obtained by upgrading raw biomethane to injection-ready quality. This data set allows to increase the confidence in the rate-based membrane model used for the simulations in this chapter.

Ten data points were chosen, where the plant was operated in steady state for 28 min up to 71 min. All recorded data was averaged over the respective time span. The flow rates of the permeate and retentate stream were recorded by gas meters, which were calibrated before the experiments. The feed flow rate was not recorded as the methanation reactor was operated and only the composition of the dried product gas was monitored. The feed flow rate was calculated as the sum of the permeate and retentate stream. The concentration measurements

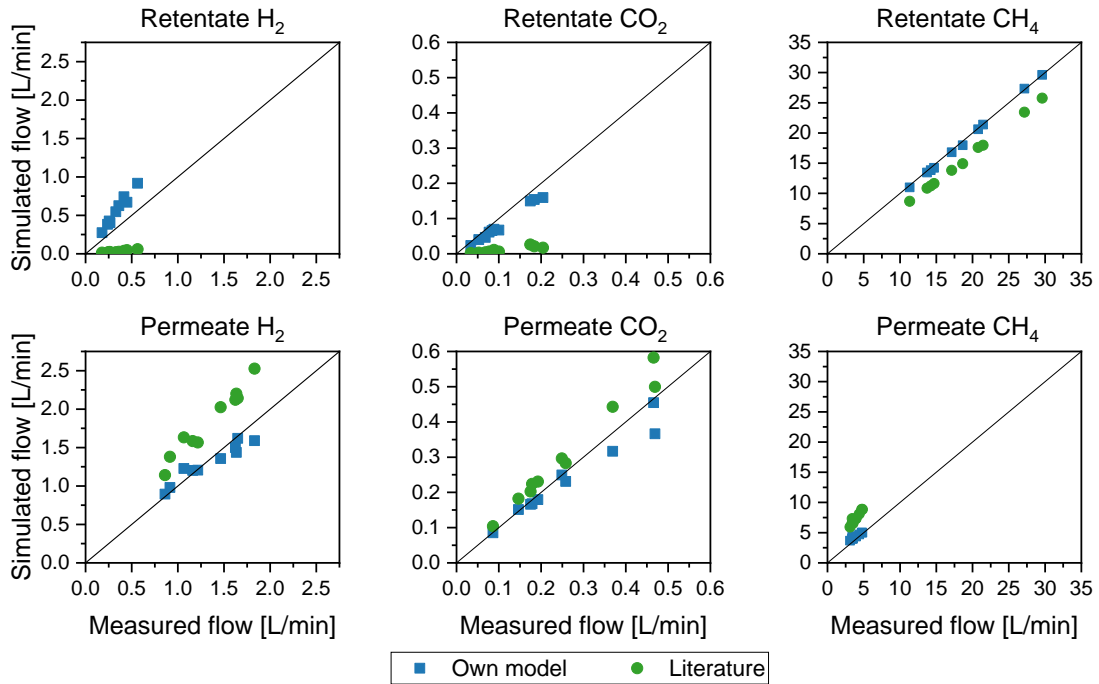


Figure 7.6: Parity plots comparing experimentally determined flow rates with results from the simulation of the membrane model. The simulations were performed with the permeation model developed in this work (own model) and permeance data of the polymer *Matrimid* from literature [119].

from the μ GC at the membrane inlet and outlets allowed the determination of the molar flows of each component. The simulation of the membrane model was run based on the feed flow rates and the feed and permeate pressures. The simulation result of the retentate and permeate flows was then compared to the experimental results. The simulation was also performed using literature data for the *Matrimid* membrane material as a benchmark.

7.3.1 Results

Generally, the simulations for the permeation model of the Evonik membrane showed satisfying agreement with the experimental data (see Figure 7.6). A slight under-estimation of H_2 permeance can be observed, which leads to a higher retentate flow and a lower permeate flow than observed in the experiments. Also in the case of CO_2 , a certain under-estimation of permeate and retentate flows can be seen. Nevertheless, since product gas from the methanation reactor was used as feed, the concentrations and subsequently the molar flows of CO_2 were very low. Methane was present in the highest concentrations, and therefore the highest molar flow rates. For methane the best agreement of simulation and experimental results can be found.

From this data, the accumulation of hydrogen and CO₂ in the permeate flow can be seen, as the permeate flow rates are higher than with methane.

In Figure 7.6, the results of the simulation with *Matrimid* permeance data are also shown and can be directly compared to the Evonik model. It can be seen that the model based on *Matrimid*-data performs worse than the Evonik model. Especially the retentate streams of CO₂ and H₂ are highly under-estimated as a result of a higher permeance. A similar, but less pronounced effect can be seen in the simulation of the methane flows.

By this comparison, the validity of the newly developed permeation model could be shown, especially the better performance compared to literature data. We therefore gain higher confidence in the simulations presented here.

7.4 Results and discussion – Asymmetrical part load scenarios

The feasibility of the simulated processes is assessed according to the following criteria:

- The grid injection limitations have to be fulfilled.
- The process is benchmarked against the limits given by the full load operation cases: the compressor duty and the recycle flow should not exceed the values given by the membrane upgrading case (60 kW and 441 m³/h) according to Chapter 5, Table 5.7. This ensures that the process can be operated with the given installations and at no additional cost, compared to the flexible processes presented there.
- Optionally, the H₂ and CH₄ concentrations in the exhaust stream should be as low as possible. On one hand due to plant safety reasons, on the other hand due to the associated efficiency decrease by product gas loss.

7.4.1 Reactor in slip stream after the compressor

The process *PtGI*, where the product gas from the methanation is merged with the bypassed biogas (see Figure 7.1) is unfeasible for operation in asymmetrical part load. As only a share of CO₂ is directed to the reactor, the overall CO₂ content in the product gas increases with increasing part load. The product gas of the methanation mixed with the bypassed raw gas being fed to the membrane separation unit resembles the biogas case. Therefore, preliminary simulations showed that even at a part load level close to full load, the system pressure has to be increased in order to separate enough CO₂ to achieve grid-ready product gas. This contradicts the fluidisation requirements in the reactor. When the part load level is decreased, the gas flow through the reactor decreases accordingly. In order to compensate the lower flow rate and still achieve a sufficiently high fluidisation state, it is required to reduce the pressure in the reactor. The two counter-acting trends of raising system pressure and decreasing reactor pressure do not allow for a design as shown in Figure 7.1. This behaviour demands a design

according to Figure 7.2, which allows different pressure levels in the membrane upgrading unit and the methanation reactor.

Obviously, in such a configuration, the plant cannot be operated in full-load, as the recycle stream would rise to infinity. Therefore, in order to simplify the process, high part load levels could be generally avoided and operation only allowed at levels of 75 % part load or lower. The plant would then have a bi-modal operation characteristics: full load operation with the raw methanation product gas being fed directly to the membrane upgrading (see Figure 7.1), and part load operation at 75 % or lower with the product gas being fed to the recycle stream, as shown in Figure 7.2.

As shown in Table 7.1, having a lower permeate pressure in the first membrane stage (2 bara), efficiently separates CO₂ and H₂ from the product gas stream. The permeate stream produced under this pressure regime is relatively low in CH₄, which has the advantage that the CH₄ concentration in the off gas is relatively low. Nevertheless, the total flow of permeate is higher than in the pure upgrading case (see Table 5.7). This larger recycle stream causes increased flow rates in the first membrane stage, which prevents reaching the grid injection limitations for CH₄ and CO₂.

p_{perm,stage 1} = 2 bara → Δp_{MEM2} = 1 bar

p _{sys}	r _{PL}	Product gas injected to grid				Gas vented			Compr.	V _{rec}	Energy loss	Feasible
		x _{H2}	x _{CO2}	x _{CH4}	Dew pt.	x _{H2,off}	x _{CO2,off}	x _{CH4,off}				
bar	-	-	-	-	°C	-	-	-	kW	m ³ /h	-	
12	0.75	0.8%	1.9%	97.2%	-8.6	13.4%	80.9%	4.7%	50.7	415.7	1.2%	x
12	0.5	0.9%	3.4%	95.6%	-9.5	8.4%	89.5%	1.6%	58.3	510.5	0.9%	
12	0.3	1.0%	7.1%	91.9%	-9.5	4.7%	94.3%	0.7%	73.5	699.2	0.6%	
14	0.5	0.9%	3.2%	95.9%	-11.4	7.6%	91.0%	1.0%	83.6	718.9	0.8%	
14	0.3	1.0%	6.6%	92.3%	-10.9	4.5%	94.8%	0.5%	98.4	888.2	0.6%	
15	0.3	0.9%	5.8%	93.2%	-11.7	4.6%	94.7%	0.5%	107.8	944.6	0.6%	

p_{perm,stage 1} = 3 bara → Δp_{MEM2} = 2 bar

12	0.75	1.0%	2.9%	95.9%	-0.1	15.6%	72.0%	10.9%	51.3	424.1	2.4%	
12	0.5	0.8%	3.7%	95.4%	-6.2	10.0%	83.9%	5.3%	39.8	283.5	2.3%	
12	0.3	0.6%	4.5%	94.9%	-12.4	5.9%	90.7%	3.1%	37.7	258.0	1.9%	
14	0.75	0.7%	1.6%	97.6%	-6.7	15.4%	73.4%	9.7%	56.4	422.0	2.4%	
14	0.5	0.5%	2.1%	97.3%	-12.2	9.9%	84.5%	4.9%	46.0	306.5	2.2%	x
14	0.3	0.4%	2.5%	97.1%	-17.4	6.0%	90.7%	2.9%	44.7	293.6	1.9%	x
15	0.75	0.5%	1.2%	98.2%	-9.7	15.4%	73.8%	9.4%	59.0	424.2	2.4%	x
15	0.5	0.4%	1.5%	98.0%	-14.6	10.1%	84.3%	4.9%	48.9	316.4	2.3%	x
15	0.3	0.3%	1.9%	97.8%	-20.0	6.0%	90.9%	2.8%	48.3	311.0	1.8%	x

Table 7.1: Selection of results of the process simulations of case *PtG1*. Fully feasible options are marked in bold.

Increasing the permeate pressure (3 bara) of membrane stage one results in a lower permeate flow. Since the pressure difference in the second membrane stage is higher, the CO₂ removal

from the system is higher. Therefore, the total flow in the recycle as well as in the first membrane stage is decreased and grid compliance can be fulfilled. On the contrary, increasing the pressure difference in the second membrane stage leads to higher losses of methane through the off gas stream. All simulations with a permeate pressure of 3 bar resulted in a CH₄ concentration higher than 1 % in the off gas. Analogously, the hydrogen losses through the off gas are also higher, in the concentration range of 15.4 % to 6.0 %.

The simulations show that part load using this configuration allows to inject the retentate in a range of 75 % down to less than 30 %. At the highest part load level, grid injection limits and technical restraints are met at 12 bar system pressure and a permeate pressure (stage one) of 2 bar. This limits the total recycle flow, as well as the CH₄ losses through the off gas.

At 50 and 30 % part load, the plant has to be operated at 15 bar and the permeate pressure of the first stage raised to 3 bar. This decreases the recycle flow below the maximum given by the membrane upgrading case.

In all feasible cases, the hydrogen losses through the off gas amount to 1.3 to 3.8 % of the feed stream coming from the electrolysis. In combination with the lost methane, this amounts to a total energy loss through the off gas stream of 1.1 to 2.4 % of the total feed energy.

7.4.2 Case *PtG2* – Slip stream to reactor after first membrane stage

This process chain consists of a membrane-upgrading unit, which produces grid-ready bio-methane during all operation conditions. The methanation unit is located in the recycling stream of the membrane upgrading; it therefore operates with a feed gas with a high CO₂-content. In the previous chapters, two sub-variations were discussed: A single-compressor option and a two-compressor option. As shown there, there is only a minor cost difference between the two options, as they are embedded in the flexible upgrading concept, which – in terms of cost – is highly dominated by the membrane-based biogas upgrading case. In the following considerations, only the variation with two compressors is further considered. The two-compressor option provides a higher degree of freedom when part load operation is desired, as the pressure of the methanation unit can be chosen independently from the membrane upgrading. Furthermore, this option is more relevant in terms of applicability, as it may enable a simple retrofitting of existing membrane upgrading plants with flexible PtG functionality.

Two versions of the *PtG2* process were considered. Since there is a bypass to the reactor required to allow for partial load operation, there are two positions to include the split stream: in the retentate of membrane stage two, *i.e.* the recycle stream, or in the permeate of membrane stage one. In the first case, a share of the CO₂ is removed from the process by the second membrane stage. At low part load levels, this loss of CO₂ is too high to provide the necessary CO₂ flow to the reactor.

Part load operation of PtG2 – Split in the feed of membrane stage two

The limits for CH₄ emissions through the off gas are assumed to be at 1 vol.-%, due to the high global warming potential (GWP) of methane. This limit is difficult to fulfil in all part load cases, often, the limit is exceeded. Although the concentration in the off-gas is relatively high, the absolute loss of methane is well below 2 % of the component's feed flow to the plant. In order to reduce the emissions, the membrane process should be further optimised, *i.e.* by adapting pressure ratios and membrane area. Alternatively, if surrounding equipment allows, the off gas can be burned in an incineration process (*e.g.* waste incinerator), maybe with catalytic support.

The nine process simulations, which resulted in conditions fulfilling the grid injection limitations, are shown in Table 7.2. Three of these cases exceed the technical limits given by the biogas upgrading case, namely the recycle flow rate to be recompressed and subsequently the duty of the main compressor unit. One of these cases only showed a slight violation of the limits. Our simulations show that a part load range of 75 % down to 30 % is feasible. Lower part loads were not tested in this case.

$p_{\text{perm, stage 1}} = 2 \text{ bara} \rightarrow \Delta p_{\text{MEM2}} = 1 \text{ bar}$

p_{sys} bar	# Modules, Stage 2	r_{PL}	Product gas injected to grid				Gas vented			1 st Compr. kW	2 nd Compr. kW	V_{rec} m ³ /h	Energy loss	Feasible
			x_{H_2}	x_{CO_2}	x_{CH_4}	Dew pt. °C	$x_{\text{H}_2, \text{off}}$	$x_{\text{CO}_2, \text{off}}$	$x_{\text{CH}_4, \text{off}}$					
10	33	0.75	1.0%	3.6%	95.3%	-8.6	11.5%	81.6%	6.3%	28.8	5.0	195.6	1.1%	
12	33	0.75	0.7%	2.1%	97.2%	-13.7	11.5%	83.1%	4.8%	37.3	4.8	251.7	1.1%	x
15	33	0.75	0.4%	0.8%	98.8%	-21.3	11.8%	82.9%	4.7%	47.0	4.8	297.1	1.1%	x
10	20	0.75	1.2%	4.6%	94.1%	-6.8	11.0%	84.9%	3.5%	33.3	4.5	258.2	0.6%	
12	20	0.75	0.9%	2.8%	96.2%	-10.8	11.1%	85.6%	2.8%	44.5	4.3	341.7	0.6%	x
15	20	0.75	0.6%	1.4%	98.0%	-16.5	11.2%	86.1%	2.2%	62.7	4.2	463.9	0.6%	
10	15	0.75	1.5%	5.9%	92.4%	-4.3	10.5%	86.9%	2.1%	39.8	4.1	345.7	0.4%	
12	15	0.75	1.2%	3.9%	94.8%	-8.0	10.5%	87.4%	1.7%	54.8	4.0	466.1	0.4%	
15	15	0.75	0.8%	1.9%	97.2%	-13.1	10.8%	87.3%	1.4%	76.8	3.9	612.9	0.4%	
10	33	0.5	1.1%	5.6%	93.2%	-9.4	7.6%	90.0%	2.0%	38.3	2.6	329.0	0.9%	
12	33	0.5	0.8%	3.5%	95.6%	-12.8	7.7%	90.3%	1.6%	51.8	2.6	432.1	0.9%	
15	33	0.5	0.5%	1.8%	97.6%	-17.7	7.8%	90.4%	1.4%	72.5	2.5	569.0	0.9%	

$p_{\text{perm, stage 1}} = 3 \text{ bara} \rightarrow \Delta p_{\text{MEM2}} = 2 \text{ bar}$

10	33	0.5	1.1%	7.2%	91.7%	-6.6	8.3%	84.0%	7.2%	24.1	2.1	131.5	2.2%	
12	33	0.5	0.7%	4.0%	95.2%	-12.0	8.4%	85.5%	5.6%	30.1	2.0	165.4	2.1%	
15	33	0.5	0.4%	1.7%	97.9%	-19.6	8.5%	86.3%	4.8%	38.9	2.0	209.3	2.1%	x
10	20	0.5	1.3%	8.6%	90.0%	-5.3	7.9%	88.0%	3.7%	27.3	1.9	175.5	1.2%	
12	20	0.5	1.0%	5.7%	93.2%	-9.2	7.7%	89.5%	2.4%	38.0	1.7	259.5	1.1%	
15	20	0.5	0.7%	3.3%	96.0%	-13.7	7.6%	90.5%	1.5%	57.6	1.6	405.2	1.0%	x
10	33	0.3	0.8%	8.1%	91.1%	-12.0	5.1%	90.7%	3.9%	25.7	1.1	154.4	1.9%	
12	33	0.3	0.6%	4.7%	94.7%	-16.6	5.2%	91.6%	3.0%	33.7	1.0	208.5	1.8%	
15	33	0.3	0.3%	2.0%	97.6%	-23.6	5.4%	91.8%	2.5%	44.9	1.0	273.6	1.7%	x

Table 7.2: Selection of results of the process simulations of the case PtG2 with a gas split in the feed of membrane stage two. Fully feasible options are marked in bold.

For the 75 % part load case, the lowest re-compression cost can be achieved using 33 2-inch membrane modules in the second stage and a system pressure of 12 bara. The permeate pressure of the first membrane stage was set to 2 bara, resulting in a pressure difference of 1 bar in the second membrane stage.

Increasing the flow rate in the second membrane stage by selectively switching off membrane modules results in a lower loss of methane through the off gas. By increasing the flow through the membrane, the permeation through the module increases due to the higher average concentration difference across the membrane. The less permeable component methane is diluted by the increasing amount of CO₂ and H₂ in the permeate. Although the permeation of CO₂ is increased, the lower number of membrane modules leads to a decreased off gas stream. Therefore, the recycle stream and recompression cost are higher.

Further decreasing the part load level results in a higher amount of CO₂ in the system. In order to decrease the recycle stream, the pressure difference in the second membrane stage has to be increased. Therefore, the feed pressure to the first membrane is raised to 15 bara and the permeate pressure to 3 bara. The plant is operated with the full number of membrane modules in the second stage. Decreasing the number of modules leads to lower methane emissions and subsequently less CO₂ separation. The higher recycle flow and higher CO₂ content also influences the first membrane stage. However, having less membrane area available in the second stage leads to a CO₂ content in the product gas, which violates the grid injection limitations.

Similarly, a part load level of 30 % can be reached: the feed pressure of stage one has to be set to 15 bara and all membrane modules of the second stage have to be in operation.

In all part load cases, the off gas concentration for methane is above 1 %, which may demand measures for the reduction for such emissions. Nevertheless, in all feasible cases the methane loss corresponds to 0.4 to 1.9 % of the feed methane. The total energy loss, which results from the composition of the off gas stream amounts to 0.6 to 2.1 % of the total incoming energy flow (CH₄ in biogas and H₂ from the electrolyser).

Part load operation of *PtG2* – Split in the retentate of membrane stage two

The highest part load level of 75 % was simulated at a system pressure of 12 bar and a permeate pressure after the first membrane stage of 2 bar (see Table 7.3). Under these conditions, the grid injection limitations and the technical restraints of the underlying processes are fulfilled. At this operation point, the CH₄ concentration in the off gas is 4.8 %. By increasing the system pressure or decreasing the number of active membrane modules in the second stage, the permeate and recycle flow could be increased and the methane concentration in the off gas lowered. Although the grid injection limitations could still be met, the recycle flow and compressor duty increased in both cases to levels beyond the limits of the membrane upgrading case.

At lower part load levels, the separation task resembles more the membrane upgrading case. Therefore, an increase of system pressure and pressure difference in stage two is required to ensure grid injection limitations. At the pressure regime given by the membrane upgrading case, part load levels of 50 % and 30 % are possible. Under these conditions, the CH₄ off-gas

$p_{\text{perm, stage 1}} = 2 \text{ bara} \rightarrow \Delta p_{\text{MEM2}} = 1 \text{ bar}$

p_{sys} bar	# Modules, Stage 2	r_{PL}	Product gas injected to grid				Gas vented			1 st Compr.	2 nd Compr.	V_{rec} m ³ /h	Energy loss	Feasible
			x_{H_2}	x_{CO_2}	x_{CH_4}	Dew pt. °C	$x_{\text{H}_2, \text{off}}$	$x_{\text{CO}_2, \text{off}}$	$x_{\text{CH}_4, \text{off}}$					
10	33	0.75	1.0%	3.6%	95.4%	-8.3	11.7%	81.5%	6.2%	28.4	5.3	190.1	1.1%	
12	33	0.75	0.7%	2.1%	97.2%	-13.4	11.6%	83.0%	4.8%	37.0	5.0	248.0	1.1%	x
15	33	0.75	0.4%	0.8%	98.8%	-21.1	11.8%	82.9%	4.6%	46.9	4.9	295.1	1.1%	x
10	20	0.75	1.2%	4.6%	94.1%	-6.7	11.0%	85.0%	3.5%	33.2	4.6	257.3	0.6%	
12	20	0.75	0.9%	2.8%	96.3%	-10.7	11.1%	85.6%	2.7%	44.4	4.4	340.6	0.6%	x
15	20	0.75	0.6%	1.4%	98.0%	-16.4	11.2%	86.1%	2.2%	62.6	4.2	462.9	0.6%	
10	15	0.75	1.3%	5.1%	93.5%	-5.5	10.8%	85.9%	2.8%	35.8	4.4	294.0	0.5%	
12	15	0.75	1.1%	3.5%	95.3%	-8.5	10.7%	86.9%	1.9%	51.5	4.1	427.8	0.5%	
15	15	0.75	0.8%	2.0%	97.2%	-13.0	10.8%	87.3%	1.4%	76.9	4.0	614.0	0.4%	
10	33	0.5	1.0%	5.5%	93.4%	-9.2	7.6%	89.9%	2.1%	37.7	2.7	321.9	0.9%	
12	33	0.5	0.8%	3.5%	95.6%	-12.7	7.7%	90.3%	1.6%	51.8	2.6	431.3	0.9%	
15	33	0.5	0.5%	1.8%	97.6%	-17.6	7.8%	90.5%	1.4%	72.6	2.5	569.8	0.9%	

$p_{\text{perm, stage 1}} = 3 \text{ bara} \rightarrow \Delta p_{\text{MEM2}} = 2 \text{ bar}$

12	20	0.75	1.0%	3.7%	95.2%	-6.3	12.2%	79.4%	7.6%	28.8	4.2	149.7	1.3%	
15	20	0.75	0.6%	1.7%	97.6%	-14.0	12.1%	81.4%	5.8%	37.8	3.7	198.4	1.3%	x
12	15	0.75	1.1%	4.2%	94.6%	-6.1	11.8%	82.0%	5.5%	30.8	3.6	174.0	1.0%	
15	15	0.75	0.7%	2.1%	97.1%	-12.8	11.5%	84.1%	3.8%	42.7	3.2	249.3	1.0%	x
10	33	0.5	1.1%	6.7%	92.2%	-4.9	8.7%	83.8%	6.9%	23.2	2.7	120.4	2.2%	
12	33	0.5	0.7%	3.8%	95.4%	-10.9	8.6%	85.3%	5.5%	29.4	2.4	157.0	2.1%	
15	33	0.5	0.4%	1.6%	97.9%	-18.9	8.6%	86.1%	4.7%	38.3	2.3	202.9	2.1%	x
10	20	0.5	1.3%	8.5%	90.2%	-4.7	8.0%	88.0%	3.6%	27.0	2.0	171.5	1.2%	
12	20	0.5	1.0%	5.4%	93.6%	-9.4	7.8%	89.2%	2.6%	36.4	1.9	242.9	1.1%	
15	20	0.5	0.6%	2.7%	96.7%	-15.2	7.9%	89.7%	2.0%	50.8	1.7	337.4	1.1%	x
10	33	0.3	0.8%	7.8%	91.4%	-10.7	5.3%	90.4%	4.0%	25.2	1.3	148.1	1.9%	
12	33	0.3	0.5%	4.5%	94.9%	-16.2	5.3%	91.4%	3.1%	33.1	1.1	202.6	1.8%	
15	33	0.3	0.3%	1.9%	97.8%	-23.3	5.4%	91.6%	2.8%	43.3	1.1	258.3	1.8%	x

Table 7.3: Selection of results of the process simulations of the case *PtG2* with split in the retentate of the second membrane stage. Fully feasible options are marked in bold.

concentrations decrease to 4.7 % and 2.8 %, respectively. Decreasing the number of active membrane modules in the second stage reduces methane emissions, but increases the recycle flow and compromise the grid injection limitations, as the CO₂ concentration rises accordingly. In this process variant, 0.6 % to 2.1 % of the total incoming energy flow are lost through the off gas stream, which is in a similar range as in the previous case.

7.4.3 Part load operation of *PtG3* – Split in the off-gas

Operating this part load process under high part load levels proofed to be difficult. Although a simple methanation of the CO₂ off gas stream and feeding the biomethane to the raw biogas seems to be a straightforward methodology, the methane-rich recycle stream has a direct influence on the membrane upgrading. Simulations showed that the feed flow to the membrane system is increased by the additional recycle flow from the reactor. The higher flow rate in the first stage of the membrane upgrading system decreases the separation performance as the partial pressure of CO₂ is decreased (see Table 7.4). This results in a CO₂ concentration in the product gas exceeding the grid limitations. None of the considered cases in the part load levels 75 % to 30 % did result in satisfactory product gas qualities. Furthermore, the

recycle flows mostly exceeded the technical limitations given by the membrane-based biogas upgrading case.

$p_{\text{perm, stage 1}} = 2 \text{ bara} \rightarrow \Delta p_{\text{MEM2}} = 1 \text{ bar}$

p_{sys} bar	# Modules, Stage 2	r_{PL}	Product gas injected to grid				Gas vented			1 st Compr. kW	2 nd Compr. kW	V_{rec} m ³ /h	Energy loss
			x_{H_2}	x_{CO_2}	x_{CH_4}	Dew pt. °C	$x_{\text{H}_2, \text{off}}$	$x_{\text{CO}_2, \text{off}}$	$x_{\text{CH}_4, \text{off}}$				
10	33	0.75	2.4%	11.9%	85.5%	0.6	10.2%	87.4%	2.0%	36.3	6.0	297.9	0.0%
12	33	0.75	2.1%	8.7%	89.1%	-1.5	10.0%	88.3%	1.3%	53.3	6.0	443.9	0.2%
15	33	0.75	1.6%	5.3%	93.0%	-5.4	9.8%	88.9%	0.9%	80.2	5.9	645.3	0.3%
10	33	0.5	1.7%	11.7%	86.6%	-4.9	7.2%	90.6%	1.8%	34.7	3.9	277.7	0.6%
12	33	0.5	1.4%	7.7%	90.8%	-7.5	7.3%	91.0%	1.4%	47.7	3.9	381.6	0.6%
15	33	0.5	1.0%	4.3%	94.6%	-11.4	7.5%	91.1%	1.1%	69.3	3.8	534.3	0.7%
10	20	0.5	2.3%	17.1%	80.5%	-0.4	6.4%	92.5%	0.8%	47.8	3.8	462.3	0.1%
12	20	0.5	2.3%	14.8%	82.8%	-0.6	6.2%	93.0%	0.5%	73.7	3.8	701.1	0.1%
15	20	0.5	2.3%	12.5%	85.1%	-0.7	6.2%	93.2%	0.3%	116.8	3.8	1040.5	0.1%
10	33	0.3	1.1%	11.7%	87.2%	-10.4	4.6%	93.6%	1.6%	34.2	2.2	270.0	0.9%
12	33	0.3	1.0%	8.6%	90.4%	-12.1	4.5%	94.2%	1.1%	50.5	2.2	410.6	0.8%
15	33	0.3	0.9%	6.4%	92.7%	-13.6	4.5%	94.7%	0.7%	81.2	2.2	651.7	0.8%
10	20	0.3	1.6%	20.2%	78.1%	-5.9	3.8%	95.5%	0.6%	51.6	2.2	509.2	0.3%
12	20	0.3	1.6%	17.5%	80.9%	-6.2	3.7%	95.7%	0.4%	75.4	2.2	718.4	0.3%
15	20	0.3	1.5%	14.4%	83.9%	-6.8	3.7%	95.8%	0.3%	111.0	2.2	979.1	0.3%
10	15	0.3	1.8%	22.8%	75.3%	-4.6	3.7%	95.7%	0.5%	56.1	2.2	576.1	0.1%
12	15	0.3	1.8%	20.6%	77.5%	-4.8	3.6%	95.9%	0.3%	81.8	2.2	800.5	0.1%
15	15	0.3	1.8%	18.6%	79.5%	-4.6	3.6%	96.0%	0.2%	120.7	2.2	1083.6	0.1%
10	33	0.1	0.4%	11.6%	88.0%	-22.9	1.6%	96.9%	1.5%	33.4	0.7	259.3	0.9%
12	33	0.1	0.3%	8.6%	91.0%	-24.3	1.6%	97.4%	1.0%	49.0	0.7	393.8	0.7%
15	33	0.1	0.3%	6.6%	93.1%	-25.6	1.6%	97.8%	0.6%	76.6	0.7	605.3	0.6%

$p_{\text{perm, stage 1}} = 3 \text{ bara} \rightarrow \Delta p_{\text{MEM2}} = 2 \text{ bar}$

10	33	0.5	2.4%	16.9%	80.5%	0.3	5.9%	93.4%	0.5%	70.5	3.7	777.8	0.0%
12	33	0.5	2.5%	15.5%	82.0%	0.3	5.8%	93.6%	0.4%	99.2	3.7	1013.1	0.0%
15	33	0.5	2.5%	13.9%	83.5%	0.6	5.9%	93.6%	0.3%	143.8	3.7	1327.4	0.1%
10	33	0.3	1.7%	17.9%	80.3%	-5.0	3.9%	95.5%	0.4%	68.2	2.2	747.0	0.2%
12	33	0.3	1.7%	16.7%	81.5%	-4.9	3.8%	95.7%	0.3%	94.3	2.2	953.9	0.2%
15	33	0.3	1.8%	16.3%	81.8%	-3.9	3.8%	95.8%	0.3%	134.2	2.2	1225.2	0.2%
10	20	0.3	1.9%	24.4%	73.6%	-3.8	3.4%	96.2%	0.3%	76.0	2.2	855.2	0.0%
12	20	0.3	2.1%	24.0%	73.9%	-3.5	3.4%	96.2%	0.3%	103.6	2.2	1067.1	0.0%
15	20	0.3	2.1%	27.1%	70.6%	-2.0	3.0%	96.7%	0.2%	144.0	2.2	1319.6	0.0%
10	33	0.1	0.7%	21.5%	77.8%	-17.0	1.3%	98.2%	0.4%	67.7	0.7	736.7	0.2%
12	33	0.1	0.7%	21.4%	77.9%	-16.5	1.3%	98.4%	0.3%	91.8	0.7	918.3	0.2%
15	33	0.1	0.7%	21.5%	77.7%	-16.2	1.2%	98.5%	0.2%	125.3	0.7	1125.2	0.2%

Table 7.4: Selection of results of the process simulations for the case *PtG3*. Grid injection limits are not met and technical limitations of the plant exceeded.

A larger membrane area in the first stage would compensate for the higher feed flow rate and ensure the separation of the CO₂. This would increase the investment cost for the process, as either more membrane modules are required. Alternatively, a re-arrangement of the configuration using the modules of the second stage may be considered. Nevertheless, as in most of the simulated cases the recycle flow exceeded the technical limits given by the membrane upgrading case, such modifications would only further increase the recycle flow and are therefore unfeasible.

Since a lower recycle flow from the reactor would lead to a similar case as the membrane-based biogas upgrading, a part load level of 10 % was simulated, but also at such low part load levels, CO₂ concentrations in the product gas exceed grid injection limits.

In certain ranges, no convergence of the process simulation could be reached, as the CO₂ flow through the product gas stream exceeded the flow required for part load operation of the reactor.

7.4.4 Comparison of the process options

Identification of a single, most promising option is difficult. Multiple, counter-acting effects have to be taken into account. Apart from the fulfilment of the grid injection limitations, further aspects play a role.

It is of special importance that the technical constraints given by the membrane-based upgrading case (*i.e.* recycle flow and main compressor duty) are not exceeded. This ensures, that no new or additional equipment is needed to operate the process. Therefore, the investment cost are not increased and operational expenses remain on the level of the membrane-based upgrading case, at maximum.

In all simulated processes, the methane loss through the off gas stream poses a problem to the ecological feasibility of the plant operation. Furthermore, high concentrations of CH₄ and H₂ in the off gas stream may violate plant safety and cause a direct efficiency loss to the system.

If a suitable process for off gas treatment (*i.e.* oxidation of CH₄ and H₂) is available, reducing the loss of CH₄ and H₂ through the off gas stream is of lower priority. For example, if an incineration process is available in proximity, the contaminated CO₂ off gas stream can be co-fed to the furnace. Although presumably no economic benefit is possible through such use, at least an energetic valorisation of the lost product gases is possible.

In order to further investigate a part load-capable process, it is of high importance to know the scheduling of the plant operation and have good estimates of the average number of part load operation hours. Plant design then has to involve an optimisation of the investment cost, possible efficiency gains, and economic benefits by part load operation, as well as operational and safety aspects. For a newly designed plant, a concept presented here can be beneficial, especially when part load operation is desirable. If an existing biogas upgrading plant is equipped with PtG functionality, such concepts may be unfeasible, even though a configuration according to *PtG3* may look promising on the first evaluation.

7.5 Experimental determination of H₂ loss under asymmetrical part load operation

Previous process simulations showed that a part of the product gas (*i.e.* CH₄ and H₂) is lost through the off gas stream from the second membrane stage along with the separated CO₂. The amount differs greatly depending on the part load level and process conditions.

In order to assess this effect under realistic conditions, the performance of the second membrane stage was simulated experimentally in our TRL 5 methanation set-up presented in previous chapters. For the experiments, raw biogas from a digester unit was available, which was mixed with additional CO₂ and H₂ to obtain the appropriate feed conditions. The concentration ranges were defined by estimates based on part load scenarios. The product gas mixture from the reactor (after condensation) was directed to the first membrane stage, where grid-ready biomethane was produced as retentate. The permeate was CO₂-rich and contained unreacted H₂, which corresponded to the feed of the second membrane stage, which was simulated in this experimental campaign.

Three settings were tested, all in co- and counter-current configuration. The pressure difference across the membrane module was set to 1 bar.

The compressor unit providing biogas to the experiment is only controlled by a set power level. Therefore, exact volumetric pump capacity is highly dependent on external factors, such as the surrounding temperature. Thus, direct setting of the biogas flow rate is difficult and only an approximate amount of biogas can be fed to the experiment. Its flow rate was calculated by subtracting the MFC flows from the Coriolis flow meter measurement. The conversion from the mass flow measured by the Coriolis device to the volumetric flow rate was done using the gas composition measurement by the μ GC in the membrane's feed.

The deviations of the volumetric flow rates of the streams entering and leaving the membrane module were lower than 2.2 % of the feed stream.

Table 7.5 presents the settings used for the experimental simulation of the second membrane upgrading stage.

In a two-stage membrane configuration, the retentate of the second membrane stage represents the recycle flow to the main compressor unit. The permeate stream corresponds to the off gas stream, which would be vented. The hydrogen loss was determined as fraction of the H₂ flow in the permeate and the H₂ feed flow rate. Figure 7.7 shows the loss of H₂ as a percentage of the partial feed flow for co- and counter-current operation, as well as the recycle rate of H₂, which correspond to the fraction of the feed flow staying in the retentate. From these results, it can be seen that the hydrogen loss decreased with higher part load levels. This can be mainly attributed to the different experimental conditions used in this set of experiments. The total flow rate was increased from 55 to 101 L min⁻¹, due to limitations in the set-up. Although the absolute amount of feed-H₂ was also increased with higher part load level (3.4 L min⁻¹ to

Config.	Experiment	\dot{V}_{f,H_2} L/min	\dot{V}_{f,CO_2} L/min	\dot{V}_{BG} L/min	$\dot{V}_{f,tot}$ L/min	x_{f,H_2} -	x_{f,CO_2} -	x_{f,CH_4} -
CC	20 % PL	3.4	37.5	16.4	54.9	6.4 %	80.0 %	13.6 %
CC	50 % PL	4.5	37.5	20.8	60.4	7.4 %	77.0 %	15.6 %
CC	75 % PL	24.5	31.9	46.2	100.7	22.0 %	52.9 %	25.1 %
CO	20 % PL	3.4	37.5	15.7	54.4	6.5 %	80.7 %	12.7 %
CO	50 % PL	4.5	37.5	19.0	59.3	7.7 %	77.5 %	14.9 %
CO	75 % PL	24.5	31.9	43.2	97.3	23.0 %	52.9 %	24.1 %

Table 7.5: Part load experiments performed for the simulation of the second membrane stage. The conditions in the membrane were simulated by setting expected concentrations at high flow rates. The retentate pressure was set to 3 bara and the permeate pressure to 2 bara. Counter-current operation is referred to with “CC”, co-current operation with “CO”.

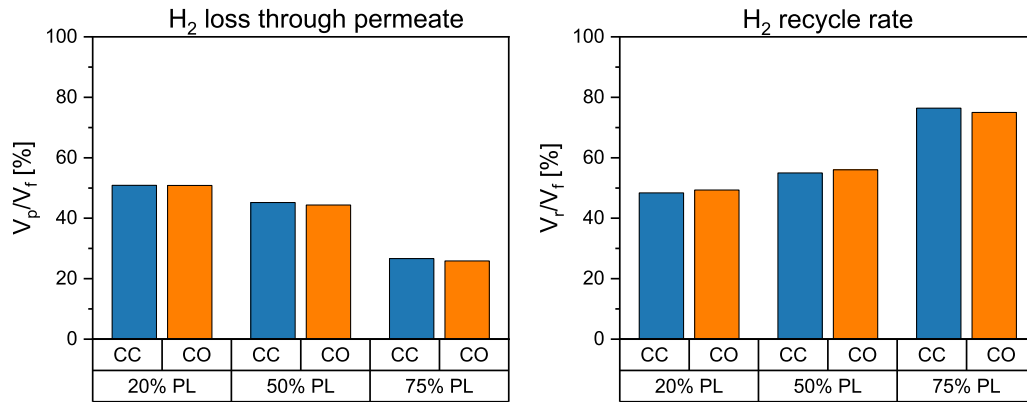


Figure 7.7: Hydrogen loss and recycle rate by the second membrane upgrading stage. Three part load levels were tested, as well as co- and counter-current configuration.

24.5 L min⁻¹), the relative flow in the permeate did not increase. Therefore, on one hand the increased total flow rate resulted in a flatter concentration profile, which generally increased the driving force for membrane permeation. The driving force was furthermore increased by a higher partial pressure of H₂ in the feed (6.4 % to 22.0 %). Nevertheless, due to the generally low pressure difference across the membrane, the permeate flow of hydrogen was low, *i.e.* the relative loss H₂ was small.

In the case where most hydrogen was expected in the second membrane stage, *i.e.* the 75 % part load case, only around one quarter of the hydrogen ending up in the permeate stream of the first stage was lost. This value increased to 51 % in case of the lowest part load. Our experiments showed that under part load conditions, H₂ loss occurred and led to an efficiency decrease of the PtG process. Due to the low H₂/CO₂ selectivity of the biogas upgrading membrane, this problem can be generalised to any membrane configuration in asymmetrical

part load operation: When CO_2 is separated from a raw biomethane stream, a share of the unreacted H_2 will always be vented together with CO_2 .

7.6 Sweep membrane concept

In this section, a further change to optimise systems for part load is introduced. It corresponds to a deviation from a standard plant capable of operating at asymmetrical part load, with the goal of decreasing the losses of CH_4 and H_2 through the off gas stream.

7.6.1 Introduction to the concept

In order to further improve the part load capabilities of a biogas-based process, it is proposed to introduce a third membrane to the previously investigated process. The goal is to increase the recycle rate of hydrogen in the process and therefore reduce its loss through the off gas stream. At the same time, we also intended to decrease the slip of CH_4 through the same path and reduce the energy loss through the off gas stream.

The third membrane could be applied in the raw product gas stream before the regular membrane upgrading unit. Under favourable conditions, the membrane would separate a part of the hydrogen already before it enters the regular membrane upgrading system. Furthermore, CO_2 may be transferred from the recycle stream to the retentate side. This leads to an accumulation of CO_2 and therefore a replacement of H_2 with CO_2 in the membrane upgrading unit.

This additional membrane is equipped with an inlet at the permeate side for a so-called sweep stream (see Figure 7.8). The recycle stream of the plant, corresponding to the retentate of the second upgrading stage, directly forms the sweep-stream. The advantage of feeding the recycle stream as a sweep stream to the permeate side is, that it lowers the partial pressure difference of CO_2 and CH_4 . Therefore, the permeation of these components should be inhibited. On the other hand, as the H_2 content in the recycle stream is already decreased by the second membrane stage, the permeation of H_2 should be favoured. Therefore, under favourable conditions, it should be possible to increase the selective recycling of H_2 without changing the membrane type.

In order to investigate the feasibility of this selective separation of H_2 and the benefits of a sweep stream on the membrane's performance, field tests were performed on the commercial biogas upgrading membrane.

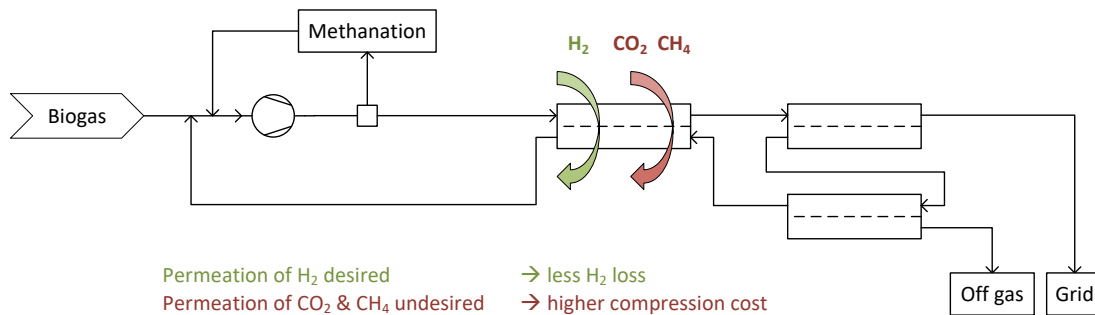


Figure 7.8: Scheme of the proposed sweep membrane process indicating the desired and undesired permeating flows.

7.6.2 Experimental

The experiments to investigate the influence of the sweep stream were conducted during the field campaign explained in the previous chapter. The membrane module was equipped with a second inlet at the permeate side, which allowed the feeding of a sweep flow.

The main feed flow to the membrane was cleaned biogas from the digester plant, mixed with CH_4 and H_2 from gas bottles to simulate product gas from a methanation reactor. The additional gases were regulated with mass flow controllers. The retentate and permeate outlets were equipped with pressure regulators, as shown in Figure 7.9.

In order to have a limited permeance of CH_4 and CO_2 in the membrane module and to favour a high concentration of H_2 in the permeate, the total flow rate in the membrane module was set as high as allowed by the set up.

We set the concentrations in the feed and sweep stream to a range corresponding to roughly a 75 % part load scenario (estimated feed composition: 10 % H_2 , 13 % CO_2 in CH_4). Two further concentration settings were also taken in consideration (high and low CO_2 content). The tests were performed with two pressure differences across the membrane, as well as a variation of the sweep stream and a reference case without sweep stream (see Table 7.6). The composition of the sweep stream corresponded to the expected concentration in the recycle stream of a PtG plant in part load operation. We used a mixture of 60 % CO_2 in CH_4 and two different total flow rates. As no direct flow and concentration measurement of the raw biogas stream was possible, the compressor duty was set to an approximated biogas flow rate. Due to fluctuations in the gas composition and ambient temperature, the raw biomethane flow varied slightly for each experiment. Nevertheless, since the full feed gas was directed through a Coriolis mass flow meter and μGC -based concentration measurements were available from the membrane feed, a sufficient characterisation of the feed flow was possible.

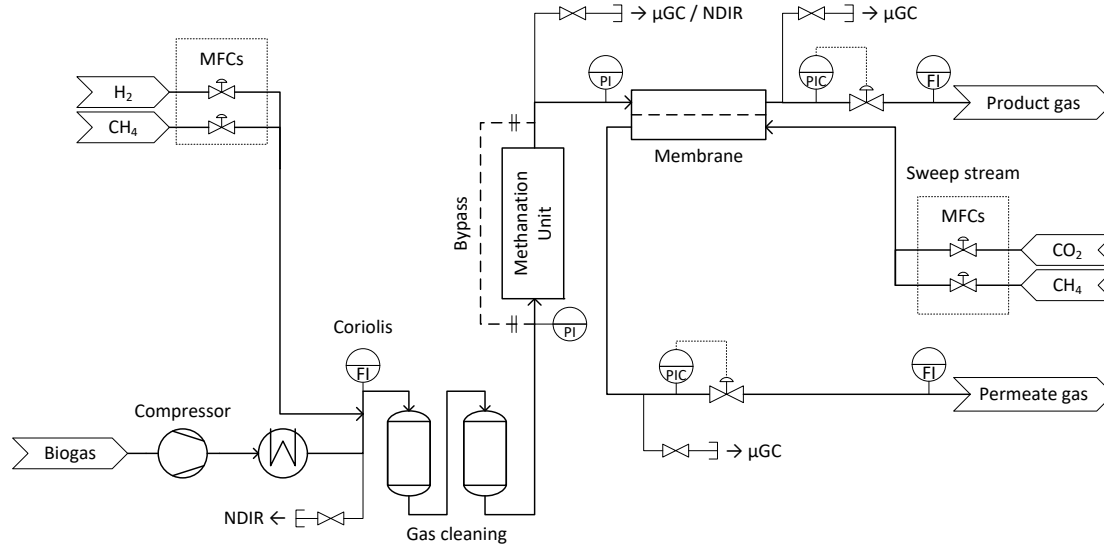


Figure 7.9: P&ID of the COSYMA plant in the configuration for membrane experiments with the sweep stream. For reasons of readability, the water bath for temperature control in the membrane module is not shown and the reactor unit is drawn in a simplified way.

The biogas stream and composition was calculated from the μGC concentration measurement at the membrane feed and the Coriolis mass flow measurement of which the MFC streams were subtracted. The total molar balance around the membrane module could be closed within $\pm 3\%$ of the sum of incoming gas streams.

7.6.3 Results and discussion

In order to compare the behaviour of the membrane module under the different conditions, the trans-membrane stream was calculated for each species. This stream corresponds to the permeate flow, from which the sweep stream was subtracted (see equation 7.5).

$$\dot{n}_{i,trans} = \dot{n}_{i,permeate} - \dot{n}_{i,sweep} \quad (7.5)$$

The integration of a third membrane step into the process should lead to a higher recycling rate of hydrogen. Ideally, with as low as possible permeation of CO_2 and CH_4 .

A reference point was recorded for each setting, where no sweep stream was applied to the module. It serves as comparison to see the direct influence of the sweep stream on the separation process.

Set-points			Sweep:						
Feed-Type			p_{sys} barg	p_{perm} barg	\dot{V}_{BG} L/min	\dot{V}_{H_2} L/min	\dot{V}_{CH_4} L/min	\dot{V}_{CO_2} L/min	\dot{V}_{CH_4} L/min
1	no sweep	$\Delta p = 4.5$ bar	7.5	3	15	5.5	30	0	0
1	sweep	$\Delta p = 4.5$ bar	7.5	3	15	5.5	30	6	4
1	no sweep	$\Delta p = 6.5$ bar	7.5	1	15	5.5	30	0	0
1	sweep	$\Delta p = 6.5$ bar	7.5	1	15	5.5	30	6	4
1	2x sweep	$\Delta p = 6.5$ bar	7.5	1	15	5.5	30	12	8
1	2x sweep	$\Delta p = 4.5$ bar	7.5	3	15	5.5	30	12	8
2	no sweep	$\Delta p = 6.5$ bar	7.5	1	10	10	40	0	0
2	sweep	$\Delta p = 6.5$ bar	7.5	1	10	10	40	6	4
3	no sweep	$\Delta p = 3$ bar	6	3	45	4.5	0	0	0
3	sweep	$\Delta p = 3$ bar	6	3	45	4.5	0	6	4
3	no sweep	$\Delta p = 5$ bar	6	1	45	4.5	0	0	0
3	sweep	$\Delta p = 5$ bar	6	1	45	4.5	0	6	4
3	2x sweep	$\Delta p = 5$ bar	6	1	45	4.5	0	12	8
3	2x sweep	$\Delta p = 3$ bar	6	3	45	4.5	0	12	8

Table 7.6: Experimental conditions used for the experiments with the sweep membrane. Three different feed concentrations were tested, wherein in each group the sweep-flow and pressure difference were varied.

In the experiments, we can clearly see the effect of the sweep stream. In Figure 7.10, the trans-membrane stream is shown for different concentration settings and pressure differences. Obviously, higher content of fast permeating species led to a higher total trans-membrane stream. Also, a higher pressure difference across the membrane increased the total permeating flow. In all cases, the permeating flow of H_2 increased when a sweep stream was applied. The respective flows for CO_2 and CH_4 showed a stable or decreasing tendency at the same time. Doubling the sweep gas stream further increased these effects.

In the first concentration setting, the CO_2 trans-membrane flow was highly decreased by the application of the sweep stream. When the sweep stream was doubled, the permeating CO_2 stream was even reversed. It was therefore possible to exchange the unreacted H_2 from the product gas stream with CO_2 from the recycle stream. This means that the recycle rate of H_2 increased, whereas the rate of CO_2 recycling decreased.

The effect for the second concentration setting was limited, as already 40 % CO_2 were present in the feed gas of the membrane. Therefore, the partial pressure difference did not allow for a back-diffusion of CO_2 . Contrarily, the concentration difference even caused high permeation rates of CO_2 .

Regarding the relative trans-membrane flow allows to see the recycle rate of the respective component (c.f. Figure 7.11). Similar trends as in the absolute permeation rates could be observed: With higher pressure difference, the permeation rate of all components increased

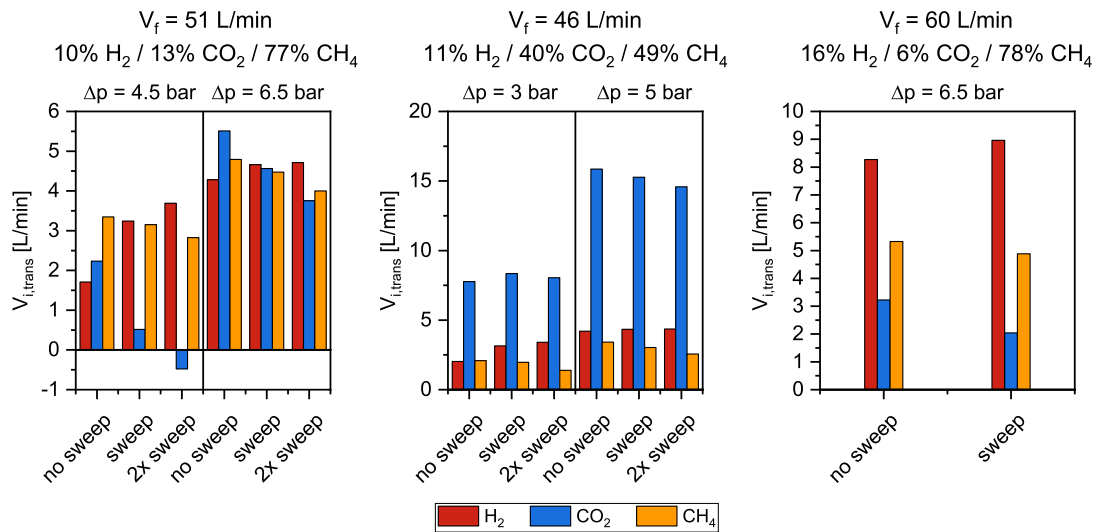


Figure 7.10: Total trans-membrane flow rate calculated from the mass balance of all incoming and leaving streams to the membrane module.

due to the higher driving force. Furthermore, the relative trans-membrane flow was increased for faster permeating species by a higher sweep stream, but not for methane. In our tests, the relative methane flow remained below 15 % of the feed flow, indicating that only around 15 % of methane passed to the recycle flow. On the other hand, more than 60 % of hydrogen could be directly recycled by the sweep membrane. At higher pressure differences, the undesired permeance of CO₂ was also increased. Therefore, the sweep membrane should only be operated with lower pressure differences.

The first set of experimental conditions was simulated with the membrane model presented in Chapters 3 and 5. In Figure 7.12, the component flow rates along the membrane length are shown. Three different conditions were simulated: the reference case where no sweep stream was applied, a case including a sweep stream, and a case with a doubled sweep flow. On the feed and retentate side of the membrane, the influence caused by the sweep flows can be clearly seen towards the retentate outlet of the module. The hydrogen flow decreased with increasing sweep stream, its separation was therefore enhanced by the lowered partial pressure on the permeate side. On the contrary, the flows of CO₂ increased on the retentate side. The model was able to depict a reversely permeating flow.

The effect of the sweep stream was even more pronounced when the profiles on the permeate side were considered. On the right side, the sweep stream was fed to the module, as visible by the non-zero values for CO₂ and CH₄. In all three considered settings, the flows of CH₄ and H₂ steadily increased along the membrane length due to the adding permeate. For the setting without a sweep stream present, also the CO₂ flow increased along the membrane. For both sweep-stream cases, the CO₂ flow decreased along the membrane, due to the components reversed permeate flow.

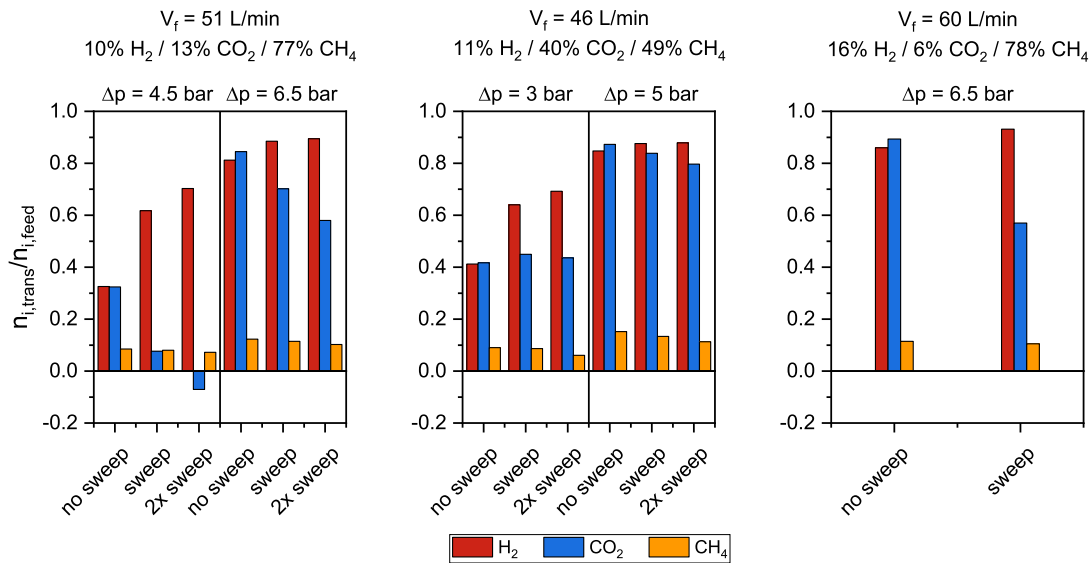


Figure 7.11: The total trans-membrane flow, relative to the respective component's feed flow are shown.

For the setting with lower sweep stream, the simulated profiles indicated a reversed CO_2 permeation. This contradicts with the experimental results shown in Figure 7.10, for which a positive trans-membrane flow was calculated. This shows that the simulation did not fully meet the experimental results in this case. The model under-estimated the CO_2 permeation, which led to a lower CO_2 trans-membrane flow and therefore to a permeating flow, which was reversed already under the conditions with the lower sweep stream.

7.6.4 Conclusion and outlook

Introducing a third membrane stage alters the flow rates and compositions in the other membrane stages. Pressure levels, as well as membrane areas (= number of modules) needed in the sweep-stage and to reach grid injection limitations require a re-optimisation of the whole plant. Due to time restrictions, this is not part of this work.

A detailed simulation of the process should be performed, which forms the base of a subsequent economic analysis of the process. Based on the cost structure, the benefit of such a design can be assessed.

A further plant design might be worth for closer evaluation: In the context of full load operation of a methanation reactor for direct methanation of biogas, a membrane with a sweep flow could facilitate the recycling of unreacted hydrogen, similar to the part load processes shown before. As a sweep stream, the uncompressed raw biogas stream can be used (see Figure 7.13). Analogously to the case presented before, H_2 permeation would be favoured, whereas CO_2 and CH_4 are less prone to pass through the membrane. If conditions can be set, which allow CO_2

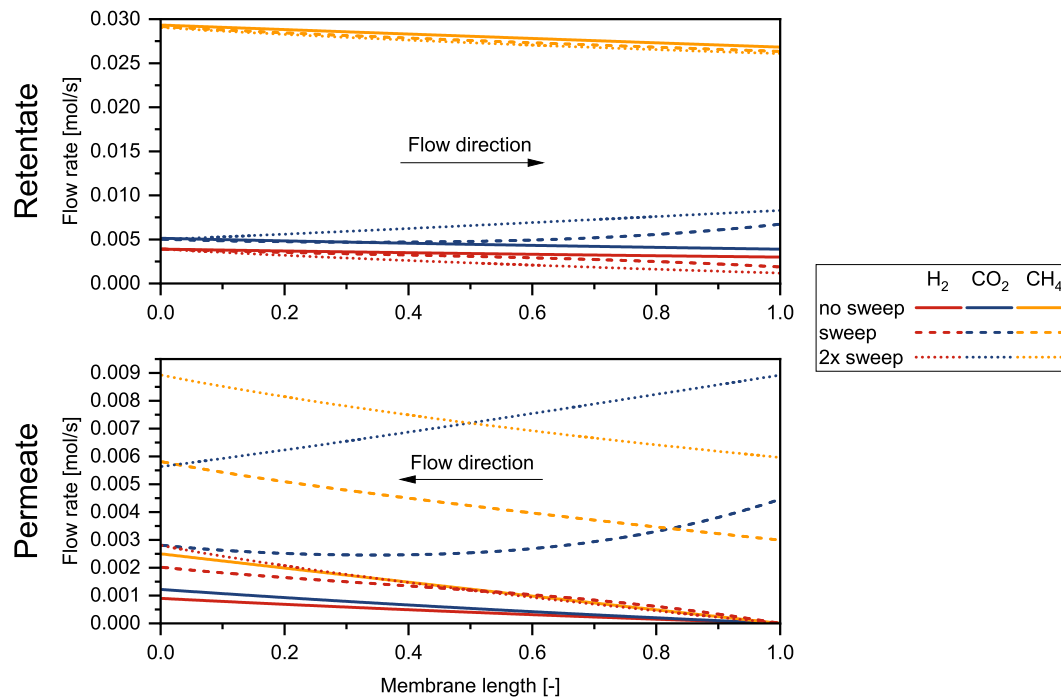


Figure 7.12: Simulation of the component flow rates along the membrane length. Data is provided for the three experiments shown in Figure 7.10 (left).

to pass through the membrane from the permeate to the retentate side, H_2 can be partially replaced by CO_2 in the product gas stream. In case the energy content of H_2 is not considered in the possible product gas revenues, this can be a way to increase the economic efficiency of grid-injecting PtG plants. Furthermore, as the CO_2 quickly passes through the polymer, the sweep membrane may have a stabilising effect to the PtG process: if an excess of CO_2 is present after the reactor, the increasing permeate flow displaces the raw biogas stream and less new CO_2 is fed to the system. The displacement is reduced as soon as more CO_2 is converted to methane.

This concept may only work in a certain operation window. Other membrane materials with a higher CO_2/CH_4 -selectivity may be more favourable for these applications. All these aspects require a closer investigation of this concept and further process simulations.

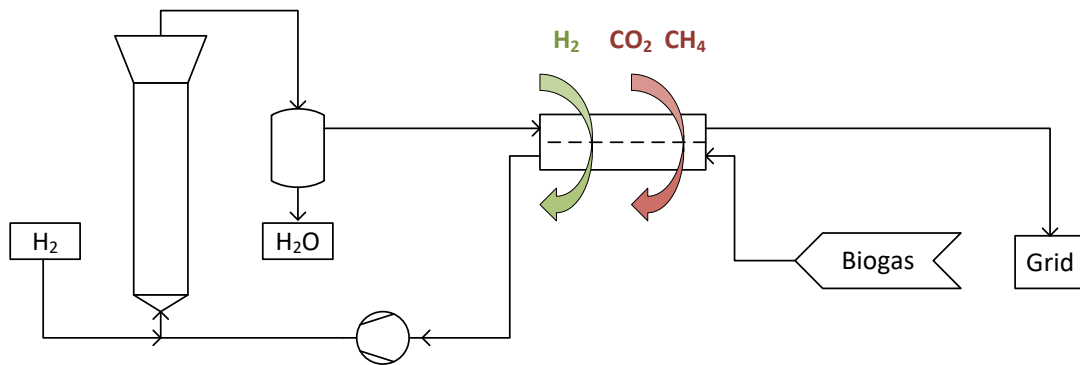


Figure 7.13: Direct methanation process making use of a sweep membrane for hydrogen recycle. The permeation of H_2 is desired, whereas the permeation of CO_2 and CH_4 is reduced by the high partial pressure of these components at the permeate side.

8 General conclusion and outlook

8.1 Achieved results and conclusions

In this work, we presented a techno-economic comparison of two CO₂-based methanation technologies. It could be shown that converting biogas without prior CO₂ separation by direct methanation leads to a clear production cost benefit. A further cost benefit arises, when high temperature electrolysis is integrated in the process: excess heat from the methanation reactor can be used to reduce the specific electricity consumption of the electrolyser. The electricity-to-methane efficiency of the process can be increased from 54 % to 73 % (LHV).

In the first part, it is assumed that the PtG process is operated throughout the whole year at a constant electricity cost. Since the availability of low-cost, renewable electricity and subsequently H₂ for methanation is not constant over the year, continuous (full load) operation of the methanation plant over the full year is economically unfeasible. In the following part of the work, process concepts are proposed, which increase the operational flexibility of the upgrading plant, allowing avoiding the use of non-renewable or expensive electricity for PtG.

In a first step, a commercial upgrading membrane (Evonik SEPURAN®) intended for CO₂ separation from biogas was tested for its capability to separate excess H₂ from methanation product gas. Characterisation experiments were performed on a full membrane module in a TRL 5 methanation set up. Compositions of methanation product gas and raw biogas were simulated in the set up. We showed that this commercial biogas upgrading membrane allows successful H₂ separation and produces grid-ready biomethane within a single separation stage. At slightly higher pressure differences, also biogas upgrading is possible, reducing the initially tested CO₂ concentration of 40 % to below the required 4 %. Based on these experimental results, an upgrading concept was proposed, which allowed an integration of membrane-based and methanation-based upgrading. The proposed concept consists of a two-stage membrane upgrading plant, which is able to separate and vent CO₂ from the raw biogas stream. When the PtG plant is operated, the first membrane stage separates H₂ from the product gas stream. The second membrane stage is bypassed and the H₂-rich recycle stream directed to the main compressor.

This upgrading concept allows a fast switching between the two operation modes, which enables the PtG unit only to operate when renewable H_2 is available. It represents a first process integration step: Compared to a membrane upgrading plant with subsequent methanation of the off gas, the membrane upgrading step after the methanation can be saved and is merged with the main membrane unit.

In order to simulate the flexible upgrading concept and enable subsequent cost analysis, reliable, rate-based unit models are required. Based on characterisation experiments performed with the commercial membrane module, the parameters of a permeation model were fitted. The model characterised the permeation of $H_2/CO_2/CH_4$ gas mixtures through the hollow fibre module. This permeation model was included into a rate-based, counter-current membrane model.

The membrane model was applied in a techno-economic assessment of the flexible upgrading concept. In this part of the work, three PtG process chain variations were considered: a first option where the full raw gas stream is fed to the reactor and the product gas is upgraded to grid-ready biomethane. A second option considers a process, where the raw gas is fed to a membrane upgrading stage ensuring grid-quality of the product gas. The CO_2 -rich permeate is fed to the methanation unit. The third option is identical to the second one, but includes a second compressor in the permeate stream, leading to lower compression duty in the main compressor unit. These three options were compared for their specific biomethane production cost in all-year operation. It could be seen that the first process chain revealed the lowest production cost, followed by the third variant.

The cost estimates of the PtG processes were combined with the cost structure of the two-stage, membrane-based upgrading process to investigate the cost structure of the integrated, flexible processes. The combined processes showed only minor cost differences among each other.

Although a two-stage, membrane upgrading process would be the option with the lowest production cost, we observed that with a low increase of production cost, PtG functionality could be added, and the carbon efficiency of the process increased. On the other hand, the specific production cost of a PtG plant, which is not operated for the full year are highly sensitive on operation hours and electricity cost, respectively. By adding an integrated membrane upgrading option, the PtG plant can be operated down to 5500 h/a without exceeding biomethane production cost of 13 €/ct./kWh.

These evaluations considered a bi-modal operation mode: PtG operation when inexpensive electricity is available and membrane-based biogas upgrading when PtG is economically not feasible. In a future electricity system with a higher penetration of renewable power sources, fluctuations in electricity production and therefore electricity price will become more frequent. Modern PEM electrolyser technology is capable of following such short term fluctuations, but a thermal process like methanation operates with higher inertia and requires a H_2 buffer tank in its feed. In order to extend the operation times of the methanation unit and therefore the

efficiency losses associated with start-up and shut down procedures, we wanted to investigate the part load capabilities of the system in a next step.

A field campaign was performed with the TRL 5 methanation set up at a commercial biogas plant, which allowed tests using real biogas as a feed and the operation of the plant with a closed hydrogen recycle loop. Experiments without a closed recycle loop showed that the fluidised bed methanation reactor could be operated down to a part load level of 20 % at a pressure of 1.5 barg. It was found that the installed membrane area was not sufficient to separate enough H_2 at this pressure difference, though. Further tests with a closed recycle loop showed that the current set up can be operated in a load range of 45 to 100 %, based on the H_2 feed. The membrane area and the compressor, which has a lower operation limit, are limiting the lower part load level.

The tests furthermore showed that it is crucial to have fast process analytics in the recycle loop or at the feed of the reactor. Especially the H_2 concentration should be closely monitored, as over- and under-stoichiometric amounts of H_2 can lead to positive and negative feedback effects in the system. Accumulation of CO_2 or H_2 in the recycle loop requires a fast adjustment of feed- H_2 and compressor duty.

The field tests were concluded with an experiment of sequential load changes. It showed that the set-up is capable of fast load changes and provides grid-quality biomethane in the full load range. After each load change, short periods occurred where the H_2 concentration in the product gas exceeded the 2 %-limit. These events were caused by a too slow adjustment of the H_2 feed stream. Such observations show the importance of fast and at least partially automated control systems in the plant, which help to regulate the H_2 feed and increase the stability of the process.

In these considerations, the operation mode of the plant corresponds to a symmetrical part load operation. In this case, H_2 and the CO_2 -source are equally reduced and fed to the reactor in an approximately stoichiometric ratio. If there is an excess of CO_2 in the feed, such as in the case of a constantly operating digester unit and reduced availability of H_2 , the overall process requires a way to remove the excess CO_2 from the system. We refer to this case as asymmetrical part load operation, as only the reactor is operated at reduced load.

As a last integration step, the asymmetrical part load behaviour of the flexible upgrading concept was investigated. The plant design was kept identical as in the previous techno-economic analyses; the investment cost is therefore also identical.

Process simulations were performed with varying the position of the reactor unit. In all technically feasible cases, a relatively large amount of methane and H_2 is lost through the off gas stream. These losses state a direct efficiency decrease of the overall process of a few %-points. A single optimal plant design could not be identified, as further factors, such as operability, plant safety, and adjacent processes have to be taken into account. Nevertheless, in case of a newly built plant, where asymmetrical part load is required, these considerations

can serve as foundation for further process optimisation according to the local boundary conditions.

As a measure to reduce the hydrogen loss through the off gas stream, the introduction of a third membrane stage is proposed. This membrane stage is installed upstream of the two-stage membrane upgrading unit and a CO₂- and CH₄-rich sweep stream is applied on its permeate side. Due to the lower partial pressure difference of CO₂ and CH₄, the permeation of these components is reduced, whereas the H₂-permeation is favoured. The permeate stream forms the recycle stream of the plant, leading to an improved recycling of H₂ and a reduced loss through the off gas.

The functionality of such a membrane arrangement was successfully tested during field experiments and was simulated with the previously developed membrane model.

The concepts presented in this work can be generalised to any PtX process, which is operated with renewable electricity and a biogenic carbon source. Both feed streams are intermittent on all time scales, either symmetrically or asymmetrically, respectively.

All biomass-derived PtX conversion processes suffer from fluctuations on the feed side. Large storage capacities of reactant gases are expensive and may render the process economically unfeasible. Especially the pathway of the carbon source involves conversion processes with low dynamics and load flexibility (*e.g.* anaerobic digestion, gasification), which are not capable of following the dynamics of the hydrogen path. It is therefore necessary to have an upgrading process with adequate flexibility in place, which allows to upgrade the full amount of biogenic gas, while only using a reduced amount of hydrogen. Especially the underlying thermal processes (*e.g.* methanation, methanol and Fischer-Tropsch synthesis) are less suited for intermittent use, as frequent start-up and shutdown procedures increase energy demand for heating and reduce the efficiency. It is therefore necessary to operate them in part load to bridge short declines in H₂ availability, which can be buffered by low-capacity storages. Fluctuations on larger time-scales must be addressed further upstream, *i.e.* the first conversion step of biomass has to be reduced and the raw biomass kept in a storable form. In such a case, it is necessary to be able to operate the reaction and the subsequent product upgrading in part load.

In this work, we show a way to increase the operational flexibility of a biogas-based PtX process, avoiding the use of expensive electricity (*e.g.* during winter). At the example of a flexible concept for direct methanation of biogas, the economic feasibility of such a process could be shown.

Our proposed concept integrates the membrane upgrading step required after the methanation reactor into a membrane-based biogas upgrading process. This allows to omit the second membrane upgrading unit after the reactor and enables a cost reduction compared to a solution with two separate plants. This integrated biogas upgrading process allows switching between two main upgrading modes (membrane upgrading and PtG). It is furthermore

shown how this process has to be operated to protect the reaction from an over-stoichiometric amount of the carbon species, either by symmetrical or asymmetrical part load operation.

Our work shows how adaptations in the process concept and relatively small intermediate storage increase the operational flexibility of the upgrading process can lead to higher economic and operational feasibility of the overall process. This gain in flexibility can be achieved without altering the dynamics of the underlying reaction process.

8.2 Outlook and recommendation for further work

The work presented in this thesis sets a base for a multitude of potential improvements. In the following, a summary of suggestions for further work is given.

The membrane unit model and the permeance model can be improved in various ways. Most importantly, the model presented in this work should be compared to the separation performance of other membrane modules with the same polymer type. Such a cross-validation would increase the confidence in the current membrane model and would identify module-specific problems.

For simulations of processes with very high H_2 content, further separation tests with hydrogen-containing gases should be performed, as in the current work no mixtures with more than 30 % H_2 were tested.

To avoid the restrictions of the COSYMA set up, it is conceivable that a new set up for membrane testing can be built. In that case, the pressure range could be increased, as well as the restrictions in the gas flow rates removed. A decreased gas consumption could be achieved by only testing a part of the fibres from a commercial module, similar to experiments performed by Sandru *et al.* [180]. The construction of a specialised membrane test set-up would require detailed engineering and safety considerations. One of the main difficulties would be the extraction of fibres from a commercial module and fixing them tightly into the new set-up. Alternatively, as realised in a set-up of FH Ost in Rapperswil, Switzerland, retentate and permeate could be mixed and pressurised to serve again as feed. Different from the mentioned set-up, a sufficient cooling of gas and membrane module (similar to the temperature control by water bath as in COSYMA) should be used to avoid over-heating of the system due to the heat accumulation from gas compression.

Nevertheless, such a set up would open room for further membrane testing. Since water vapour plays an important role in biogas upgrading and methanation, it may be interesting to further investigate its influence on gas permeation through the tested membrane. From these experiments, parameters can be fitted to be included in the permeation model. Further influences to test could be the temperature dependency, resistance against common biogas contaminants, as well as tars and terpenes.

Overall, the construction of such a set-up states a great effort and may not justify the expense. A clear analysis of possible knowledge gain should be performed.

The membrane model should be equipped with a term quantifying pressure loss on the bore-side of the hollow fibre. This is especially relevant at higher flow rates and low pressure differences across the membrane, as the accuracy of the model may be further improved. The equation of Hagen-Poiseuille is a simple, but effective way to do so.

For several years, our group has been working on a multi-purpose, TRL 6, bubbling fluidised bed methanation plant (160 – 200 kW, GanyMeth). The plant is a crucial step for implementing the fluidised bed methanation in the market and for the investigation of phenomena only occurring in industrial scale (heat/mass transfer, mixing, and their interaction with the chemical reactions) and a deduction of further research questions thereof.

The plant is equipped with extensive diagnostics, which allow gas sampling and temperature measurements along the bed height. Further analytical devices are installed in the feed and product gas streams, which enables detailed balancing. By evaluating reactive experiments, the output of the reactor model can be directly compared to experimental data obtained in industrial scale. A concept for process and scientific diagnostics for the GanyMeth plant was developed during the work for this thesis, but is not documented here.

The GanyMeth reactor can be operated at different load levels with varying gas composition. Therefore, a variety of scenarios can be experimentally simulated, such as methanation of CO₂ and CO, direct methanation of biogas, as well as upgrading of gasification-derived producer gases. These tests allow a direct comparison of the real plant performance to model predictions. This increases the confidence in scale-up predictions and the feasibility of subsequent cost estimates needed for the implementation of the technology in the market. Especially part load operation of the methanation reactor and the inherent changes in the temperature and concentration profiles can be studied in more detail than in the smaller COSYMA plant. In addition, start-up and shutdown ramps can be simulated with the GanyMeth installation, and according control strategies can be derived. Knowing the dynamics of this plant allows estimating the thermal restraints of a possible industrial application and a prediction of the flexibility of a BFB-based PtX process. Application of this data in simulations of the PtX process chain, or on a systemic level allows furthermore for a better prediction of required intermediate storage of feed gases.

The plant allows introducing raw gas contaminants (*e.g.* aromatics) to the feed gas stream. Investigation of their influence on the methanation kinetics and catalyst state are therefore also possible. Such data allow for a more detailed modelling of the reactor, especially when facing specific applications, such as methanation of producer gases or contaminated raw gas streams.

This facility allows the detailed investigation of fluid dynamics in the catalyst bed in presence of heat exchange internals using optical and pressure fluctuation probes [176, 181]. As a part

of this ongoing research, detailed bubble size correlations are developed, which allow a better description of hydrodynamics in bubbling fluidised bed reactors with vertical internals. These correlations should be implemented in the reactor model, which allow a better prediction of reactor performance and size estimates of higher precision.

The sweep membrane process should be modelled and further investigated, such that its economic feasibility can be assessed. Alternative membrane configurations may allow further reducing the product gas losses, enhancing the selectivity of the separation and therefore reducing the required membrane area.

Nevertheless, it should be kept in mind that for implementation of an integrated, flexible upgrading process at a biogas plant, the process complexity should not be underestimated. Since simpler processes require less maintenance and less knowledge on the part of the plant operators, they are more likely to be considered as a possible variant for implementation.

The feasibility of methanation-based PtG processes will be highly increased as soon as grid injection limitations are adjusted towards higher allowed hydrogen contents. In this case, the underlying design questions will be fundamentally changed, as a BFB reactor with sufficiently high CO_2 -conversion fulfils the concentration demands after condensation of the reactant water. Apart from drying, no further separation steps are required under operation at design specifications. Nevertheless, under asymmetrical part load conditions, questions concerning the fate of excess CO_2 are still relevant and should be further investigated.

A Membrane characterisation experiments

Component [-]	Config. co/cc	\dot{V}_f L/min	p_r bar	\dot{V}_p L/min	\dot{V}_r L/min	p_f bar
CH ₄	co	20	4.0	2.4	17.6	4.2
CH ₄	co	20	7.0	5.0	15.1	7.2
CH ₄	co	20	9.0	6.9	13.3	9.2
CH ₄	co	30	4.0	2.5	27.4	4.2
CH ₄	co	30	7.0	5.3	24.4	7.2
CH ₄	co	30	10.0	8.2	21.6	10.2
CO ₂	co	40	2.0	32.0	10.0	2.3
H ₂	co	90	1.5	73.5	16.5	1.9
CH ₄	cc	20	4.0	2.4	17.6	4.2

Table A.1: Single gas characterisation experiments in co- and counter-current configuration. All data points shown here are used in the parameter estimation.

Config. co/cc	\dot{V}_f L/min	p_r bar	x_{f,CH_4} %	x_{f,CO_2} %	\dot{V}_p L/min	x_{p,CH_4} %	x_{p,CO_2} %	\dot{V}_r L/min	x_{r,CH_4} %	x_{r,CO_2} %	p_f bar	p_p bar	Param. est.
co	40.2	4.0	97.1	2.9	2.6	90.1	9.9	37.3	97.5	2.5	4.3	1	x
co	41.5	7.0	94.1	5.9	7.3	78.3	21.7	34.2	97.4	2.6	7.2	1	
co	41.6	4.0	94.1	5.9	2.9	80.7	19.3	38.2	95.1	4.9	4.3	1	x
co	42.0	4.0	87.1	12.9	3.8	63.2	36.7	37.3	90.7	9.3	4.2	1	
co	42.0	7.0	87.1	12.9	8.2	60.1	39.8	33.0	95.2	4.8	7.2	1	
co	42.0	10.0	87.0	13.0	12.3	65.0	34.9	29.4	97.9	2.2	10.2	1	
co	42.6	7.0	93.5	6.5	6.5	77.3	22.6	35.0	97.1	2.9	7.2	1	
co	44.5	7.0	87.4	12.6	9.7	58.4	41.6	35.1	95.1	4.9	7.2	1	
co	44.6	4.0	87.6	12.4	3.8	60.7	39.3	40.4	90.1	9.9	4.3	1	x
co	56.1	4.0	70.6	29.4	9.6	23.7	76.3	45.6	80.1	19.9	4.3	1	x
co	56.2	9.0	70.5	29.5	21.1	33.1	66.9	33.8	94.6	5.4	9.2	1	
co	56.3	7.0	70.5	29.5	18.2	28.7	71.3	36.9	91.4	8.6	7.2	1	
co	71.2	4.0	97.2	2.8	3.1	90.1	9.9	69.5	97.5	2.5	4.3	1	x
co	73.6	7.0	94.0	6.0	7.6	73.1	26.9	67.4	96.2	3.8	7.3	1	
co	73.8	5.5	93.8	6.2	5.6	74.8	25.2	68.7	95.4	4.6	5.8	1	x
co	73.9	4.0	93.8	6.2	3.7	79.0	21.0	70.9	94.7	5.3	4.4	1	x
co	78.9	7.0	88.0	12.0	10.6	51.9	48.1	69.3	93.3	6.7	7.3	1	
co	79.3	4.2	88.0	12.0	5.0	59.0	41.0	74.3	89.9	10.1	4.5	1	x
co	79.3	5.5	87.9	12.1	7.7	53.9	46.1	71.7	91.5	8.5	5.8	1	x
co	101.5	5.5	69.6	30.4	20.3	17.9	82.1	79.7	82.9	17.1	5.9	1	x
co	101.7	7.0	69.4	30.6	25.3	18.8	81.2	75.4	87.2	12.8	7.3	1	x

Table A.2: Binary characterisation experiments using mixtures of CO₂ and CH₄ in co-current configuration. Data points used for the parameter estimations are marked with "x".

Config. co/cc	\dot{V}_f L/min	p_r bar	x_{f,CH_4} %	x_{f,CO_2} %	\dot{V}_p L/min	x_{p,CH_4} %	x_{p,CO_2} %	\dot{V}_r L/min	x_{r,CH_4} %	x_{r,CO_2} %	p_f bar	p_p bar	Param. est.
cc	28.3	4.0	88.2	11.8	4.1	63.1	36.9	25.2	92.3	7.7	4	1	x
cc	28.3	7.0	88.0	12.0	8.4	63.9	36.1	21.2	98.0	2.0	7	1	x
cc	28.7	7.0	60.4	39.6	16.0	31.6	68.4	13.6	98.3	1.7	7	1	x
cc	28.7	9.0	60.3	39.7	18.0	38.0	62.0	11.7	99.8	0.2	9	1	x
cc	28.8	4.0	60.3	39.7	11.6	21.5	78.5	18.2	86.3	13.7	4.1	1	x
cc	28.9	7.0	25.9	74.1	24.9	18.8	81.2	4.1	100.0	0.0	7	1	x
cc	36.0	7.0	96.5	3.5	5.8	86.4	13.5	30.0	98.9	1.1	7.2	1	x
cc	36.0	7.0	96.5	3.5	5.7	87.9	12.0	30.2	98.5	1.5	7.2	1	x
cc	41.2	4.0	96.6	3.4	2.7	89.7	10.2	37.9	97.4	2.6	4.2	1	x
cc	41.2	10.0	96.4	3.6	9.3	88.4	11.6	31.2	99.2	0.8	10.2	1	x
cc	41.3	4.0	96.6	3.4	2.7	88.7	11.2	37.8	97.5	2.5	4.2	1	x
cc	41.3	10.0	96.5	3.5	9.5	87.4	12.6	31.0	99.6	0.4	10.2	1	x
cc	41.6	4.0	60.2	39.8	13.7	17.1	82.9	28.2	81.2	18.8	4.1	1	x
cc	41.6	8.5	60.2	39.8	21.6	27.7	72.3	20.0	98.1	1.9	8.6	1	x
cc	41.7	7.0	60.3	39.7	19.8	24.0	76.0	21.8	95.6	4.4	7.1	1	x
cc	41.7	9.0	60.3	39.7	22.2	29.7	70.3	19.5	98.8	1.2	9	1	x
cc	42.0	4.0	87.1	12.9	4.0	60.4	39.5	37.1	91.2	8.9	4.2	1	x
cc	42.0	4.0	25.4	74.6	29.6	5.9	94.1	11.7	83.6	16.4	4.1	1	x
cc	42.0	7.0	87.0	13.0	8.8	57.3	42.6	32.5	96.5	3.5	7.2	1	x
cc	42.0	7.0	25.2	74.8	32.5	11.9	88.1	7.8	99.1	0.9	7	1	x
cc	42.0	10.0	87.0	13.0	13.0	63.9	36.1	28.1	99.2	0.8	10.2	1	x
cc	42.6	7.0	93.5	6.5	6.8	75.0	24.9	34.7	97.7	2.3	7.2	1	x
cc	52.3	2.2	25.3	74.7	22.1	2.8	97.2	30.3	42.2	57.8	2.5	1	x
cc	64.4	9.0	59.1	40.9	28.9	20.8	79.2	34.2	95.9	4.1	9.1	1	x
cc	65.3	7.0	58.0	42.0	27.7	16.0	84.0	37.4	91.1	8.9	7.1	1	x
cc	65.3	8.5	58.5	41.5	29.3	18.9	81.1	35.1	94.9	5.1	8.6	1	x
cc	65.4	4.0	58.6	41.4	18.0	12.4	87.6	47.5	75.9	24.1	4.2	1	x

Table A.3: Binary characterisation experiments using mixtures of CO₂ and CH₄ in counter-current configuration. Data points used for the parameter estimations are marked with "x".

Config. co/cc	\dot{V}_f L/min	p_r bar	x_{f,CH_4} %	x_{f,H_2} %	\dot{V}_p L/min	x_{p,CH_4} %	x_{p,H_2} %	\dot{V}_r L/min	x_{r,CH_4} %	x_{r,H_2} %	p_f bar	p_p bar	Param. est.
co	39.9	4.0	97.0	3.0	3.3	90.6	9.4	36.3	97.7	2.3	4.2	1	x
co	40.9	10.0	97.1	2.9	9.2	90.2	9.7	30.8	99.3	0.7	10.2	1	
co	41.0	4.0	97.3	2.7	2.7	90.3	9.5	37.3	97.7	2.3	4.2	1	
co	41.0	7.0	97.3	2.7	5.7	88.8	11.1	34.5	98.6	1.4	7.2	1	
co	41.0	8.7	97.3	2.7	7.5	89.1	10.7	33.3	99.0	1.0	8.9	1	
co	41.8	4.0	93.6	6.4	3.8	80.3	19.7	37.2	95.0	5.0	4.3	1	x
co	41.8	7.0	93.6	6.4	7.7	78.5	21.5	33.7	97.2	2.8	7.2	1	
co	42.0	4.0	88.2	11.8	3.8	62.4	37.4	37.1	90.8	9.3	4.2	1	
co	42.0	7.0	88.3	11.7	8.2	60.6	39.4	32.9	95.1	4.9	7.2	1	
co	42.0	10.0	88.4	11.6	12.5	66.9	33.1	28.6	97.6	2.4	10.2	1	
co	43.0	7.0	94.2	5.8	6.7	77.3	22.6	35.2	97.1	2.9	7.2	1	
co	43.9	4.0	87.4	12.6	4.8	62.6	37.4	38.9	90.6	9.4	4.3	1	x
co	43.9	10.0	87.5	12.5	13.9	66.2	33.8	30.6	97.5	2.5	10.2	1	
co	44.0	7.0	87.4	12.6	10.0	61.5	38.5	34.3	95.2	4.8	7.2	1	
co	44.0	9.0	87.5	12.5	12.7	64.5	35.5	31.8	96.9	3.1	9.2	1	
co	55.3	7.0	69.8	30.2	20.0	30.4	69.6	35.6	91.9	8.1	7.2	1	
co	55.4	4.0	69.8	30.2	12.1	25.0	75.0	42.9	82.2	17.8	4.3	1	
co	55.4	9.0	69.9	30.1	23.2	35.2	64.8	32.6	94.7	5.3	9.2	1	
co	70.8	4.0	96.8	3.2	3.2	89.0	11.0	69.2	97.2	2.8	4.3	1	x
co	73.7	5.5	94.0	6.0	5.8	73.9	26.1	69.2	95.3	4.7	5.7	1	x
co	73.8	4.0	93.5	6.5	3.7	78.1	21.9	70.9	94.4	5.6	4.3	1	x
co	73.8	5.5	93.5	6.5	5.7	73.9	26.1	69.6	95.2	4.8	5.7	1	x
co	78.6	5.5	87.3	12.7	8.3	52.3	47.7	71.0	91.5	8.5	5.8	1	
co	100.5	4.0	69.0	31.0	17.8	16.4	83.6	82.9	80.0	20.0	4.4	1	

Table A.4: Binary characterisation experiments using mixtures of H₂ and CH₄ in co-current configuration. Data points used for the parameter estimations are marked with "x".

Config. co/cc	\dot{V}_f L/min	p_r bar	x_{f,CH_4} %	x_{f,H_2} %	\dot{V}_p L/min	x_{p,CH_4} %	x_{p,H_2} %	\dot{V}_r L/min	x_{r,CH_4} %	x_{r,H_2} %	p_f bar	p_p bar	Param. est.
cc	40.1	7.0	60.1	39.9	21.6	25.8	74.2	20.1	99.0	1.0	7	1	x
cc	41.0	4.0	97.3	2.7	2.7	88.9	10.9	37.1	97.8	2.2	4.2	1	x
cc	41.0	7.0	97.3	2.7	5.9	85.7	14.2	34.3	99.2	0.8	7.2	1	x
cc	41.0	8.7	97.3	2.7	7.8	86.6	13.3	32.9	99.7	0.3	8.9	1	x
cc	41.0	10.0	97.1	2.9	9.5	88.5	11.4	30.6	99.9	0.1	10.2	1	x
cc	42.0	4.0	88.3	11.7	4.2	56.7	43.2	36.9	91.7	8.3	4.2	1	x
cc	42.0	7.0	88.4	11.6	9.4	55.0	44.9	31.9	98.1	1.9	7.2	1	x
cc	42.0	10.0	88.4	11.6	13.5	64.7	35.3	27.6	99.9	0.1	10.2	1	x
cc	42.4	7.0	70.6	29.4	15.5	33.5	66.5	26.0	92.4	7.6	7.2	1	x
cc	42.4	7.0	70.6	29.4	17.3	31.2	68.9	24.4	98.5	1.5	7.2	1	x
cc	43.0	7.0	94.2	5.8	7.2	72.2	27.7	34.7	98.5	1.5	7.2	1	x

Table A.5: Binary characterisation experiments using mixtures of H₂ and CH₄ in counter-current configuration. Data points used for the parameter estimations are marked with "x"

Config. co/cc	\dot{V}_f L/min	p_r bar	x_{f,CH_4} %	x_{f,CO_2} %	x_{f,H_2} %	\dot{V}_p L/min	x_{p,CH_4} %	x_{p,CO_2} %	x_{p,H_2} %	\dot{V}_r L/min	x_{r,CH_4} %	x_{r,CO_2} %	x_{r,H_2} %	p_f bar	p_p bar	Param. est.
co	39.5	2.0	84.9	2.8	12.3	1.3	71.2	5.5	23.3	38.1	85.4	2.8	11.8	2.3	1	x
co	40.9	2.1	81.9	5.8	12.3	1.7	63.4	12.0	24.6	39.5	82.8	5.6	11.7	2.4	1	x
co	46.1	4.0	84.5	3.0	12.5	5.3	54.5	9.0	36.6	40.0	88.6	2.2	9.2	4.3	1	
co	46.1	7.0	84.5	3.0	12.5	10.8	53.7	9.5	36.8	34.8	94.4	1.0	4.6	7.2	1	
co	46.2	9.0	84.5	3.1	12.4	13.7	57.2	8.9	33.8	32.2	96.5	0.6	2.9	9.2	1	
co	47.7	4.0	81.7	5.9	12.4	6.1	47.3	17.5	35.2	40.9	87.0	4.2	8.8	4.3	1	
co	47.7	7.0	81.7	5.9	12.4	12.1	47.2	18.0	34.8	35.1	93.8	1.9	4.3	7.2	1	
co	47.7	9.0	81.6	5.9	12.4	15.1	51.2	16.7	32.1	32.5	96.1	1.1	2.7	9.2	1	
co	52.0	2.3	64.2	5.7	30.2	4.6	26.1	11.8	62.0	47.3	67.8	5.2	27.0	2.6	1	x
co	61.3	4.0	63.9	6.1	30.0	16.1	17.8	13.7	68.5	44.1	80.6	3.4	16.0	4.3	1	
co	61.3	7.0	63.9	6.1	30.0	24.4	23.6	13.1	63.3	36.3	91.2	1.5	7.3	7.2	1	
co	61.3	9.0	64.0	6.0	30.0	27.4	28.1	12.3	59.6	33.2	94.2	1.0	4.8	9.2	1	
co	82.3	5.5	84.5	2.9	12.6	9.5	43.2	10.8	45.9	73.7	89.9	1.9	8.2	5.8	1	
co	82.4	3.9	84.4	2.9	12.6	5.5	49.8	9.6	40.6	76.6	87.0	2.5	10.5	4.3	1	x
co	85.1	5.5	80.8	6.8	12.5	11.9	33.2	24.6	42.1	75.0	88.2	4.3	7.5	5.8	1	
co	85.2	4.0	81.4	6.0	12.6	4.7	40.2	20.0	39.9	78.6	85.0	4.9	10.0	4.4	1	x
co	85.3	4.1	81.2	6.2	12.6	7.2	39.6	20.5	39.9	78.1	85.1	5.0	9.9	4.4	1	x
co	110.4	4.2	63.2	6.1	30.7	25.8	11.0	13.6	75.4	85.5	78.8	4.0	17.2	4.6	1	
cc	45.4	8.0	84.5	2.9	12.6	12.9	50.9	9.0	40.1	32.6	98.6	0.5	0.9	8.1	1	x
cc	45.5	7.0	84.5	2.9	12.6	11.6	48.4	9.2	42.5	33.8	97.4	0.8	1.8	7.1	1	x
cc	45.6	4.0	84.6	2.8	12.6	5.9	48.7	8.9	42.5	39.3	90.1	2.0	7.9	4.2	1	x
cc	47.0	8.0	81.7	5.8	12.5	14.3	45.3	17.2	37.5	32.8	98.2	1.0	0.8	8.1	1	x
cc	47.1	4.0	81.8	5.7	12.5	6.7	41.8	17.4	40.8	40.0	88.7	3.8	7.5	4.2	1	x
cc	47.1	7.0	81.7	5.7	12.5	12.9	42.9	17.4	39.7	34.1	96.9	1.5	1.6	7.1	1	x
cc	60.6	4.0	63.9	6.0	30.1	18.0	15.5	12.3	72.2	42.1	84.6	3.4	12.0	4.3	1	x
cc	60.6	7.0	63.8	6.0	30.2	25.0	21.4	12.2	66.4	34.5	96.2	1.4	2.4	7.2	1	x
cc	60.6	8.0	63.9	6.0	30.1	27.1	23.8	12.3	64.0	33.1	97.9	1.0	1.2	8.1	1	x

Table A.6: Ternary characterisation experiments using mixtures of H₂, CO₂ and CH₄ in co- and counter-current configuration. Data points used for the parameter estimations are marked with "x".

B Process simulations

$p_{\text{perm, stage 1}} = 2 \text{ bara} \rightarrow \Delta p_{\text{MEM2}} = 1 \text{ bar}$

Product gas injected to the grid									Off gas										
p_{sys}	p_{react}	r_{PL}	x_{H_2}	x_{CO_2}	x_{CH_4}	$x_{\text{H}_2\text{O}}$	n_{tot}	Dew pt.	$x_{\text{H}_2, \text{off}}$	$x_{\text{CO}_2, \text{off}}$	$x_{\text{CH}_4, \text{off}}$	$x_{\text{H}_2\text{O}, \text{off}}$	$n_{\text{tot}, \text{off}}$	Compr.	V_{rec}	r_{split}	$r_{\text{CH}_4, \text{loss}}$	$r_{\text{H}_2, \text{loss}}$	Energy loss
bar	bar	-	-	-	-	-	mol/s	°C	-	-	-	-	mol/s	kW	m ³ /h	-	-	-	-
12	8	0.75	0.7%	2.0%	97.3%	0.04%	2.23	-12.0	12.3%	82.0%	4.9%	0.72%	0.31	50.1	407.6	0.26	1.0%	1.3%	1.1%
12	6	0.75	0.8%	1.9%	97.2%	0.05%	2.23	-8.6	13.4%	80.9%	4.7%	0.95%	0.31	50.7	415.7	0.26	1.0%	1.5%	1.2%
12	4	0.75	0.8%	1.8%	97.2%	0.08%	2.23	-3.6	15.2%	79.0%	4.4%	1.39%	0.33	52.0	430.8	0.25	1.0%	1.8%	1.3%
12	8	0.5	0.8%	3.5%	95.7%	0.04%	2.04	-13.1	7.8%	90.2%	1.7%	0.36%	0.46	57.0	495.0	0.10	0.5%	1.8%	0.9%
12	6	0.5	0.9%	3.4%	95.6%	0.05%	2.04	-9.5	8.4%	89.5%	1.6%	0.48%	0.46	58.3	510.5	0.10	0.5%	2.0%	0.9%
12	4	0.5	1.0%	3.3%	95.6%	0.07%	2.04	-4.2	9.6%	88.2%	1.5%	0.71%	0.47	60.9	541.7	0.09	0.5%	2.4%	1.0%
12	8	0.3	0.9%	7.1%	91.9%	0.04%	1.93	-13.2	4.4%	94.7%	0.7%	0.18%	0.53	72.4	686.0	0.04	0.3%	2.0%	0.6%
12	6	0.3	1.0%	7.1%	91.9%	0.05%	1.93	-9.5	4.7%	94.3%	0.7%	0.24%	0.53	73.5	699.2	0.04	0.3%	2.1%	0.6%
12	4	0.3	1.1%	7.0%	91.7%	0.08%	1.93	-4.0	5.4%	93.6%	0.7%	0.36%	0.54	76.1	729.8	0.04	0.2%	2.5%	0.7%
14	8	0.5	0.8%	3.3%	95.9%	0.03%	2.04	-14.9	7.0%	91.7%	1.0%	0.29%	0.51	81.7	697.9	0.07	0.3%	1.8%	0.8%
14	6	0.5	0.9%	3.2%	95.9%	0.04%	2.03	-11.4	7.6%	91.0%	1.0%	0.38%	0.51	83.6	718.9	0.06	0.3%	2.0%	0.8%
14	4	0.5	1.0%	3.0%	95.9%	0.06%	2.03	-6.4	8.7%	89.8%	0.9%	0.57%	0.52	87.8	765.2	0.06	0.3%	2.4%	0.9%
14	8	0.3	0.9%	6.7%	92.4%	0.03%	1.92	-14.5	4.2%	95.1%	0.5%	0.15%	0.55	96.9	871.5	0.03	0.2%	2.0%	0.6%
14	6	0.3	1.0%	6.6%	92.3%	0.04%	1.92	-10.9	4.5%	94.8%	0.5%	0.21%	0.55	98.4	888.2	0.03	0.2%	2.1%	0.6%
14	4	0.3	1.1%	6.6%	92.2%	0.07%	1.92	-5.5	5.2%	94.0%	0.5%	0.31%	0.55	102.1	929.1	0.03	0.2%	2.4%	0.6%
15	8	0.3	0.8%	5.8%	93.3%	0.03%	1.90	-15.4	4.3%	95.1%	0.5%	0.16%	0.55	105.9	923.9	0.03	0.2%	2.0%	0.6%
15	6	0.3	0.9%	5.8%	93.2%	0.04%	1.90	-11.7	4.6%	94.7%	0.5%	0.21%	0.55	107.8	944.6	0.03	0.2%	2.1%	0.6%
15	4	0.3	1.0%	5.7%	93.2%	0.06%	1.90	-6.4	5.2%	94.0%	0.5%	0.32%	0.56	112.0	988.9	0.03	0.2%	2.5%	0.6%

$p_{\text{perm, stage 1}} = 3 \text{ bara} \rightarrow \Delta p_{\text{MEM2}} = 2 \text{ bar}$

12	8	0.75	0.9%	3.0%	96.0%	0.08%	2.19	-3.8	14.3%	73.2%	11.3%	1.17%	0.35	51.0	421.7	0.48	2.7%	1.8%	2.3%
12	8	0.5	0.8%	3.8%	95.4%	0.05%	2.01	-9.8	9.2%	84.9%	5.4%	0.58%	0.55	39.6	280.5	0.25	2.0%	2.6%	2.2%
12	8	0.3	0.6%	4.4%	95.0%	0.03%	1.84	-15.8	5.6%	90.9%	3.2%	0.30%	0.69	37.2	252.4	0.12	1.5%	3.3%	1.8%
14	8	0.5	0.5%	2.1%	97.3%	0.03%	1.98	-15.4	9.2%	85.2%	5.0%	0.57%	0.57	45.6	302.4	0.23	1.9%	2.7%	2.2%
14	8	0.3	0.4%	2.5%	97.1%	0.02%	1.80	-20.8	5.6%	91.2%	2.9%	0.29%	0.72	44.5	291.1	0.10	1.4%	3.4%	1.8%
15	8	0.3	0.3%	1.9%	97.8%	0.02%	1.79	-23.2	5.6%	91.3%	2.8%	0.29%	0.73	48.0	307.9	0.10	1.4%	3.5%	1.8%
12	6	0.75	1.0%	2.9%	95.9%	0.10%	2.19	-0.1	15.6%	72.0%	10.9%	1.53%	0.36	51.3	424.1	0.47	2.7%	2.0%	2.4%
12	6	0.5	0.8%	3.7%	95.4%	0.06%	2.01	-6.2	10.0%	83.9%	5.3%	0.77%	0.56	39.8	283.5	0.25	2.0%	2.9%	2.3%
12	6	0.3	0.6%	4.5%	94.9%	0.04%	1.84	-12.4	5.9%	90.7%	3.1%	0.38%	0.70	37.7	258.0	0.12	1.4%	3.5%	1.9%
14	6	0.75	0.7%	1.6%	97.6%	0.06%	2.15	-6.7	15.4%	73.4%	9.7%	1.44%	0.39	56.4	422.0	0.43	2.6%	2.2%	2.4%
14	6	0.5	0.5%	2.1%	97.3%	0.04%	1.97	-12.2	9.9%	84.5%	4.9%	0.74%	0.59	46.0	306.5	0.22	1.9%	3.0%	2.2%
14	6	0.3	0.4%	2.5%	97.1%	0.03%	1.80	-17.4	6.0%	90.7%	2.9%	0.39%	0.72	44.7	293.6	0.10	1.4%	3.7%	1.9%
15	6	0.75	0.5%	1.2%	98.2%	0.05%	2.14	-9.7	15.4%	73.8%	9.4%	1.42%	0.40	59.0	424.2	0.42	2.6%	2.2%	2.4%
15	6	0.5	0.4%	1.5%	98.0%	0.03%	1.97	-14.6	10.1%	84.3%	4.9%	0.76%	0.59	48.9	316.4	0.22	1.9%	3.1%	2.3%
15	6	0.3	0.3%	1.9%	97.8%	0.02%	1.79	-20.0	6.0%	90.9%	2.8%	0.38%	0.73	48.3	311.0	0.10	1.4%	3.8%	1.8%

Table B.1: Process simulations of the PtG1 process in asymmetrical part load operation.

$p_{\text{perm, stage 1}} = 2 \text{ bara} \rightarrow \Delta p_{\text{MEM2}} = 1 \text{ bar}$

p_{sys} bar	# Modules, Stage 2	Product gas injected to the grid							Off gas					1 st Compr.	2 nd Compr.	V_{rec} m ³ /h	r_{split}	$r_{\text{CH}_4, \text{loss}}$	$r_{\text{H}_2, \text{loss}}$	Energy loss
		r_{PL}	x_{H_2}	x_{CO_2}	x_{CH_4}	$x_{\text{H}_2\text{O}}$	n_{tot}	Dew pt. °C	$x_{\text{H}_2, \text{off}}$	$x_{\text{CO}_2, \text{off}}$	$x_{\text{CH}_4, \text{off}}$	$x_{\text{H}_2\text{O}, \text{off}}$	$n_{\text{tot}, \text{off}}$							
		-	-	-	-	-	mol/s		-	-	-	-	mol/s	kW	kW		-	-	-	-
10	33	0.75	1.0%	3.6%	95.3%	0.1%	2.28	-8.6	11.5%	81.6%	6.3%	0.63%	0.27	28.8	5.0	195.6	0.47	1.1%	1.1%	1.1%
12	33	0.75	0.7%	2.1%	97.2%	0.0%	2.24	-13.7	11.5%	83.1%	4.8%	0.60%	0.31	37.3	4.8	251.7	0.35	1.0%	1.2%	1.1%
15	33	0.75	0.4%	0.8%	98.8%	0.0%	2.20	-21.3	11.8%	82.9%	4.7%	0.62%	0.31	47.0	4.8	297.1	0.30	1.0%	1.3%	1.1%
10	20	0.75	1.2%	4.6%	94.1%	0.1%	2.32	-6.8	11.0%	84.9%	3.5%	0.56%	0.22	33.3	4.5	258.2	0.33	0.5%	0.8%	0.6%
12	20	0.75	0.9%	2.8%	96.2%	0.0%	2.27	-10.8	11.1%	85.6%	2.8%	0.56%	0.24	44.5	4.3	341.7	0.24	0.4%	0.9%	0.6%
15	20	0.75	0.6%	1.4%	98.0%	0.0%	2.23	-16.5	11.2%	86.1%	2.2%	0.55%	0.26	62.7	4.2	463.9	0.17	0.4%	1.0%	0.6%
10	15	0.75	1.5%	5.9%	92.4%	0.1%	2.37	-4.3	10.5%	86.9%	2.1%	0.51%	0.20	39.8	4.1	345.7	0.23	0.3%	0.7%	0.4%
12	15	0.75	1.2%	3.9%	94.8%	0.1%	2.31	-8.0	10.5%	87.4%	1.7%	0.49%	0.21	54.8	4.0	466.1	0.17	0.2%	0.8%	0.4%
15	15	0.75	0.8%	1.9%	97.2%	0.0%	2.26	-13.1	10.8%	87.3%	1.4%	0.51%	0.22	76.8	3.9	612.9	0.13	0.2%	0.8%	0.4%
10	33	0.5	1.1%	5.6%	93.2%	0.0%	2.09	-9.4	7.6%	90.0%	2.0%	0.36%	0.43	38.3	2.6	329.0	0.15	0.6%	1.7%	0.9%
12	33	0.5	0.8%	3.5%	95.6%	0.0%	2.04	-12.8	7.7%	90.3%	1.6%	0.36%	0.46	51.8	2.6	432.1	0.11	0.5%	1.8%	0.9%
15	33	0.5	0.5%	1.8%	97.6%	0.0%	2.00	-17.7	7.8%	90.4%	1.4%	0.37%	0.48	72.5	2.5	569.0	0.08	0.4%	1.9%	0.9%
10	20	0.5	1.5%	8.9%	89.5%	0.1%	2.19	-4.9	6.9%	91.8%	1.0%	0.32%	0.31	50.6	2.4	501.2	0.09	0.2%	1.1%	0.5%
12	20	0.5	1.4%	7.1%	91.4%	0.1%	2.14	-6.4	6.8%	92.2%	0.7%	0.30%	0.32	73.7	2.4	700.0	0.07	0.2%	1.1%	0.4%
15	20	0.5	1.3%	5.2%	93.4%	0.1%	2.10	-7.9	6.9%	92.2%	0.6%	0.31%	0.34	110.1	2.3	968.8	0.05	0.1%	1.2%	0.4%
10	15	0.5	1.8%	11.4%	86.7%	0.1%	2.26	-3.1	6.4%	92.6%	0.7%	0.28%	0.24	58.0	2.3	602.7	0.08	0.1%	0.8%	0.3%
12	15	0.5	1.7%	9.3%	88.9%	0.1%	2.21	-3.9	6.4%	92.7%	0.6%	0.29%	0.25	82.5	2.3	808.5	0.06	0.1%	0.8%	0.3%
15	15	0.5	1.6%	7.5%	90.7%	0.1%	2.16	-4.5	6.5%	92.8%	0.4%	0.29%	0.26	123.0	2.3	1106.8	0.04	0.1%	0.9%	0.3%
10	33	0.3	1.0%	9.1%	89.8%	0.0%	1.97	-10.4	4.4%	94.4%	0.9%	0.20%	0.51	49.9	1.4	492.1	0.05	0.3%	1.9%	0.6%
12	33	0.3	0.9%	7.2%	91.8%	0.0%	1.93	-11.7	4.4%	94.6%	0.7%	0.20%	0.53	70.3	1.4	659.5	0.04	0.3%	2.0%	0.6%
15	33	0.3	0.8%	5.2%	93.9%	0.0%	1.89	-13.4	4.5%	94.7%	0.6%	0.20%	0.55	101.0	1.3	873.4	0.03	0.2%	2.1%	0.6%
10	20	0.3	1.5%	15.1%	83.3%	0.1%	2.13	-6.0	3.9%	95.4%	0.5%	0.17%	0.33	63.4	1.3	680.2	0.04	0.1%	1.1%	0.3%
12	20	0.3	1.5%	13.7%	84.7%	0.1%	2.09	-6.6	3.9%	95.5%	0.4%	0.17%	0.34	88.6	1.3	885.2	0.03	0.1%	1.1%	0.3%
15	20	0.3	1.5%	12.3%	86.1%	0.1%	2.06	-6.4	3.9%	95.6%	0.3%	0.17%	0.35	126.0	1.3	1140.1	0.02	0.1%	1.2%	0.3%
10	15	0.3	1.7%	17.8%	80.5%	0.1%	2.20	-5.5	3.8%	95.6%	0.4%	0.16%	0.25	67.9	1.3	742.2	0.03	0.1%	0.8%	0.2%
12	15	0.3	1.7%	16.6%	81.7%	0.1%	2.17	-5.3	3.7%	95.8%	0.3%	0.15%	0.26	93.7	1.3	946.8	0.03	0.1%	0.8%	0.2%
15	15	0.3	1.8%	16.2%	81.9%	0.1%	2.17	-4.3	3.7%	95.9%	0.3%	0.16%	0.26	133.3	1.3	1216.4	0.02	0.0%	0.8%	0.2%

$p_{\text{perm, stage 1}} = 3 \text{ bara} \rightarrow \Delta p_{\text{MEM2}} = 2 \text{ bar}$

10	33	0.5	1.1%	7.2%	91.7%	0.1%	2.10	-6.6	8.3%	84.0%	7.2%	0.47%	0.46	24.1	2.1	131.5	0.43	2.2%	2.0%	2.2%
12	33	0.5	0.7%	4.0%	95.2%	0.0%	2.02	-12.0	8.4%	85.5%	5.6%	0.47%	0.53	30.1	2.0	165.4	0.33	2.0%	2.3%	2.1%
15	33	0.5	0.4%	1.7%	97.9%	0.0%	1.97	-19.6	8.5%	86.3%	4.8%	0.47%	0.59	38.9	2.0	209.3	0.26	1.9%	2.6%	2.1%
10	20	0.5	1.3%	8.6%	90.0%	0.1%	2.16	-5.3	7.9%	88.0%	3.7%	0.42%	0.40	27.3	1.9	175.5	0.31	1.0%	1.6%	1.2%
12	20	0.5	1.0%	5.7%	93.2%	0.1%	2.09	-9.2	7.7%	89.5%	2.4%	0.39%	0.48	38.0	1.7	259.5	0.19	0.8%	1.9%	1.1%
15	20	0.5	0.7%	3.3%	96.0%	0.0%	2.03	-13.7	7.6%	90.5%	1.5%	0.37%	0.54	57.6	1.6	405.2	0.12	0.6%	2.1%	1.0%
10	15	0.5	1.5%	10.1%	88.3%	0.1%	2.20	-4.2	7.5%	89.8%	2.4%	0.38%	0.36	30.8	1.7	223.4	0.23	0.6%	1.4%	0.8%
12	15	0.5	1.4%	7.9%	90.7%	0.1%	2.15	-6.3	7.1%	91.3%	1.3%	0.33%	0.42	48.3	1.6	383.8	0.12	0.4%	1.5%	0.7%
15	15	0.5	1.0%	4.7%	94.2%	0.0%	2.07	-10.6	7.1%	91.6%	1.0%	0.32%	0.45	71.4	1.5	554.8	0.08	0.3%	1.6%	0.7%
10	33	0.3	0.8%	8.1%	91.1%	0.0%	1.91	-12.0	5.1%	90.7%	3.9%	0.27%	0.63	25.7	1.1	154.4	0.18	1.6%	2.8%	1.9%
12	33	0.3	0.6%	4.7%	94.7%	0.0%	1.84	-16.6	5.2%	91.6%	3.0%	0.26%	0.70	33.7	1.0	208.5	0.13	1.4%	3.1%	1.8%
15	33	0.3	0.3%	2.0%	97.6%	0.0%	1.79	-23.6	5.4%	91.8%	2.5%	0.26%	0.75	44.9	1.0	273.6	0.10	1.3%	3.4%	1.7%
10	20	0.3	1.1%	11.5%	87.3%	0.1%	2.02	-9.4	4.7%	93.5%	1.6%	0.21%	0.52	33.8	0.9	266.5	0.10	0.6%	2.1%	0.9%
12	20	0.3	1.0%	9.3%	89.6%	0.0%	1.97	-11.1	4.5%	94.4%	0.9%	0.19%	0.58	53.1	0.9	443.6	0.06	0.4%	2.2%	0.7%
15	20	0.3	0.8%	5.5%	93.7%	0.0%	1.89	-14.5	4.6%	94.5%	0.7%	0.20%	0.60	75.3	0.8	598.3	0.04	0.3%	2.3%	0.7%
10	15	0.3	1.4%	15.7%	82.8%	0.1%	2.13	-7.2	4.2%	94.8%	0.9%	0.18%	0.44	43.2	0.9	392.4	0.07	0.3%	1.5%	0.5%
12	15	0.3	1.2%	12.1%	86.6%	0.1%	2.04	-8.6	4.1%	95.0%	0.6%	0.18%	0.46	62.2	0.8	558.7	0.05	0.2%	1.6%	0.5%
15	15	0.3	1.1%	9.0%	89.9%	0.0%	1.97	-10.0	4.2%	95.2%	0.5%	0.18%	0.47	93.2	0.8	791.0	0.03	0.1%	1.7%	0.5%

Table B.2: Process simulations of the PtG2 process with split in the permeate of the first stage in asymmetrical part load operation.

$p_{\text{perm, stage 1}} = 2 \text{ bara} \rightarrow \Delta p_{\text{MEM2}} = 1 \text{ bar}$

p _{sys} bar	# Modules, Stage 2	Product gas injected to the grid						Off gas						1 st Compr.	2 nd Compr.	V _{rec} m ³ /h	f _{split}	f _{CH4,loss}	f _{H2,loss}	Energy loss
		f _{PL}	x _{H2}	x _{CO2}	x _{CH4}	x _{H2O}	n _{tot}	Dew pt.	x _{H2,off}	x _{CO2,off}	x _{CH4,off}	x _{H2O,off}	n _{tot,off}							
							mol/s	°C					mol/s	kW	kW					
10	33	0.75	1.0%	3.6%	95.4%	0.1%	2.28	-8.3	11.7%	81.5%	6.2%	0.7%	0.27	28.4	5.3	190.1	0.57	1.1%	1.1%	1.1%
12	33	0.75	0.7%	2.1%	97.2%	0.0%	2.24	-13.4	11.6%	83.0%	4.8%	0.6%	0.31	37.0	5.0	248.0	0.41	1.0%	1.3%	1.1%
15	33	0.75	0.4%	0.8%	98.8%	0.0%	2.20	-21.1	11.8%	82.9%	4.6%	0.6%	0.31	46.9	4.9	295.1	0.34	1.0%	1.3%	1.1%
10	20	0.75	1.2%	4.6%	94.1%	0.1%	2.32	-6.7	11.0%	85.0%	3.5%	0.6%	0.22	33.2	4.6	257.3	0.36	0.5%	0.8%	0.6%
12	20	0.75	0.9%	2.8%	96.3%	0.0%	2.27	-10.7	11.1%	85.6%	2.7%	0.6%	0.24	44.4	4.4	340.6	0.26	0.4%	0.9%	0.6%
15	20	0.75	0.6%	1.4%	98.0%	0.0%	2.23	-16.4	11.2%	86.1%	2.2%	0.6%	0.26	62.6	4.2	462.9	0.18	0.4%	1.0%	0.6%
10	15	0.75	1.3%	5.1%	93.5%	0.1%	2.34	-5.5	10.8%	85.9%	2.8%	0.5%	0.18	35.8	4.4	294.0	0.30	0.3%	0.7%	0.5%
12	15	0.75	1.1%	3.5%	95.3%	0.1%	2.30	-8.5	10.7%	86.9%	1.9%	0.5%	0.20	51.5	4.1	427.8	0.19	0.3%	0.8%	0.5%
15	15	0.75	0.8%	2.0%	97.2%	0.0%	2.26	-13.0	10.8%	87.3%	1.4%	0.5%	0.22	76.9	4.0	614.0	0.13	0.2%	0.8%	0.4%
10	33	0.5	1.0%	5.5%	93.4%	0.1%	2.09	-9.2	7.6%	89.9%	2.1%	0.4%	0.43	37.7	2.7	321.9	0.17	0.6%	1.7%	0.9%
12	33	0.5	0.8%	3.5%	95.6%	0.0%	2.04	-12.7	7.7%	90.3%	1.6%	0.4%	0.46	51.8	2.6	431.3	0.12	0.5%	1.8%	0.9%
15	33	0.5	0.5%	1.8%	97.6%	0.0%	2.00	-17.6	7.8%	90.5%	1.4%	0.4%	0.48	72.6	2.5	569.8	0.09	0.4%	1.9%	0.9%
10	20	0.5	1.5%	8.9%	89.5%	0.1%	2.19	-4.8	6.9%	91.8%	1.0%	0.3%	0.31	50.6	2.4	501.5	0.10	0.2%	1.1%	0.5%
12	20	0.5	1.4%	7.1%	91.4%	0.1%	2.14	-6.0	6.8%	92.1%	0.7%	0.3%	0.32	73.8	2.4	701.4	0.07	0.2%	1.1%	0.5%
15	20	0.5	1.3%	5.2%	93.5%	0.1%	2.10	-7.7	6.9%	92.2%	0.6%	0.3%	0.34	110.0	2.3	968.5	0.05	0.1%	1.2%	0.4%
10	15	0.5	1.8%	10.8%	87.3%	0.1%	2.24	-3.0	6.6%	92.4%	0.8%	0.3%	0.24	56.7	2.4	585.6	0.08	0.1%	0.8%	0.3%
12	15	0.5	1.7%	9.3%	88.9%	0.1%	2.21	-3.5	6.5%	92.7%	0.6%	0.3%	0.25	82.7	2.3	811.1	0.06	0.1%	0.8%	0.3%
15	15	0.5	1.6%	7.5%	90.8%	0.1%	2.16	-4.4	6.5%	92.7%	0.4%	0.3%	0.26	123.0	2.3	####	0.04	0.1%	0.9%	0.3%

$p_{\text{perm, stage 1}} = 3 \text{ bara} \rightarrow \Delta p_{\text{MEM2}} = 2 \text{ bar}$

10	33	0.75	No convergence reached																	
12	33	0.75																		
15	33	0.75																		
10	20	0.75	No convergence reached																	
12	20	0.75																		
15	20	0.75																		
10	15	0.75	No convergence reached																	
12	15	0.75																		
15	15	0.75																		
10	33	0.5	1.1%	6.7%	92.2%	0.1%	2.08	-4.9	8.7%	83.8%	6.9%	0.6%	0.47	23.2	2.7	120.4	0.78	2.2%	2.1%	2.2%
12	33	0.5	0.7%	3.8%	95.4%	0.0%	2.02	-10.9	8.6%	85.3%	5.5%	0.5%	0.54	29.4	2.4	157.0	0.53	2.0%	2.4%	2.1%
15	33	0.5	0.4%	1.6%	97.9%	0.0%	1.97	-18.9	8.6%	86.1%	4.7%	0.5%	0.59	38.3	2.3	202.9	0.38	1.9%	2.6%	2.1%
10	20	0.5	1.3%	8.5%	90.2%	0.1%	2.15	-4.7	8.0%	88.0%	3.6%	0.4%	0.41	27.0	2.0	171.5	0.41	1.0%	1.7%	1.2%
12	20	0.5	1.0%	5.4%	93.6%	0.0%	2.08	-9.4	7.8%	89.2%	2.6%	0.4%	0.46	36.4	1.9	242.9	0.26	0.8%	1.9%	1.1%
15	20	0.5	0.6%	2.7%	96.7%	0.0%	2.01	-15.2	7.9%	89.7%	2.0%	0.4%	0.50	50.8	1.7	337.4	0.17	0.7%	2.0%	1.1%
10	15	0.5	1.5%	9.9%	88.6%	0.1%	2.20	-4.2	7.5%	89.7%	2.4%	0.4%	0.35	30.3	1.8	217.6	0.28	0.6%	1.4%	0.8%
12	15	0.5	1.2%	6.8%	92.0%	0.1%	2.12	-7.4	7.4%	90.6%	1.7%	0.4%	0.40	43.0	1.7	324.6	0.17	0.4%	1.5%	0.8%
15	15	0.5	0.9%	4.1%	95.0%	0.0%	2.06	-11.3	7.3%	91.2%	1.1%	0.4%	0.43	66.0	1.6	499.6	0.10	0.3%	1.6%	0.7%
10	33	0.3	0.8%	7.8%	91.4%	0.0%	1.91	-10.7	5.3%	90.4%	4.0%	0.3%	0.62	25.2	1.3	148.1	0.29	1.7%	2.8%	1.9%
12	33	0.3	0.5%	4.5%	94.9%	0.0%	1.84	-16.2	5.3%	91.4%	3.1%	0.3%	0.70	33.1	1.1	202.6	0.19	1.4%	3.1%	1.8%
15	33	0.3	0.3%	1.9%	97.8%	0.0%	1.79	-23.3	5.4%	91.6%	2.8%	0.3%	0.73	43.3	1.1	258.3	0.14	1.3%	3.3%	1.8%
10	20	0.3	1.0%	11.0%	87.9%	0.1%	2.00	-9.1	4.7%	93.4%	1.7%	0.2%	0.51	32.7	1.0	252.5	0.13	0.6%	2.0%	0.9%
12	20	0.3	0.9%	8.0%	91.1%	0.0%	1.94	-11.6	4.6%	94.0%	1.2%	0.2%	0.56	47.9	0.9	384.5	0.08	0.4%	2.2%	0.8%
15	20	0.3	0.7%	5.1%	94.1%	0.0%	1.88	-14.6	4.6%	94.4%	0.8%	0.2%	0.59	72.7	0.9	572.1	0.05	0.3%	2.3%	0.7%
10	15	0.3	1.2%	13.8%	84.9%	0.1%	2.08	-7.4	4.3%	94.4%	1.1%	0.2%	0.42	39.0	0.9	340.0	0.09	0.3%	1.5%	0.6%
12	15	0.3	1.2%	11.4%	87.4%	0.1%	2.02	-8.5	4.2%	94.9%	0.7%	0.2%	0.45	59.9	0.8	531.9	0.05	0.2%	1.6%	0.5%
15	15	0.3	1.1%	9.0%	89.9%	0.0%	1.97	-9.6	4.1%	95.2%	0.5%	0.2%	0.47	93.1	0.8	789.8	0.03	0.1%	1.7%	0.5%

Table B.3: Process simulations of the PtG2 process with split in the retentate of the second stage in asymmetrical part load operation.

$p_{perm,stage\ 1} = 2\text{ bara} \rightarrow \Delta p_{MEM2} = 1\text{ bar}$

			Product gas injected to the grid						Off gas																
p _{sys}	# Modules, Stage 2	r _{FL}	x _{H2}	x _{CO2}	x _{CH4}	x _{H2O}	n _{tot}	Dew pt.	x _{H2,off}	x _{CO2,off}	x _{CH4,off}	x _{H2O,off}	n _{tot,off}	1 st Compr.	2 nd Compr.	V _{rec}	r _{split}	r _{CH4,loss}	r _{H2,loss}	Energy loss					
bar	-	-	-	-	-	-	mol/s	°C	-	-	-	-	mol/s	kW	kW	m ³ /h	-	-	-	-	-				
10	33	0.75	2.4%	11.9%	85.5%	0.1%	2.56	0.6	10.2%	87.4%	2.0%	0.4%	0.00	36.3	6.0	297.9	1.00	0.0%	0.0%	0.0%					
12	33	0.75	2.1%	8.7%	89.1%	0.1%	2.46	-1.5	10.0%	88.3%	1.3%	0.4%	0.12	53.3	6.0	443.9	0.88	0.1%	0.4%	0.2%					
15	33	0.75	1.6%	5.3%	93.0%	0.1%	2.35	-5.4	9.8%	88.9%	0.9%	0.4%	0.19	80.2	5.9	645.3	0.82	0.1%	0.6%	0.3%					
10	20	0.75	Convergence not reached																						
12	20	0.75																							
15	20	0.75																							
10	15	0.75																							
12	15	0.75																							
15	15	0.75																							
10	33	0.5	1.7%	11.7%	86.6%	0.1%	2.26	-4.9	7.2%	90.6%	1.8%	0.3%	0.30	34.7	3.9	277.7	0.65	0.4%	1.1%	0.6%					
12	33	0.5	1.4%	7.7%	90.8%	0.1%	2.15	-7.5	7.3%	91.0%	1.4%	0.3%	0.37	47.7	3.9	381.6	0.60	0.3%	1.4%	0.6%					
15	33	0.5	1.0%	4.3%	94.6%	0.0%	2.07	-11.4	7.5%	91.1%	1.1%	0.3%	0.42	69.3	3.8	534.3	0.56	0.3%	1.6%	0.7%					
10	20	0.5	2.3%	17.1%	80.5%	0.1%	2.44	-0.4	6.4%	92.5%	0.8%	0.3%	0.07	47.8	3.8	462.3	0.89	0.0%	0.2%	0.1%					
12	20	0.5	2.3%	14.8%	82.8%	0.1%	2.37	-0.6	6.2%	93.0%	0.5%	0.3%	0.11	73.7	3.8	701.1	0.83	0.0%	0.3%	0.1%					
15	20	0.5	2.3%	12.5%	85.1%	0.1%	2.31	-0.7	6.2%	93.2%	0.3%	0.3%	0.13	116.8	3.8	1040.5	0.80	0.0%	0.4%	0.1%					
10	15	0.5	Convergence not reached																						
12	15	0.5																							
15	15	0.5																							
10	33	0.3	1.1%	11.7%	87.2%	0.0%	2.02	-10.4	4.6%	93.6%	1.6%	0.2%	0.53	34.2	2.2	270.0	0.37	0.6%	2.1%	0.9%					
12	33	0.3	1.0%	8.6%	90.4%	0.0%	1.95	-12.1	4.5%	94.2%	1.1%	0.2%	0.62	50.5	2.2	410.6	0.34	0.4%	2.4%	0.8%					
15	33	0.3	0.9%	6.4%	92.7%	0.0%	1.90	-13.6	4.5%	94.7%	0.7%	0.2%	0.69	81.2	2.2	651.7	0.31	0.3%	2.6%	0.8%					
10	20	0.3	1.6%	20.2%	78.1%	0.1%	2.26	-5.9	3.8%	95.5%	0.6%	0.2%	0.30	51.6	2.2	509.2	0.51	0.1%	1.0%	0.3%					
12	20	0.3	1.6%	17.5%	80.9%	0.1%	2.19	-6.2	3.7%	95.7%	0.4%	0.1%	0.32	75.4	2.2	718.4	0.49	0.1%	1.0%	0.3%					
15	20	0.3	1.5%	14.4%	83.9%	0.1%	2.11	-6.8	3.7%	95.8%	0.3%	0.1%	0.33	111.0	2.2	979.1	0.48	0.1%	1.1%	0.3%					
10	15	0.3	1.8%	22.8%	75.3%	0.1%	2.35	-4.6	3.7%	95.7%	0.5%	0.1%	0.16	56.1	2.2	576.1	0.67	0.0%	0.5%	0.1%					
12	15	0.3	1.8%	20.6%	77.5%	0.1%	2.29	-4.8	3.6%	95.9%	0.3%	0.1%	0.17	81.8	2.2	800.5	0.65	0.0%	0.5%	0.1%					
15	15	0.3	1.8%	18.6%	79.5%	0.1%	2.24	-4.6	3.6%	96.0%	0.2%	0.1%	0.18	120.7	2.2	1083.6	0.64	0.0%	0.5%	0.1%					
10	33	0.1	0.4%	11.6%	88.0%	0.0%	1.78	-22.9	1.6%	96.9%	1.5%	0.1%	0.74	33.4	0.7	259.3	0.12	0.7%	3.0%	0.9%					
12	33	0.1	0.3%	8.6%	91.0%	0.0%	1.73	-24.3	1.6%	97.4%	1.0%	0.1%	0.81	49.0	0.7	393.8	0.11	0.5%	3.3%	0.7%					
15	33	0.1	0.3%	6.6%	93.1%	0.0%	1.69	-25.6	1.6%	97.8%	0.6%	0.1%	0.87	76.6	0.7	605.3	0.10	0.4%	3.4%	0.6%					

$p_{perm,stage\ 1} = 3\text{ bara} \rightarrow \Delta p_{MEM2} = 2\text{ bar}$

10	33	0.5	2.4%	16.9%	80.5%	0.1%	2.44	0.3	5.9%	93.4%	0.5%	0.2%	0.03	70.5	3.7	777.8	0.95	0.0%	0.1%	0.0%
12	33	0.5	2.5%	15.5%	82.0%	0.1%	2.40	0.3	5.8%	93.6%	0.4%	0.2%	0.04	99.2	3.7	1013.1	0.92	0.0%	0.1%	0.0%
15	33	0.5	2.5%	13.9%	83.5%	0.1%	2.36	0.6	5.9%	93.6%	0.3%	0.2%	0.05	143.8	3.7	1327.4	0.91	0.0%	0.2%	0.1%
10	20	0.5	Convergence not reached																	
12	20	0.5																		
15	20	0.5																		
10	15	0.5																		
12	15	0.5																		
15	15	0.5																		
10	33	0.3	1.7%	17.9%	80.3%	0.1%	2.21	-5.0	3.9%	95.5%	0.4%	0.2%	0.25	68.2	2.2	747.0	0.56	0.1%	0.8%	0.2%
12	33	0.3	1.7%	16.7%	81.5%	0.1%	2.18	-4.9	3.8%	95.7%	0.3%	0.2%	0.26	94.3	2.2	953.9	0.55	0.1%	0.8%	0.2%
15	33	0.3	1.8%	16.3%	81.8%	0.1%	2.17	-3.9	3.8%	95.8%	0.3%	0.2%	0.27	134.2	2.2	1225.2	0.54	0.0%	0.9%	0.2%
10	20	0.3	1.9%	24.4%	73.6%	0.1%	2.41	-3.8	3.4%	96.2%	0.3%	0.1%	0.04	76.0	2.2	855.2	0.90	0.0%	0.1%	0.0%
12	20	0.3	2.1%	24.0%	73.9%	0.1%	2.41	-3.5	3.4%	96.2%	0.3%	0.1%	0.04	103.6	2.2	1067.1	0.88	0.0%	0.1%	0.0%
15	20	0.3	2.1%	27.1%	70.6%	0.1%	2.51	-2.0	3.0%	96.7%	0.2%	0.1%	0.05	144.0	2.2	1319.6	0.87	0.0%	0.1%	0.0%
10	15	0.3	Convergence not reached																	
12	15	0.3																		
15	15	0.3																		
10	33	0.1	0.7%	21.5%	77.8%	0.0%	2.03	-17.0	1.3%	98.2%	0.4%	0.1%	0.46	67.7	0.7	736.7	0.18	0.1%	1.5%	0.2%
12	33	0.1	0.7%	21.4%	77.9%	0.0%	2.03	-16.5	1.3%	98.4%	0.3%	0.1%	0.47	91.8	0.7	918.3	0.18	0.1%	1.5%	0.2%
15	33	0.1	0.7%	21.5%	77.7%	0.0%	2.03	-16.2	1.2%	98.5%	0.2%	0.0%	0.47	125.3	0.7	1125.2	0.18	0.1%	1.5%	0.2%

Table B.4: Process simulations of the PtG3 process in asymmetrical part load operation.

Bibliography

- [1] International Energy Agency (IEA). 'Data and statistics', [Online]. Available: <https://www.iea.org/data-and-statistics> (visited on 19/07/2022).
- [2] Intergovernmental Panel on Climate Change (IPCC), *Climate Change 2014: Synthesis Report. Contribution of Working Groups I, II and III to the Fifth Assessment Report of the Intergovernmental Panel on Climate Change*, R. K. Pachauri and L. Meyer, Eds. 2014, p. 151.
- [3] NOAA Global Monitoring Laboratory. 'Trends in Atmospheric Carbon Dioxide', [Online]. Available: <https://gml.noaa.gov/ccgg/trends/global.html> (visited on 18/07/2022).
- [4] United Nations Framework Convention on Climate Change. 'The Paris Agreement', [Online]. Available: <https://unfccc.int/process-and-meetings/the-paris-agreement/the-paris-agreement> (visited on 18/07/2022).
- [5] H. D. Matthews *et al.*, 'Opportunities and challenges in using remaining carbon budgets to guide climate policy', *Nature Geoscience*, vol. 13, no. 12, pp. 769–779, 2020. DOI: 10.1038/s41561-020-00663-3.
- [6] Intergovernmental Panel on Climate Change (IPCC), 'IPCC report Global warming of 1.5°C', Tech. Rep., 2018, p. 630.
- [7] M. Meinshausen *et al.*, 'Realization of Paris Agreement pledges may limit warming just below 2 °C', *Nature*, vol. 604, no. 7905, pp. 304–309, 2022. DOI: 10.1038/s41586-022-04553-z.
- [8] Swiss Federal Office of Energy (SFOE). 'Energy Strategy 2050'. (2020), [Online]. Available: <https://www.bfe.admin.ch/bfe/en/home/policy/energy-strategy-2050.html> (visited on 10/07/2020).
- [9] M. Rüdisüli, S. L. Teske and U. Elber, 'Impacts of an Increased Substitution of Fossil Energy Carriers with Electricity-Based Technologies on the Swiss Electricity System', *Energies*, vol. 12, no. 12, p. 2399, 2019. DOI: 10.3390/en12122399.
- [10] Swiss Federal Office of Energy (SFOE), 'Schweizerische Elektrizitätsstatistik 2019', Tech. Rep., 2020.

-
- [11] L. Geissbühler *et al.*, ‘Pilot-scale demonstration of advanced adiabatic compressed air energy storage, Part 1: Plant description and tests with sensible thermal-energy storage’, *Journal of Energy Storage*, vol. 17, pp. 129–139, 2018. DOI: 10.1016/j.est.2018.02.004.
- [12] T. Schaaf, J. Grünig, M. R. Schuster, T. Rothenfluh and A. Orth, ‘Methanation of CO₂ – storage of renewable energy in a gas distribution system’, *Energy, Sustainability and Society*, vol. 4, no. 1, p. 2, 2014. DOI: 10.1186/s13705-014-0029-1.
- [13] X. Luo, J. Wang, M. Dooner and J. Clarke, ‘Overview of current development in electrical energy storage technologies and the application potential in power system operation’, *Applied Energy*, vol. 137, pp. 511–536, 2015. DOI: 10.1016/j.apenergy.2014.09.081.
- [14] O. Schmidt, S. Melchior, A. Hawkes and I. Staffell, ‘Projecting the Future Levelized Cost of Electricity Storage Technologies’, *Joule*, vol. 3, no. 1, pp. 81–100, 2019. DOI: 10.1016/j.joule.2018.12.008.
- [15] A. Abdon, X. Zhang, D. Parra, M. K. Patel, C. Bauer and J. Worlitschek, ‘Techno-economic and environmental assessment of stationary electricity storage technologies for different time scales’, *Energy*, vol. 139, pp. 1173–1187, 2017. DOI: 10.1016/j.energy.2017.07.097.
- [16] H. Blanco and A. Faaij, ‘A review at the role of storage in energy systems with a focus on Power to Gas and long-term storage’, *Renewable and Sustainable Energy Reviews*, vol. 81, pp. 1049–1086, 2018. DOI: 10.1016/j.rser.2017.07.062.
- [17] V. Venkataraman *et al.*, ‘Reversible solid oxide systems for energy and chemical applications – Review & perspectives’, *Journal of Energy Storage*, vol. 24, no. June, p. 100 782, 2019. DOI: 10.1016/j.est.2019.100782.
- [18] Swiss Federal Office of Energy (SFOE), ‘Schweizerische Gesamtenergiestatistik 2019’, Tech. Rep., 2019.
- [19] Verband der Schweizerischen Gasindustrie (gazenergie). ‘Web Page gazenergie’, [Online]. Available: <https://gazenergie.ch/> (visited on 19/07/2022).
- [20] T. Kober *et al.*, *Perspectives of Power-to-X technologies in Switzerland – A White Paper*, 2019. DOI: 10.3929/ethz-b-000352294.
- [21] T. Estermann, M. Newborough and M. Sterner, ‘Power-to-gas systems for absorbing excess solar power in electricity distribution networks’, *International Journal of Hydrogen Energy*, vol. 41, no. 32, pp. 13 950–13 959, 2016. DOI: 10.1016/j.ijhydene.2016.05.278.
- [22] B. Simonis and M. Newborough, ‘Sizing and operating power-to-gas systems to absorb excess renewable electricity’, *International Journal of Hydrogen Energy*, vol. 42, no. 34, pp. 21 635–21 647, 2017. DOI: 10.1016/j.ijhydene.2017.07.121.
- [23] Swiss Federal Office for the Environment (FOEN), ‘Emissionen von Treibhausgasen nach CO₂-Gesetz und Kyoto-Protokoll, 2. Verpflichtungsperiode (2013–2020)’, Bundesamt für Umwelt (BAFU), Tech. Rep., 2021, pp. 1–23.

BIBLIOGRAPHY

- [24] M. Held, L. Küng, E. Çabukoglu, G. Pareschi, G. Georges and K. Boulouchos, 'Future mobility demand estimation based on socio-demographic information: A data-driven approach using machine learning algorithms', in *18th Swiss Transport Research Conference*, ETH Zurich, 2018. DOI: 10.3929/ethz-b-000266653.
- [25] Schweizerischer Verein des Gas- und Wasserfaches (SVGW), 'Richtlinie für die Einspeisung von erneuerbaren Gasen - G13/G18', Tech. Rep., 2016.
- [26] V. Burg, G. Bowman, M. Erni, R. Lemm and O. Thees, 'Analyzing the potential of domestic biomass resources for the energy transition in Switzerland', *Biomass and Bioenergy*, vol. 111, pp. 60–69, 2018. DOI: 10.1016/j.biombioe.2018.02.007.
- [27] O. Thees, V. Burg, M. Erni, G. Bowman and R. Lemm, 'Biomassepotenziale der Schweiz für die energetische Nutzung. Ergebnisse des Schweizerischen Energiekompetenzzentrums SCCER BIOSWEET', *WSL Berichte*, no. 57, p. 299, 2017.
- [28] V. Burg *et al.*, 'White paper: Biogas from animal manure in Switzerland. Energy potential, technology development and resource mobilization.', Swiss Federal Research Institute WSL, Tech. Rep., 2021, p. 20. DOI: 10.16904/envidat.255.
- [29] V. Burg, G. Bowman, M. Haubensak, U. Baier and O. Thees, 'Valorization of an untapped resource: Energy and greenhouse gas emissions benefits of converting manure to biogas through anaerobic digestion', *Resources, Conservation and Recycling*, vol. 136, no. April, pp. 53–62, 2018. DOI: 10.1016/j.resconrec.2018.04.004.
- [30] E. Moioli and T. Schildhauer, 'Negative CO₂ emissions from flexible biofuel synthesis: Concepts, potentials, technologies', *Renewable and Sustainable Energy Reviews*, vol. 158, no. December 2021, p. 112 120, 2022. DOI: 10.1016/j.rser.2022.112120.
- [31] A. Larsson, M. Kuba, T. Berdugo Vilches, M. Seemann, H. Hofbauer and H. Thunman, 'Steam gasification of biomass – Typical gas quality and operational strategies derived from industrial-scale plants', *Fuel Processing Technology*, vol. 212, p. 106 609, 2021. DOI: 10.1016/j.fuproc.2020.106609.
- [32] Swiss Federal Office of Energy (SFOE), 'Schweizerische Statistik der erneuerbaren Energien. Ausgabe 2019', Swiss Federal Office of Energy (SFOE), Tech. Rep., 2020.
- [33] A. Calbry-Muzyka, H. Madi, F. Rüsch-Pfund, M. Gandiglio and S. Biollaz, 'Biogas composition from agricultural sources and organic fraction of municipal solid waste', *Renewable Energy*, vol. 181, pp. 1000–1007, 2022. DOI: 10.1016/j.renene.2021.09.100.
- [34] N. H. Garcia, A. Mattioli, A. Gil, N. Frison, F. Battista and D. Bolzonella, 'Evaluation of the methane potential of different agricultural and food processing substrates for improved biogas production in rural areas', *Renewable and Sustainable Energy Reviews*, vol. 112, pp. 1–10, 2019. DOI: 10.1016/j.rser.2019.05.040.
- [35] L. P. Rabou and L. Bos, 'High efficiency production of substitute natural gas from biomass', *Applied Catalysis B: Environmental*, vol. 111–112, pp. 456–460, 2012. DOI: 10.1016/j.apcatb.2011.10.034.

-
- [36] F. Osorio and J. Torres, 'Biogas purification from anaerobic digestion in a wastewater treatment plant for biofuel production', *Renewable Energy*, vol. 34, no. 10, pp. 2164–2171, 2009. DOI: 10.1016/j.renene.2009.02.023.
- [37] A. S. Calbry-Muzyka *et al.*, 'Deep removal of sulfur and trace organic compounds from biogas to protect a catalytic methanation reactor', *Chemical Engineering Journal*, vol. 360, pp. 577–590, 2019. DOI: 10.1016/j.cej.2018.12.012.
- [38] Q. Sun, H. Li, J. Yan, L. Liu, Z. Yu and X. Yu, 'Selection of appropriate biogas upgrading technology-a review of biogas cleaning, upgrading and utilisation', *Renewable and Sustainable Energy Reviews*, vol. 51, pp. 521–532, 2015. DOI: 10.1016/j.rser.2015.06.029.
- [39] S. Rasi, A. Veijanen and J. Rintala, 'Trace compounds of biogas from different biogas production plants', *Energy*, vol. 32, no. 8, pp. 1375–1380, 2007. DOI: 10.1016/j.energy.2006.10.018.
- [40] D. Foppiano, M. Tarik, J. Schneebeli, A. Calbry-Muzyka, S. Biollaz and C. Ludwig, 'Siloxane compounds in biogas from manure and mixed organic waste: Method development and speciation analysis with GC-ICP-MS', *Talanta*, vol. 208, p. 120398, 2020. DOI: 10.1016/j.talanta.2019.120398.
- [41] R. Dewil, L. Appels and J. Baeyens, 'Energy use of biogas hampered by the presence of siloxanes', *Energy Conversion and Management*, vol. 47, no. 13-14, pp. 1711–1722, 2006. DOI: 10.1016/j.enconman.2005.10.016.
- [42] A. S. Calbry-Muzyka and T. J. Schildhauer, 'Direct Methanation of Biogas – Technical Challenges and Recent Progress', *Frontiers in Energy Research*, vol. 8, no. December, 2020. DOI: 10.3389/fenrg.2020.570887.
- [43] A. Lanzini *et al.*, 'Dealing with fuel contaminants in biogas-fed solid oxide fuel cell (SOFC) and molten carbonate fuel cell (MCFC) plants: Degradation of catalytic and electro-catalytic active surfaces and related gas purification methods', *Progress in Energy and Combustion Science*, vol. 61, pp. 150–188, 2017. DOI: 10.1016/j.pecs.2017.04.002.
- [44] F. Bauer, T. Persson, C. Hulteberg and D. Tamm, 'Biogas upgrading – technology overview, comparison and perspectives for the future', *Biofuels, Bioproducts and Biorefining*, vol. 7, no. 5, pp. 499–511, 2013. DOI: 10.1002/bbb.1423.
- [45] M. Ravina and G. Genon, 'Global and local emissions of a biogas plant considering the production of biomethane as an alternative end-use solution', *Journal of Cleaner Production*, vol. 102, no. 2015, pp. 115–126, 2015. DOI: 10.1016/j.jclepro.2015.04.056.
- [46] IEA Bioenergy. 'Task 37: Energy from Biogas'. (2019), [Online]. Available: <http://task37.ieabioenergy.com> (visited on 19/07/2022).
- [47] M. Miltner, A. Makaruk and M. Harasek, 'Review on available biogas upgrading technologies and innovations towards advanced solutions', *Journal of Cleaner Production*, vol. 161, pp. 1329–1337, 2017. DOI: 10.1016/j.jclepro.2017.06.045.

BIBLIOGRAPHY

- [48] R. W. Baker, 'Future Directions of Membrane Gas Separation Technology', *Industrial & Engineering Chemistry Research*, vol. 41, no. 6, pp. 1393–1411, 2002. DOI: 10.1021/ie0108088.
- [49] R. W. Baker, 'Membrane Technology', in *Encyclopedia of Polymer Science and Technology*, Hoboken, NJ, USA: John Wiley & Sons, Inc., 2001. DOI: 10.1002/0471440264.pst194.
- [50] X. Y. Chen, H. Vinh-Thang, A. A. Ramirez, D. Rodrigue and S. Kaliaguine, 'Membrane gas separation technologies for biogas upgrading', *RSC Advances*, vol. 5, no. 31, pp. 24 399–24 448, 2015. DOI: 10.1039/C5RA00666J.
- [51] Evonik Industries AG. 'SEPURAN®: Efficient gas separation using hollow-fiber membranes', [Online]. Available: <https://www.membrane-separation.com/en/upgrading-of-biogas-to-biomethane-with-sepuran-green> (visited on 19/07/2022).
- [52] J. Witte, 'Experimental and Techno-Economic Assessment of Catalytic Methanation of Biogas for Power-to-Gas Processes', Ph.D. dissertation, ETH Zurich, 2018, p. 215. DOI: 10.3929/ETHZ-B-000304900.
- [53] C. Vogt, M. Monai, G. J. Kramer and B. M. Weckhuysen, 'The renaissance of the Sabatier reaction and its applications on Earth and in space', *Nature Catalysis*, vol. 2, no. 3, pp. 188–197, 2019. DOI: 10.1038/s41929-019-0244-4.
- [54] S. Rönsch *et al.*, 'Review on methanation – From fundamentals to current projects', *Fuel*, vol. 166, pp. 276–296, 2016. DOI: 10.1016/j.fuel.2015.10.111.
- [55] G. A. Mills and F. W. Steffgen, 'Catalytic Methanation', *Catalysis Reviews*, vol. 8, no. 1, pp. 159–210, 1974. DOI: 10.1080/01614947408071860.
- [56] M. Götz *et al.*, 'Renewable Power-to-Gas: A technological and economic review', *Renewable Energy*, vol. 85, pp. 1371–1390, 2016. DOI: 10.1016/j.renene.2015.07.066.
- [57] J. Kopyscinski, T. J. Schildhauer and S. M. Biollaz, 'Production of synthetic natural gas (SNG) from coal and dry biomass – A technology review from 1950 to 2009', *Fuel*, vol. 89, no. 8, pp. 1763–1783, 2010. DOI: 10.1016/j.fuel.2010.01.027.
- [58] C. Dannesboe, J. B. Hansen and I. Johannsen, 'Catalytic methanation of CO₂ in biogas: experimental results from a reactor at full scale', *Reaction Chemistry & Engineering*, vol. 5, no. 1, pp. 183–189, 2020. DOI: 10.1039/C9RE00351G.
- [59] D. Rusmanis, R. O'Shea, D. M. Wall and J. D. Murphy, 'Biological hydrogen methanation systems – an overview of design and efficiency', *Bioengineered*, vol. 10, no. 1, pp. 604–634, 2019. DOI: 10.1080/21655979.2019.1684607.
- [60] J. Guilera *et al.*, 'Synthetic natural gas production from biogas in a waste water treatment plant', *Renewable Energy*, vol. 146, pp. 1301–1308, 2020. DOI: 10.1016/j.renene.2019.07.044.
- [61] C. H. Bartholomew, 'Mechanisms of catalyst deactivation', *Applied Catalysis A: General*, vol. 212, no. 1-2, pp. 17–60, 2001. DOI: 10.1016/S0926-860X(00)00843-7.

- [62] M. C. Seemann, T. J. Schildhauer and S. M. A. Biollaz, 'Fluidized Bed Methanation of Wood-Derived Producer Gas for the Production of Synthetic Natural Gas', *Industrial & Engineering Chemistry Research*, vol. 49, no. 21, pp. 11 119–11 119, 2010. DOI: 10.1021/ie101898w.
- [63] T. J. Schildhauer and S. M. Biollaz, Eds., *Synthetic Natural Gas from Coal, Dry Biomass, and Power-to-Gas Applications*. Hoboken, NJ, USA: John Wiley & Sons, Inc., 2016, pp. 231–248. DOI: 10.1002/9781119191339.
- [64] D. Strübing, B. Huber, M. Lebuhn, J. E. Drewes and K. Koch, 'High performance biological methanation in a thermophilic anaerobic trickle bed reactor', *Bioresource Technology*, vol. 245, pp. 1176–1183, 2017. DOI: 10.1016/j.biortech.2017.08.088.
- [65] L. Rachbauer, G. Voitl, G. Bochmann and W. Fuchs, 'Biological biogas upgrading capacity of a hydrogenotrophic community in a trickle-bed reactor', *Applied Energy*, vol. 180, pp. 483–490, 2016. DOI: 10.1016/j.apenergy.2016.07.109.
- [66] J.-P. Peillex, M.-L. Fardeau, R. Boussand, J.-M. Navarro and J.-P. Belaich, 'Growth of *Methanococcus thermolithotrophicus* in batch and continuous culture on H₂ and CO₂: influence of agitation', *Applied Microbiology and Biotechnology*, vol. 29, no. 6, pp. 560–564, 1988. DOI: 10.1007/BF00260985.
- [67] M. Thema *et al.*, 'Optimized biological CO₂-methanation with a pure culture of thermophilic methanogenic archaea in a trickle-bed reactor', *Bioresource Technology*, vol. 333, p. 125 135, 2021. DOI: 10.1016/j.biortech.2021.125135.
- [68] N. Schill, W. M. van Gulik, D. Voisard and U. von Stockar, 'Continuous cultures limited by a gaseous substrate: Development of a simple, unstructured mathematical model and experimental verification with *Methanobacterium thermoautotrophicum*', *Biotechnology and Bioengineering*, vol. 51, no. 6, pp. 645–658, 2000. DOI: 10.1002/(SICI)1097-0290(19960920)51:6<645::AID-BIT4>3.0.CO;2-H.
- [69] T. Ullrich and A. Lemmer, 'Performance enhancement of biological methanation with trickle bed reactors by liquid flow modulation', *GCB Bioenergy*, vol. 11, no. 1, pp. 63–71, 2019. DOI: 10.1111/gcbb.12547.
- [70] A. Vintiloiu, A. Lemmer, H. Oechsner and T. Jungbluth, 'Mineral substances and macronutrients in the anaerobic conversion of biomass: An impact evaluation', *Engineering in Life Sciences*, vol. 12, no. 3, pp. 287–294, 2012. DOI: 10.1002/elsc.201100159.
- [71] microbEnergy GmbH. 'Web Page microbEnergy'. (2019), [Online]. Available: <https://www.microbenergy.de/> (visited on 19/07/2022).
- [72] F. Graf, A. Krajete and U. Schmack, 'Abschlussbericht: Techno-ökonomische Studie zur biologischen Methanisierung bei Power-to-Gas-Konzepten', DVGW Deutscher Verein des Gas- und Wasserfaches, Tech. Rep., 2014, p. 66.

BIBLIOGRAPHY

- [73] A. Seifert, S. Rittmann and C. Herwig, 'Analysis of process related factors to increase volumetric productivity and quality of biomethane with *Methanothermobacter marburgensis*', *Applied Energy*, vol. 132, pp. 155–162, 2014. DOI: 10.1016/j.apenergy.2014.07.002.
- [74] Electrochaea.dk ApS. 'Power-to-Gas via Biological Catalysis (P2G-BioCat)'. (2014), [Online]. Available: <https://energiforskning.dk/en/node/15072> (visited on 19/07/2022).
- [75] E. Inkeri, T. Tynjälä, A. Laari and T. Hyppänen, 'Dynamic one-dimensional model for biological methanation in a stirred tank reactor', *Applied Energy*, vol. 209, pp. 95–107, 2018. DOI: 10.1016/j.apenergy.2017.10.073.
- [76] D. Hafenbradl, *Oral Presentation: Biological methanation*, 2019.
- [77] T. Ullrich, J. Lindner, K. Bär, F. Mörs, F. Graf and A. Lemmer, 'Influence of operating pressure on the biological hydrogen methanation in trickle-bed reactors', *Bioresource Technology*, vol. 247, pp. 7–13, 2018. DOI: 10.1016/j.biortech.2017.09.069.
- [78] T. Peyer, J. Flückiger, T. Di Lorenzo and N. Gündel, 'Das Stadtgas der Zukunft', *Aqua & Gas*, no. 9, pp. 34–39, 2018.
- [79] Limeco. 'Project Web Page: Power-to-Gas Plant Dietikon (Switzerland)'. (2020), [Online]. Available: <https://www.powertogas.ch/> (visited on 19/07/2022).
- [80] M. Specht, J. Brellochs, V. Frick, B. Stürmer and U. Zuberbühler, 'The Power To Gas Process', in *Synthetic Natural Gas from Coal, Dry Biomass, and Power-to-Gas Applications*, T. J. Schildhauer and S. M. Biollaz, Eds., Hoboken, NJ, USA: John Wiley & Sons, Inc., 2016, pp. 191–220. DOI: 10.1002/9781119191339.ch7.
- [81] J. Witte, A. Calbry-Muzyka, T. Wieseler, P. Hottinger, S. M. Biollaz and T. J. Schildhauer, 'Demonstrating direct methanation of real biogas in a fluidised bed reactor', *Applied Energy*, vol. 240, pp. 359–371, 2019. DOI: 10.1016/j.apenergy.2019.01.230.
- [82] S. Matthischke, S. Roensch and R. Güttel, 'Start-up Time and Load Range for the Methanation of Carbon Dioxide in a Fixed-Bed Recycle Reactor', *Industrial & Engineering Chemistry Research*, vol. 57, no. 18, pp. 6391–6400, 2018. DOI: 10.1021/acs.iecr.8b00755.
- [83] S. Matthischke, R. Krüger, S. Rönsch and R. Güttel, 'Unsteady-state methanation of carbon dioxide in a fixed-bed recycle reactor — Experimental results for transient flow rate ramps', *Fuel Processing Technology*, vol. 153, pp. 87–93, 2016. DOI: 10.1016/j.fuproc.2016.07.021.
- [84] J. Lefebvre, M. Götz, S. Bajohr, R. Reimert and T. Kolb, 'Improvement of three-phase methanation reactor performance for steady-state and transient operation', *Fuel Processing Technology*, vol. 132, pp. 83–90, 2015. DOI: 10.1016/j.fuproc.2014.10.040.
- [85] E. Giglio, R. Pirone and S. Bensaid, 'Dynamic modelling of methanation reactors during start-up and regulation in intermittent power-to-gas applications', *Renewable Energy*, vol. 170, pp. 1040–1051, 2021. DOI: 10.1016/j.renene.2021.01.153.

- [86] J. Bremer, K. H. G. Rätze and K. Sundmacher, 'Co₂ methanation: optimal start-up control of a fixed-bed reactor for power-to-gas applications', *AIChE Journal*, vol. 63, no. 1, pp. 23–31, 2017. DOI: 10.1002/aic.15496.
- [87] R. T. Zimmermann, J. Bremer and K. Sundmacher, 'Load-flexible fixed-bed reactors by multi-period design optimization', *Chemical Engineering Journal*, vol. 428, no. May 2021, p. 130 771, 2022. DOI: 10.1016/j.cej.2021.130771.
- [88] M. Lasser, 'Partial-load behaviour of fluidized-bed methanation', M.S. thesis, Montanuniversität Leoben, Leoben, Austria, 2021, p. 64.
- [89] A. Ursua, L. M. Gandia and P. Sanchis, 'Hydrogen Production From Water Electrolysis: Current Status and Future Trends', *Proceedings of the IEEE*, vol. 100, no. 2, pp. 410–426, 2012. DOI: 10.1109/JPROC.2011.2156750.
- [90] A. Buttler and H. Spliethoff, 'Current status of water electrolysis for energy storage, grid balancing and sector coupling via power-to-gas and power-to-liquids: A review', *Renewable and Sustainable Energy Reviews*, vol. 82, pp. 2440–2454, 2018. DOI: <https://doi.org/10.1016/j.rser.2017.09.003>.
- [91] M. Gruber *et al.*, 'Power-to-Gas through thermal integration of high-temperature steam electrolysis and carbon dioxide methanation - Experimental results', *Fuel Processing Technology*, vol. 181, pp. 61–74, 2018. DOI: 10.1016/j.fuproc.2018.09.003.
- [92] O. Schmidt, A. Gambhir, I. Staffell, A. Hawkes, J. Nelson and S. Few, 'Future cost and performance of water electrolysis: An expert elicitation study', *International Journal of Hydrogen Energy*, vol. 42, no. 52, pp. 30 470–30 492, 2017. DOI: 10.1016/j.ijhydene.2017.10.045.
- [93] M. Carmo, D. L. Fritz, J. Mergel and D. Stolten, 'A comprehensive review on PEM water electrolysis', *International Journal of Hydrogen Energy*, vol. 38, no. 12, pp. 4901–4934, 2013. DOI: 10.1016/j.ijhydene.2013.01.151.
- [94] L. Bertuccioli, A. Chan, D. Hart, F. Lehner, B. Madden and E. Standen, 'Study on development of water electrolysis in the EU', Tech. Rep. February, 2014, pp. 1–160.
- [95] T. Norman and M. Hamdan, 'Unitized Design for Home Refueling Appliance for Hydrogen Generation to 5,000 psi', DOE Hydrogen and Fuel Cells Program, Tech. Rep., 2012, pp. II-31 –II-34.
- [96] K. E. Ayers *et al.*, 'Research Advances Towards Low Cost, High Efficiency PEM Electrolysis', *ECS Meeting Abstracts*, vol. MA2010-02, no. 10, pp. 603–603, 2010. DOI: 10.1149/ma2010-02/10/603.
- [97] M. Laguna-Bercero, 'Recent advances in high temperature electrolysis using solid oxide fuel cells: A review', *Journal of Power Sources*, vol. 203, pp. 4–16, 2012. DOI: 10.1016/j.jpowsour.2011.12.019.
- [98] Karlsruher Institut für Technologie (KIT). 'Helmeth Project', [Online]. Available: <http://helmeth.eu/> (visited on 19/07/2022).

BIBLIOGRAPHY

- [99] M. Schmid and D. Decurtins, 'Energieversorgung der Zukunft', Verband der Schweizerischen Gasindustrie (VSG), Tech. Rep., 2018, p. 12.
- [100] H. Böhm, A. Zauner, D. C. Rosenfeld and R. Tichler, 'Projecting cost development for future large-scale power-to-gas implementations by scaling effects', *Applied Energy*, vol. 264, p. 114 780, 2020. DOI: 10.1016/j.apenergy.2020.114780.
- [101] M. Thema, F. Bauer and M. Sterner, 'Power-to-Gas: Electrolysis and methanation status review', *Renewable and Sustainable Energy Reviews*, vol. 112, pp. 775–787, 2019. DOI: 10.1016/j.rser.2019.06.030.
- [102] J. Witte, A. Kunz, S. M. Biollaz and T. J. Schildhauer, 'Direct catalytic methanation of biogas – Part II: Techno-economic process assessment and feasibility reflections', *Energy Conversion and Management*, vol. 178, pp. 26–43, 2018. DOI: 10.1016/j.enconman.2018.09.079.
- [103] J. Witte, J. Settino, S. M. Biollaz and T. J. Schildhauer, 'Direct catalytic methanation of biogas – Part I: New insights into biomethane production using rate-based modelling and detailed process analysis', *Energy Conversion and Management*, vol. 171, pp. 750–768, 2018. DOI: 10.1016/j.enconman.2018.05.056.
- [104] 'Store&Go Project'. (2016), [Online]. Available: <https://www.storeandgo.info/> (visited on 11/02/2020).
- [105] Energie360°. 'Gaspreise'. (2021), [Online]. Available: <https://www.energie360.ch/de/energie-360/wissen/erdgas-biogas/gaspreise/> (visited on 19/07/2022).
- [106] O. Posdziech, K. Schwarze and J. Brabandt, 'Efficient hydrogen production for industry and electricity storage via high-temperature electrolysis', *International Journal of Hydrogen Energy*, vol. 44, no. 35, pp. 19 089–19 101, 2019. DOI: 10.1016/j.ijhydene.2018.05.169.
- [107] J. Huettenrauch, M. Hoffmann and H. Föcker, 'Store&Go – Innovative large-scale energy storage technologies and power-to-gas concepts after optimisation. Report on economic analysis of test cases (D5.10)', Tech. Rep., 2020, p. 39.
- [108] E. Giglio, A. Lanzini, M. Santarelli and P. Leone, 'Synthetic natural gas via integrated high-temperature electrolysis and methanation: Part I—Energy performance', *Journal of Energy Storage*, vol. 2, no. 1, pp. 64–79, 2015. DOI: 10.1016/j.est.2015.06.004.
- [109] J. Kopyscinski, T. J. Schildhauer and S. M. Biollaz, 'Methanation in a fluidized bed reactor with high initial CO partial pressure: Part II— Modeling and sensitivity study', *Chemical Engineering Science*, vol. 66, no. 8, pp. 1612–1621, 2011. DOI: 10.1016/j.ces.2010.12.029.
- [110] K. Hilligardt and J. Werther, 'Lokaler Blasengas-Holdup und Expansionsverhalten von Gas/Feststoff-Wirbelschichten', *Chemie Ingenieur Technik*, vol. 57, no. 7, pp. 622–623, 1985. DOI: 10.1002/cite.330570713.
- [111] D. Geldart, 'Types of gas fluidization', *Powder Technology*, vol. 7, no. 5, pp. 285–292, 1973. DOI: 10.1016/0032-5910(73)80037-3.

- [112] L. S. Teske, 'Integrating Rate Based Models into a Multi-Objective Process Design & Optimisation Framework using Surrogate Models', Ph.D. dissertation, Lausanne, 2014. DOI: 10.5075/epfl-thesis-6302.
- [113] J. Kopyscinski, T. J. Schildhauer, F. Vogel, S. M. Biollaz and A. Wokaun, 'Applying spatially resolved concentration and temperature measurements in a catalytic plate reactor for the kinetic study of CO methanation', *Journal of Catalysis*, vol. 271, no. 2, pp. 262–279, 2010. DOI: 10.1016/j.jcat.2010.02.008.
- [114] J. Werther, 'Die Bedeutung der Blasenkoaleszenz für die Auslegung von Gas/Feststoff-Wirbelschichten', *Chemie Ingenieur Technik*, vol. 48, no. 4, pp. 339–339, 1976. DOI: 10.1002/cite.330480421.
- [115] S. Maurer *et al.*, 'Correlating bubble size and velocity distribution in bubbling fluidized bed based on X-ray tomography', *Chemical Engineering Journal*, vol. 298, pp. 17–25, 2016. DOI: 10.1016/J.CEJ.2016.02.012.
- [116] F. Schillinger, S. Maurer, E. C. Wagner, J. R. van Ommen, R. F. Mudde and T. J. Schildhauer, 'Influence of vertical heat exchanger tubes, their arrangement and the column diameter on the hydrodynamics in a gas–solid bubbling fluidized bed', *International Journal of Multiphase Flow*, vol. 97, pp. 46–59, 2017. DOI: 10.1016/j.ijmultiphaseflow.2017.07.013.
- [117] Store&Go Project. 'Store&Go Demonstration Site in Switzerland'. (2016), [Online]. Available: <https://www.storeandgo.info/demonstration-sites/switzerland/> (visited on 11/02/2020).
- [118] A. Makaruk and M. Harasek, 'Numerical algorithm for modelling multicomponent multipermeator systems', *Journal of Membrane Science*, vol. 344, no. 1-2, pp. 258–265, 2009. DOI: 10.1016/j.memsci.2009.08.013.
- [119] Y. Zhang, I. H. Musselman, J. P. Ferraris and K. J. Balkus, 'Gas permeability properties of Matrimid® membranes containing the metal-organic framework Cu-BPY-HFS', *Journal of Membrane Science*, vol. 313, no. 1-2, pp. 170–181, 2008. DOI: 10.1016/j.memsci.2008.01.005.
- [120] G. D. Ulrich and P. T. Vasudevan, *Chemical Engineering Process Design and Economics: A Practical Guide*, 2nd ed. Durham, N.H.: Process Publishing, 2004, p. 776.
- [121] DIN 1343:1990-01, *Reference conditions, normal conditions, normal volume; concepts and values*, 1990. DOI: 10.31030/2333155.
- [122] D. E. Garrett, *Chemical Engineering Economics*, 4. Dordrecht: Springer Netherlands, 1989, vol. 5, pp. 52–55. DOI: 10.1007/978-94-011-6544-0.
- [123] C. Bauer *et al.*, 'Potentials, costs and environmental assessment of electricity generation technologies', Paul Scherrer Institut (PSI), Villigen PSI, Tech. Rep., 2017, p. 783.
- [124] 'Chemical Engineering plant cost index (CEPCI)', *Chemical Engineering*, vol. 127, no. 9, p. 72, 2020.

BIBLIOGRAPHY

- [125] C. Flaviana *et al.*, 'Selective laser melting for heat exchanger', in *Proceeding of 6th International Conference on Additive Technologies*, 2016, pp. 383–388.
- [126] A. Buttler, R. Koltun, R. Wolf and H. Spliethoff, 'A detailed techno-economic analysis of heat integration in high temperature electrolysis for efficient hydrogen production', *International Journal of Hydrogen Energy*, vol. 40, no. 1, pp. 38–50, 2015. DOI: 10.1016/j.ijhydene.2014.10.048.
- [127] E. Giglio *et al.*, 'Power-to-Gas through High Temperature Electrolysis and Carbon Dioxide Methanation: Reactor Design and Process Modeling', *Industrial & Engineering Chemistry Research*, vol. 57, no. 11, pp. 4007–4018, 2018. DOI: 10.1021/acs.iecr.8b00477.
- [128] M. Tribe and R. Alpine, 'Scale economies and the "0.6 rule"', *Engineering Costs and Production Economics*, vol. 10, no. 1, pp. 271–278, 1986. DOI: 10.1016/0167-188X(86)90053-4.
- [129] F. Mörs, R. Schlautmann, J. Gorre, R. Leonhard and F. Graf, 'Store&Go – Innovative large-scale energy storage technologies and power-to-gas concepts after optimisation. Final report on evaluation of technologies and processes (D5.9)', Tech. Rep., 2020, p. 92.
- [130] R. Schlautmann *et al.*, 'Renewable Power-to-Gas: A Technical and Economic Evaluation of Three Demo Sites Within the STORE&GO Project', *Chemie Ingenieur Technik*, vol. 93, no. 4, pp. 568–579, 2021. DOI: 10.1002/cite.202000187.
- [131] Adam Christensen, 'Assessment of Hydrogen Production Costs from Electrolysis: United States and Europe', Tech. Rep., 2020, pp. 1–73.
- [132] P. Graichen, F. Peter, A. Sakhel, C. Podewils, T. Lenck and F. Hein, 'Die Energiewende im Stromsektor: Stand der Dinge 2018', Agora Energiewende, Tech. Rep., 2019, p. 74.
- [133] Swiss Federal Office of Energy (SFOE), 'Energiesstrategie 2050: Erstes Massnahmenpaket', Tech. Rep., 2012, p. 84.
- [134] Deutscher Verein des Gas- und Wasserfaches (DVGW), 'Arbeitsblatt G 262 2011-09: Nutzung von Gasen aus regenerativen Quellen in der öffentlichen Gasversorgung', Tech. Rep., 2011.
- [135] Österreichische Vereinigung für das Gas- und Wasserfach (ÖVGW), 'Erdgas in Österreich - Gasbeschaffenheit (Richtlinie G 31)', Tech. Rep. ÖVGW G 31, 2001.
- [136] A. Makaruk, M. Miltner and M. Harasek, 'Membrane biogas upgrading processes for the production of natural gas substitute', *Separation and Purification Technology*, vol. 74, no. 1, pp. 83–92, 2010. DOI: 10.1016/j.seppur.2010.05.010.
- [137] F. M. Baena-Moreno, M. Rodríguez-Galán, F. Vega, L. F. Vilches and B. Navarrete, 'Review: recent advances in biogas purifying technologies', *International Journal of Green Energy*, vol. 16, no. 5, pp. 401–412, 2019. DOI: 10.1080/15435075.2019.1572610.

- [138] F. Kirchbacher, P. Biegger, M. Miltner, M. Lehner and M. Harasek, 'A new methanation and membrane based power-to-gas process for the direct integration of raw biogas – Feasability and comparison', *Energy*, vol. 146, pp. 34–46, 2018. DOI: 10.1016/j.energy.2017.05.026.
- [139] Hitachi Zosen Inova AG. 'HZI Etogas'. (2020), [Online]. Available: <https://www.hz-inova.com/de/renewable-gas/etogas/> (visited on 19/07/2022).
- [140] INERATEC GmbH. 'INERATEC - Innovative Chemical Reactor Technologies'. (2017), [Online]. Available: <https://ineratec.de/en/home/> (visited on 11/02/2020).
- [141] P. Collet *et al.*, 'Techno-economic and Life Cycle Assessment of methane production via biogas upgrading and power to gas technology', *Applied Energy*, vol. 192, pp. 282–295, 2017. DOI: 10.1016/j.apenergy.2016.08.181.
- [142] E. Saracevic *et al.*, 'Utilization of Food and Agricultural Residues for a Flexible Biogas Production: Process Stability and Effects on Needed Biogas Storage Capacities', *Energies*, vol. 12, no. 14, p. 2678, 2019. DOI: 10.3390/en12142678.
- [143] D. G. Mulat, H. F. Jacobi, A. Feilberg, A. P. S. Adamsen, H.-H. Richnow and M. Nikolausz, 'Changing Feeding Regimes To Demonstrate Flexible Biogas Production: Effects on Process Performance, Microbial Community Structure, and Methanogenesis Pathways', *Applied and Environmental Microbiology*, vol. 82, no. 2, R. M. Kelly, Ed., pp. 438–449, 2016. DOI: 10.1128/AEM.02320-15.
- [144] H. Hahn, B. Krautkremer, K. Hartmann and M. Wachendorf, 'Review of concepts for a demand-driven biogas supply for flexible power generation', *Renewable and Sustainable Energy Reviews*, vol. 29, pp. 383–393, 2014. DOI: 10.1016/j.rser.2013.08.085.
- [145] Bronkhorst (Schweiz) AG, *General instructions digital Mass Flow / Pressure instruments laboratory style / IN-FLOW*, 2020.
- [146] V. Tshedanoﬀ, T. J. Schildhauer, S. M. Biollaz and A. Wokaun, 'Portable gas chromatograph calibration with gases of varying viscosities', *Talanta*, vol. 225, p. 121 077, 2021. DOI: 10.1016/j.talanta.2020.121077.
- [147] J. R. Fried, 'Molecular Simulation of Gas and Vapor Transport in Highly Permeable Polymers', in *Materials Science of Membranes for Gas and Vapor Separation*, Y. Yampolskii, I. Pinnau and B. Freeman, Eds., Chichester, UK: John Wiley & Sons, Ltd, 2006, pp. 95–136. DOI: 10.1002/047002903X.ch3.
- [148] R. M. Barrer, J. A. Barrie and J. Slater, 'Sorption and diffusion in ethyl cellulose. Part III. Comparison between ethyl cellulose and rubber', *Journal of Polymer Science*, vol. 27, no. 115, pp. 177–197, 1958. DOI: 10.1002/pol.1958.1202711515.
- [149] O. C. David, D. Gorri, A. Urtiaga and I. Ortiz, 'Mixed gas separation study for the hydrogen recovery from H₂/CO/N₂/CO₂ post combustion mixtures using a Matrimid membrane', *Journal of Membrane Science*, vol. 378, no. 1-2, pp. 359–368, 2011. DOI: 10.1016/j.memsci.2011.05.029.

BIBLIOGRAPHY

- [150] J. M. Henis and M. K. Tripodi, 'Composite hollow fiber membranes for gas separation: the resistance model approach', *Journal of Membrane Science*, vol. 8, no. 3, pp. 233–246, 1981. DOI: 10.1016/S0376-7388(00)82312-1.
- [151] T. Pettersen and K. Lien, 'A new robust design model for gas separating membrane modules, based on analogy with counter-current heat exchangers', *Computers & Chemical Engineering*, vol. 18, no. 5, pp. 427–439, 1994. DOI: 10.1016/0098-1354(94)88021-2.
- [152] D. T. Coker, B. D. Freeman and G. K. Fleming, 'Modeling multicomponent gas separation using hollow-fiber membrane contactors', *AIChE Journal*, vol. 44, no. 6, pp. 1289–1302, 1998. DOI: 10.1002/aic.690440607.
- [153] M. H. Murad Chowdhury, X. Feng, P. Douglas and E. Croiset, 'A New Numerical Approach for a Detailed Multicomponent Gas Separation Membrane Model and Aspen-Plus Simulation', *Chemical Engineering & Technology*, vol. 28, no. 7, pp. 773–782, 2005. DOI: 10.1002/ceat.200500077.
- [154] C. Y. Pan, 'Gas separation by high-flux, asymmetric hollow-fiber membrane', *AIChE Journal*, vol. 32, no. 12, pp. 2020–2027, 1986. DOI: 10.1002/aic.690321212.
- [155] T. Kvist and N. Aryal, 'Methane loss from commercially operating biogas upgrading plants', *Waste Management*, vol. 87, pp. 295–300, 2019. DOI: 10.1016/j.wasman.2019.02.023.
- [156] International Energy Agency (IEA), 'Renewables 2021 – Analysis and forecast to 2026', Tech. Rep., 2021.
- [157] J. Gorre, F. Ruoss, H. Karjunen, J. Schaffert and T. Tynjälä, 'Cost benefits of optimizing hydrogen storage and methanation capacities for Power-to-Gas plants in dynamic operation', *Applied Energy*, vol. 257, p. 113967, 2020. DOI: 10.1016/j.apenergy.2019.113967.
- [158] L. M. Robeson, 'Correlation of separation factor versus permeability for polymeric membranes', *Journal of Membrane Science*, vol. 62, no. 2, pp. 165–185, 1991. DOI: 10.1016/0376-7388(91)80060-J.
- [159] T.-S. Chung, L. Shao and P. S. Tin, 'Surface Modification of Polyimide Membranes by Diamines for H₂ and CO₂ Separation', *Macromolecular Rapid Communications*, vol. 27, no. 13, pp. 998–1003, 2006. DOI: 10.1002/marc.200600147.
- [160] F. Wu, L. Li, Z. Xu, S. Tan and Z. Zhang, 'Transport study of pure and mixed gases through PDMS membrane', *Chemical Engineering Journal*, vol. 117, no. 1, pp. 51–59, 2006. DOI: 10.1016/j.cej.2005.12.010.
- [161] W. J. Koros, R. T. Chern, V. Stannett and H. B. Hopfenberg, 'A model for permeation of mixed gases and vapors in glassy polymers', *Journal of Polymer Science: Polymer Physics Edition*, vol. 19, no. 10, pp. 1513–1530, 1981. DOI: 10.1002/pol.1981.180191004.
- [162] W. Koros, A. Chan and D. Paul, 'Sorption and transport of various gases in polycarbonate', *Journal of Membrane Science*, vol. 2, pp. 165–190, 1977. DOI: 10.1016/S0376-7388(00)83242-1.

- [163] J. D. Wind, 'Improving Polyimide Membrane Resistance to Carbon Dioxide Plasticization in Natural Gas Separations', Ph.D. dissertation, University of Texas at Austin, 2002, pp. 2605–2621.
- [164] A. S. Michaels, W. R. Vieth and J. A. Barrie, 'Solution of Gases in Polyethylene Terephthalate', *Journal of Applied Physics*, vol. 34, no. 1, pp. 1–12, 1963. DOI: 10.1063/1.1729066.
- [165] K. Toi, G. Morel and D. R. Paul, 'Gas sorption and transport in poly(phenylene oxide) and comparisons with other glassy polymers', *Journal of Applied Polymer Science*, vol. 27, no. 8, pp. 2997–3005, 1982. DOI: 10.1002/app.1982.070270823.
- [166] A. Gantenbein, J. Witte, S. M. Biollaz, O. Kröcher and T. J. Schildhauer, 'Flexible application of biogas upgrading membranes for hydrogen recycle in power-to-methane processes', *Chemical Engineering Science*, vol. 229, p. 116 012, 2021. DOI: 10.1016/j.ces.2020.116012.
- [167] A. Gantenbein, O. Kröcher, S. M. A. Biollaz and T. J. Schildhauer, 'Techno-Economic Evaluation of Biological and Fluidised-Bed Based Methanation Process Chains for Grid-Ready Biomethane Production', *Frontiers in Energy Research*, vol. 9, 2022. DOI: 10.3389/fenrg.2021.775259.
- [168] C. Müller and U. Oester, 'Biogasaufbereitungsanlage – Aufbereitung von 40 Nm³/h Klärgas zu Reingas und Einspeisung ins 5 bar-Erdgasnetz', Tech. Rep., 2019.
- [169] M. Ungerank, G. Baumgarten, M. Piske and H. Roegl, 'PROCESS FOR SEPARATION OF GASES', United States Patent No. 8999038B2.
- [170] J. Kopyscinski, 'Production of synthetic natural gas in a fluidized bed reactor', Ph.D. dissertation, ETH Zurich, 2010, pp. 1–252. DOI: 10.3929/ETHZ-A-006031831.
- [171] European Energy Exchange (EEX). 'Electricity Spot Price', [Online]. Available: <https://www.epexspot.com/> (visited on 19/07/2022).
- [172] Swiss Federal Office of Energy (SFOE), 'Schweizerische Elektrizitätsstatistik 2020', Tech. Rep., 2020.
- [173] MeteoSchweiz. 'Climate normals', [Online]. Available: <https://www.meteoschweiz.admin.ch/home/klima/schweizer-klima-im-detail/klima-normwerte/normwerte-pro-messgroesse-und-station.html> (visited on 19/07/2022).
- [174] European Energy Exchange (EEX). 'Emission trading spot market price', [Online]. Available: <https://www.eex.com/en/market-data/environmental-markets/spot-market> (visited on 15/02/2022).
- [175] E. Inkeri, T. Tynjälä and H. Karjunen, 'Significance of methanation reactor dynamics on the annual efficiency of power-to-gas -system', *Renewable Energy*, vol. 163, pp. 1113–1126, 2021. DOI: 10.1016/j.renene.2020.09.029.
- [176] F. Schillinger, 'Systematic assessment and application of local optical and two-dimensional X-ray measurement techniques for hydrodynamic characterization of bubbling fluidized beds', Ph.D. dissertation, ETH Zurich, 2018, p. 215. DOI: 10.3929/ethz-b-000306127.

BIBLIOGRAPHY

- [177] Energy Science Center of ETH Zurich. 'ReMaP - Renewable Management and Real-Time Control Platform', [Online]. Available: <https://remap.ch/> (visited on 19/07/2022).
- [178] J. Witte, H. Madi, U. Elber, P. Jansohn and T. J. Schildhauer, 'Grid-Neutral Hydrogen Mobility: Dynamic Modelling and Techno-Economic Assessment of a Renewable-Powered Hydrogen Plant', *manuscript in preparation*,
- [179] M. Hofer and P. Jansohn, 'ESI Achievements Report', Paul Scherrer Institute (PSI), Villigen, Tech. Rep. June, 2022, p. 52. DOI: 10.3929/ethz-b-000553744.
- [180] M. Sandru, S. H. Haukebo and M.-B. Hägg, 'Composite hollow fiber membranes for CO₂ capture', *Journal of Membrane Science*, vol. 346, no. 1, pp. 172–186, 2010. DOI: 10.1016/j.memsci.2009.09.039.
- [181] S. Maurer, 'Hydrodynamic Characterization and Scale-Up of Bubbling Fluidized Beds for Catalytic Conversion', Ph.D. dissertation, ETH Zurich, 2015, p. 219. DOI: 10.3929/ethz-a-010453120.

List of publications

Peer-reviewed publications

- A. S. Calbry-Muzyka, A. Gantenbein, J. Schneebeil, A. Frei, A. J. Knorpp, T. J. Schildhauer, S. M. A. Biollaz, 'Deep removal of sulfur and trace organic compounds from biogas to protect a catalytic methanation reactor', *Chemical Engineering Journal*, vol. 360, pp. 577–590, Mar. 2019. DOI: 10.1016/j.cej.2018.12.012
- A. Gantenbein, J. Witte, S. M. A. Biollaz, O. Kröcher, T. J. Schildhauer, 'Flexible application of biogas upgrading membranes for hydrogen recycle in power-to-methane processes', *Chemical Engineering Science*, vol. 229, p. 116 012, Jan. 2021. DOI: 10.1016/j.ces.2020.116012
- A. Gantenbein, S. M. A. Biollaz, O. Kröcher, T. J. Schildhauer, 'Techno-Economic Evaluation of Biological and Fluidised-Bed Based Methanation Process Chains for Grid-Ready Biomethane Production', *Frontiers in Energy Research*, vol. 9, Mar. 2022. DOI: 10.3389/fenrg.2021.775259

Conference oral presentations

- A. Gantenbein, J. Witte, O. Kröcher, S.M.A. Biollaz, T.J. Schildhauer, 'Applying biogas upgrading membranes for hydrogen recycle in Power-to-Methane processes', *XXIV International Conference on Chemical Reactors*, September 2021, Milan, Italy (online).
- A. Gantenbein, J. Witte, O. Kröcher, S.M.A. Biollaz, T.J. Schildhauer, 'Applying biogas upgrading membranes for hydrogen recycle in Power-to-Methane processes', *13th European Congress of Chemical Engineering and 6th European Congress of Applied Biotechnology (ECCE/ECAB)*, September 2021, Berlin, Germany (online).
- A. Gantenbein, J. Witte, O. Kröcher, S.M.A. Biollaz, T.J. Schildhauer, 'Applying biogas upgrading membranes for hydrogen recycle in Power-to-Methane processes', *26th International Symposium on Chemical Reaction Engineering (ISCRE 26)*, December 2021, Delhi, India (online).

- A. Gantenbein, O. Kröcher, S.M.A. Biollaz, T.J. Schildhauer, 'Flexible application of biogas upgrading membranes for hydrogen recycle in Power-to-Methane processes', *30th European Biomass Conference & Exhibition*, Mai 2022, online.

Conference posters

- A. Gantenbein, J. Witte, O. Kröcher, S.M.A. Biollaz, T.J. Schildhauer, 'Application of Biogas Upgrading Membranes for Hydrogen Recycle in Power-to-Methane Processes', *DECHEMA Jahrestreffen Reaktionstechnik 2019*, May 2019, Würzburg, Germany.
- A. Gantenbein, J. Witte, O. Kröcher, S.M.A. Biollaz, T.J. Schildhauer, 'Flexible Application of Biogas Upgrading Membranes in Power-to-Methane Processes', *6th Biomass for Swiss Energy Future Conference*, September 2019, Horw, Switzerland.
- A. Gantenbein, J. Witte, O. Kröcher, S.M.A. Biollaz, T.J. Schildhauer, 'Flexible Application of Biogas Upgrading Membranes in Power-to-Methane Processes', *PSI ENE/NES Poster event*, December 2019, Villigen PSI, Switzerland.
- A. Gantenbein, J. Witte, O. Kröcher, S.M.A. Biollaz, T.J. Schildhauer, 'Flexible Application of Biogas Upgrading Membranes in Power-to-Methane Processes', *3rd Doctoral Colloquium Bioenergy*, September 2020, Leipzig, Germany (online).

Andreas Gantenbein – Curriculum Vitae

Nationality: Swiss, citizen of Grabs SG
Date of Birth: 16th May 1990

Education

- May 2018 – July 2022 **PhD Student, EPF Lausanne, at PSI Villigen**
Doctoral thesis in the Thermochemical Processes Group,
supervised by Prof. O. Kröcher and Dr. T. J. Schildhauer
- Feb. 2016 – Aug. 2017 **Master studies in Chemical and Bioengineering, ETH Zurich**
- Mar. – June 2016 **Master's thesis, Thermochemical Processes Group, PSI Villigen**
“Purification of Biogas for Methanation: Siloxane Adsorption on Sulphur
Removing Sorbents”
Supervision: Prof. Alexander Wokaun
- Sept. – Dec. 2015 **Semester project, Safety & Environmental Technology Group, ETH Zurich**
Topic: Data visualisation and interpretation for an industrial waste
incineration process optimisation.
Supervision: Prof. Konrad Hungerbühler
- Sept. 2011 – Feb. 2016 **Bachelor studies in Chemical Engineering, ETH Zurich**

Professional and Research Experience

- May 2018 – July 2022 **Research Assistant, Thermochemical Processes Group, PSI Villigen**
Part of the engineering team of a TRL 6 PtG facility, plant commissioning and
development of a concept for process and scientific analytics
- Oct. 2017 – Mar. 2018 **Intern, GMP & Production Services, F. Hoffmann-La Roche AG, Basel**
Work in the technical compliance team of the late stage development and
small molecules launch facility
- Mar. – July 2017 **Visiting Scientist, PSI Villigen**
Gas sampling and data evaluation during a long-duration field campaign with
a TRL 4 – 5 PtG plant
- Mar. – Sept. 2011 **Internship, EMS-Chemie, Domat-Ems**
Part of the engineering department (EMS-Services)
- Oct. – Dec. 2010 **Internship, DOW Chemical Company (former ACIMA AG), Buchs SG**
Work in chemical and biological laboratories